

# **HYDRODYNAMIC INVESTIGATION OF POLYSACCHARIDES AND THEIR INTERACTIONS WITH CASEIN**

**by Gordon Alistair Morris, BSc., MSc.**

Thesis submitted to the University of Nottingham for the degree of Doctor of  
Philosophy, January 2001.

**Supervisors** - Prof. Stephen E. Harding (NCMH Unit, Division of Food Sciences)  
Dr. Tim J. Foster (Product Microstructure, Unilever Research)



**“What one usually means by research, I suppose, is the systematic questing for enlightenment”**

**Thé Svedberg, 1947\***

\*Thé Svedberg in his address “Forskningens mål och medel” at the inauguration of the Research Laboratory, Höganäs-Billesholms AB, Sweden, September 10<sup>th</sup> 1947. Translated by DS MacQueen (Uppsala University) and appearing in Physical Chemistry of Colloids and Macromolecules – The Svedberg Symposium, Rångby B (Ed.), Blackwell Science, Oxford, 1987.

# LIST OF CONTENTS

<b>LIST OF CONTENTS</b> .....	<b>i</b>
<b>LIST OF FIGURES</b> .....	<b>ix</b>
<b>LIST OF TABLES</b> .....	<b>xix</b>
<b>ABSTRACT</b> .....	<b>xxi</b>
<b>ACKNOWLEDGEMENTS</b> .....	<b>xxii</b>
<b>GLOSSARY OF IMPORTANT TERMS</b> .....	<b>xxiii</b>
<b>1 CHAPTER 1 - PROTEIN – POLYSACCHARIDE INTERACTIONS</b> .....	<b>1</b>
1.1 MIXED BIOPOLYMERS.....	1
1.2 TYPES OF PROTEIN – POLYSACCHARIDE INTERACTIONS .....	1
1.2.1 Phase Separation .....	2
1.2.1.1 Two – phase system .....	3
1.2.1.2 One – phase system .....	5
1.2.2 Complexation.....	6
1.2.2.1 One – phase system .....	6
1.2.2.2 Two – phase system .....	7
1.3 FLOCCULATION.....	8
1.4 APPLICATION OF HYDRODYNAMIC TECHNIQUES .....	10
1.4.1 Sedimentation Velocity .....	11
1.4.2 Sedimentation Equilibrium.....	11
1.4.3 Capillary Viscometry .....	12
1.4.4 SEC-MALLS-RI .....	12
1.4.5 Dynamic Light Scattering.....	12
1.4.6 Particle Size Analysis using the Malvern Mastersizer™ .....	13
1.5 AIMS AND OBJECTIVES.....	13
1.6 REFERENCES .....	14
<b>2 CHAPTER 2 – HYDRODYNAMIC TOOLS FOR THE STUDY OF PROTEIN – POLYSACCHARIDE INTERACTIONS</b> .....	<b>21</b>
2.1 THE USE OF HYDRODYNAMICS TOOLS FOR THE ANALYSIS OF THE SOLUTION PROPERTIES OF MACROMOLECULES.....	21
2.1.1 Hydrodynamic Techniques.....	22

2.2	THEORY OF SEDIMENTATION IN THE ANALYTICAL ULTRACENTRIFUGE .....	25
2.2.1	Sedimentation Velocity in the Analytical Ultracentrifuge .....	28
2.2.2	Sedimentation Equilibrium in the Analytical Ultracentrifuge.....	40
2.2.2.1	MSTAR .....	41
2.3	VISCOMETRY .....	47
2.3.1	Theory of Viscosity.....	47
2.3.2	Measurement of Viscosity (in dilute solution) .....	50
2.3.3	Measurement of Viscosity (in concentrated solution) .....	56
2.4	SIZE EXCLUSION CHROMATOGRAPHY – MULTI-ANGLE LASER LIGHT SCATTERING .....	59
2.4.1	Light Scattering.....	59
2.4.2	Size Exclusion Chromatography (SEC).....	63
2.4.3	SEC-MALLS .....	65
2.5	DYNAMIC LIGHT SCATTERING (DLS).....	68
2.6	PARTICLE SIZE DISTRIBUTION – LASER DIFFRACTION .....	71
2.7	DENSIMETRY .....	75
2.8	COMBINED HYDRODYNAMIC APPROACHES.....	75
2.9	REFERENCES .....	83
<b>3</b>	<b>CHAPTER 3 – DETAILED CHARACTERISATION OF THE POLYSACCHARIDE SUBSTRATES .....</b>	<b>90</b>
3.1	CHARACTERISATION OF CITRUS PECTINS .....	94
3.1.1	Characterisation of Pectin 7000 Series.....	94
3.1.1.1	Background.....	94
3.1.1.2	Materials .....	95
3.1.1.3	Methods .....	96
3.1.1.4	Results and Discussion .....	98
3.1.1.5	Concluding Remarks .....	106
3.1.2	Effect of High Temperature.....	109
3.1.2.1	Background.....	109
3.1.2.2	LM Pectin .....	109
3.1.2.3	HM Pectin.....	116
3.1.2.4	Concluding Remarks .....	126

3.1.3	Effect of Carboxybenzyl Derivatisation .....	127
3.1.3.1	Background.....	127
3.1.3.2	Materials .....	127
3.1.3.3	Methods .....	128
3.1.3.4	Results and Discussion.....	130
3.1.3.5	Concluding Remarks .....	135
3.2	CHARACTERISATION OF CARRAGEENANS.....	136
3.2.1	Background.....	136
3.2.2	$\kappa$ -carrageenan.....	141
3.2.3	$\iota$ -carrageenan .....	141
3.2.4	Methods.....	141
3.2.4.1	Capillary Viscometry .....	141
3.2.4.2	Sedimentation Velocity in the Analytical Ultracentrifuge .....	141
3.2.4.3	Sedimentation Equilibrium in the Analytical Ultracentrifuge .....	142
3.2.4.4	SEC-MALLS .....	142
3.2.5	Results and Discussion.....	143
3.2.5.1	Capillary Viscometry .....	143
3.2.5.2	Sedimentation Velocity in the Analytical Ultracentrifuge .....	143
3.2.5.3	Sedimentation Equilibrium in the Analytical Ultracentrifuge .....	146
3.2.5.4	SEC-MALLS .....	147
3.2.6	Concluding Remarks.....	148
3.3	CHARACTERISATION OF GALACTOMANNANS.....	150
3.3.1	Background.....	150
3.3.2	Materials .....	151
3.3.2.1	Guar M150, Guar M90, Guar M30 and LBG M175 .....	151
3.3.3	Methods.....	152
3.3.3.1	Capillary Viscometry .....	152
3.3.3.2	Sedimentation Velocity in the Analytical Ultracentrifuge .....	152
3.3.3.3	SEC-MALLS .....	153
3.3.4	Results and Discussion.....	153
3.3.4.1	Capillary Viscometry .....	153
3.3.4.2	Sedimentation Velocity in the Analytical Ultracentrifuge .....	153
3.3.4.3	SEC-MALLS .....	156

3.3.5	Concluding Remarks .....	160
3.4	CHARACTERISATION OF TWO BACTERIAL POLYSACCHARIDES - <i>APHANOTHECE HALOPHYTICA</i> AND XANTHAN.....	165
3.4.1	Background.....	165
3.4.2	Materials .....	166
3.4.3	Methods.....	167
3.4.3.1	Capillary Viscometry .....	167
3.4.3.2	Rotational Viscometry.....	167
3.4.3.3	Sedimentation Velocity in the Analytical Ultracentrifuge .....	168
3.4.3.4	Sedimentation Equilibrium in the Analytical Ultracentrifuge .....	168
3.4.4	Results and Discussion.....	169
3.4.4.1	Capillary Viscometry for AH-EPS.....	169
3.4.4.2	Capillary Viscometry for Xanthan .....	170
3.4.4.3	Rotational Viscometry for AH-EPS.....	170
3.4.4.4	Rotational Viscometry for Xanthan .....	173
3.4.4.5	Sedimentation Velocity for AH-EPS .....	173
3.4.4.6	Sedimentation Velocity for Xanthan.....	175
3.4.4.7	Sedimentation Equilibrium for AH-EPS .....	175
3.4.4.8	Sedimentation Equilibrium for Xanthan .....	179
3.4.5	Concluding Remarks.....	179
3.5	CHARACTERISATION OF NATIVE AND MODIFIED ARABINO- XYLANS .....	181
3.5.1	Background.....	181
3.5.2	Materials .....	184
3.5.3	Methods.....	185
3.5.3.1	UV Absorption.....	185
3.5.3.2	Capillary Viscometry .....	185
3.5.3.3	Sedimentation Velocity in the Analytical Ultracentrifuge .....	185
3.5.3.4	Sedimentation Equilibrium in the Analytical Ultracentrifuge.....	186
3.5.4	Results and Discussion.....	186
3.5.4.1	UV Absorption.....	186
3.5.4.2	Capillary Viscometry .....	186
3.5.4.3	Sedimentation Velocity in the Analytical Ultracentrifuge .....	188

3.5.4.4	Sedimentation Equilibrium in the Analytical Ultracentrifuge.....	189
3.5.5	Concluding Remarks .....	190
3.6	REFERENCES .....	191
<b>4</b>	<b>CHAPTER 4 – DETAILED CHARACTERISATION OF THE MILK PROTEIN SUBSTRATES .....</b>	<b>207</b>
4.1	CASEIN MICELLES IN SKIM MILK .....	210
4.1.1	Background.....	210
4.1.2	Materials .....	212
4.1.3	Methods.....	212
4.1.3.1	Sedimentation Velocity in the Analytical Ultracentrifuge .....	212
4.1.3.2	Capillary Viscometry .....	213
4.1.4	Results and Discussion.....	214
4.1.4.1	Sedimentation Velocity in the Analytical Ultracentrifuge .....	214
4.1.4.2	Capillary Viscometry .....	215
4.1.5	Concluding Remarks .....	221
4.2	SODIUM CASEINATE.....	222
4.2.1	Background.....	222
4.2.2	Materials .....	223
4.2.2.1	Solutions .....	223
4.2.3	Methods.....	223
4.2.3.1	Capillary Viscometry .....	223
4.2.3.2	Sedimentation Velocity in the Analytical Ultracentrifuge .....	223
4.2.3.3	Sedimentation Equilibrium in the Analytical Ultracentrifuge.....	224
4.2.4	Results and Discussion.....	224
4.2.4.1	Capillary Viscometry .....	224
4.2.4.2	Sedimentation Velocity .....	225
4.2.4.3	Sedimentation Equilibrium.....	228
4.2.5	Concluding Remarks.....	230
4.3	INDIVIDUAL CASEINS .....	232
4.3.1	$\beta$ -casein.....	232
4.3.1.1	Background.....	232
4.3.1.2	Methods .....	233
4.3.1.3	Results and Discussion.....	234

4.3.1.4	Concluding Remarks .....	239
4.3.2	$\kappa$ -casein.....	240
4.3.2.1	Background.....	240
4.3.2.2	Methods .....	243
4.3.2.3	Results and Discussion .....	244
4.3.2.4	Concluding Remarks .....	248
4.4	$\beta$ -LACTOGLOBULIN.....	250
4.4.1	Background.....	250
4.4.2	Materials .....	252
4.4.3	Methods .....	252
4.4.3.1	Capillary Viscometry .....	252
4.4.3.2	Sedimentation Velocity in the Analytical Ultracentrifuge at High Temperature .....	252
4.4.3.3	SEC-MALLS .....	253
4.4.4	Results and Discussion.....	253
4.4.4.1	Capillary Viscometry .....	253
4.4.4.2	Sedimentation Velocity in the Analytical Ultracentrifuge at High Temperature .....	255
4.4.4.3	SEC-MALLS .....	256
4.4.5	Concluding Remarks .....	258
4.5	REFERENCES .....	259
<b>5</b>	<b>CHAPTER 5 – MIXED CASEIN MICELLE – POLYSACCHARIDE SYSTEMS.....</b>	<b>269</b>
5.1	MALVERN MASTERSIZER™ ANALYSIS OF MIXED SYSTEMS ...	269
5.1.1	Experimental considerations of particle size analysis.....	269
5.2	ANALYSIS OF MIXED CASEIN MICELLE – POLYSACCHARIDE SYSTEMS .....	270
5.2.1	Preliminary results of particle size analysis of mixed casein micelle – polysaccharide systems.....	271
5.2.2	Analysis of mixed casein micelle – $\kappa$ -carrageenan systems.....	272
5.2.2.1	Particle size analysis.....	272
5.2.2.2	Sedimentation velocity in the analytical ultracentrifuge.....	273

5.3	EVIDENCE FOR CASEIN MICELLE – $\kappa$ -CARRAGEENAN INTERACTIONS.....	276
5.4	REFERENCES .....	280
<b>6</b>	<b>CHAPTER 6 – GENERAL DISCUSSION .....</b>	<b>282</b>
6.1	REVIEW OF RESULTS IN CHAPTER 3 – DETAILED CHARACTERISATION OF POLYSACCHARIDE SUBSTRATES.....	282
6.1.1	Effect of DE on hydrodynamic properties of citrus pectin.....	283
6.1.2	Effect of elevated temperature on citrus pectin .....	283
6.1.2.1	LM pectin.....	284
6.1.2.2	HM pectin .....	284
6.1.3	Effect of chemical substitution on citrus pectin.....	285
6.1.4	Carrageenans.....	286
6.1.4.1	$\kappa$ -carrageenan.....	286
6.1.4.2	$\iota$ -carrageenan.....	286
6.1.5	Galactomannans .....	287
6.1.6	Bacterial polysaccharides .....	287
6.1.7	Effect of chemical substitution on xylans .....	288
6.2	REVIEW OF RESULTS IN CHAPTER 4 – DETAILED CHARACTERISATION OF MILK PROTEIN SUBSTRATES .....	289
6.2.1	Casein micelles .....	289
6.2.2	Sodium Caseinate.....	290
6.2.3	Individual caseins.....	291
6.2.3.1	$\beta$ -casein.....	291
6.2.3.2	$\kappa$ -casein.....	292
6.2.4	$\beta$ -lactoglobulin.....	292
6.3	REVIEW OF RESULTS IN CHAPTER 5 – MIXED CASEIN MICELLE – POLYSACCHARIDE SYSTEMS.....	293
6.4	CONCLUDING REMARKS AND SUGGESTIONS FOR FUTURE WORK.....	294
6.5	REFERENCES .....	296
<b>A.</b>	<b>APPENDIX A – TYPES OF AVERAGE MOLECULAR WEIGHTS.....</b>	<b>303</b>
<b>B.</b>	<b>APPENDIX B – PUBLICATIONS .....</b>	<b>305</b>

B1	UV TAGGING LEAVES THE STRUCTURAL INTEGRITY OF AN ARABINO-(4-O-METHYLGLUCURONO) XYLAN POLYSACCHARIDE UNAFFECTED.....	305
B2	ELEVATED-TEMPERATURE ANALYTICAL ULTRACENTRIFUGATION ON A LOW-METHOXY POLYURONIDE.....	306
B3	THE EFFECT OF DEGREE OF ESTERIFICATION ON THE HYDRODYNAMIC PROPERTIES OF CITRUS PECTIN.....	307
B4	HYDRODYNAMIC CHARACTERISATION OF THE EXOPOLYSACCHARIDE FROM THE HALOPHILIC CYANOBACTERIA <i>APHANOTHECE HALOPHTYICA</i> GR02: A COMPARISON WITH XANTHAN.....	308
B5	FURTHER OBSERVATIONS ON THE SIZE, SHAPE AND HYDRATION OF CASEIN MICELLES FROM NOVEL ANALYTICAL ULTRACENTRIFUGATION AND CAPILLARY VISCOMETRY APPROACHES.....	309
B6	A HYDRODYNAMIC STUDY ON THE DEPOLYMERISATION OF A HIGH METHOXY PECTIN AT ELEVATED TEMPERATURES .....	310
B7	MODIFICATION OF PECTIN WITH UV-ABSORBING SUBSTITUENTS AND ITS EFFECT ON THE STRUCTURAL AND HYDRODYNAMIC PROPERTIES OF THE WATER-SOLUBLE DERIVATIVES .....	311

## LIST OF FIGURES

- Figure 1-1** Tolstoguzov diagram representing the possible consequences on mixing two soluble biopolymers in an aqueous environment. Adapted from Tolstoguzov, 1990, 1991 and Harding, 1997..... 2
- Figure 1-2** Schematic representation of segregative phase separation (adapted from Picullel *et. al.*, 1995 see also Picullel and Lindman, 1992; Bergfeldt *et. al.*, 1996 and Syrbe *et. al.*, 1998). Where  $S_1$  is the solvent and  $P_2$  and  $P_3$  are polymers. ... 4
- Figure 1-3** Schematic representation of associative phase separation (adapted from Picullel *et. al.*, 1995 see also Picullel and Lindman, 1992; Bergfeldt *et. al.*, 1996 and Syrbe *et. al.*, 1998)..... 5
- Figure 1-4** Schematic representation of bridging flocculation (adapted from Furusawa *et. al.*, 1999) ..... 8
- Figure 1-5** Schematic representation of steric stabilisation (adapted from Furusawa *et. al.*, 1999). ..... 9
- Figure 1-6** Schematic representation of a polymer depletion layer (adapted from Williams and Smith, 1995). .....10
- Figure 1-7** Schematic representation of the exclusion of polymer molecules from between particles at close separations leading to depletion flocculation (adapted from Williams and Smith, 1995).....10
- Figure 2-1** Double - sector centrepiece. The sample is placed in one sector, and a reference solvent in dialysis equilibrium with the sample is placed in the reference sector. The reference sector is usually filled slightly more than the sample sector, so that the reference meniscus does not obscure the sample profile (adapted from Ralston, 1993).....26
- Figure 2-2** Comparison of the optical records for a sedimenting boundary obtained from the (a) Schlieren, (b) interference, (c) photographic absorbance (Turbidity), and (d) photoelectric absorbance optical systems (adapted from Schachman, 1959, Ralston, 1993).....27
- Figure 2-3** The forces acting on a solute particle in a gravitational field (adapted from van Holde, 1985). A sector shaped cell is in a rotor spinning about the axis, A at an angular velocity,  $\omega$ . The cell is sector shaped because sedimentation proceeds

along radial lines; and any other shape would lead to concentration accumulation near the edges and accompanying convection. ....28

**Figure 2-4** A moving sedimenting boundary for the chemically modified xylan CB-GX at concentration 0.40 mg/ml, speed 50,000 rpm, temperature 20°C: scanning at 30 minute intervals. The sedimentation coefficient can be measured by following the mid-point (or, more precisely the “second moment”) of the boundary. The boundary broadens with time due to diffusion. [Note – modern software measures sedimentation coefficient by following the change in time of the whole concentration profile, and not just the boundary mid-point]. ....31

**Figure 2-5** A schematic representation of the scanning absorption optical system. The diffraction grating allows the choice of monochromatic light in the region of 200-800nm (from Ralston, 1993). ....32

**Figure 2-6** A schematic representation of the interference optical system for the Beckman Optima XLI (adapted from Beckman, 1996). ....33

**Figure 2-7** A plot of  $\ln \frac{r_b(t)}{r_b(t_0)}$  vs.  $\omega^2 t$  for the high methoxy pectin HR 7021 at 50°C using the Schlieren optical system on a Beckman Model E analytical ultracentrifuge. ....35

**Figure 2-8** The concentration dependency of sedimentation, for casein micelles at 20°C, data from Beckman Optima XLI using the interference optical system. ....36

**Figure 2-9** MHKS sedimentation plot for sodium caseinate at different concentrations. ....39

**Figure 2-10** Schematic representation of sedimentation equilibrium. At equilibrium, the resulting concentration distribution is exponential with the square of the radial position (adapted from Ralston, 1993). ....40

**Figure 2-11**  $\ln(c)$  vs.  $\xi$  (or  $r^2$ ) showing deviations from ideality (adapted from McRorie & Voelker, 1993). ....45

**Figure 2-12** Concentration dependency of apparent molecular weight for the halophilic cyanobacterium *Aphanothece Halophytica GR02*. ....46

**Figure 2-13** A schematic representation of the shearing of a liquid between 2 parallel plates. The arrows represent fluid velocities at different values of  $y$  (adapted from van Holde, 1985). ....47

<b>Figure 2-14</b>	Schematic representation of an Ostwald viscometer (adapted from van Holde, 1985).....	50
<b>Figure 2-15</b>	The Huggins (black squares), Kraemer (red circles) and Solomon-Ciuta (blue triangles) plots for the low methoxy pectin HL 7192.....	54
<b>Figure 2-16</b>	The pseudo Mark-Houwink (MHKS) plot for the high-methoxy pectin HR 7021 at different temperatures. [Note – this is a pseudo MHKS plot in the sense that it does convey results for a fractionated system]. .....	55
<b>Figure 2-17</b>	A schematic representation of a cone and plate viscometer (adapted from van Holde, 1985 see also Jumel, 1994).....	56
<b>Figure 2-18</b>	Representation of (a) macromolecules in dilute solution (e.g. $c < c^*$ ); (b) onset of overlapping coils ( $c = c^*$ ) and (c) polymer network ( $c > c^*$ ) (adapted from Morris <i>et. al.</i> , 1981 see also Jumel, 1994). .....	58
<b>Figure 2-19</b>	Construction of a Zimm plot - Abscissa $\sin^2(\theta/2) + kc$ and ordinate $Kc/R_\theta$ adapted from Harding <i>et. al.</i> , 1991. Molecular weight, radius of gyration and virial coefficients can then be calculated from Equation 2-59. ....	63
<b>Figure 2-20</b>	Schematic representation of the SEC-MALLS system (adapted from Jumel, 1994).....	66
<b>Figure 2-21</b>	Examples of elution traces from SEC-MALLS, (a) from the concentration ( $dn/dc$ ) detector, (b) light scattering detector (adapted from Jumel, 1994).....	67
<b>Figure 2-22</b>	The Haug triangle (adapted from Tombs and Harding, 1998).....	78
<b>Figure 2-23</b>	The persistence and contour lengths for a linear macromolecule in the limits of $L_c \rightarrow \infty$ . Where $L_p$ corresponds to the average projection (onto a line of the initial direction projected from one end of the macromolecule) that $L_c$ would have in the hypothetical limit that $L_c \rightarrow \infty$ . Adapted from Harding, 1997.....	79
<b>Figure 3-1</b>	The Fischer projection for the D-hexoses with the chiral carbons labelled in red they are from left to right D-Allose, D-Altrose, D-Glucose, D-Mannose, D-Gulose, D-Idose, D-Galactose and D-Talose (adapted from Lehninger <i>et. al.</i> , 1990).....	90
<b>Figure 3-2</b>	Formation of the two cyclic forms of D-glucopyranose (adapted from Lehninger <i>et. al.</i> , 1990).....	91
<b>Figure 3-3</b>	The chemical structure of sucrose - $\alpha$ -D-glucopyranosyl (1 $\rightarrow$ 2) $\beta$ -D-fructofuranoside (adapted from Lehninger <i>et. al.</i> , 1990).....	92

<b>Figure 3-4</b> Chemical structures for lactose and trehalose - $\beta$ -D-galactopyranosyl (1 $\rightarrow$ 4) $\beta$ -D-glucopyranorose and $\alpha$ -D-glucopyranosyl (1 $\rightarrow$ 1) $\alpha$ -D-glucopyranorose respectively (from Lehninger <i>et. al.</i> , 1990).....	92
<b>Figure 3-5</b> Idealised structure of pectic acid <i>i.e.</i> pectin of DE 0% (adapted from Glicksman, 1969). .....	94
<b>Figure 3-6</b> Dependence of density increment $\Delta\rho = \rho - \rho_0$ (where $\rho$ and $\rho_0$ are the densities of the pectin solution and the buffer respectively in g/ml) for a high methoxy pectin in pH 6.8, I=0.1M phosphate/ chloride buffer.....	98
<b>Figure 3-7</b> Intrinsic viscosity vs. DE for Pectin 7000 Series in pH 6.8, I=0.1M phosphate/ chloride buffer. Where the DEs are 77.8, 65.0, 53.9, 37.8 and 27.9% for pectins 7000, 7001, 7002, 7003 and 7004 respectively. ....	99
<b>Figure 3-8</b> $g(s^*)$ profiles for pectin samples in pH 6.8, I=0.1M phosphate/ chloride buffer. Where the DEs are 77.8, 65.0, 53.9, 37.8 and 27.9% for pectins 7000, 7001, 7002, 7003 and 7004 respectively. ....	100
<b>Figure 3-9</b> Sedimentation coefficient vs. concentration for Pectin 7000 series in pH 6.8, I=0.1M phosphate/ chloride buffer. <b>a</b> – Pectin 7000, <b>b</b> – Pectin 7001, <b>c</b> – Pectin 7002, <b>d</b> – Pectin 7003, <b>e</b> – Pectin 7004.....	101
<b>Figure 3-10</b> Sedimentation coefficient vs. DE for Pectin 7000 series in pH 6.8, I=0.1M phosphate/ chloride buffer. Where the DEs are 77.8, 65.0, 53.9, 37.8 and 27.9% for pectins 7000, 7001, 7002, 7003 and 7004 respectively. ....	102
<b>Figure 3-11</b> Apparent weight average molecular weight vs. concentration in pH 6.8, I=0.1M phosphate/ chloride buffer. <b>a</b> – Pectin 7000, <b>b</b> – Pectin 7001, <b>c</b> – Pectin 7002, <b>d</b> – Pectin 7003, <b>e</b> – Pectin 7004 .....	104
<b>Figure 3-12</b> Molecular weight vs. DE for Pectin 7000 Series, from two independent techniques: sedimentation equilibrium and SEC-MALLS in pH 6.8, I=0.1M phosphate/ chloride buffer. Where the DEs are 77.8, 65.0, 53.9, 37.8 and 27.9% for pectins 7000, 7001, 7002, 7003 and 7004 respectively. ....	105
<b>Figure 3-13</b> Wales-van Holde and frictional ratios vs. DE for the Pectin 7000 Series in pH 6.8, I=0.1M phosphate/ chloride buffer. Where the DEs are 77.8, 65.0, 53.9, 37.8 and 27.9% for pectins 7000, 7001, 7002, 7003 and 7004 respectively. ....	107
<b>Figure 3-14</b> Schlieren peak for LM Pectin HL7192 in pH 6.8, I=0.1M phosphate/ chloride buffer, Temperature = 60°C; Concentration 2.3mg/ml; Rotor Speed	

52640rpm; $t = 3240\text{sec}$ , $s_{\text{obs}} = 4.22\text{S}$ and $s_{20,w} = 1.92\text{S}$ . Direction of sedimentation is from left to right. ....	112
<b>Figure 3-15</b> The effect of increased temperature on $s_{\text{obs}}$ and $s_{20,w}$ for LM Pectin HL7192 in pH 6.8, $I=0.1\text{M}$ phosphate/ chloride buffer. ....	113
<b>Figure 3-16</b> The effect of increased temperature on the reduced viscosity for LM Pectin HL7192 in pH 6.8, $I=0.1\text{M}$ phosphate/ chloride buffer. ....	114
<b>Figure 3-17</b> The effect of increased temperature on the weight average molecular weight for LM Pectin HL7192 in pH 6.8, $I=0.1\text{M}$ phosphate/ chloride buffer. ....	115
<b>Figure 3-18</b> Effect of increased temperature on the intrinsic viscosity, $[\eta]$ for a high-methoxy pectin in standard phosphate chloride buffer (pH = 6.8, $I=0.1\text{M}$ ). ....	118
<b>Figure 3-19</b> Schlieren peak for a high methoxy pectin in standard phosphate chloride buffer (pH = 6.8, $I=0.1\text{M}$ ), direction of sedimentation left to right. ....	119
<b>Figure 3-20</b> Effect of increased temperature on sedimentation coefficient, $s_{20,w}^0$ for a high-methoxy pectin in standard phosphate chloride buffer (pH = 6.8, $I=0.1\text{M}$ ). ....	120
<b>Figure 3-21</b> Effect of increased temperature on the weight average molecular weight, $M_w$ for a high-methoxy pectin in standard phosphate chloride buffer (pH = 6.8, $I=0.1\text{M}$ ). ....	122
<b>Figure 3-22</b> Effect of increased temperature on the translation frictional ratio, $f/f_0$ for a high-methoxy pectin in standard phosphate chloride buffer (pH = 6.8, $I=0.1\text{M}$ ). ....	122
<b>Figure 3-23</b> Mark-Houwink (MHKS) plot for a high-methoxy pectin at different temperatures in standard phosphate chloride buffer (pH = 6.8, $I=0.1\text{M}$ ). ....	123
<b>Figure 3-24</b> “Blob” model plot of $\frac{[\eta]}{M^{0.5}}$ vs. $M^{3\nu-1.5}$ for a high methoxy pectin sample at elevated temperatures in standard phosphate chloride buffer (pH = 6.8, $I=0.1\text{M}$ ) (as explained in section 2.7 and Dondos, 2001). ....	124
<b>Figure 3-25</b> Stockmayer-Fixman-Burchard plot of $\frac{[\eta]}{M^{0.5}}$ vs. $M^{0.5}$ for a high methoxy pectin sample at elevated temperatures in standard phosphate chloride buffer (pH = 6.8, $I=0.1\text{M}$ ). ....	125
<b>Figure 3-26</b> FT-IR spectra for parent and derivatised pectin samples 1)LMP, 2)LMPG3, 3)LMPG2, 4)KP and 5)CB-KP. ....	131

<b>Figure 3-27</b> $g^*(s^*)$ profiles for parent and substituted pectins. Legend – KP – navy squares, CB-KP – green circles, LMP – orange up-triangle, LMPG2 – pink down-triangle and LMPG3 – cyan diamond.....	133
<b>Figure 3-28</b> Elution profiles for parent and substituted pectins. Legend – KP – navy squares, CB-KP – green circles, LMP – orange up-triangle, LMPG2 – pink down-triangle and LMPG3 – cyan diamond.....	134
<b>Figure 3-29</b> Idealised structure for the commercial carrageenans (adapted from Tombs and Harding, 1998). .....	137
<b>Figure 3-30</b> The sedimentation distributions for $\kappa$ -carrageenan at different concentrations. Legend – 3.0mg/ml (black squares); 2.5mg/ml (red circles); 2.0mg/ml (green up-triangle); 1.5mg/ml (blue down-triangle); 1.0mg/ml (cyan diamonds) and 0.5mg/ml (magenta crosses).....	144
<b>Figure 3-31</b> The concentration dependency of sedimentation for $\kappa$ -carrageenan in standard phosphate buffer at 20°C. ....	145
<b>Figure 3-32</b> The concentration dependency of sedimentation for $\iota$ -carrageenan in standard phosphate buffer at 20°C. ....	146
<b>Figure 3-33</b> Idealised structures for locust bean and guar gums (adapted from Glicksman, 1969). .....	151
<b>Figure 3-34</b> The sedimenting boundaries for from top to bottom guar M150, M90 and M30, recorded using the XLI interference optical system on the XLI. Speed = 50,000rpm; temperature = 20°C; solvent = water and concentration 1.5mg/ml. ....	154
<b>Figure 3-35</b> $g^*(s^*)$ peaks for guar samples. Legend guar M150 – blue squares, M90 – red open circles and M30 – green open triangles under same conditions described in <b>Figure 3-34</b> . [Note – due to concentration dependency the apparent sedimentation coefficient of M90 is greater than that of M150, however the sedimentation coefficient for M150 is greater when extrapolated to infinite dilution ( <b>Figure 3-36</b> )]. .....	154
<b>Figure 3-36</b> Concentration dependency of sedimentation for guar samples. Legend guar M150 – blue squares, M90 – red open circles and M30 – green open triangles.....	155

<b>Figure 3-37</b>	Elution profiles for guar samples in standard “Paley” buffer. Legend guar M150 – blue squares, M90 – red open circles and M30 – green open triangles.....	157
<b>Figure 3-38</b>	Plots of log RMS radius vs. log $M_w$ for guar samples. The average slope is $0.51\pm 0.04$ . Legend guar M150 – blue squares, M90 – red open circles and M30 – green open triangles.....	158
<b>Figure 3-39</b>	The MHKS viscosity plot for guar samples. Slope is $0.69\pm 0.01$ . ....	158
<b>Figure 3-40</b>	The MHKS sedimentation plot for guar samples. Slope is $0.40\pm 0.01$ . .....	161
<b>Figure 3-41</b>	“Blob” model plot of $\frac{[\eta]}{M^{0.5}}$ vs. $M^{3\nu-1.5}$ for guar samples.....	162
<b>Figure 3-42</b>	Stockmayer-Fixman-Burchard plot $\frac{[\eta]}{M^{0.5}}$ vs. $M^{0.5}$ for guar samples.	163
<b>Figure 3-43</b>	Huggins (red) and Kraemer (black) plots for AH-EPS from capillary viscometry.....	170
<b>Figure 3-44</b>	Viscosity and fitting of AH-EPS at 0.6g/l measured at 25°C. Circles: points not used for fitting. Square: points used for fitting. Line: fitted curve. ..	171
<b>Figure 3-45</b>	Huggins (square) and Kraemer (circle) plots for AH-EPS. Extrapolation towards zero concentration was performed on the points with a large marker..	172
<b>Figure 3-46</b>	Coil overlap plot obtained with an intrinsic viscosity value of 8000 ml/g (see text for explanation). ....	172
<b>Figure 3-47</b>	$g(s^*)$ profile for AH-EPS at 40,000 rpm at 25°C in 1M guanidine hydrochloride and concentration 1.0mg/ml. ....	174
<b>Figure 3-48</b>	Concentration dependency of sedimentation of AH-EPS – conventional plot at 25°C in 1M guanidine hydrochloride. ....	174
<b>Figure 3-49</b>	Concentration dependency of sedimentation of AH-EPS – reciprocal plot at 25°C in 1M guanidine hydrochloride. ....	175
<b>Figure 3-50</b>	Concentration dependency of apparent molecular weight of AH-EPS – conventional plot at 25°C in 1M guanidine hydrochloride.....	176
<b>Figure 3-51</b>	Concentration dependency of apparent molecular weight of AH-EPS – reciprocal plot at 25°C in 1M guanidine hydrochloride. ....	177
<b>Figure 3-52</b>	Partial chemical structure of arabino-4-O-methylglucuronoxylan from softwood (adapted from de Gruyter, 1984). ....	182

<b>Figure 3-53</b> UV absorption data for modified and native arabinoxylans. ....	183
<b>Figure 3-54</b> Reduced viscosity vs. concentration for AGX and CB-AGX in I= 0.1, pH 7.5 phosphate chloride buffer. ....	187
<b>Figure 3-55</b> Apparent sedimentation coefficient vs. sedimenting concentration for AGX and CB-AGX in I= 0.1, pH 7.5 phosphate chloride buffer. ....	188
<b>Figure 3-56</b> Apparent molecular weight (from low speed sedimentation equilibrium) vs. cell loading concentration for AGX and CB-AGX in I= 0.1, pH 7.5 phosphate chloride buffer. ....	189
<b>Figure 4-1</b> Sub-unit model for the casein micelle. From Dickinson and Stainsby (1982). ....	211
<b>Figure 4-2</b> $g(s^*)$ profiles for casein micelles at differing concentrations in skim milk at 12600rpm. ....	214
<b>Figure 4-3</b> Concentration dependence of sedimentation for casein micelles in skim milk. From the plot above $s_{T,b}^0 = (845 \pm 2)S$ and $k_s = (16.9 \pm 0.1)ml/g$ . ....	215
<b>Figure 4-4</b> Concentration dependence of reduced viscosity (Huggins plot) of casein micelles in skim milk. From the plot above $[\eta] = (10.4 \pm 0.4)ml/g$ and $k_\eta = (61 \pm 4)ml/g$ and $K_H = 5.9 \pm 0.5$ . ....	216
<b>Figure 4-5</b> Concentration dependence of diffusion of casein micelles in skim milk. From the graph above $D_{T,b}^0 = (2.8 \pm 0.2) \times 10^{-8} cm^2 sec^{-1}$ and $k_D = (105 \pm 13)ml/g$ . ....	218
<b>Figure 4-6</b> The proposed structure of the casein “sub-micelle”. (A is the hydrophobic core and B is the $\kappa$ -casein rich exterior). From Dickinson and Stainsby (1982). ....	222
<b>Figure 4-7</b> The Huggins (squares) and Kraemer (circles) plots for sodium caseinate in standard pH 6.8, I=0.1M “Paley” buffer. ....	225
<b>Figure 4-8</b> Sedimentation velocity diagram for sodium caseinate at 40,000rpm, 20.0°C at 280nm, boundary concentration, initial $c = 3.5mg/ml$ , scanned every 5 minutes in standard pH 6.8, I=0.1M “Paley” buffer. ....	226
<b>Figure 4-9</b> $s_{20,w}$ vs. concentration for sodium caseinate in standard pH 6.8, I=0.1M “Paley” buffer. ....	227
<b>Figure 4-10</b> $M_{w,app}$ vs. concentration for sodium caseinate. Where “X” marks the “monomer” molecular weight in standard pH 6.8, I=0.1M “Paley” buffer. Line fitted manually. ....	228

<b>Figure 4-11</b> MHKS sedimentation plot for sodium caseinate in standard pH 6.8, I=0.1M “Paley” buffer. The line fitted corresponds to $s=0.0035M^{0.63}$ .....	229
<b>Figure 4-12</b> Typical sedimenting boundary for $\beta$ -casein at 8.5°C in barbiturate buffer pH 7.5, I = 0.2M (adapted from Payens and van Markwijk, 1963).....	233
<b>Figure 4-13</b> Sedimentation coefficient distribution for $\beta$ -casein at concentration 2mg/ml in standard “Paley” buffer at 20°C. ....	235
<b>Figure 4-14</b> Change in sedimentation coefficient with concentration for $\beta$ -casein in standard “Paley” buffer at 20°C. Legend – black squares (slow peak); red circles (fast peak) and green triangles (weight average).....	236
<b>Figure 4-15</b> Change in molecular weight with concentration for $\beta$ -casein in standard “Paley” buffer at 20°C. Legend – black squares (monomer), red circles (polymer) and green triangles (weight average). ....	237
<b>Figure 4-16</b> A space filling model of $\kappa$ -casein. The peptide backbone is coloured cyan, hydrophobic side chains green, acidic side chains red, basic side chains purple and the Phe-Met (105-106) bond in orange (adapted from Kumosinski <i>et al.</i> , 1991a). ....	240
<b>Figure 4-17</b> Sedimentation coefficient distribution for $\kappa$ -casein at 2mg/ml – a typical sedimenting boundary inset in standard “Paley” buffer at 20°C. Sedimenting boundary recorded every 2 minutes at 50,000 rpm. ....	245
<b>Figure 4-18</b> Concentration dependence of sedimentation of $\kappa$ -casein in standard “Paley” buffer at 20°C. ....	246
<b>Figure 4-19</b> Concentration dependence of molecular weight of $\kappa$ -casein in standard “Paley” buffer at 20°C. ....	247
<b>Figure 4-20</b> A space filling model of a $\beta$ -lactoglobulin dimer. Where carbon is grey, hydrogen – white, oxygen – red, nitrogen – blue and sulphur – yellow.....	251
<b>Figure 4-21</b> Effect of temperature on reduced viscosity of $\beta$ -lactoglobulin in pH 6.8, I = 0.1M phosphate/ chloride buffer. ....	254
<b>Figure 4-22</b> Effect of increased temperature on corrected sedimentation coefficient of $\beta$ -lactoglobulin in pH 6.8, I = 0.1M phosphate/ chloride buffer.....	255
<b>Figure 4-23</b> Effect of increased temperature on the weight average molecular weight of $\beta$ -lactoglobulin in pH 6.8, I = 0.1M phosphate/ chloride buffer.....	256

<b>Figure 4-24</b> Effect of increased temperature on the translational frictional ratio of $\beta$ -lactoglobulin in pH 6.8, I = 0.1M phosphate/ chloride buffer. ....	257
<b>Figure 5-1</b> Particle size distribution for skim milk – polysaccharide mixtures. Legend – black – skim milk; red – skim milk + low methoxy pectin; green – skim milk + high methoxy pectin; navy – skim milk + $\kappa$ -carrageenan; cyan – skim milk + $\iota$ -carrageenan; magenta – skim milk + guar gum and yellow – skim milk + locust bean gum.....	271
<b>Figure 5-2</b> Particle size distribution for skim milk – $\kappa$ -carrageenan mixtures. Legend – black – skim milk; red – skim milk + 0.2mg/ml $\kappa$ -carrageenan; green – skim milk + 0.4mg/ml $\kappa$ -carrageenan; navy – skim milk + 0.6mg/ml $\kappa$ -carrageenan and cyan – skim milk + 0.8mg/ml $\kappa$ -carrageenan. ....	273
<b>Figure 5-3</b> Schematic representation of bridging flocculation in casein micelle - $\kappa$ -carrageenan systems (adapted from Furusawa <i>et. al.</i> , 1999).....	277
<b>Figure 5-4</b> Schematic representation of steric stabilisation in casein micelle - $\kappa$ -carrageenan systems (adapted from Furusawa <i>et. al.</i> , 1999).....	277
<b>Figure 5-5</b> Schematic representation of a $\kappa$ -carrageenan depletion layer (adapted from Williams and Smith, 1995).....	278
<b>Figure 5-6</b> Schematic representation of the exclusion of $\kappa$ -carrageenan molecules from between casein micelles at close separations leading to depletion flocculation (adapted from Williams and Smith, 1995). ....	279
<b>Figure A-1</b> A graph showing the distribution of molecular weight “averages” in a polydisperse system (adapted from McRorie DK and Voelker PJ (1993) <i>Self-Associating Systems in the Analytical Ultracentrifuge</i> . Beckman Instruments Inc., California). ....	304

## LIST OF TABLES

<b>Table 2-1</b>	Molecular weight averages from different techniques (adapted from Harding <i>et. al.</i> , 1991).....	24
<b>Table 2-2</b>	Mark – Houwink (MHKS) conformational parameters from Equations 2-42, 2-15 and 2-66 – see <i>e.g.</i> Tombs and Harding (1998). .....	76
<b>Table 3-1</b>	Hydrodynamic data for pectin 7000 series in pH 6.8, I=0.1M phosphate/chloride buffer.....	103
<b>Table 3-2</b>	Calculated parameters for pectin 7000 series in pH 6.8, I=0.1M phosphate/chloride buffer.....	108
<b>Table 3-3</b>	The effect of temperature on the sedimentation coefficient, reduced viscosity and weight average molecular weight for LM pectin HL7192 in pH 6.8, I=0.1M phosphate/ chloride buffer.....	111
<b>Table 3-4</b>	Effect of temperature on a high methoxy pectin .....	118
<b>Table 3-5</b>	Results of the “blob” model approach for calculating the number of Kuhn statistical segments per chain for a high methyl pectin sample at elevated temperature, from the equations 2-84 - 2-91and the plots above.....	126
<b>Table 3-6</b>	Analytical data for parent and derivatised pectins.....	130
<b>Table 3-7</b>	Hydrodynamic data for parent and derivatised pectins.....	132
<b>Table 3-8</b>	Major uses of carrageenans in the food industry (adapted from Tombs and Harding, 1998) .....	138
<b>Table 3-9</b>	Hydrodynamic data for $\kappa$ - and $\iota$ -carrageenan in dilute solution .....	148
<b>Table 3-10</b>	The hydrodynamic data for guar M150, M90, M30 and LBG M175 ..	159
<b>Table 3-11</b>	Results of the “blob” model approach for calculating the number of Kuhn statistical segments per chain for the three guar samples, from the equations 2-84 - 2-91and the graphs above. ....	163
<b>Table 3-12</b>	Experimental and calculated parameters for AH-EPS and xanthan in 1M guanidine hydrochloride .....	178
<b>Table 3-13</b>	Typical composition and physical properties for arabinoxylan AGX ...	184
<b>Table 4-1</b>	Some properties of the major components of Bovine milk. Adapted from Jennes, 1970. Assumes total protein = 36g/l and ~78% casein. ....	208

<b>Table 4-2</b> Major components of bovine milk. Adapted from Dickinson and Stainsby (1982).....	210
<b>Table 4-3</b> Experimental hydrodynamic parameters for casein micelles in skim milk .....	219
<b>Table 4-4</b> Calculated hydrodynamic parameters for casein micelles in skim milk...	220
<b>Table 4-5</b> Hydrodynamic parameters for sodium caseinate in standard pH 6.8, I=0.1M “Paley” buffer .....	231
<b>Table 4-6</b> Hydrodynamic properties for $\beta$ -casein in pH 6.8, I=0.1M phosphate buffer at 20°C .....	238
<b>Table 4-7</b> Hydrodynamic properties of $\kappa$ -casein in pH 6.8, I = 0.1M phosphate buffer at 20°C .....	248
<b>Table 4-8</b> Effect of elevated temperature on hydrodynamic properties of $\beta$ -lactoglobulin in pH 6.8, I = 0.1M phosphate/ chloride buffer .....	257
<b>Table 5-1</b> Sedimentation coefficient and area of the first peak for skim milk – $\kappa$ -carrageenan mixtures .....	274
<b>Table 5-2</b> Normalised peak areas from particle size and sedimentation time derivative analysis .....	275

## ABSTRACT

Polysaccharide systems (pectin, carrageenan, guar, locust bean gum, xanthan and xylan) have been characterised using a variety of hydrodynamic techniques including sedimentation velocity, sedimentation equilibrium, size exclusion chromatography – multi-angle laser light scattering (SEC-MALLS), and viscometry. Results suggest that the polysaccharides selected are, in general, rigid or semi-rigid molecules with a large hydrated volume, this is important in relation to polysaccharide structure - function relationships. In addition the effect of incorporating a UV absorbing substituent group was also investigated for two pectin samples and an arabinoxylan polysaccharide, the reaction conditions result in  $\beta$ -elimination of the pectin chain in one case, but there was no significant effect on the other pectin or arabinoxylan. The effect of increased temperature was also investigated with respect to high and low methoxy pectins, this resulted in  $\beta$ -elimination of high methoxy pectin and a mild conformational change in low methoxy pectin.

Milk protein systems have also been studied using the above techniques, and it was proven that casein micelles are large, spherical hydrated molecules and sodium caseinate undergoes complex concentration dependant self-association under the conditions studied, which is significant even at low concentrations.  $\beta$ - and  $\kappa$ -casein also undergo self-association reactions, the former of which was concentration dependent. An investigation into the effect of high temperature on  $\beta$ -lactoglobulin suggested that temperature induced aggregation is a two-step process (denaturation and aggregation), the first of which is thermo-reversible denaturation as indicated by capillary viscometry.

The characterisation of the polysaccharide and milk protein substrates then allowed an investigation into the interactions of casein micelles with polysaccharide molecules. It was estimated that only  $\kappa$ - and  $\iota$ -carrageenan interacted significantly with casein micelles in the reaction conditions studied (pH  $\sim$  6.8, I  $\sim$  0.1M). A more detailed investigation into the  $\kappa$ -carrageenan interaction suggests that at low concentration a sterically stabilised complex is formed, which undergoes depletion flocculation upon increasing  $\kappa$ -carrageenan concentration.

## ACKNOWLEDGEMENTS

To my supervisors, Prof. Stephen E. Harding and Dr. Tim J. Foster, for their advice, support and encouragement over the last 3 years.

I would also like to thank -

Dr. Anna Ebringerova, Dr. Zdenka Hromadkova, Dr. Eva Machova and Dr. Jan Hirsch of the Slovak Academy of Sciences in Bratislava for their help and advice in our collaboration and their enthusiastic welcome on my two visits to Slovakia.

Dr. Pengfu Li, Dr. Max Puaud and Prof. John Mitchell for their help on the work on bacterial exopolysaccharides.

Dr. David Picout and Prof. Simon Ross-Murphy for their participation in the guar and locust bean gum study.

Nick Butler and Putri Saril, my project students for their help on the high temperature work and Dr. Pierre Aymard for his discussions with regard to  $\beta$ -lactoglobulin.

My friends and colleagues (past and present) at the NCMH and the Division of Food Sciences - Chris Walters, Taewee Tongdang (Krim), Jana Kogulanathan, Dr. Matthew Deacon, Dr. George Pavlov, Dr. Natalia Chebotnereva, Mr. Phil Grover, Mr. Pete Husbands, Mr. Les Sarcoe, Dr. Gaëlle Roudaunt, Prof. Don Winzor and especially Dr. Conny Jumel, Dr. Neil Errington and Prof. Arthur Rowe.

My housemates – Anne, Antje, Baltasar, Gökhan, Julian, Pascal, Rachael and Vanessa.

The BBSRC and Unilever Research for the financial support.

Cécile without whom I would have gone mad.

And, finally to my parents, brother Graham and sister Julie and the rest of my family for their love and support.

## GLOSSARY OF IMPORTANT TERMS

- a** Mark-Houwink-Kuhn-Sakurada exponent for viscosity
- A** absorption
- b** Mark-Houwink-Kuhn-Sakurada exponent for sedimentation
- B** 2<sup>nd</sup> thermodynamic virial coefficient ( $\text{ml.mol.g}^{-2}$ ) (usually expressed as  $A_2$  in light scattering studies)
- $\beta$**  Scheraga-Mandelkern conformational parameter
- c** Mark-Houwink-Kuhn-Sakurada exponent for diffusion
- $c^*$**  critical coil overlap concentration ( $\text{g.ml}^{-1}$ )
- $dc/dt$**  change in concentration with time ( $\text{g.ml}^{-1}.\text{s}^{-1}$ )
- $dc/dr$**  change in concentration with radius ( $\text{g.ml}^{-1}.\text{cm}^{-1}$ )
- $dn/dc$**  refractive index increment ( $\text{ml.g}^{-1}$ )
- $D^0_{20,w}$**  translational diffusion coefficient at infinite dilution and solvent standard conditions viscosity of water at 20°C ( $\text{cm}^2.\text{s}^{-1}$ )
- $\delta$**  hydration (g of solvent/ g of solute)
- $\epsilon$**  Mark-Houwink-Kuhn-Sakurada exponent for root mean square radius

$f$	frictional coefficient ( $\text{g}\cdot\text{s}^{-1}$ )
$f/f_0$	translational frictional ratio
$\phi$	volume fraction
$\phi_{0,\infty}$	Flory-Fox parameter
$g^*(s^*)$	<i>apparent</i> distribution of sedimentation coefficients, <i>i.e.</i> not corrected for diffusion and non-ideality
$[\eta]$	intrinsic viscosity ( $\text{ml}\cdot\text{g}^{-1}$ )
$\eta_{T,b}$	viscosity of solvent at experimental temperature (Poise = $\text{cm}\cdot\text{g}^{-1}\cdot\text{s}^{-1}$ )
$\eta_0$	zero shear viscosity (Poise)
$\eta_{20,w}$	viscosity of water at 20°C (0.01002 Poise)
$\eta_{\text{rel}}$	relative viscosity
$\eta_{\text{sp}}$	specific viscosity
$\eta_{\text{red}}$	reduced viscosity ( $\text{ml}\cdot\text{g}^{-1}$ )
$\eta_{\text{inh}}$	inherent viscosity ( $\text{ml}\cdot\text{g}^{-1}$ )
$j(a)$	meniscus concentration in fringe units
$J$	fringe displacement
$J_0$	total concentration across the whole centrifuge cell in fringe units

$k_B$	Stefan-Boltzmann constant ( $1.381 \times 10^{-16}$ erg.K <sup>-1</sup> .mol <sup>-1</sup> )
$k_D$	concentration dependency of diffusion (ml.g <sup>-1</sup> )
$k_s$	concentration dependency of sedimentation (ml.g <sup>-1</sup> )
$K_H$	Huggins constant
$K_K$	Kraemer constant
$k_\eta$	viscosity “regression” coefficient (ml.g <sup>-1</sup> )
$L_c$	contour length (cm)
$L_p$	persistence length (cm)
$\lambda^{-1}$	Kuhn statistical length (cm)
$M$	molecular weight (molar mass) (g.mol <sup>-1</sup> )
$M^*$	“star average” molecular weight (g.mol <sup>-1</sup> )
$M_L$	mass per unit length (g.mol <sup>-1</sup> .cm <sup>-1</sup> )
$M_n$	“number average” molecular weight (g.mol <sup>-1</sup> )
$M_w$	“weight average” molecular weight (g.mol <sup>-1</sup> )
$M_{w, app}$	<i>apparent</i> “weight average” molecular weight (g.mol <sup>-1</sup> )
$M_z$	“z-average” molecular weight (g.mol <sup>-1</sup> )
$n_0$	refractive index of solvent
$N_A$	Avogadro’s number ( $6.023 \times 10^{23}$ mol <sup>-1</sup> )

$\nu$	Einstein viscosity increment
P	Perrin function
$P(\theta)$	particle scattering function
$P_2, P_3$	polymer fractions
$\Pi$	conformational parameter
$\Pi$	osmotic pressure ( $\text{dyn.cm}^{-2}$ )
$r$	radial position (cm)
$r_H$	hydrodynamic (Stokes) radius (cm)
R	Wales – van Holde ratio
R	universal gas constant ( $8.314 \times 10^7 \text{ erg.K}^{-1}.\text{mol}^{-1}$ )
$R_g$	radius of gyration (cm)
RMS	root mean square radius (cm)
$\rho_{T,b}$	density of solvent at experimental temperature ( $\text{g.ml}^{-1}$ )
$\rho_{20,w}$	density of water at $20^\circ\text{C}$ ( $0.99823 \text{ g.ml}^{-1}$ )
$s_{20,w}$	sedimentation coefficient at standard conditions of water at $20^\circ\text{C}$ (s or S)
$s_{20,w}^0$	sedimentation coefficient at infinite dilution and standard conditions of water at $20^\circ\text{C}$ (s or S)
S	the Svedberg unit $1\text{S} = 10^{-13}$ seconds

$S_1$	solvent
$\bar{v}$	partial specific volume (ml.g <sup>-1</sup> )
$v_s$	swollen volume (ml.g <sup>-1</sup> )
$\omega$	angular velocity (rad.s <sup>-1</sup> )
$\xi$	normalised radial position squared, $\xi = \left( \frac{r^2 - a^2}{b^2 - a^2} \right)$

# 1 CHAPTER 1 - PROTEIN – POLYSACCHARIDE INTERACTIONS

## 1.1 MIXED BIOPOLYMERS

The behaviour of mixed biopolymer systems and whether or not they chemically interact is a very important question in biological science in general and in food sciences in particular. Food products are by their very nature mixed biopolymer systems and it is therefore of great interest to the food industry to understand the structure (or microstructure) of such mixed systems.

The structural properties of such systems can have a significant affect on many physical properties including gelling, foaming, emulsifying, plasticising, aggregation, precipitation and phase separation all of which are important physical properties to food chemists.

## 1.2 TYPES OF PROTEIN – POLYSACCHARIDE INTERACTIONS

When two (or more) biopolymers are mixed together in an aqueous medium one of three things can occur (Syrbe *et. al.*, 1998; Harding, 1995; Harding, 1997; Hoskins *et. al.*, 1998 and Tolstoguzov, 1990, 1991) (Figure 1-1).

- (i) nothing (miscibility)
- (ii) thermodynamic incompatibility *i.e.* phase separation (1.2.1)
- (iii) macromolecular interaction *i.e.* complexation (1.2.2)

The boundaries between these arbitrary divisions are somewhat blurred and the equilibrium is dependent on biopolymer concentration, ionic strength, pH and temperature (Harding, 1997 and Tolstoguzov, 1990, 1991).

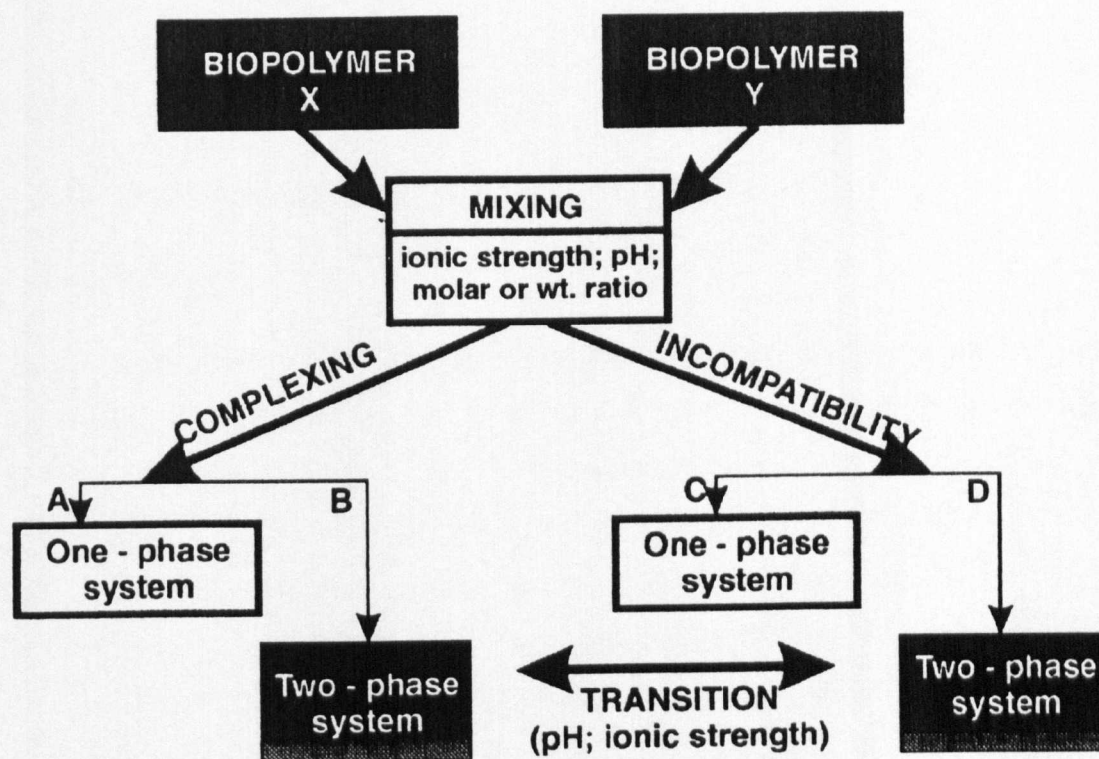


**Figure 1-1** Tolstoguzov diagram representing the possible consequences on mixing two soluble biopolymers in an aqueous environment. Adapted from Tolstoguzov, 1990, 1991 and Harding, 1997.

Any of the above scenarios for the mixed polysaccharide – protein systems can have an effect on functional properties of both the polysaccharide and protein components (Tolstoguzov, 1986).

### 1.2.1 Phase Separation

In most cases, solutions of mixed polymers reach their thermodynamic minimum due to phase separation (Michon *et. al.*, 2000). Phase separation occurs due to the relatively low entropy of mixing of high molecular weight polymers. This is dominated by the fact that the interaction between polymer segments is the critical factor in the free energy of mixing (Tolstoguzov, 1986; Albertsson, 1995; Antonov and Gonçalves, 1999). There are many factors, which can influence phase separation phenomena –

- (i) polymer pair
- (ii) polymer concentration
- (iii) polymer molecular weight
- (iv) polymer charge (which itself depends on pH and ionic strength)
- (v) temperature

It has been reported (Grinberg and Tolstoguzov, 1997) that polysaccharide incompatibility towards proteins decreases in the order carboxyl group containing polysaccharides (*e.g.* pectin) > neutral polysaccharides (*e.g.* guar) > sulphated polysaccharides (*e.g.*  $\kappa$ -carrageenan). Phase separation can occur by one of two distinct mechanisms – two-phase (segregative) (1.2.1.1) or one-phase (associative) phase separation (1.2.1.2) and in under very special circumstances “borderline” phase separation (Picullel *et. al.*, 1995, Ramzi *et. al.*, 1999). This depends primarily on polymer-polymer and polymer-solvent interactions (enthalpic effects) and the polymer size (exclusion volume) and structural conformation (entropic effects) (Tolstoguzov, 1991; Schmitt *et. al.*, 1999), for example  $\kappa$ -carrageenan in the helical form gives rise to greater thermodynamic incompatibility when mixed with 11S globulin (*Vicia faba*) than in random state, this is probably due to excluded volume effects (Semenova *et. al.*, 1991). The more usual situation is however for interactions between segments of two different polymers to be less favourable than the interactions between like segments and therefore two phase (segregative) phase separation predominant (Kasapis *et. al.*, 1993, Schmitt *et. al.*, 1998), this often achieved by lowering the temperature (Lundin *et. al.*, 2000).

### 1.2.1.1 Two – phase system

If the interactions between polymer/ polymer/ solvent systems are repulsive, two phases are obtained; each enriched in one of the biopolymers this is termed “segregative” phase separation (Picullel *et. al.*, 1995; Michon *et. al.* 2000). Segregative (two-phase) separation involves the partition of the two biopolymers  $P_2$  and  $P_3$  into different phases (**Figure 1-2**) and is therefore referred to as “polymer

incompatibility” or “simple coacervation” or “de-mixing” and the two polymers are confined entirely to their respective phases [Note – the term “simple coacervation” does not suggest any complex formation and it is meant in the sense that it is an opposite effect to “complex coacervation”], (Clark, 1995; Kasapis, 1995) *e.g.* locust bean gum/ casein micelle suspensions (Bourriot *et. al.*, 1999b; Schorsch *et. al.*, 1999)  $\kappa$ -carrageenan/ casein micelle suspensions (Bourriot *et. al.*, 1999a). The degree of incompatibility is therefore dependent on solvent quality (Schorsch *et. al.*, 1999) and it is possible to pass from complete to limited compatibility by changing solvent quality (Schorsch *et. al.*, 1999). A detailed list of protein - polysaccharide and protein – protein systems and the conditions under which they are thermodynamically incompatible can be found in Grinberg and Tolstoguzov (1997) and Polyakov *et. al.* (1997) respectively.

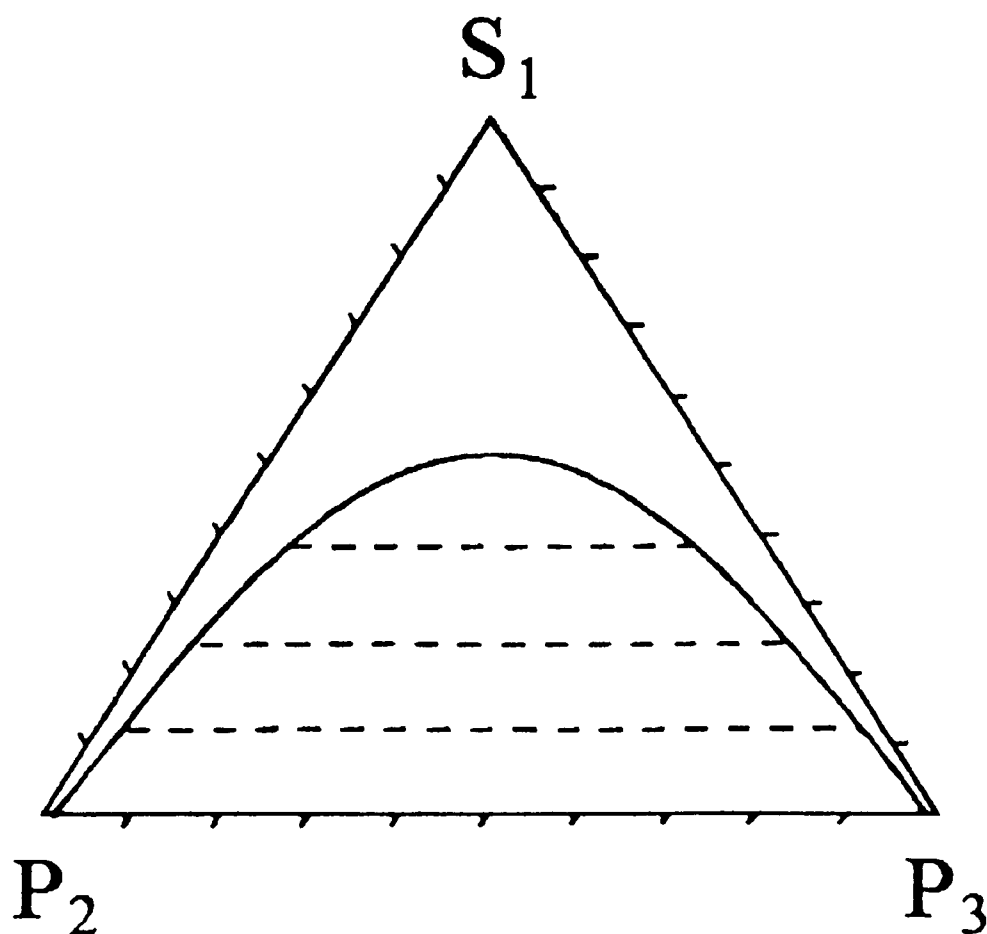


**Figure 1-2** Schematic representation of segregative phase separation (adapted from Picullel *et. al.*, 1995 see also Picullel and Lindman, 1992; Bergfeldt *et. al.*, 1996 and Syrbe *et. al.*, 1998). Where  $S_1$  is the solvent and  $P_2$  and  $P_3$  are polymers.

## 1.2.1.2 One – phase system

In an associative (one-phase) phase separation the two biopolymers  $P_2$  and  $P_3$  are enriched in the same phase (**Figure 1-3**) and this is often known as “complex coacervation”. This is more common if the biopolymers are oppositely charged *i.e.* the two phases one containing the so-called “co-acervate” phase composed of electrostatically (or non-specifically) stabilised polymer complexes the other a dilute phase containing large amounts of solvent *e.g.* gelatin and pectin,  $\beta$ -lactoglobulin and acacia gum (Tolstoguzov, 1990; Schmitt *et. al.*, 1999). [Note – in this case associative refers to the formation of complexes between dissimilar molecules (Michon *et. al.*, 2000)].

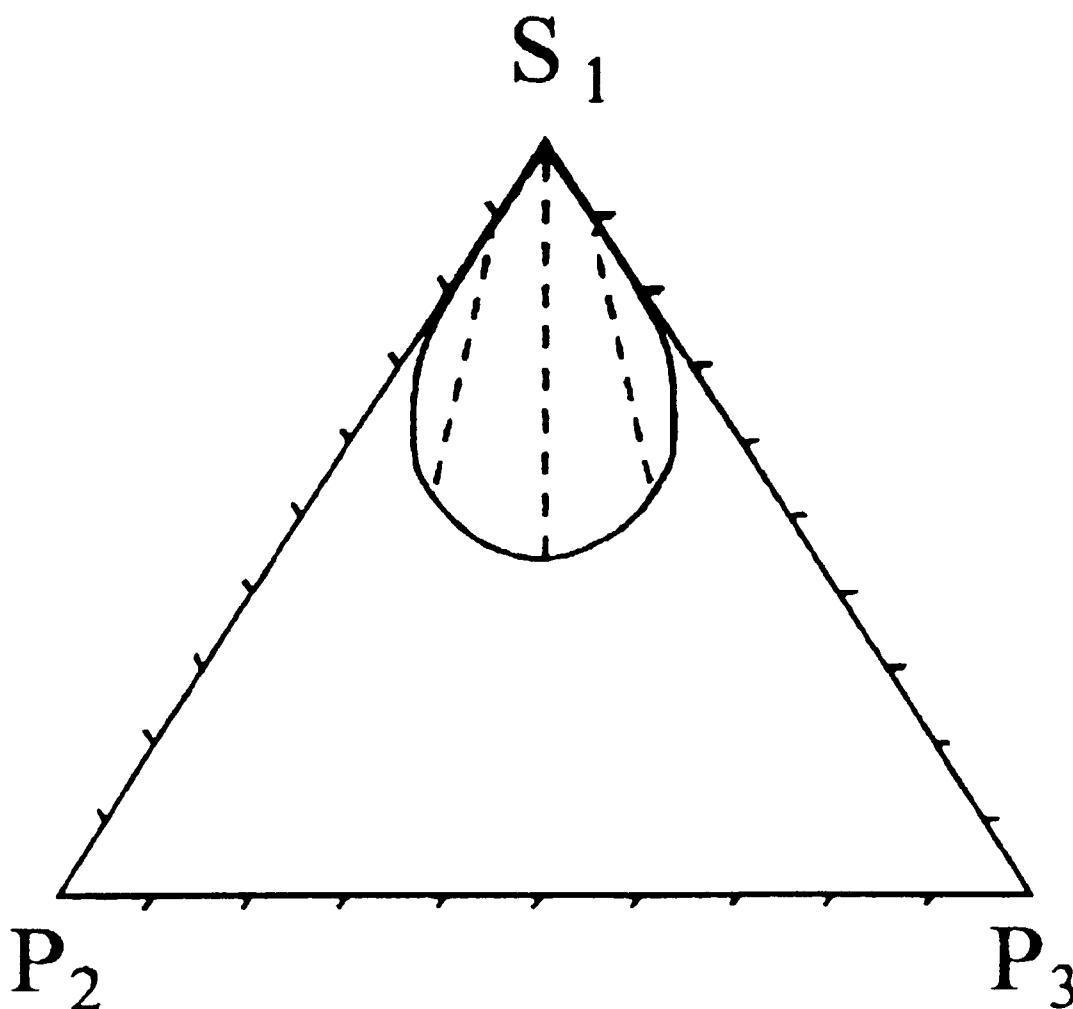


**Figure 1-3** Schematic representation of associative phase separation (adapted from Picullel *et. al.*, 1995 see also Picullel and Lindman, 1992; Bergfeldt *et. al.*, 1996 and Syrbe *et. al.*, 1998).

It has however been reported that shear effects can modify the phase behaviour mixed biopolymer systems (Brown *et. al.*, 1995).

### 1.2.2 Complexation

Complexation is a very broad term, which in general describes “biopolymers which can interact covalently or non-covalently in either a reversible or irreversible manner” (see *e.g.* Harding, 1997). Complexes can be soluble (1.2.2.1) or insoluble (1.2.2.2) in aqueous solvent depending on biopolymer concentration, ionic strength, pH and temperature (**Figure 1-1**) (Harding, 1997; Schmitt *et. al.*, 1998 Tolstoguzov, 1990, 1991). Protein – polysaccharide complexes can exhibit “better” functional properties than proteins and polysaccharides alone *e.g.* hydration, structuration, interfacial and adsorption properties (Schmitt *et. al.*, 1998).

#### 1.2.2.1 One – phase system

The soluble complex can be stabilised by a variety of intermolecular forces of significantly different strengths (see *e.g.* Dickinson, 1998) -

- (i) covalent - very strong specific linkage between reactive groups
- (ii) electrostatic - Coulombic interaction between charged molecules, can be either attractive or repulsive
- (iii) steric interactions - repulsive interaction between electron clouds due to their close proximity
- (iv) hydrogen bonding - specific short-range interaction between polar groups *e.g.*  $\text{O-H}^{\delta+} \dots \delta^- \text{O-R}$
- (v) hydrophobic interactions - attractive interaction between non-polar groups

(vi) ion-bridging - the binding of two (or more) anions by a polycation e.g.  $\text{Ca}^{2+}$  ions stabilising a low-methoxy pectin gel network - “egg-box model”.

(vii) van der Waals forces - weak interaction between molecules in close proximity

(viii) “Synergistic” interactions e.g. locust bean gum with xanthan (E.R. Morris, 1995) or  $\kappa$ -carrageenan with locust bean gum or konjac mannan (Williams *et al.*, 1991, 1992; V.J. Morris, 1995).

As with most interaction phenomena protein – polysaccharide complexation depends on many variables e.g. pH, ionic strength, biopolymer ratio, biopolymer molecular weights, charge density, temperature, shear-rate and pressure (Schmitt *et al.*, 1998). Of the types of interactions listed (i-vii) are the most important with respect to protein-polysaccharide complexation, of the single most important is the attractive electrostatic interaction. This is usually between positively charged regions in proteins (depends on pH and ionic strength) and negatively charged polysaccharides. Electrostatic interactions have been used to describe many protein-polysaccharide interactions e.g. casein - carrageenan complexes (Snoeren, 1976; Dalgleish and Morris, 1988; Schorsch *et al.*, 2000; Augustin *et al.*, 1999, Bourriot *et al.*, 1999a and Drohan *et al.*, 1997); casein - pectin complexes (Oakenfull and Scott, 1998 and Kravtchenko *et al.*, 1994); gelatin - pectin interactions (Tolstogustov, 1990); ovalbumin -  $\iota$ -carrageenan and dextran sulphate complexes (Galazka *et al.*, 1999), lysozyme – chitosan (Cölfen *et al.*, 1996), myoglobin – pectate/ alginate/ CMC, bovine serum albumin – pectate/ alginate/ CMC (Imeson *et al.*, 1977).

#### 1.2.2.2 Two – phase system

The formation of an electrically neutral complex between two oppositely charged biopolymers can lead to a precipitation and therefore the two-phase complex situation (**Figure 1-1**), where the aqueous phase is solvent and excess of one or other biopolymer. An example of this type of interaction is the chitosan - mucin complex (Harding, 1994; Fiebrig, 1995; Harding, 1997; Deacon *et al.*, 1998 and Deacon, 1999).

### 1.3 FLOCCULATION

As the stability of colloidal dispersions is greatly influenced by addition of polyelectrolytes any of the situations discussed in 1.2 can lead to a number of specific interactions (Williams and Smith, 1995 and Furusawa *et. al.*, 1999)

- (i) bridging flocculation
- (ii) steric stabilisation
- (iii) depletion flocculation

At very low polymer concentrations the bridging phenomenon is predominant, that is where the polymer is able to adsorb on to the surface of more than one colloidal particle (**Figure 1-4**).

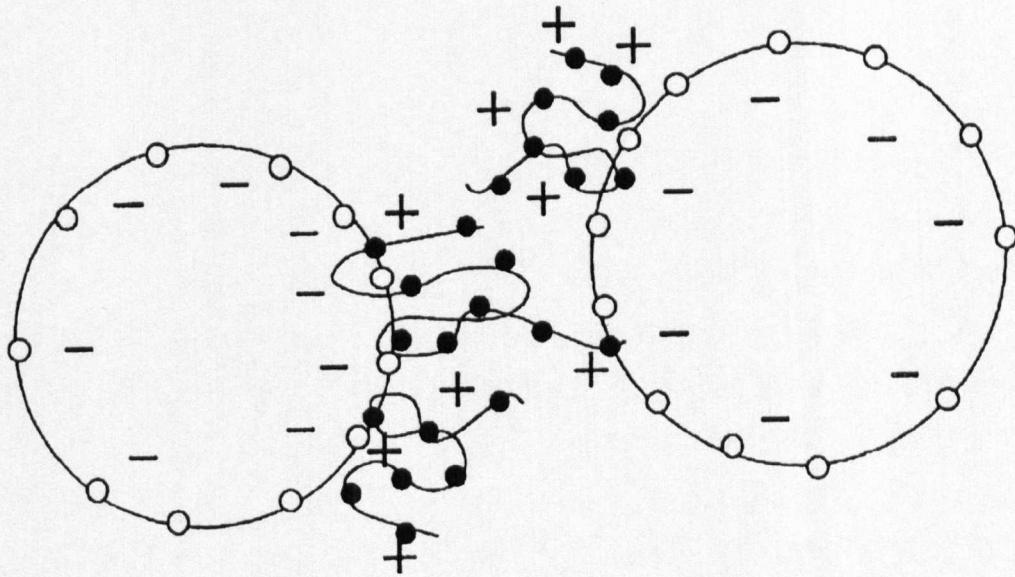


**Figure 1-4** Schematic representation of bridging flocculation (adapted from Furusawa *et. al.*, 1999)

When a sufficient polymer concentration is reached the colloidal particle will be universally coated this is called steric stabilisation (Koltay and Feke, 1999; Furusawa *et. al.*, 1999) (**Figure 1-5**).

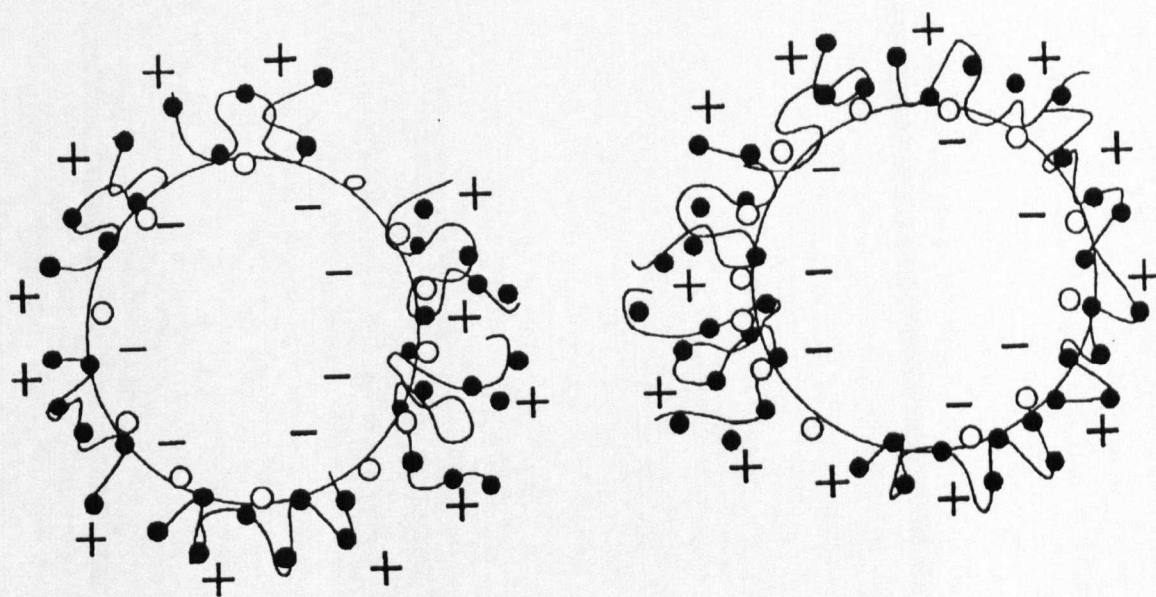


**Figure 1-5** Schematic representation of steric stabilisation (adapted from Furusawa *et. al.*, 1999).

Finally after the addition of an excess of polymer a depletion layer (**Figure 1-6**) is formed where the polymer concentration at the surface is less than that of the bulk, this results in an osmotic pressure difference between the bulk polymer solution and the depleted region containing pure solvent, this results in an attractive force being set up and therefore when two (or more) colloidal particles come close together depletion flocculation will occur (**Figure 1-7**)(Williams and Smith, 1995; Jenkins and Snowden, 1996; Warren, 1997; Soga *et. al.*, 1998; Chatterjee and Schweizer, 1998; Koltay and Feke, 1999; Kiratzis *et. al.*, 1999; Furusawa *et. al.*, 1999; McClements, 2000).

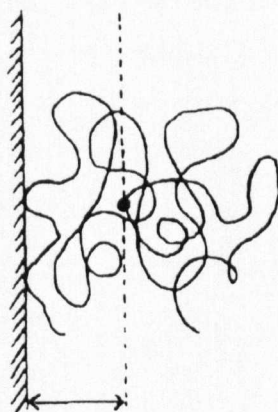


**Figure 1-6** Schematic representation of a polymer depletion layer (adapted from Williams and Smith, 1995).

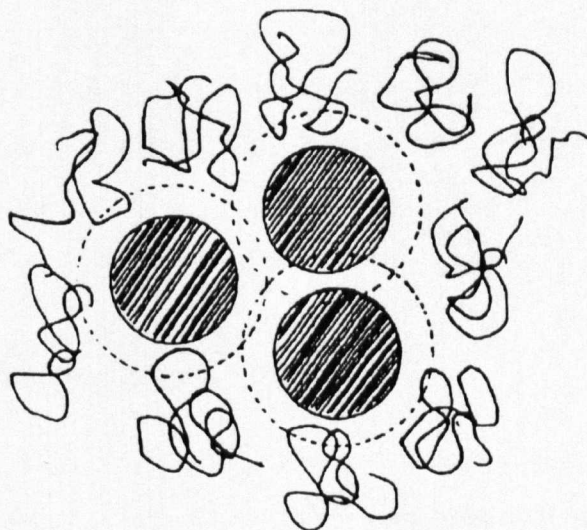


**Figure 1-7** Schematic representation of the exclusion of polymer molecules from between particles at close separations leading to depletion flocculation (adapted from Williams and Smith, 1995).

#### 1.4 APPLICATION OF HYDRODYNAMIC TECHNIQUES

Hydrodynamic techniques such as sedimentation velocity, sedimentation equilibrium, capillary viscometry, size exclusion chromatography - multi-angle laser light

scattering, dynamic light scattering and particle size analysis (Chapter 2) are particularly useful for the analysis of macromolecule complexes *i.e.* sections 1.2.2.1 and 1.2.2.2 (see for example Cölfen *et. al.*, 1996; Harding, 1994; Fiebrig, 1995; Deacon *et. al.*, 1998; Deacon, 1999).

#### 1.4.1 Sedimentation Velocity

Sedimentation velocity allows the determination of the sedimentation coefficient,  $s_{20,w}$  and sedimentation coefficient distribution,  $g(s_{20,w})$  of a complex, which can be compared with the distributions of the “pure” components. One can also determine qualitatively and quantitatively the amounts of each component not involved in complex formation and hence calculate the relative amounts of each component involved in the interaction. Thus by varying the relative amounts of each component sedimentation velocity provides the opportunity for the estimation of strengths and stoichiometries of a particular interaction. Sedimentation velocity can also be used to give an indication of the shape of the complex and hence an idea of the spatial geometry of interaction.

#### 1.4.2 Sedimentation Equilibrium

Sedimentation equilibrium allows the determination of weight average molecular weights,  $M_w$ . Therefore the molecular weight of a complex can then be compared with the individual components and by varying the concentrations of each species, interaction strengths and stoichiometries can be estimated.

### 1.4.3 Capillary Viscometry

The intrinsic viscosity of a macromolecule can give an indication of molecular weight and therefore can be used as a non-specific probe to determine complex formation. The intrinsic viscosity may also give an approximate indication of shape.

### 1.4.4 SEC-MALLS-RI

Size Exclusion Chromatography coupled to Multi-Angle Laser Light Scattering with on-line Refractive Index detection is another useful technique for looking at macromolecular interaction, but is perhaps most useful in assaying the molecular integrity of polysaccharide reactants. Size Exclusion Chromatography (SEC) allows the separation of macromolecules based on hydrodynamic volume; this prior separation allows the on-line determination of molecular weights, molecular weight distributions and gyration radii from light scattering measurements at different angles (MALLS). The Refractive Index (RI) detector allows the determination of species concentration; therefore by varying the concentrations of each species, interaction strengths and stoichiometries can be estimated.

### 1.4.5 Dynamic Light Scattering

Dynamic Light Scattering (DLS) allows the determination of the translational diffusion coefficients (and their distribution) from which hydrodynamic (Stokes) radii can be estimated. This therefore can give valuable information on the complex size *i.e.* molecular weight and on complex geometry. As with sedimentation experiments and SEC-MALLS one can estimate strengths and stoichiometries by varying concentrations.

#### 1.4.6 Particle Size Analysis using the Malvern Mastersizer™

Essentially gives the same information as DLS, and is therefore useful as a “look-and-see” method to probe complex formation.

### 1.5 AIMS AND OBJECTIVES

The aim of the PhD study is to characterise the interactions between the native milk protein – casein and a number of commercially available polysaccharides, using a variety of hydrodynamic techniques. The type of reaction (if any) can then be estimated, if one knows the detailed properties of the individual reactants.

The specific objectives are to use the techniques described in Chapter 2 to estimate the dilute solution hydrodynamic properties and predict the solution conformation of a number of commercially available polysaccharides (Chapter 3) and of milk protein solutions (Chapter 4). We can then use the information described in chapters 3 and 4 as a platform for the investigation of the mixed systems (Chapter 5). Finally Chapter 6 will draw specific conclusions on the results in Chapters 3-5, some general conclusions and suggestions for future work.

## 1.6 REFERENCES

- Albertsson P-Å (1995) Aqueous Polymer Phase Systems: Properties and Applications in Bioseparation. In: Harding SE, Hill SE and Mitchell JR (Eds.) *Biopolymer Mixtures*, pp. 1-12. Nottingham University Press, Nottingham.
- Antonov YA and Goncalves MP (1999) Phase Separation in Aqueous Gelatin –  $\kappa$  - Carrageenan Systems. *Food Hydrocolloids*, **13**, 517-524.
- Augustin MA, Puvanenthiran A and McKinnon IR (1999) The Effect of  $\kappa$ -Carrageenan Conformation on its Interaction with Casein Micelles. *International Dairy Journal*, **9**, 413-414.
- Bergfeldt K, Picullel L and Linse P (1996) Segregation and Association in Mixed Polymer Solutions from Flory-Huggins Model Calculations. *Journal of Physical Chemistry*, **100**, 3680-3687.
- Bourriot S, Garnier C and Doublier J-L (1999a) Micellular-Casein-  $\kappa$ -Carrageenan Mixtures. I. Phase Separation and Ultrastructure. *Carbohydrate Polymers*, **40**, 145-157.
- Bourriot S, Garnier C and Doublier J-L (1999b) Phase Separation, Rheology and Structure of Micellular Casein-Galactomannan Mixtures. *International Dairy Journal*, **9**, 353-357.
- Brown CRT, Foster TJ, Norton IT and Underwood J. (1995) Influence of Shear on the Microstructure of Mixed Biopolymer Systems. In: Harding SE, Hill SE and Mitchell JR (Eds.) *Biopolymer Mixtures*, pp. 65-84. Nottingham University Press, Nottingham

- Chatterjee AP and Schweizer KS (1998) Microscopic Theory of Polymer-Mediated Interactions between Spherical Particles. *Journal of Chemical Physics*, **109**, 10464-10476.
- Clark AH (1995) Kinetics of De-mixing. In: Harding SE, Hill SE and Mitchell JR (Eds.) *Biopolymer Mixtures*, pp. 37-64. Nottingham University Press, Nottingham.
- Cölfen H, Harding SE, Varum KM and Winzor DJ (1996) A Study by Analytical Ultracentrifugation on the Interaction between Lysozyme and Extensively Deacylated Chitin (Chitosan). *Carbohydrate Polymers*, **30**, 45-53.
- Dagleish DG and Morris ER (1988) Interactions Between Carrageenans and Casein Micelles: Electrophoretic and Hydrodynamic Properties of the Particles. *Food Hydrocolloids*, **2**, 311-320.
- Deacon MP (1999) Polymer Bioadhesives for Drug Delivery. University of Nottingham, PhD.
- Deacon MP, Davis SS, White RJ, Nordman H, Carlstedt I, Errington N, Rowe AJ and Harding SE (1999) Are Chitosan-Mucin Interactions Specific to Different Regions of the Stomach? Velocity Ultracentrifugation Offers a Clue. *Carbohydrate Polymers*, **38**, 235-238.
- Dickinson E (1998) Stability and Rheological Implications of Electrostatic Milk Protein - Polysaccharide Interactions. *Trends in Food Science and Technology*, **9**, 347-354.
- Drohan DD, Tziboula A, McNulty D and Horne DS (1997) Milk Protein-Carrageenan Interactions. *Food Hydrocolloids*, **11**, 101-107.

- Fiebrig I (1995) Solution Studies on the Mucoadhesive Potential of Various Polymers for Uses in Gastrointestinal Drug Delivery Systems. University of Nottingham, PhD.
- Furusawa K, Ueda M and Nashima T (1999) Bridging and Depletion Flocculation of Synthetic Latices Induced by Polyelectrolytes. *Colloids and Surfaces A: Physicochemical and Engineering Aspects*, **153**, 575-581.
- Galazka VB, Smith D, Ledward DA and Dickinson E (1999) Interactions of Ovalbumin with Sulphated Polysaccharides: Effects of pH, Ionic strength, Heat and High Pressure Treatment. *Food Hydrocolloids*, **13**, 81-88.
- Grinberg VY and Tolstoguzov VB (1997) Thermodynamic Incompatibility of Proteins and Polysaccharides in Solutions. *Food Hydrocolloids*, **11**, 145-158.
- Harding SE (1994) Shapes and Sizes of Food Polysaccharides by Sedimentation Analysis - Recent Developments. In: Phillips GO, Williams PA and Wedlock DJ (Eds.) *Gums and Stabilisers for the Food Industry 7*, pp. 55-68. IRL Press, Oxford.
- Harding SE (1995) On the Hydrodynamic Analysis of Macromolecular Conformation. *Biophysical Chemistry*, **55**, 69-93.
- Harding SE (1997) Characterisation of Chitosan-Mucin Complexes by Sedimentation Velocity Analytical Ultracentrifugation. In: Muzzarelli RAA and Peters MG (Eds.) *Chitin Handbook*, pp 457-466. European Chitin Society, Torrette, Italy.
- Hoskins AR, Robb ID and Williams PA (1998) Selective Separation of Proteins from Mixtures using Polysaccharides. *Biopolymers*, **45**, 97-104.

- Imeson AP, Ledward DA and Mitchell JR (1977) On the Nature of the Interaction Between Some Anionic Polysaccharides and Proteins. *Journal of the Science of Food and Agriculture*, **28**, 661-668.
- Jenkins P and Snowden M (1996) Depletion Flocculation in Colloidal Dispersions. *Advances in Colloid and Interface Science*, **68**, 57-96.
- Kasapis S (1995) Phase Separation in Hydrocolloid Gels. In: Harding SE, Hill SE and Mitchell JR (Eds.) *Biopolymer Mixtures*, pp. 193-224. Nottingham University Press, Nottingham.
- Kasapis S, Morris ER, Norton IT and Gidley MJ (1993) Phase Equilibria and Gelation in Gelatin/ Maltodextrin Systems – Part II: Polymer Incompatibility in Solution. *Carbohydrate Polymers*, **21**, 249-259.
- Kiratzis N, Faers M and Luckham PF (1999) Depletion Flocculation of Particulate Systems Induced by Hydroxyethylcellulose. *Colloids and Surfaces A: Physicochemical and Engineering Aspects*, **151**, 461-471.
- Koltay JA and Feke DL (1999) Preparation of Continuous Fiber Ceramic Composites using a Combination of Steric-Stabilization and Depletion-Flocculation Phenomena. *Composites Part A: Applied Science and Manufacturing*, **30**, 231-237.
- Kravtchenko TP, Voragen AGJ and Pilnik W (1994) Characterisation of Industrial High Methoxy Pectin. In: Phillips GO, Williams PA and Wedlock DJ (Eds.) *Gums and Stabilisers for the Food Industry 7*, pp. 27-36. IRL Press, Oxford.
- Lundin L, Norton IT, Foster TJ, Williams MAK, Hermansson A-M and Bergström E (2000) Phase Separation in Mixed Biopolymer Systems. In: Phillips GO, Williams PA and Wedlock DJ (Eds.) *Gums and Stabilisers for the Food Industry 10*, pp. 167-180. Royal Society of Chemistry, Cambridge.

- McClements DJ (2000) Comments on Viscosity Enhancement and Depletion Flocculation by Polysaccharides. *Food Hydrocolloids*, **14**, 173-177.
- Michon C, Vigouroux F, Boulenguer P, Cuvelier G and Launay B (2000) Gelatin/Iota Carrageenan Interactions in Non-gelling Conditions. *Food Hydrocolloids*, **14**, 203-208.
- Morris ER (1995) Polysaccharide Synergism - More Questions than Answers? In: Harding SE, Hill SE and Mitchell JR (Eds.) *Biopolymer Mixtures*, pp. 247-288. Nottingham University Press, Nottingham.
- Morris VJ (1995) Synergistic Interactions with Galactomannans and Glucomannans. In: Harding SE, Hill SE and Mitchell JR (Eds.) *Biopolymer Mixtures*, pp. 289-314. Nottingham University Press, Nottingham.
- Oakenfull DG and Scott A (1998) Milk Gels with Low Methoxy Pectins. In: Phillips GO, Williams PA and Wedlock DJ (Eds.) *Gums and Stabilisers for the Food Industry 9*, pp. 212-221. Royal Society of Chemistry, Cambridge.
- Picullel L and Lindman B (1992) Association and Segregation in Aqueous Polymer/Polymer, Polymer/Surfactant, and Surfactant/ Surfactant Mixtures: Similarities and Differences. *Advances in Colloid and Interface Science*, **41**, 149-178.
- Picullel L, Bergfeldt K and Nilsson S (1995) Factors Determining Phase Behaviour of Multi Component Polymer Systems. In: Harding SE, Hill SE and Mitchell JR (Eds.) *Biopolymer Mixtures*, pp. 13-36. Nottingham University Press, Nottingham.
- Polyakov VI, Grinberg VY and Tolstoguzov VB (1997) Thermodynamic Incompatibility of Proteins. *Food Hydrocolloids*, **11**, 171-180.

- Ramzi M, Borgström J and Piculell L (1999) Effects of Added Polysaccharide on the Isotropic/ Nematic Phase Equilibria of  $\kappa$ -Carrageenan. *Macromolecules*, **32**, 2250-2255.
- Schmitt C, Sanchez C, Desorby-Baron S and Hardy J (1998) Structure and Technofunctional Properties of Protein – Polysaccharide Complexes: A Review. *Critical Reviews in Food Science and Nutrition*, **38**, 689-753.
- Schmitt C, Sanchez C, Thomas F and Hardy J (1999) Complex Coacervation Between  $\beta$ -Lactoglobulin and Acacia Gum in Aqueous Media. *Food Hydrocolloids*, **13**, 483-496.
- Schorsch C, Jones MG and Norton IT (1999) Thermodynamic Incompatibility and Microstructure of Milk Protein/ Locust Bean Gum/ Sucrose Systems. *Food Hydrocolloids*, **13**, 89-99.
- Schorsch C, Jones MG and Norton IT (2000) Phase Behaviour of Pure Micellar Casein/  $\kappa$ -carrageenan Systems in Milk Salt Ultrafiltrate. *Food Hydrocolloids*, **14**, 347-358.
- Semenova MG, Pavlovskaya GE and Tolstoguzov VB (1991) Light Scattering and Thermodynamic Phase Behaviour of the System 11S Globulin –  $\kappa$ -Carrageenan – Water. *Food Hydrocolloids*, **4**, 469-479.
- Snoeren THM, Both P and Schmitt DG (1976) An Electron-Microscopy Study of Carrageenan and its Interaction with  $\kappa$ -Casein. *Netherlands Milk and Dairy Journal*, **30**, 132-141.
- Soga KG, Melrose JR and Ball RC (1998) Continuum Percolation and Depletion Flocculation. *Journal of Chemical Physics*, **108**, 6026-6032.

Syrbe A, Bauer WJ and Klostermeyer H (1998) Polymer Science Concepts in Dairy Systems – An Overview of Milk Protein and Food Hydrocolloid Interaction. *International Dairy Journal*, **8**, 179-193.

Tolstoguzov VB (1986) Functional Properties of Protein – Polysaccharide Mixtures. In: Mitchell JR and Ledward DJ (Eds.) *Functional Properties of Food Macromolecules*, pp. 385-415. Elsevier, London.

Tolstoguzov VB (1990) Interactions of Gelatin with Polysaccharides. In: Phillips GO, Williams PA and Wedlock DJ (Eds.) *Gums and Stabilisers for the Food Industry 5*, pp. 157-176. IRL Press, Oxford.

Tolstoguzov VB (1991) Functional Properties of Food Proteins. *Food Hydrocolloids*, **4**, 429-468.

Warren PB (1997) Phase Behaviour of a Colloid + Binary Polymer Mixture: Theory. *Langmuir*, **13**, 4588-4594.

Williams PA, Clegg SM, Day DH and Phillips GO (1991) Mixed Gels Formed by Konjac Mannan and Xanthan Gum. In: Dickinson E (Ed.) *Food Polymers, Gels and Colloids*, pp 339-348. Royal Society of Chemistry, Cambridge.

Williams PA, Clegg SM, Langdon MJ, Nishinari K and Phillips GO (1992) Studies on the Synergistic Interaction of Konjac Mannan and Locust Bean Gum with  $\kappa$ -Carrageenan. In: Phillips GO, Williams PA and Wedlock DJ (Eds.) *Gums and Stabilisers for the Food Industry 6*, pp. 209-216. IRL Press, Oxford.

Williams PA and Smith NJ (1995) Depletion Flocculation. In: Harding SE, Hill SE and Mitchell JR (Eds.) *Biopolymer Mixtures*, pp. 161-172. Nottingham University Press, Nottingham.

## **2 CHAPTER 2 – HYDRODYNAMIC TOOLS FOR THE STUDY OF PROTEIN – POLYSACCHARIDE INTERACTIONS**

### **2.1 THE USE OF HYDRODYNAMICS TOOLS FOR THE ANALYSIS OF THE SOLUTION PROPERTIES OF MACROMOLECULES**

Modern hydrodynamic techniques provide the bioscientist with an array of powerful techniques for the investigation of mass, conformation, and interaction properties under solution conditions. Although regarded as being low resolution compared to structural probes such as X-ray crystallography and nuclear magnetic resonance (NMR) hydrodynamic techniques have found a niche in many leading biochemistry and molecular biology laboratories. Hydrodynamic tools play an important role as a complementary technique, which can give rapid “low resolution” information on macromolecular structure prior to a detailed crystallographic, or NMR analysis. This has proved invaluable for molecular biologists who often only have very small amounts of sample and therefore a rapid, non-destructive estimate of molecular conformation, which supplies useful extra information to support their “high resolution” data, is imperative. Furthermore because of the high concentrations required to give satisfactory NMR spectra, simple hydrodynamic approaches can give vital information on self-association phenomenon, which may lead to misinterpretation of NMR chemical shift spectra.

There are also many circumstances where techniques such as X-ray crystallography and NMR are inappropriate, for example many macromolecules cannot be crystallised or when working under physiological conditions concentrations are too low for a more detailed investigation. Polysaccharides are not readily available in a form suitable for “high resolution” techniques. Due to their polydisperse nature and large water binding capacity, hydrodynamic methods are appropriate for providing an estimate for molecular conformation and interactions in solution.

### 2.1.1 Hydrodynamic Techniques

The word “hydrodynamic” is from the Greek for “water-movement”, which encompasses any technique involving the motion of a macromolecule with, or relative to, the aqueous solvent in which it is dissolved or suspended (Harding, 1999b). The main hydrodynamic tools for the analysis of macromolecular conformation are (see *e.g.* Harding, 1995a, 1995b and Dhimi *et. al.*, 1995) –

- (i) sedimentation velocity – information on sample homogeneity/ purity, macromolecular size (sedimentation coefficient), macromolecular shape and macromolecular interactions (including self-association and disassociation)
- (ii) sedimentation equilibrium – information on molar mass, molar mass distributions and interaction phenomena
- (iii) viscometry – information on macromolecular size, shape, critical coil overlap concentration, shear behaviour and interactions
- (iv) size exclusion chromatography coupled to multi-angle laser light scattering – information on molar mass and molar mass distributions, radius of gyration and interactions
- (v) dynamic light scattering (quasi-elastic scattering or photon correlation spectroscopy) – information on diffusion coefficient, shape, size (hydrodynamic radius) and interactions
- (vi) Mie scattering – information on size (hydrodynamic radius), size distributions and interactions
- (vii) densimetry – information on density and on partial specific volumes,  $\bar{v}$  (essential for both sedimentation velocity and sedimentation equilibrium evaluation).

Even an apparently simple technique such as viscosity can give important information on size and shape and therefore be useful in estimating gross macromolecular conformation (Harding, 1997).

Although individually each technique can give important information it is the use of combined techniques, which is the real advantage of these tools as a probe for gross conformation. In the remainder of this chapter each method will be described (2.2-2.7) and combined approaches will be considered in section 2.8.

**Table 2-1** Molecular weight averages from different techniques (adapted from Harding *et. al.*, 1991).

Method	Type of average (see Appendix A)
<i>Absolute techniques</i>	
Osmotic pressure	$M_n$
Classical light scattering	$M_w$
Sedimentation equilibrium	$M_w$ ( $M_z$ , $M_{y1}$ and $M_{y2}$ )
<i>Relative techniques</i>	
Intrinsic viscosity	$M_\eta$
Sedimentation velocity	$M_s$
Dynamic light scattering	$M_{dif}$
Size exclusion chromatography	$M_n$ , $M_w$ and $M_z$ (distribution)
<i>Combined approaches</i>	
Sedimentation velocity and	$M_w$
Dynamic light scattering	
SEC + Classical light scattering	$M_n$ , $M_w$ and $M_z$ (distribution)

[Note - *Absolute* techniques do not require any calibration, *Relative* techniques require either assumptions over conformation or calibration with standards of known molecular weight and the combination of two or more *relative* techniques can also yield *absolute* molecular weights (for example sedimentation velocity and dynamic light scattering via the Svedberg equation 2-12)].

## 2.2 THEORY OF SEDIMENTATION IN THE ANALYTICAL ULTRACENTRIFUGE

Although often thought of as a rather outdated technique, analytical ultracentrifugation is still the most versatile method for the determination of the molecular weight and hydrodynamic properties of macromolecules. The development of the analytical ultracentrifuge by Thé(odor) Svedberg and co-workers in Uppsala, Sweden and Madison, Wisconsin in the mid-1920s was a major breakthrough in macromolecular chemistry in general and protein chemistry in particular, as the analytical ultracentrifuge (AUC) enabled absolute molecular weight determination. Recent developments in data analysis software (DCDT, DCDT+, SVEDBERG) together with the introduction of two new instruments the Beckman Optima XLA and XLI, have rekindled interest in this field. The analytical ultracentrifuge allows the concentration distribution of a sample to be determined at an accurately controlled rotor speed and accurately controlled temperature. As the rotor often spins at high angular velocities, both the rotor and sample cells should be able to withstand high gravitational stresses. Double sector cells are often used in order to correct for the activity of the solvent. The solution containing the sample is injected into one sector and the solvent into the other (Figure 2-1).

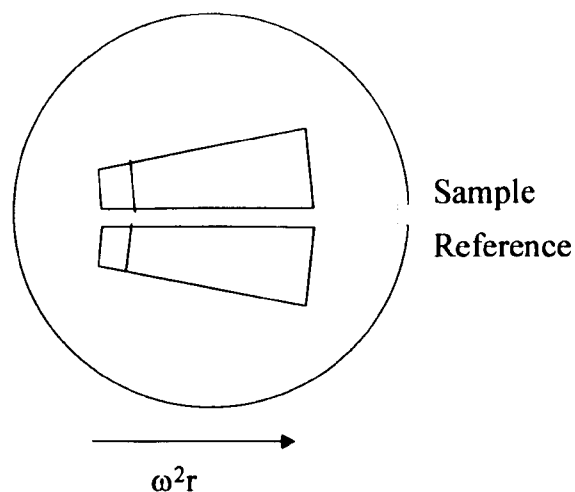


**Figure 2-1** Double - sector centrepiece. The sample is placed in one sector, and a reference solvent in dialysis equilibrium with the sample is placed in the reference sector. The reference sector is usually filled slightly more than the sample sector, so that the reference meniscus does not obscure the sample profile (adapted from Ralston, 1993).

There are four main methods of detection -

- (i) Schlieren (**Figure 2-2a**),
- (ii) Interference (**Figure 2-2b**)
- (iii) Photographic absorption “Turbidity” (**Figure 2-2c**) and
- (iv) Molecular/ photoelectric absorbance (**Figure 2-2d**)

Both Schlieren and Interference optics are related to refractive index, in the former the light is deviated as it passes through the sample and this displacement is proportional to the concentration gradient. The displacement is converted optically to a vertical displacement of the image. Interference optics on the other hand are based on the principle that the velocity of light is decreased as it passes through a region of higher refractive index. When monochromatic light passes through the two sectors of the double sector cell, the emerging waves interfere and a pattern of alternating light and

dark fringes are produced. If the refractive index of the sample is higher than that of the solvent the fringes are shifted vertically relative to a reference point of known concentration.

The simplest optical system is UV-visible absorption: this however relies on the presence of an absorbing chromophore in the sample and is therefore usually highly suitable for proteins (Figure 2-2).

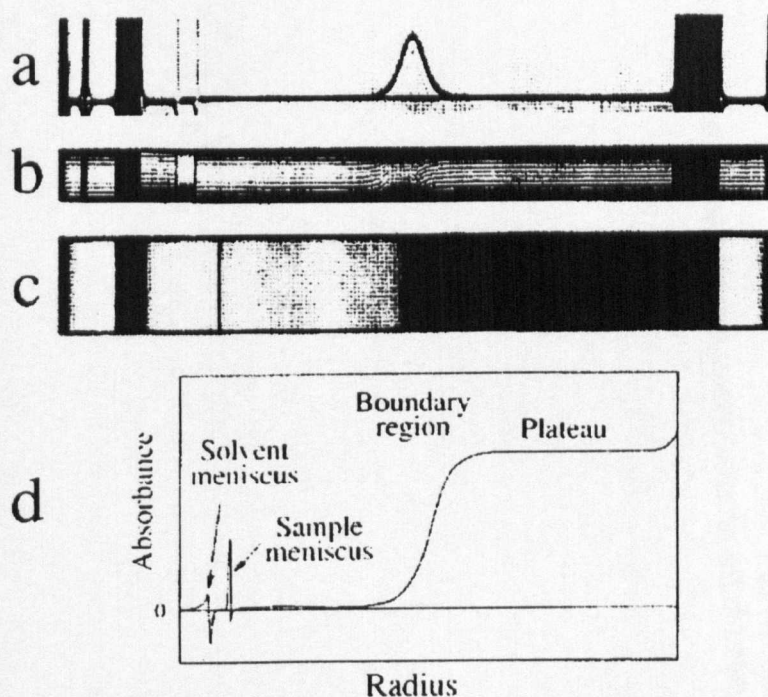


**Figure 2-2** Comparison of the optical records for a sedimenting boundary obtained from the (a) Schlieren, (b) interference, (c) photographic absorbance (Turbidity), and (d) photoelectric absorbance optical systems (adapted from Schachman, 1959, Ralston, 1993).

There are two main types of experiment commonly undertaken using the AUC.

- (i) Sedimentation Velocity – which measures the rate of movement of solute through a solvent in a centrifugal field, therefore there is net transport of solute.
- (ii) Sedimentation Equilibrium – no net movement of solute due to centrifugal and diffusion forces being equal as long as the rotor speed is not changed. The concentration gradient of solute is the determining factor.

## 2.2.1 Sedimentation Velocity in the Analytical Ultracentrifuge

When the solution of the sample of interest is subjected to a gravitational field, the solute is subjected to three forces - sedimenting (gravitational) force,  $F_c$ ; the buoyant force,  $F_b$  and the frictional force,  $F_d$  (**Figure 2-3**).

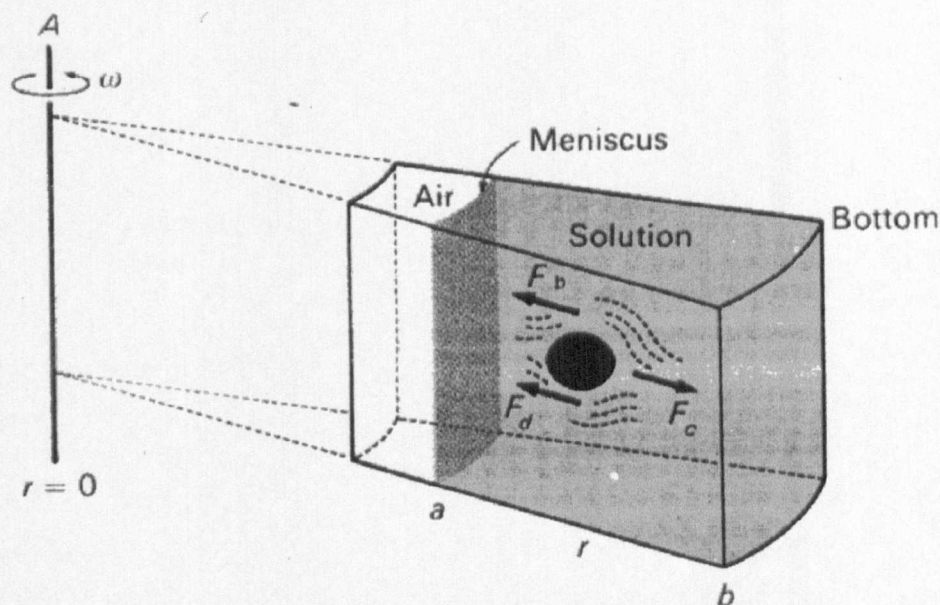


**Figure 2-3** The forces acting on a solute particle in a gravitational field (adapted from van Holde, 1985). A sector shaped cell is in a rotor spinning about the axis, A at an angular velocity,  $\omega$ . The cell is sector shaped because sedimentation proceeds along radial lines; and any other shape would lead to concentration accumulation near the edges and accompanying convection.

In a spinning rotor (up to 60,000 rpm), the acceleration is determined by the distance of the particle from the axis of the rotation,  $r$  and the square of the angular velocity,  $\omega$ .

$$F_c = m\omega^2 r = \frac{M}{N_A} \omega^2 r \quad (2-1)$$

where  $m$  is the mass in grams of a single particle,  $M$  is the molecular weight in g/mol,  $N_A$  is Avogadro's number and  $\omega = 2\pi\text{rpm}/60$

The Buoyant force,  $F_b$ , is determined using Archimedes' principle of fluid displacement.

$$F_b = -m_0\omega^2 r \quad (2-2)$$

where  $m_0$  is the mass of fluid displaced

$$m_0 = m\bar{v}\rho \quad (2-3)$$

where  $\bar{v}$  is the partial specific volume and  $\rho$  is the density of the solvent

As the particle sediments toward the cell base, the effective velocity,  $v$  will increase and the particle will experience frictional drag.

$$F_d = -fv \quad (2-4)$$

where  $f$  is the frictional coefficient, which depends on the shape and size of the macromolecule of interest.

Within a short period of time ( $\sim 1\mu\text{sec}$ ) these forces will come into balance. After rearrangement the following expression is derived (Ralston, 1993)-

$$\frac{M(1 - \bar{v}\rho)}{N_A f} = \frac{v}{\omega^2 r} = s \quad (2-5)$$

where  $s$  is the sedimentation coefficient

The sedimentation coefficient has the dimensions of seconds, however as for most macromolecules  $s$  values lie in the region of  $10^{-13}$  seconds, the Svedberg unit;  $S$  is used for convenience.  $1S = 1 \times 10^{-13}s$ .

As a centrifugal field is applied to a solution, the solute molecules will start to migrate through the cell towards the cell base. The distribution of solute is no longer uniform, as the region near the meniscus will be depleted of solute and there will be a region nearer the cell base where the solute concentration is uniform – plateau region (**Figure 2-4**). Between this plateau region and the supernatant there is a transitional region where the solute concentration varies with distance from the axis of rotation. This is the boundary region and it is the rate of movement of this boundary, which is observed in sedimentation velocity experiments, which allows the calculation of sedimentation coefficients (see *e.g.* van Holde, 1985; Ralston, 1993).

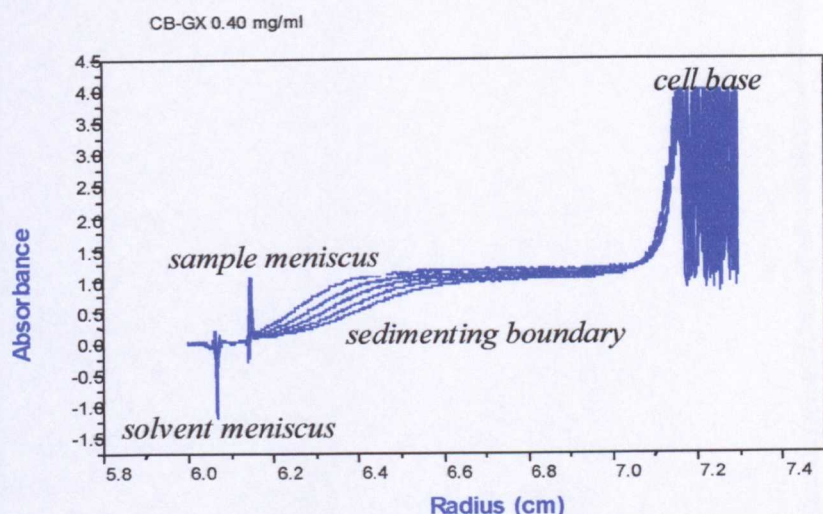


**Figure 2-4** A moving sedimenting boundary for the chemically modified xylan CB-GX at concentration 0.40 mg/ml, speed 50,000 rpm, temperature 20°C: scanning at 30 minute intervals. The sedimentation coefficient can be measured by following the mid-point (or, more precisely the “second moment”) of the boundary. The boundary broadens with time due to diffusion. [Note – modern software measures sedimentation coefficient by following the change in time of the whole concentration profile, and not just the boundary mid-point].

The progression of the sedimenting boundary is recorded by an optical system (Figure 2-2). The ultracentrifuge cell is illuminated by a light source each time it revolves through the optical path. Focussing mirrors are arranged to form an image of the cell, this image is then scanned by a photomultiplier and displaced in the  $r$  direction (Figure 2-5 and Figure 2-6). A double-sector cell (Figure 2-1) is employed so that solution and solvent are alternatively observed; this is essentially analogous to a double beam spectrophotometer.

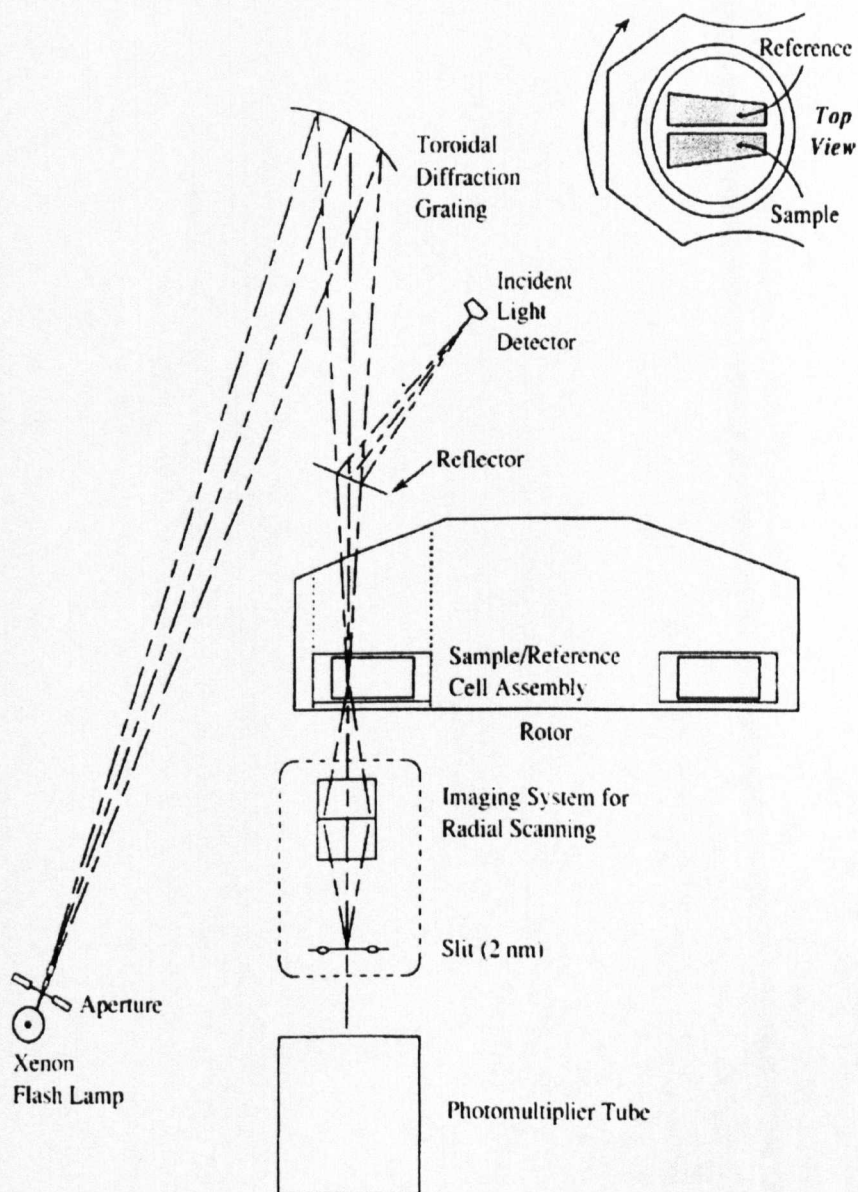


**Figure 2-5** A schematic representation of the scanning absorption optical system. The diffraction grating allows the choice of monochromatic light in the region of 200-800nm (from Ralston, 1993).

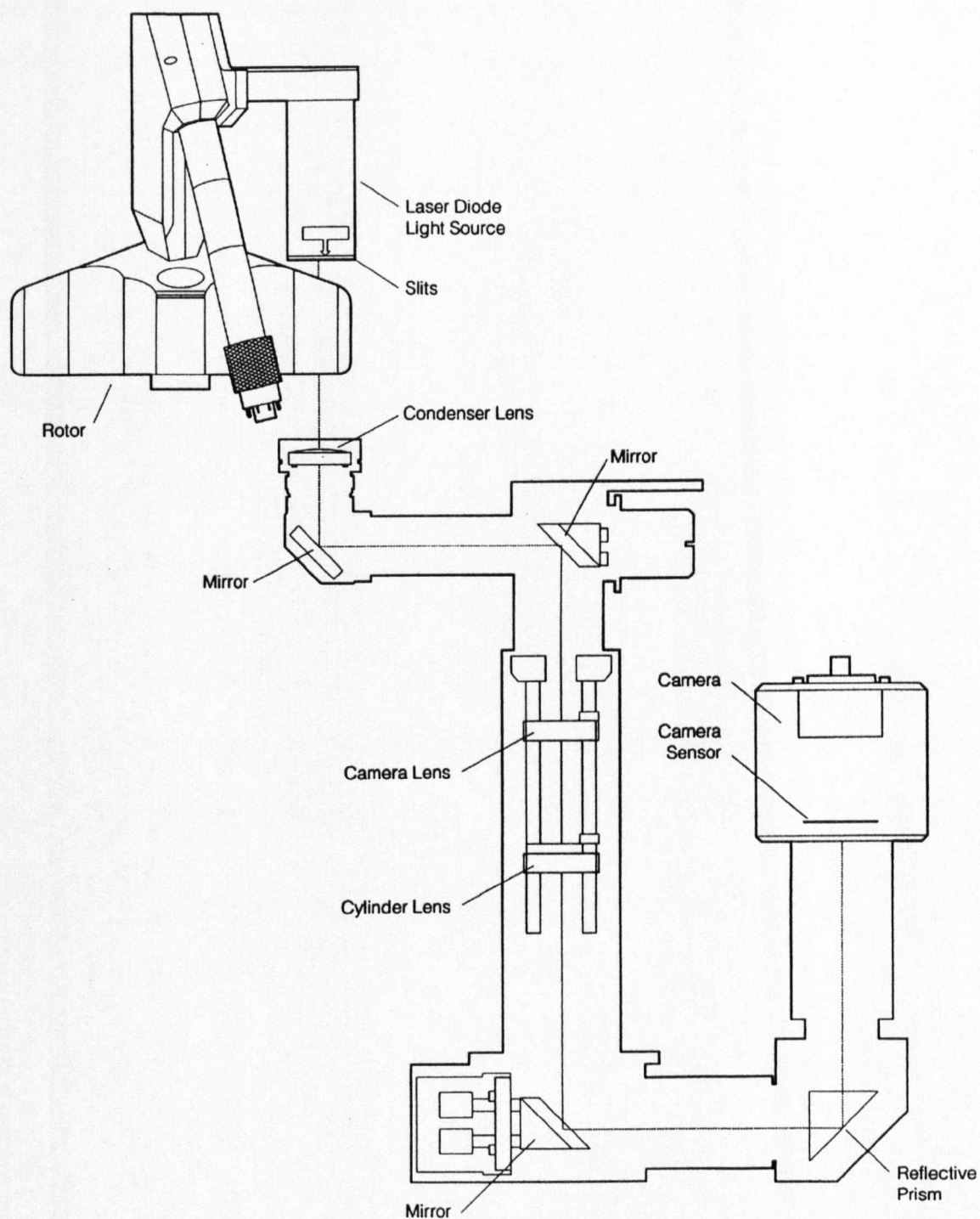


**Figure 2-6** A schematic representation of the interference optical system for the Beckman Optima XLI (adapted from Beckman, 1996).

Therefore at each radial position,  $r$  the absorption (or refractive index) difference between the solution sector and the reference sector is recorded. A series of graphs of absorbance (or fringe shift) against  $r$  is obtained and the boundary position is usually the mid-point of the step and can be recorded several time intervals throughout the

experiment. As the velocity of sedimentation,  $v$  can be set to equal  $dr_b/dt$  (the change in boundary position with time), therefore from equation 2-5 -

$$\frac{dr_b}{dt} = r_b \omega^2 s \quad (2-6)$$

therefore upon integration –

$$\ln \frac{r_b(t)}{r_b(t_0)} = \omega^2 s(t - t_0) \quad (2-7)$$

where  $r_b(t)$  and  $r_b(t_0)$  are the boundary positions at times  $t$  and  $0$  respectively ( $r_b(t_0)$  is the solution meniscus). Therefore a plot of  $\ln \frac{r_b(t)}{r_b(t_0)}$  vs.  $\omega^2 t$ , yields a straight line of slope  $s$  (Figure 2-7).

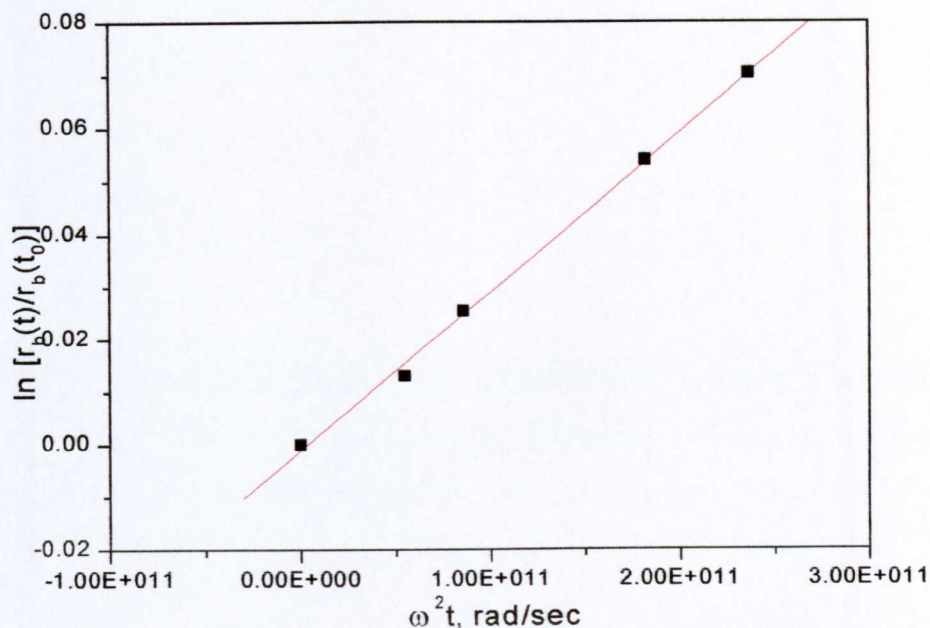


**Figure 2-7** A plot of  $\ln \frac{r_b(t)}{r_b(t_0)}$  vs.  $\omega^2 t$  for the high methoxy pectin HR 7021 at 50°C using the Schlieren optical system on a Beckman Model E analytical ultracentrifuge.

With the advent of the new XL ultracentrifuges a revolution in data analysis has heralded a new age for the AUC. A major development in software for data analysis has been the routine of DCDT (dc/dt) which measures the change in solute concentration with time, this can be converted into a distribution of sedimentation coefficients,  $g^*(s^*)$  (usually pronounced “g of s”). Where the \* is indicative of an *apparent* sedimentation coefficient distribution *i.e.* not corrected for diffusion, and an *apparent* sedimentation coefficient *i.e.* not corrected for non-ideality and not necessarily to standard solvent conditions (Stafford, 1992a,b and Laue and Stafford, 1999).

As all sedimentation coefficients are apparent due to non-ideality and will decrease with increasing concentration (assuming no self-association) and hence an extrapolation to zero concentration is required (Equations 2-8 and 2-9); (Harding, 1994; Jumel, 1994; Gralén, 1944; Pavlov, 1997; Morris *et. al.*, 2000; Creeth and Pain, 1967; van Holde, 1985 and Ralston, 1993) – **Figure 2-8**.

$$s = s^0(1 - k_s c) \tag{2-8}$$

$$\frac{1}{s} = \frac{1}{s^0(1 + k_s c)} \tag{2-9}$$

where  $\eta_{T,b}$ ,  $\eta_{20,w}$  are respectively the viscosities of the solvent at temperature T and water at 20.0°C, and  $\rho_T$  and  $\rho_{20,w}$  are the corresponding solvent densities. This correction can be done before (convention) or after the concentration extrapolation of equation 2-8 or 2-9. In general  $k_s$  values from the reciprocal plot (Equation 2-9) are more reliable in non-ideal systems (see *e.g.* Harding, 1995b).

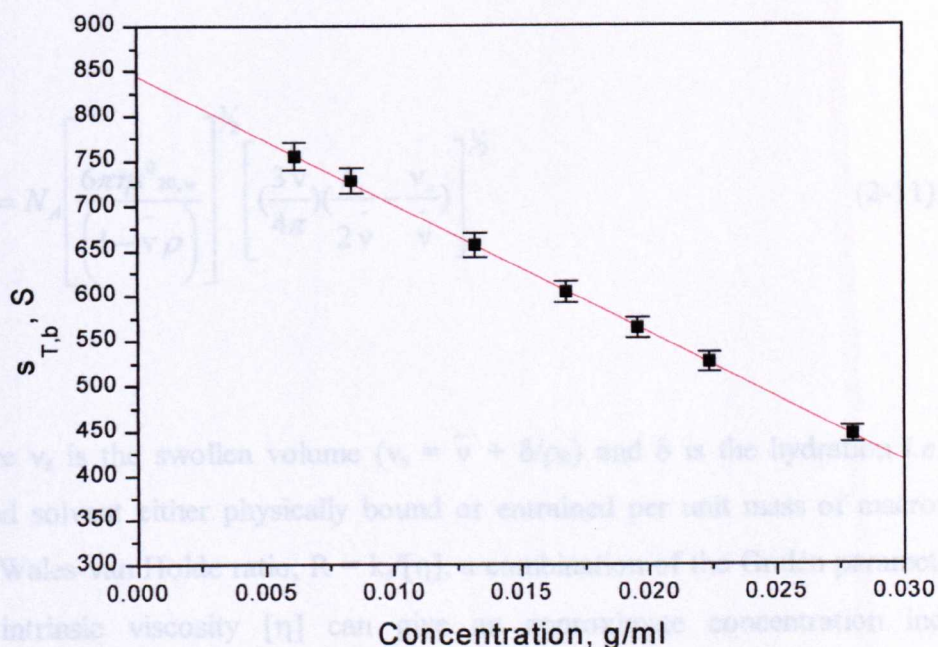


**Figure 2-8** The concentration dependency of sedimentation, for casein micelles at 20°C, data from Beckman Optima XLI using the interference optical system.

As sedimentation coefficients are also temperature and solvent sensitive, it is the convention that all sedimentation coefficient values are quoted at the standard conditions of 20°C and water as the solvent using Equation 2-10 (see *e.g.* Ralston, 1993).

$$s_{20,w} = s^* \left[ \frac{(1 - \bar{v} \rho_{20,w}) \eta_{T,b}}{(1 - \bar{v} \rho_{T,b}) \eta_{20,w}} \right] \quad (2-10)$$

where  $\eta_{T,b}$ ,  $\eta_{20,w}$  are respectively the viscosities of the solvent at temperature T and water at 20.0°C, and  $\rho_{T,b}$  and  $\rho_{20,w}$ , are the corresponding solvent densities. This correction can be done before (convention) or after the concentration extrapolation of equation 2-8 or 2-9.

Values of  $s_{20,w}^0$  and  $k_s$  can be used in the determination of molecular weights and conformational parameters (van Holde, 1985; Jumel, 1994; Rowe, 1977, Harding, 1997).

$$M_w = N_A \left[ \frac{6\pi\eta s_{20,w}^0}{(1 - \bar{v} \rho)} \right]^{3/2} \left[ \left( \frac{3\bar{v}}{4\pi} \right) \left( \frac{k_s}{2\bar{v}} - \frac{v_s}{\bar{v}} \right) \right]^{1/2} \quad (2-11)$$

where  $v_s$  is the swollen volume ( $v_s = \bar{v} + \delta/\rho_0$ ) and  $\delta$  is the hydration *i.e.* mass of bound solvent either physically bound or entrained per unit mass of macromolecule. The Wales-van Holde ratio,  $R = k_s/[\eta]$ , a combination of the Gralén parameter,  $k_s$  and the intrinsic viscosity  $[\eta]$  can give an approximate concentration independent indication of macromolecular shape, which is also independent of an assumed value of the hydration,  $\delta$ .

$$\frac{s_{20,w}^0}{D_{20,w}^0} = \frac{M_w(1 - \bar{v} \rho)}{RT} \quad (2-12)$$

Where  $R$  is the universal gas constant ( $8.314 \times 10^7 \text{ ergK}^{-1}\text{mol}^{-1}$ ) and  $D_{20,w}^0$  in the Svedberg equation (2-12) is the infinite dilution diffusion coefficient at standard conditions, which can be measured directly from dynamic light scattering or indirectly from boundary spreading during sedimentation velocity (this can be estimated from the width of a  $g^*(s^*)$  or  $dc/dr$  peak from Schlieren optics). This proves difficult in polydisperse systems and therefore direct measurement from light scattering or sedimentation equilibrium would be preferable (Tanford, 1961). The translational frictional ratio,  $f/f_0$  (Tanford, 1961) a parameter that depends on conformation and molecular hydration can also be derived from the knowledge of sedimentation coefficient and weight average molecular weight.

$$\frac{f}{f_0} = \frac{M_w(1 - \bar{v}\rho)}{(N_A 6\pi\eta_0 s_{20,w}^0) \left(\frac{4\pi N_A}{3\bar{v}M_w}\right)^{1/3}} \quad (2-13)$$

knowledge of hydration,  $\delta$  (or swollen volume,  $v_s$ ) allows the estimation of the Perrin function (the frictional ratio due to shape),  $P$  (see *e.g.* Dhimi *et. al.*, 1995 and Harding, 1997).

$$P = \left(\frac{f}{f_0}\right) \left[\frac{\bar{v}}{v_s}\right]^{1/3} \quad (2-14)$$

Standardised sedimentation coefficient values can also be related to molecular weight via the Mark-Houwink-Kuhn-Sakurada (MHKS) equation (see *e.g.* Harding, 1992; Jumel 1994, Tombs and Harding, 1998).

$$s_{20,w}^0 = K'' M_w^b \quad (2-15)$$

where  $K''$  and  $b$  are obtained from the intercept and slope of the double log plot of  $s_{20,w}^0$  vs.  $M_w$  respectively (**Figure 2-9**). The value of  $b$  can be used as an estimation of gross macromolecular conformation and hence  $b$  values of  $\sim 0.67$  correspond to spheres, 0.4-0.5 to random coils, and  $\sim 0.15$  to rigid rods (see *e.g.* Tombs and Harding, 1998; Jumel, 1994).

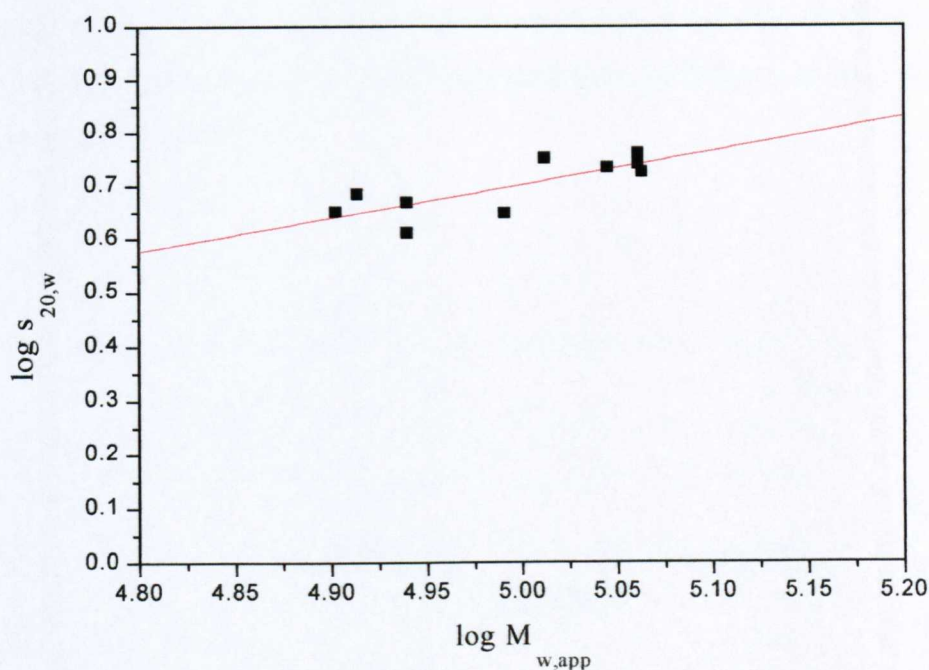


**Figure 2-9** MHKS sedimentation plot for sodium caseinate at different concentrations.

### 2.2.2 Sedimentation Equilibrium in the Analytical Ultracentrifuge

In contrast to sedimentation velocity, sedimentation equilibrium requires only moderate angular velocities (up to 25,000 rpm), depending on the size of the macromolecule (van Holde, 1985). As the solute sediments towards the cell base the concentration therefore increases at base, this sets up a diffusion gradient, which opposes that of sedimentation. After a certain amount of time the two processes reach dynamic equilibrium and the solute concentration increases exponentially towards the cell base (**Figure 2-10**).

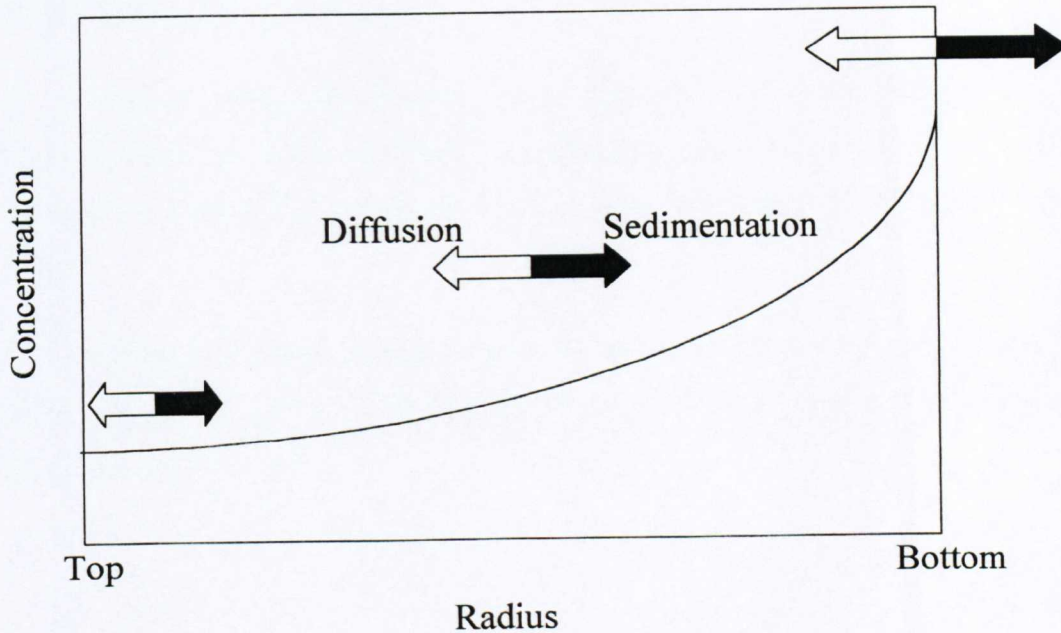


**Figure 2-10** Schematic representation of sedimentation equilibrium. At equilibrium, the resulting concentration distribution is exponential with the square of the radial position (adapted from Ralston, 1993).

It can be shown that for a single, ideal solute –

$$M = \frac{2RT}{(1 - \bar{v}\rho)\omega^2 \frac{d(\ln c)}{dr^2}} \quad (2-16)$$

where  $M$  is the molecular weight and  $c$  is the concentration of solute in g/ml, thus a plot of  $\ln(\text{concentration})$  vs.  $r^2$  yields a slope proportional to  $M$ . Sedimentation equilibrium can be used to determine molecular weights of molecules from 342 g/mol *e.g.* sucrose up to several million g/mol *e.g.* bushy stunt virus (van Holde, 1985). Information can also be gained on regarding polydispersity, association/ dissociation and non-ideality (Creeth and Harding, 1982). Solute distributions at sedimentation equilibrium and data subsequently analysed using the QUICKBASIC algorithm MSTAR (Cölfen & Harding, 1997).

### 2.2.2.1 MSTAR

The MSTAR program estimates

- (i) molecular weight for the whole distribution of solute in the ultracentrifuge cell (from meniscus to cell base) using the operational point average, the “star average”  $M^*$ , and the identity  $M^*(\text{cell base}) = M_{w,app}$ . (the apparent weight average molecular weight).
- (ii) the apparent point average weight average molecular weight as a function of radial position,  $M_{w,app}(r)$ . These values are obtained by the sliding strip procedure as described in Teller (1973).

There are 2 forms of this program MSTARA and MSTARI

**MSTARA:** For the analyses of UV (or visible) absorption records from sedimentation equilibrium.

Molecular weights are obtained from the MSTARA program using the  $M^*$  function defined by –

$$M^*(r) = \frac{(A(r) - A_{Meniscus})}{kA_{Meniscus}(r^2 - Meniscus^2) + 2k \int_{Meniscus}^r [A(r) - A_{meniscus}] dr} \quad (2-17)$$

where  $M^*$  is known as the star average molecular weight and

$$k = \frac{(1 - \bar{v}\rho)\omega^2}{2RT} \quad (2-18)$$

The  $M^*$  function is then plotted against  $\xi$ , the normalised squared radial position

$$\xi = \left( \frac{r^2 - a^2}{b^2 - a^2} \right) \text{ (at the meniscus (a), } \xi=0 \text{ and cell base (b) } \xi=1\text{). Creeth and Harding}$$

(1982) have shown that the  $M^*$  function at the cell base is identical to the *apparent* weight average molecular weight,  $M_{w,app}$  for the whole distribution of macromolecules in the centrifuge cell, *i.e.*

$$M^*_{at\xi=1} = M_{w,app} \quad (2-19)$$

Therefore an extrapolation of the  $M^*$  function to the cell base (usually linear) yields the apparent weight average molecular weight,  $M_{w, app}$ .

Point average molecular weights ( $M_{w, app}(r)$ ) can also be calculated from plots of  $\ln A(r)$  vs.  $r$ . Local slopes along the curve give the local or “point” average for that position in the centrifuge cell.

$$M_{w, app}(r) = \frac{d \ln A(r)}{kd(r^2)} \quad (2-20)$$

Due to the small amount of data points for absorption optics (compared to interference optics) point average molecular weight plots from absorption optics may be noisy. Since each  $r$  corresponds to a particular concentration or absorption  $A(r)$ , a plot of  $M_{w, app}$  versus not only  $r$ , but also versus  $A(r)$  can be produced.

**MSTARI:** A similar procedure also applies for  $M_w$  calculation from Rayleigh interference optics. However, since interference optical records are of concentration *relative to the meniscus*, the meniscus concentration needs to be calculated before absolute concentrations can be obtained and (i) and (ii) subsequently performed. For this, the “intercept over slope” method as described in Creeth and Harding, (1982) is employed in the initial stage of running MSTARI.

$$[\text{Note - } J(a) = \int \frac{2 \times \text{int ercept (at meniscus)}}{\text{lim ing slope (at meniscus)}} \text{ of a plot of } \frac{j(r)}{r^2 - a^2} \text{ vs. } \frac{\int_r^r j(r) dr}{r^2 - a^2}].$$

The value can be checked if the total initial loading concentration is known,  $J_0$ , due the principal conservation of mass and hence  $J(a)$  is correct if  $J_{0, calc} = J_0$ .  $J_0$  can be measured by a separate experiment using a special synthetic boundary cell (see *e.g.* Hall *et al*, 1999)

$$J_{0,calc} = \frac{2}{b^2 - a^2} \int_{Meniscus}^{Bottom} [J(a) + j(r)] r dr \quad (2-21)$$

and therefore

$$M^*(r) = \frac{(J(r) - J(a))}{kJ(a)(r^2 - a^2) + 2k \int_a^r [J(r) - J(a)] dr} \quad (2-22)$$

Molecular weight is then calculated from the M\* function in the same way as for absorption optics, and point average molecular weights as follows –

$$M_{w,app}(r) = \frac{d \ln J(r)}{kd(r^2)} \quad (2-23)$$

**Polydispersity and Non-ideality:** The use of MSTARA (Absorption optics) and MSTARI (Interference optics) facilitates the estimation of non-ideality/ polydispersity from the slope of  $\ln J(r)$  vs.  $\xi$  for interference ( $\ln A(r)$  vs.  $\xi$  for Absorbance). Where  $J(r)$  is the concentration in fringes at a specific radial position ( $A(r)$  is the concentration in Absorption units). A straight line in the graph of  $\ln(c)$  vs.  $\xi$  (or  $r^2$ ) indicates ideal behaviour (**Figure 2-11a**), an upward curvature indicates polydispersity or self-association (**Figure 2-11b**) and a downward curvature indicates non-ideality (**Figure 2-11c**). It must be noted that both processes could cancel out producing a pseudo-ideal linear plot.

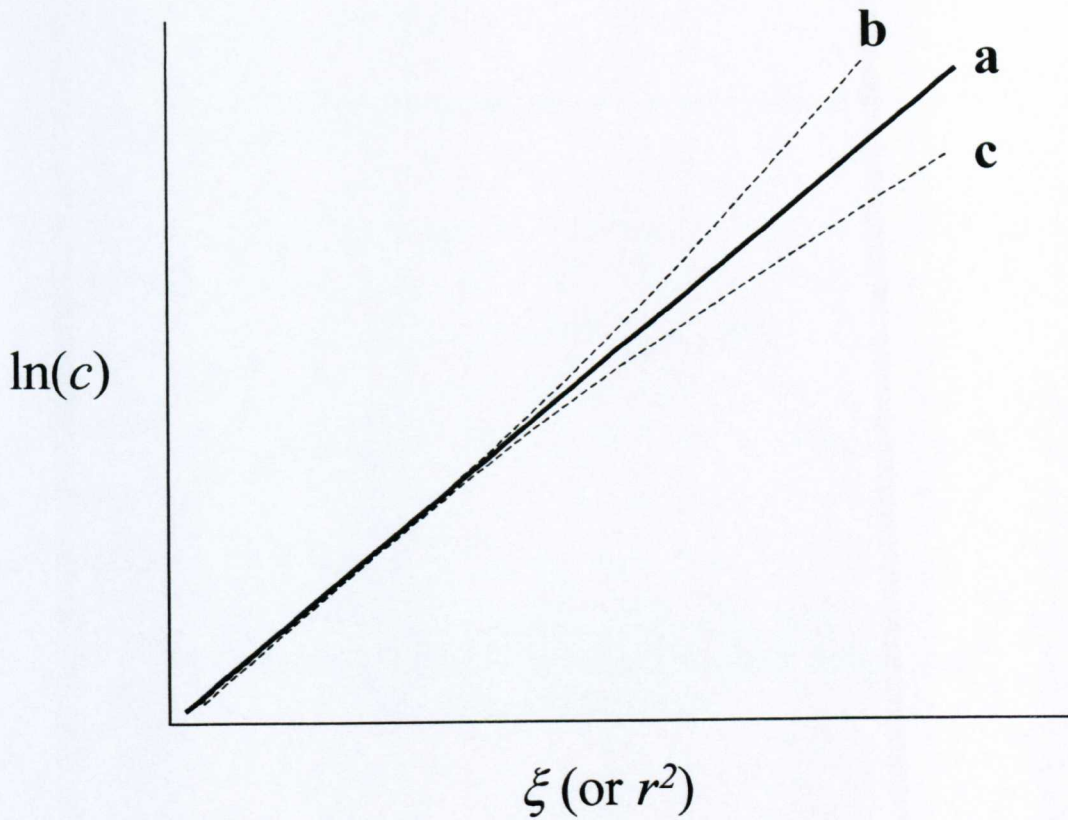


**Figure 2-11**  $\ln(c)$  vs.  $\xi$  (or  $r^2$ ) showing deviations from ideality (adapted from McRorie & Voelker, 1993).

In order to account for thermodynamic non-ideality, calculated apparent molecular weights should be extrapolated to zero concentration (**Figure 2-12**).

$$\frac{1}{M_{w,app}} = \frac{1}{M_w} + 2Bc + \dots \quad (2-24)$$

where  $B$  is the 2<sup>nd</sup> thermodynamic (osmotic pressure) virial coefficient. Equation 2-24 applies to dilute solutions. At higher concentrations and/ or highly non-ideal solutions such as alginate or xanthan higher order terms *i.e.* ( $c^2$  and  $c^3$  etc.) may be necessary.

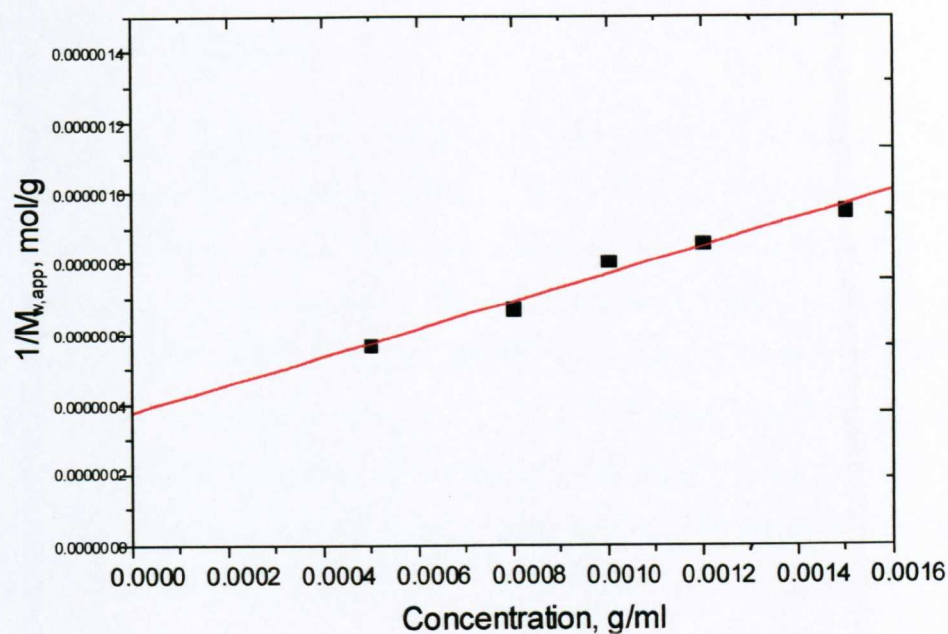


**Figure 2-12** Concentration dependency of apparent molecular weight for the halophilic cyanobacterium *Aphanothece Halophytica GR02*.

High non-ideality of polysaccharides derives from their large excluded volume due molecular asymmetry (*i.e.* axial ratio) and hydration and/ or polyelectrolyte behaviour (Harding *et. al.*, 1991).

It is always highly useful to obtain complementary evidence from other independent and absolute technique for example light scattering (see for example, Harding *et. al.*, 1990; Jumel, 1994; Morris *et. al.*, 2000).

## 2.3 VISCOMETRY

### 2.3.1 Theory of Viscosity

The viscosity of a fluid is a measure of resistance to flow and is dependent on occupied volume (Einstein 1906, 1911). The mechanics of viscous flow are however quite complex (for a more detailed explanation see *e.g.* van Holde, 1985 – we give a summary here). If we consider the simple arrangement (**Figure 2-13**) where liquid is held between two infinitely large parallel plates, one of which is moving in the direction  $x$  with a constant velocity  $v$ . It is the resistance to sliding that is measured by viscosity. This deformation experience by the liquid is known as shear and the shear strain at any point can be referred to as  $dx/dy$ . When a liquid is subjected to a constant shear strain it will shear at a constant rate (as long as the stress is maintained).

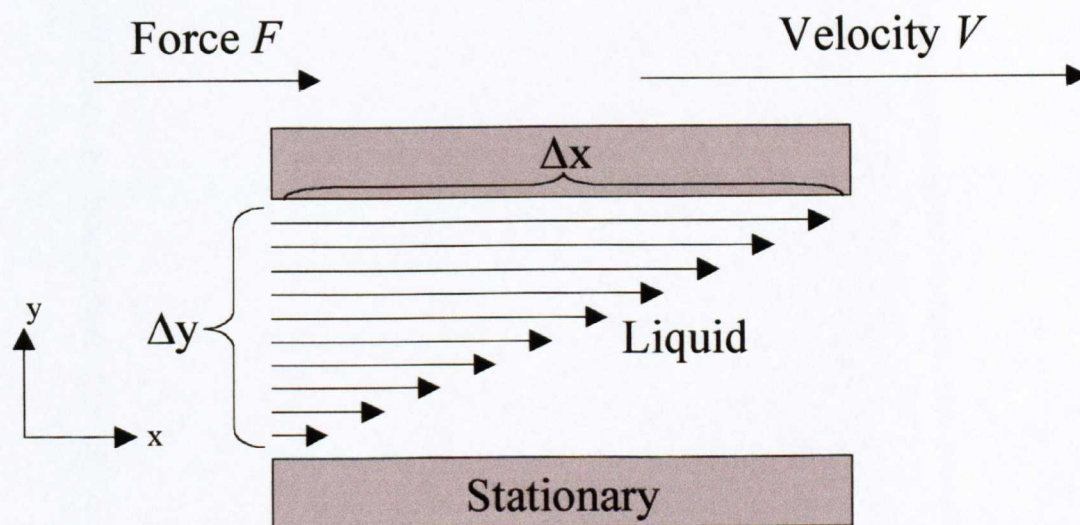


**Figure 2-13** A schematic representation of the shearing of a liquid between 2 parallel plates. The arrows represent fluid velocities at different values of  $y$  (adapted from van Holde, 1985).

Therefore, for Newtonian liquids -

$$\sigma = \eta \frac{d}{dt} \left( \frac{dx}{dy} \right) = \eta \frac{d}{dy} \left( \frac{dx}{dt} \right) \quad (2-25)$$

where  $\eta$  is the viscosity of the liquid and has the units  $\text{g.cm}^{-1}.\text{s}^{-1}$  more commonly abbreviated to poise (P).

According to Einstein, viscosity could also be defined as a measure of the rate of energy dissipation of flow and shear rate can then be defined as  $v/\Delta y$ .

$$\frac{F}{A\Delta y} \frac{dx}{dt} = \eta \left( \frac{v}{\Delta y} \right)^2 \quad (2-26)$$

In equation (2-26)  $F.dx$  is the energy expended in the time  $dt$  and  $A.\Delta y$  is the volume of fluid.

$$\eta \left( \frac{v}{\Delta y} \right)^2 = \frac{dE}{dt} \quad (2-27)$$

When measuring viscosity one must first measure the viscosity of the solvent by calculating the shear force required to maintain the shear rate, if we then add a number of rigid particles, which occupy the fraction,  $\phi$  of the solution volume. A greater force is then required to maintain a constant shear rate.

$$\left(\frac{dE}{dt}\right) > \left(\frac{dE}{dt}\right)_0 \quad (2-28)$$

This new rate of energy dissipation is related to the rate of the pure solvent as follows

$$\left(\frac{dE}{dt}\right) \approx \left(\frac{dE}{dt}\right)_0 (1 + \nu\phi) \quad (2-29)$$

and the simple ratio of viscosities can be formulated

$$\frac{\eta}{\eta_0} = (1 + \nu\phi) \quad (2-30)$$

where  $\nu$  is 2.5 for a sphere (Einstein, 1906, 1911).

### 2.3.2 Measurement of Viscosity (in dilute solution)

Viscosity can be measured in many different ways (Figure 2-14), however here we consider the Ostwald viscometer (the most common and simplest).

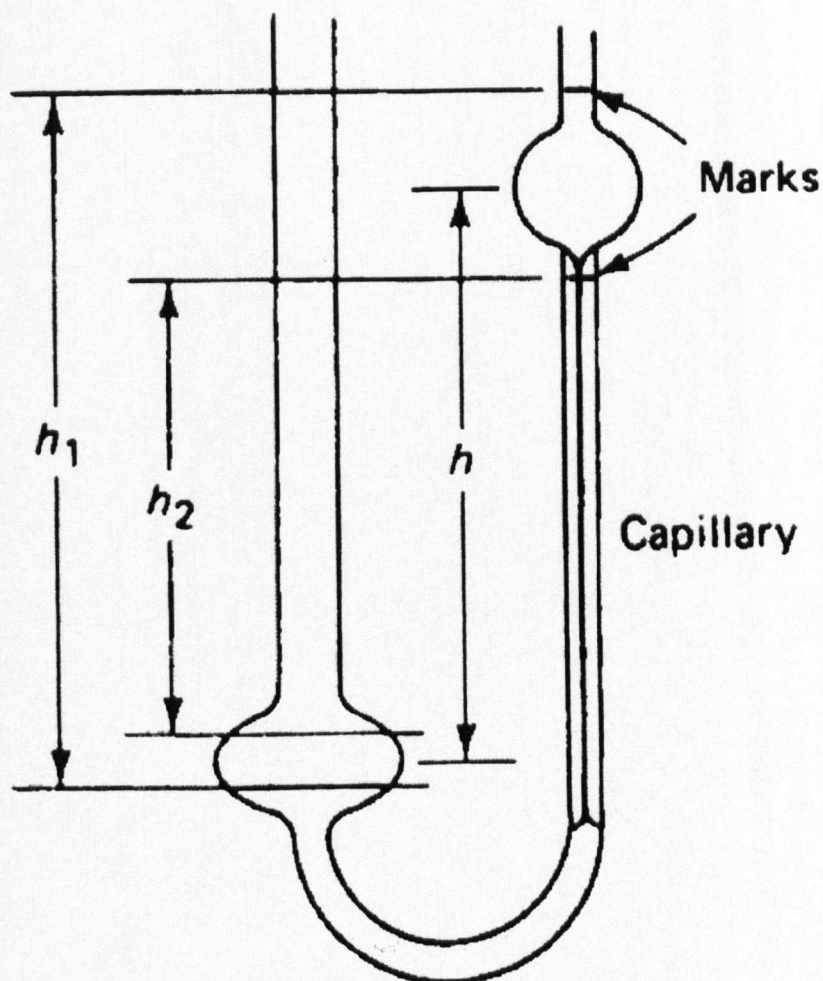


Figure 2-14 Schematic representation of an Ostwald viscometer (adapted from van Holde, 1985).

The rate of flow of a solvent through a capillary (radius,  $a$  and length,  $l$ ) when driven by pressure,  $P$  will according to Poiseuille's law be

$$\left(\frac{dV}{dt}\right) = \frac{\pi a^4 P}{8\eta l} \quad (2-31)$$

$$P = hg\rho \quad (2-32)$$

where  $g$  is the gravitational constant.

As the bulb empties from  $h_1$  to  $h_2$ , the height,  $h$  will vary slightly  $\therefore$  on integration

$$t = \frac{\eta}{\eta_0} = \left(\frac{8l}{\pi g a^4} \int_{h_1}^{h_2} \frac{dV}{h}\right) \quad (2-33)$$

where all parameters in brackets are instrumental constants (van Holde, 1985). Therefore the simple ratio of viscosities can be given and is known as the relative viscosity,  $\eta_{rel}$ .

$$\frac{\eta}{\eta_0} = \left(\frac{t}{t_0}\right)\left(\frac{\rho}{\rho_0}\right) = \eta_{rel} \quad (2-34)$$

where  $t$  is the flow time for the macromolecular solution,  $t_0$  is the flow time for the solvent in seconds. Because of the low concentration used ( $\rho/\rho_0$ ) is usually taken as unity (see *e.g.* Harding, 1997). The specific,  $\eta_{sp}$  and the reduced viscosities,  $\eta_{red}$  can then be defined as follows

$$\eta_{sp} = \eta_{rel} - 1 \quad (2-35)$$

$$\eta_{red} = \frac{\eta_{sp}}{c} \quad (2-36)$$

A further viscosity term, the inherent viscosity  $\eta_{inh}$  can also be defined.

$$\eta_{inh} = \frac{(\ln \eta_{rel})}{c} \quad (2-37)$$

Due to non-ideality both the reduced and inherent viscosities are concentration dependent. The value of the parameters in the limit  $c \rightarrow 0$ , is known as the intrinsic viscosity (IUPAC nomenclature – limiting viscosity number),  $[\eta]$  (van Holde, 1985; Harding, 1997; Arias *et. al.*, 1998). This value is either extrapolated to zero concentration on a Huggins (Huggins, 1942) plot  $\eta_{red}$  vs.  $c$  (Equation 2-38) or a Kraemer plot  $\eta_{inh}$  vs.  $c$  (Equation 2-40) (see *e.g.* Harding, 1997) (**Figure 2-15**).

$$\eta_{red} = [\eta](1 + K_H [\eta]c) \quad (2-38)$$

$$\eta_{red} = [\eta](1 + k_{\eta}c) \quad (2-39)$$

$$\frac{\ln(\eta_{rel})}{c} = [\eta](1 - K_K[\eta]c) \quad (2-40)$$

where  $K_H$ ,  $k_{\eta}$  (Rowe, 1977) and  $K_K$  are the Huggins, “viscosity regression” and Kraemer coefficients respectively.

A common method for measuring intrinsic viscosities is to calculate the relative and specific viscosities at one concentration and invoke the Solomon/ Ciuta approximation (Harding, 1997, Morris *et. al* 2000, Abel-Azim *et. al*, 1999, Kravtchenko and Pilnik, 1990) (**Figure 2-15**). According to Kravtchenko and Pilnik (1990), the intrinsic viscosity can be accurately estimated (error 1%) by a single measurement at low concentration. In the same article he achieved good agreement between single point measurements and traditional multi-point extrapolations (see *e.g.* Harding, 1997, Kravtchenko and Pilnik, 1990, Morris *et. al*, 2000), this is in good agreement with **Figure 2-15** (Morris, unpublished).

$$[\eta] \approx \frac{[2\eta_{sp} - 2 \ln \eta_{rel}]^{1/2}}{c} \quad (2-41)$$

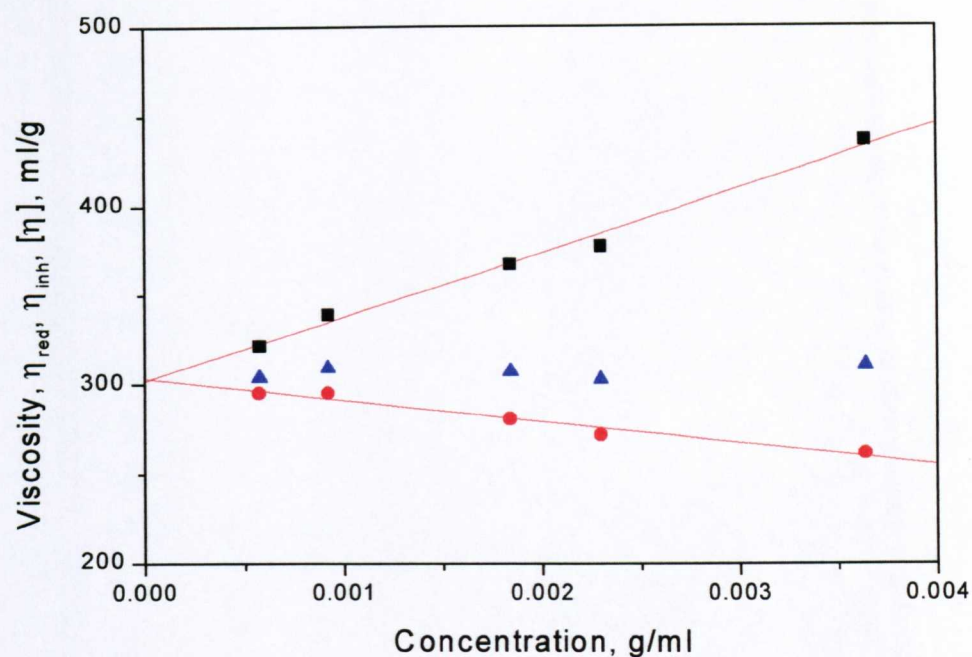


**Figure 2-15** The Huggins (black squares), Kraemer (red circles) and Solomon-Ciuta (blue triangles) plots for the low methoxy pectin HL 7192.

Intrinsic viscosity can also be related to molecular weight via a Mark- Houwink (MHKS) relationship.

$$[\eta] = k' M_w^a \quad (2-42)$$

where  $k'$  and  $a$  are obtained from the intercept and slope of the double log plot of  $[\eta]$  vs.  $M_w$  respectively (**Figure 2-16**). The value of  $a$  can be used as an estimation of gross macromolecular conformation and hence  $a$  values of  $\sim 0$  correspond to spheres, 0.5-0.8 to random coils, and up to 1.8 to rigid rods (see *e.g.* Jumel, 1994; Tombs & Harding, 1998).

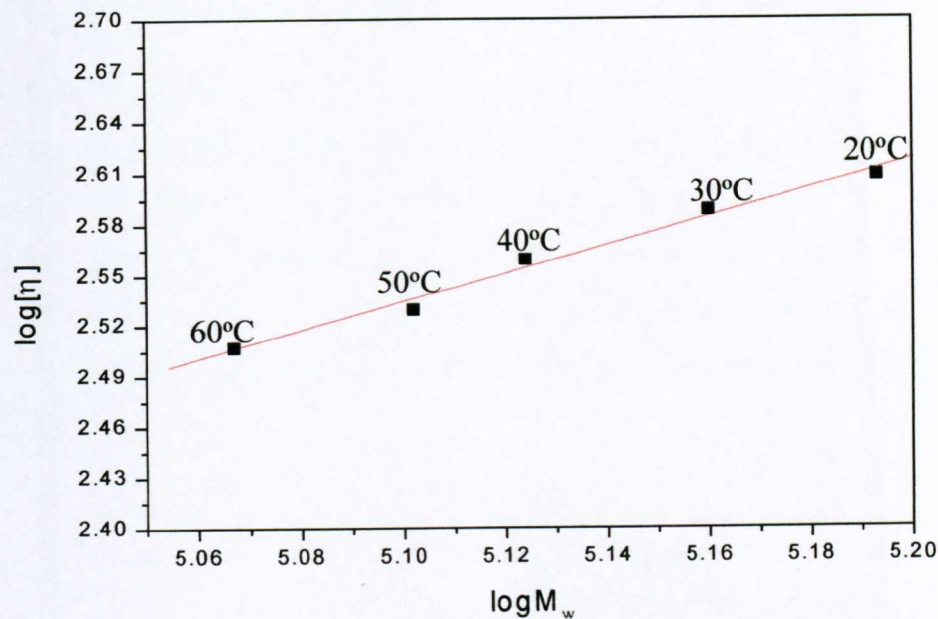


**Figure 2-16** The pseudo Mark-Houwink (MHKS) plot for the high-methoxy pectin HR 7021 at different temperatures. [Note – this is a pseudo MHKS plot in the sense that it does convey results for a fractionated system].

$$[\eta] = \nu v_s \quad (2-43)$$

where  $\nu$  (the Einstein viscosity increment) has a minimum value of 2.5 for a sphere and increases for more asymmetric molecules (Einstein, 1906, 1911; Jumel, 1994 and Harding, 1997) and  $v_s$  is the swollen volume (see Equation 2-11).

### 2.3.3 Measurement of Viscosity (in concentrated solution)

Capillary viscometers are more than adequate for the evaluation of viscosities of a many macromolecules at low concentration, however in the capillary the shear rate varies with distance from the capillary wall. This is important for non-Newtonian liquids where the viscosities are dependent on shear rate. Many viscometers have been designed to counter the shear-rate dependency, the simplest being the cone and plate viscometer (Figure 2-17). Flow is induced by the rotation of the either the cone or plate.

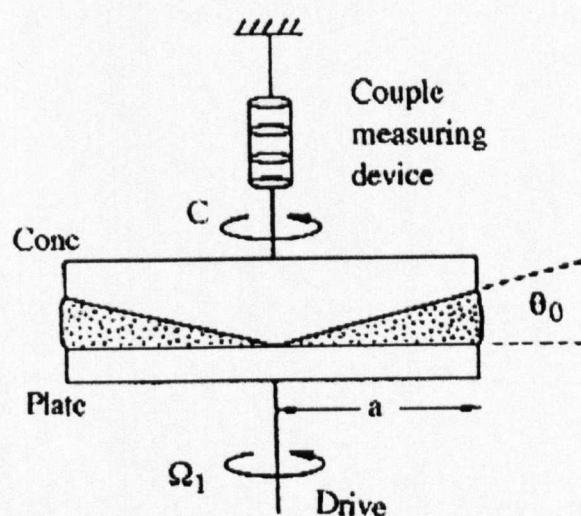


**Figure 2-17** A schematic representation of a cone and plate viscometer (adapted from van Holde, 1985 see also Jumel, 1994)

If the gap angle  $\theta_0$  is sufficiently small, the shear rate is approximately uniform in the entire liquid and is given by –

$$\dot{\gamma} = \frac{\Omega_1}{\theta_0} \quad (2-44)$$

where  $\Omega_1$  is the angular velocity of the rotating plate.

The shear stress is

$$\sigma = \frac{3c}{2\pi a^3} \quad (2-45)$$

where  $a$  is the radius of the cone and  $c$  is the torque experienced by the cone or plate and the viscosity can therefore be defined as –

$$\eta = \frac{3c\theta_0}{2\pi a^3 \Omega_1} \quad (2-46)$$

In order to fit the shape of a general flow curve for polymer solutions, at least four parameters are needed. The Cross-equation (Cross, 1965) is a very useful semi-empirical relation to calculate these parameters –

$$\frac{\eta - \eta_\infty}{\eta_0 - \eta_\infty} = \frac{1}{(1 + (K \dot{\gamma})^m)} \quad (2-47)$$

where  $\eta_0$  and  $\eta_\infty$  refer to the values of viscosity at very low and very high shear rates respectively.  $K$  is a constant with dimensions of time and  $m$  is a dimensionless constant.

Viscosities are usually extrapolated to zero shear and  $\eta_{red,0}$  (or  $\eta_{inh,0}$ ) are then plotted against concentration as with capillary viscometry to calculate the intrinsic viscosity. For many polysaccharides a distinct curvature in the Huggins's plot ( $\eta_{red,0}$  vs.  $c$ ) is a common manifestation of the critical coil overlap concentration,  $c^*$ .  $c^*$  is defined as the onset of significant coil overlap in concentrated solution and is dependant on molecular size (and shape) (**Figure 2-18**).

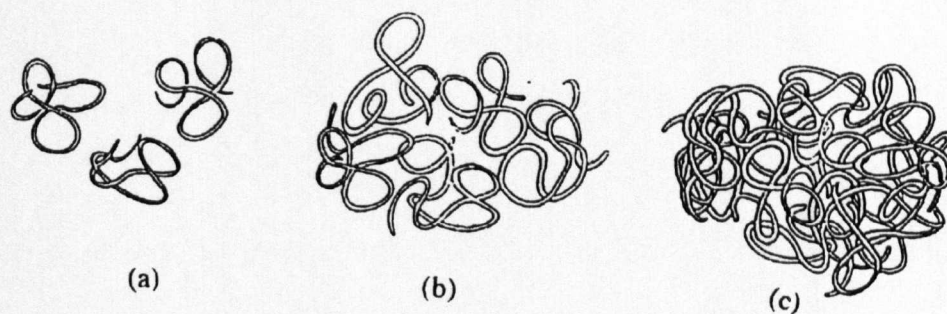


**Figure 2-18** Representation of (a) macromolecules in dilute solution (e.g.  $c < c^*$ ); (b) onset of overlapping coils ( $c = c^*$ ) and (c) polymer network ( $c > c^*$ ) (adapted from Morris *et. al.*, 1981 see also Jumel, 1994).

## 2.4 SIZE EXCLUSION CHROMATOGRAPHY – MULTI-ANGLE LASER LIGHT SCATTERING

Before considering the combined size exclusion chromatography – multi-angle laser light scattering system it is first necessary to consider each process separately.

### 2.4.1 Light Scattering

Light scattering is one of the few absolute, thermodynamically rigorously founded methods for the determination of molar masses and is therefore one of the most fundamental methods in polymer science. More detailed explanations of the physics behind light scattering can be found in Wyatt, 1992; Kratochvil, 1972, Jumel, 1994 van Holde, 1985 and Kratochvil, 1987.

For small molecules, where the radius of gyration,  $R_g$  is considerably less than the wavelength of incident light *e.g.*  $R_g < \lambda/20$  then

$$i_\theta = \frac{I_0 n}{r^2} \frac{16\pi^2 \alpha^2}{\lambda^4} \cos^2 \theta \quad (2-48)$$

where  $\theta$ , is the scattering angle;  $i_\theta$  is the intensity of scattered light;  $I_0$  is the incident light intensity;  $r$  is the distance between the scattering molecule and the detector;  $n$  is the refractive index of the solution,  $\alpha$  is the polarisability of the scattering molecule and  $\lambda$  is wavelength of incident light.

The introduction of the scattering volume,  $V$ , containing  $n$  scattering centres, we can then define the Rayleigh ratio (or factor),  $R_\theta$  (Equation 2-49).

$$R_{\theta} = \frac{16\pi^4 \alpha^2 n}{\lambda^4 V} \quad (2-49)$$

where  $\alpha$  is the polarisability and is proportional to the specific refractive index,  $dn/dc$ .

$$\alpha = \frac{Mn_0}{2\pi N_A} \frac{dn}{dc} \quad (2-50)$$

where  $n_0$  is the refractive index and  $dn/dc$  is the change in refractive index with concentration (see *e.g.* Cassassa and Eisenberg, 1961; Huglin, 1972). We can define the total number of scattering centres with a certain scattering volume as

$$\frac{n}{V} = \frac{cN_A}{M} \quad (2-51)$$

then equation (2-51) can be rewritten as

$$R_{\theta} = \frac{2\pi^2 Mn_0^2 c}{N_A \lambda^4} \left(\frac{dn}{dc}\right)^2 \text{ or} \quad (2-52)$$

$$R_{\theta} = KMc \quad (2-53)$$

where  $K$  is a constant for a given polymer

$$K = \frac{2\pi^2 n_0^2}{N_A \lambda^4} \left( \frac{dn}{dc} \right)^2 \quad (2-54)$$

In terms of thermodynamics this can be described as the free energy required to create a concentration gradient in a solution due to osmotic pressure,  $\Pi$

$$\frac{Kc}{R_\theta} = \frac{1}{RT} \frac{d\Pi}{dc} \quad (2-55)$$

$\Pi$  can be expanded in the form of the virial expansion as for osmotic pressure experiments

$$\frac{Kc}{R_\theta} = \frac{1}{M_w} + 2Bc + 3Cc^2 + \dots \quad (2-56)$$

where B, C, etc. are the 2<sup>nd</sup>, 3<sup>rd</sup> and subsequent virial coefficients respectively (as in sedimentation equilibrium), however in dilute solutions virial coefficients of the third and higher are usually ignored [**Note** – the virial coefficients are usually called  $A_2$  and  $A_3$  in light scattering terminology, but are called B and C here in order to be consistent with the analytical ultracentrifugation explanation].

Most macromolecules (molecular weight greater than 30,000g/mol) have a radius of gyration  $R_g > \lambda/20$ . Larger molecular dimensions mean that a single molecule can have many scattering points and the light from these different scattering points will reach the detectors in different phases, due to intramolecular interference. Therefore as the Rayleigh factor,  $R_\theta$  is a function of  $\theta$ , the scattering intensity is reduced due to interference at all angles except zero. However, this internal interference depends on the size and shape of the macromolecule. Therefore the angular dependency in itself

can yield important information on size and conformation and can be explained in terms of a scattering function,  $P(\theta)$

$$P(\theta) = \frac{R_\theta}{R_0} \quad (2-57)$$

where at zero angle  $P(\theta) = 1$ . In practice  $R_0$  is difficult to measure and is usually calculated by extrapolation of  $R_\theta$  to zero angle. This has the added advantage of calculating  $R_g$  without any prior assumptions of shape (Tanford, 1961).

$$\lim_{\theta \rightarrow 0} \frac{1}{P(\theta)} = 1 + \frac{16\pi^2}{3\lambda^2} \langle R_g^2 \rangle \sin^2\left(\frac{\theta}{2}\right) \quad (2-58)$$

and by the further extrapolation to zero concentration (Zimm, 1948, see also Harding *et. al.*, 1991; Jumel, 1994).

$$\lim_{\theta \rightarrow 0}(c \rightarrow 0) \frac{Kc}{R_\theta} = \frac{1}{M_w P(\theta)} = \frac{1}{M_w} \left(1 + \frac{16\pi^2}{3\lambda^2} \langle R_g^2 \rangle \sin^2\left(\frac{\theta}{2}\right)\right) \quad (2-59)$$

One then constructs the double Zimm plot  $\frac{Kc}{R_\theta}$  vs.  $Kc$  which yields  $\frac{1}{M_w}$  from the

intercept and B from the slope, furthermore from  $\frac{Kc}{R_\theta}$  vs.  $\sin^2\left(\frac{\theta}{2}\right)$  we can measure  $R_g$

from the limiting slope  $\frac{16\pi^2}{3\lambda^2} \langle R_g^2 \rangle$  (Figure 2-19).

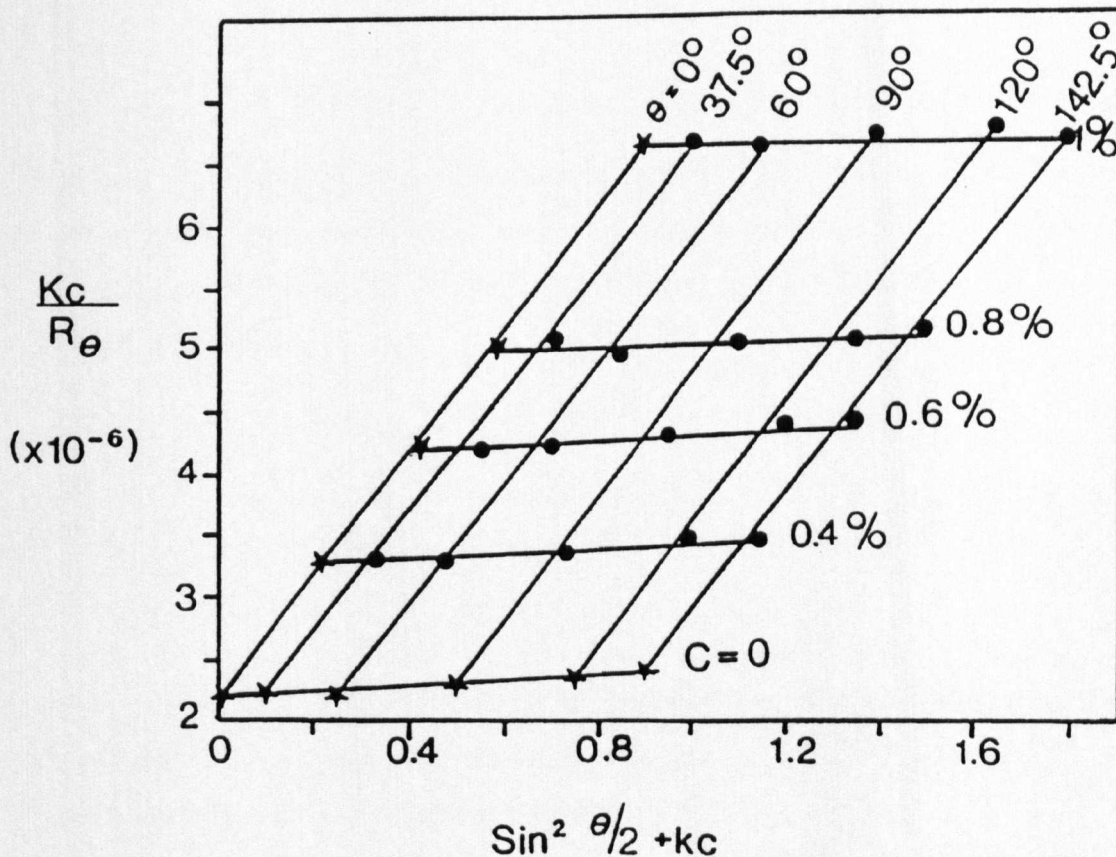


**Figure 2-19** Construction of a Zimm plot - Abscissa  $\sin^2(\theta/2) + kc$  and ordinate  $Kc/R_\theta$  adapted from Harding *et. al.*, 1991. Molecular weight, radius of gyration and virial coefficients can then be calculated from Equation 2-59.

#### 2.4.2 Size Exclusion Chromatography (SEC)

Size exclusion chromatography is based on the simple principle of the separation of molecules due to size (hydrodynamic volume). The chromatographic column consists of a matrix of porous polymer beads and solute molecules will penetrate in and out of these pores, thus setting up an equilibrium between the concentration (of solute) inside and outside the polymer beads. The volume of mobile phase inside and outside the pores is collectively known as  $V_M$ , and the internal pore volume  $V_i$  is essentially the stationary phase. The remaining mobile phase the interstitial liquid between the packing particles is the void volume,  $V_0$  (Jumel, 1994).

$$V_M = V_i + V_0 \quad (2-60)$$

The partition of solvent between phases can be described  $K_D$  ( $0 \leq K_D \leq 1$ ), which is the ratio of average solute concentration inside and outside the pores and is independent of flow rates or column length. Therefore the total accessible volume for the solute is the retention volume  $V_R$ .

$$V_R = V_0 + K_D V_i \quad (2-61)$$

If  $K_D=0$ , then  $V_R=V_0$  and the molecule is therefore too large to diffuse into the column matrix, this is known as the total exclusion volume, and when  $K_D=1$  the polymer can penetrate the entire bead matrix and  $V_R=V_M$ , which is called to total permeation volume. Retention in an SEC system is governed by changes in entropy between phases.

### 2.4.3 SEC-MALLS

SEC- MALLS (Size Exclusion Chromatography Coupled to Multi-Angle Laser Light Scattering). However, the major disadvantage of a stand alone SEC system is that one can only assign *relative* molecular weights by comparison with known standards, this relies on both the standards and sample of interest behaving at least similarly in the SEC column and that non-size exclusion processes due to molecular charge *etc* are kept to a minimum. As multi-angle laser light scattering is an *absolute* method of determining average molecular weights, it is clear that a prior separation technique such as an SEC system will enable detailed evaluation of the molecular weight of each fraction. With the addition of an on-line differential refractive index detector (or UV detector) one can calculate concentrations and can therefore calculate  $M_w$ , B and  $R_g$ . Hence SEC-MALLS has become the quickest and easiest method of determining absolute molecular weights and molecular weight distributions for many different macromolecules (Wyatt, 1992; Jumel, 1994) (**Figure 2-20** and **Figure 2-21**).

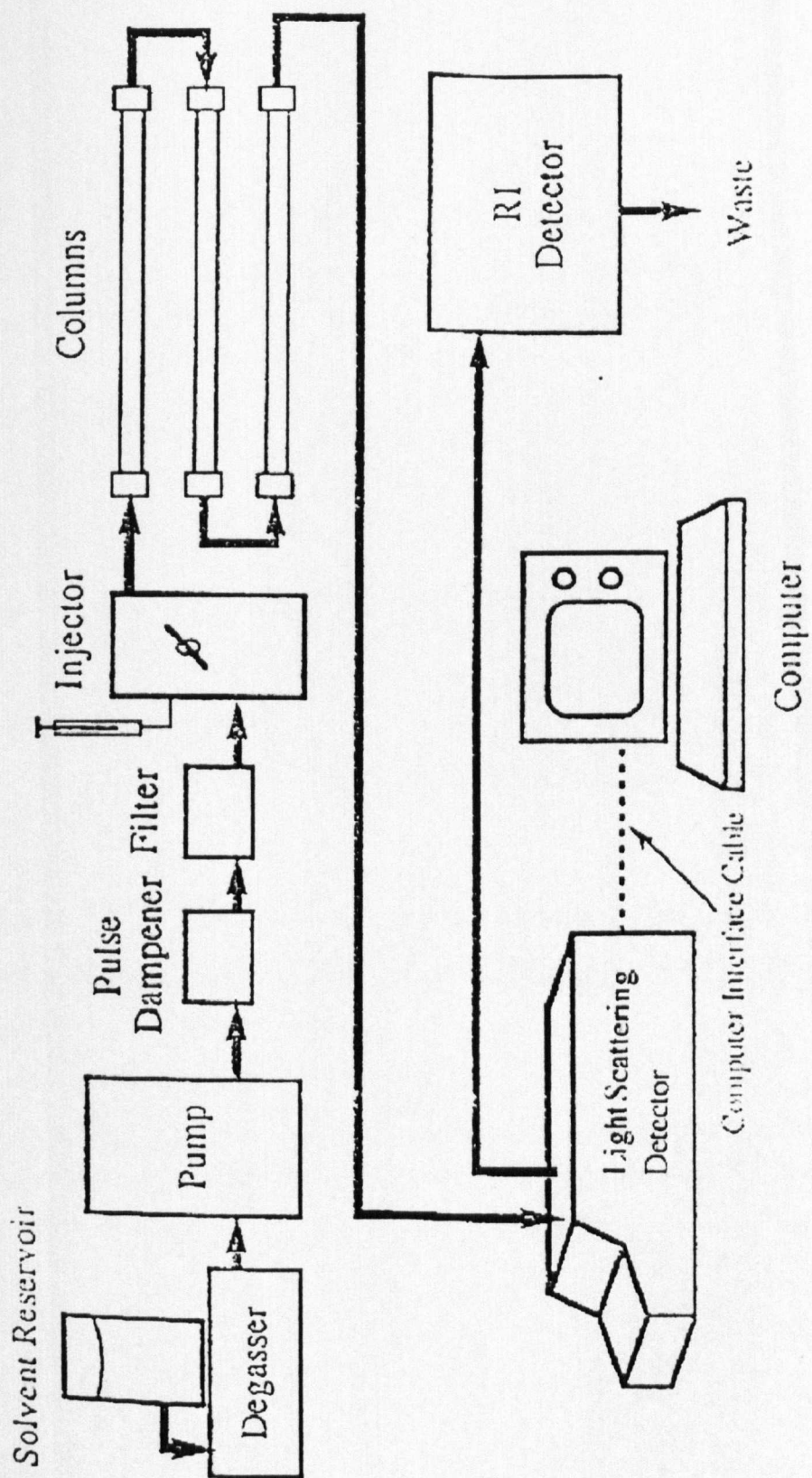
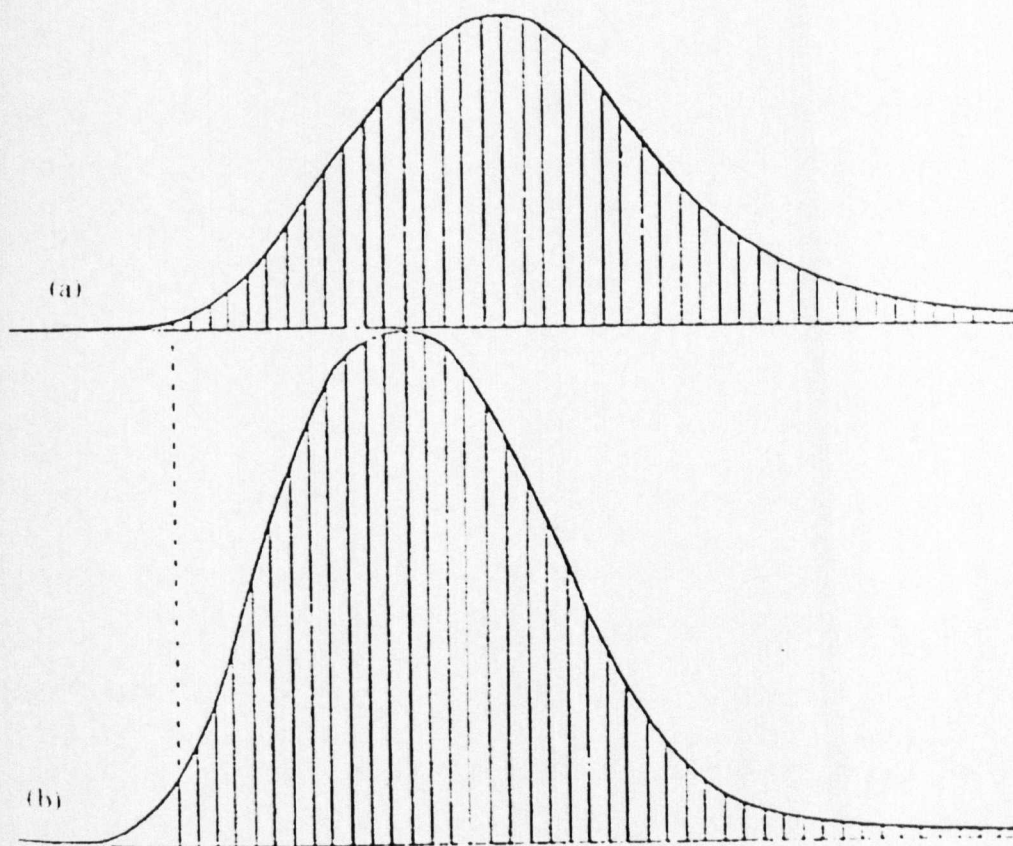


Figure 2-20 Schematic representation of the SEC-MALLS system (adapted from Jumel, 1994).



**Figure 2-21** Examples of elution traces from SEC-MALLS, (a) from the concentration ( $dn/dc$ ) detector, (b) light scattering detector (adapted from Jumel, 1994).

Information from each peak slice is used to calculate molecular weight and radius of gyration averages.

## 2.5 DYNAMIC LIGHT SCATTERING (DLS)

Dynamic Light Scattering is the technique used to calculate translational diffusion coefficients,  $D_t$ . The hydrodynamic radius can also be calculated from the Stokes-Einstein equation –

$$r_H = \frac{k_B T}{6\pi\eta D_t} \quad (2-62)$$

where  $k_B$  is the Stefan-Boltzmann constant ( $1.381 \times 10^{-16} \text{ ergK}^{-1}\text{mol}^{-1}$ ) (see *e.g.* Harding, 1999a).

DLS measures the diffusion of a macromolecule within a solution due to Brownian motion and measures the intensity fluctuations of scattered light as a function of time ( $10^{-3} \rightarrow 10^{-9}$ secs) (Harding, 1999a). The frequency of these fluctuations depends on how rapidly the solute molecules are moving due to diffusion. Due to the necessity for high light intensity, collimation, monochromaticity, and most importantly spatial and temporal coherence (light in the form of a continuous wave rather than short bursts) a laser is required (Harding, 1999a). Moving macromolecules will Doppler-broaden monochromatic incident light and the scattered intensity will fluctuate due to interference from scattered waves of different wavelengths, therefore this technique is often known as Quasi-Electric Scattering (QLS). Data from the intensity detectors is then sent to an autocorrelator, which compares the intensity at different times and the technique is therefore called Photon Correlation Spectroscopy (PCS). The rapidity of this fluctuation over time,  $\tau$  is represented by the normalised intensity autocorrelation function,  $g^{(2)}\tau$  where the (2) is indicative of intensity fluctuation as opposed to (1) electric field autocorrelation function.  $g^{(2)}\tau$  can be averaged as a function of  $\tau$  and can be used to calculate the translation diffusion coefficient,  $D_t$  (see *e.g.* Harding, 1999a)–

$$\ln[g^{(2)}(\tau) - 1] = 2D_t k^2 \tau \quad (2-63)$$

where  $k$  is the Bragg wave vector  $k = \frac{4\pi n}{\lambda} \sin \frac{\theta}{2}$  and  $n$  is the refractive index of the medium,  $\theta$  is the scattering angle and  $\lambda$  is wavelength of incident light. Extrapolation to zero angle is usually necessary, however the for near-spherical molecules, *e.g.* casein micelles, the decay is not affected by rotational diffusion effects and this extrapolation is not required. The translation diffusion coefficient is temperature dependent and is usually converted to standard conditions (20°C and water *c.f.* sedimentation coefficient, see Equation 2-10).

$$D_{20,w} = D^* \left( \frac{293.2}{T} \right) \left( \frac{\eta_{T,w}}{\eta_{20,w}} \right) \left( \frac{\eta_s}{\eta_w} \right) \quad (2-64)$$

As with sedimentation coefficients (Equations 2-8 and 2-9), diffusion coefficients are concentration dependent and extrapolation to zero concentration is necessary.

$$D_{20,w} = D^0_{20,w} (1 + k_D C + \dots) \quad (2-65)$$

where  $D^0_{20,w}$  is the translation diffusion coefficient at infinite dilution,  $D_{20,w}$  is the value at concentration,  $C$  and  $k_D$  is the concentration dependency (Harding and Johnson, 1985). The extrapolated diffusion coefficient can then be combined with the sedimentation coefficient to calculate  $M_w$  via the Svedberg equation (2-12). The translation diffusion coefficient can also be related to molecular weight through a Mark-Houwink (MHKS) relationship.

$$D^0_{20,w} = K'''' M^{-c} \quad (2-66)$$

where  $k''''$  and  $c$  are obtained from the intercept and slope of the double log plot of  $D_{20,w}^0$  vs.  $M_w$  respectively. The value of  $c$  can be used as an estimation of gross macromolecular conformation and hence  $c$  values of  $\sim 0.333$  correspond to spheres, 0.5-0.6 to random coils, and 0.85 to rigid rods (Tombs & Harding, 1998).

The translational frictional ratio (Tanford, 1961) can also be calculated from the following equation –

$$\frac{f}{f_0} = \frac{k_B T}{6\pi\eta_{20,w}} \left( \frac{4\pi N_A}{3V M_w} \right)^{1/3} \frac{1}{D_{20,w}^0} \quad (2-67)$$

For asymmetric molecules extrapolation to zero angle is also required – Dynamic Zimm plot (see *e.g.* Burchard, 1992; Štěpánek, 1993). At lower angles there increased problems due to dust particles. Many modern DLS instruments are fixed angle (90°) and are therefore only applicable for spherical or globular molecules for which angular dependency is very small.

## 2.6 PARTICLE SIZE DISTRIBUTION – LASER DIFFRACTION

When light interacts with a particle, one of three results can occur, the incident light can be absorbed, scattered or transmitted. Due to the law of the conservation of energies, the sum of these three energies should be equal to energy of the incident beam *i.e.*  $\Delta E = 0$ . For large particles it can be assumed that all light has interacted due to scattering. Therefore the measurement of scattered light,  $x$  can give information about the particle size. If one assumes that the particles are spherical (a sphere is unique since it can be characterised by a single linear dimension, the diameter or radius) then –

$$x = \frac{2\pi r}{\lambda} = \frac{\pi d}{\lambda} \quad (2-68)$$

where  $\lambda$  is the wavelength of incident light in the scattering medium. There is a general relationship between particle size and various scattering theories (see for example Errington, 1993) –

$d \ll \lambda$	$d < \frac{\lambda}{10}$	- Rayleigh scattering
$d = \lambda$		- Lorenz – Mie theory
$d \gg \lambda$	$d > 4\lambda$	- Diffraction (Fraunhofer theory)

Perhaps a more useful parameter is the relative index of diffraction (van der Hulst, 1957).

$$P = \frac{2\pi d |m - 1|}{\lambda} \quad (2-69)$$

where  $m$  is the refractive index of the particle with respect to the medium.

$P \ll 0.3$  - Rayleigh scattering

$P = 1$  - Lorenz – Mie theory

$P \gg 30$  - Diffraction (Fraunhofer theory)

For a sphere, disc or aperture of radius,  $r$  the resultant intensity of diffraction pattern is

$$i = i_0 \left[ \frac{2J_1(x)}{x} \right]^2 \quad (2-70)$$

where  $J_1$  is the first order spherical Bessel function and  $x = \frac{2\pi r s}{\lambda F}$  and  $s$  is the radial distance in the diffraction plane as measured from the optical axis and  $F$  is the focal length of the lens. The general Bessel equation is –

$$J_m(u) = \frac{i^{-m}}{2\pi} \int_0^{2\pi} e^{i(ms+u \cos \nu)} d\nu \quad (2-71)$$

where  $m$  is the order.

The intensity pattern can be measured and used to infer particle size distribution, Eq. (2-71) is integrated in order to give the fraction of light energy contained within a circle radius,  $s$  of the detector.

$$L = 1 - J_0^2(x) - J_1^2(x) \quad (2-72)$$

As the detector consists of a series of concentric rings one can determine the energy falling between two radii,  $s_1$  and  $s_2$  as

$$L_{s_1, s_2} = C\pi r^2 [J_0^2(x) - J_1^2(x)]_{s_1} - [J_0^2(x) - J_1^2(x)]_{s_2} \quad (2-73)$$

where  $\pi r^2$  is the cross-sectional area and  $C$  is the optical constant (depends on detector sensitivity and the power of the light source). Neglecting multiple diffraction, for  $N$  particles of radius,  $r$  we get –

$$L_{s_1, s_2} = C\pi \sum_{i=1}^M N_i r_i^2 [J_0^2(x) - J_1^2(x)]_{s_1} - [J_0^2(x) - J_1^2(x)]_{s_2} \quad (2-74)$$

this can be rewritten in terms of the weight of particles (W) assuming density of the particle is size independent –

$$L_{s_1, s_2} = K \sum \frac{W_i}{r_i} [J_0^2(x) - J_1^2(x)]_{s_1} - [J_0^2(x) - J_1^2(x)]_{s_2} \quad (2-75)$$

where K is a constant depending on the optical constant, C and particle density.

## 2.7 DENSIMETRY

Densimetry is widely used in physical biochemistry to calculate the partial specific volume,  $\bar{v}$  of the solute of interest. The Anton Paar (Graz, Austria) precision density meter consists of a U-shaped glass tube; the natural frequency of vibration of such a U-shaped tube filled with sample solution is dependant on the mechanical properties of the vibrating tube and on the density of the liquid within the tube (Kratky, *et. al.*, 1973). The densities of solvent and samples solutions can be estimated by measuring the time taken to perform a known number of oscillations *e.g.*  $1 \times 10^4$  (assuming one knows the oscillation time for a standard of known density, usually water). Therefore by calculating solution densities at different concentrations one can estimate the buoyancy factor  $(1 - \bar{v}\rho_0) = \Delta\rho/\Delta c$  and hence the partial specific volume,  $\bar{v}$ , where  $(1 - \bar{v}\rho_0)$  is slope of  $\rho - \rho_0$  versus concentration (where  $\rho$  and  $\rho_0$  are the densities of the sample solution and the buffer respectively).

## 2.8 COMBINED HYDRODYNAMIC APPROACHES

Although in the previous sections 2.2-2.7 the main hydrodynamic techniques have in general been discussed individually it is of course possible to combine two or more different types of measurement to give a more detailed picture of hydrodynamic structure (Rowe, 1977; Jumel, 1994 and Harding, 1997)

For instance one can compare the  $M_w$  values from the two *independent* and *absolute* techniques of SEC-MALLS and low speed sedimentation equilibrium. Molecular weights can also be equated to  $[\eta]$ ,  $s_{20,w}^0$  and  $D_{20,w}^0$  through a series of MHKS equations which have been defined in the relevant sections (Equations 2-42, 2-15 and 2-66 respectively). See Table 2-2.

**Table 2-2** Mark – Houwink (MHKS) conformational parameters from Equations 2-42, 2-15 and 2-66 – see *e.g.* Tombs and Harding (1998).

Conformation	a	b	c
Compact sphere	0	0.667	0.333
Rigid rod	1.8	0.15	0.85
Random coil	0.5-0.8	0.4-0.5	0.5-0.6

where a, b, and c are the exponents from viscosity, sedimentation and diffusion respectively.

One can further combine  $M_w$  with  $s^0_{20,w}$  (or  $D^0_{20,w}$ ) in the calculation of the translation frictional ratio (2-13 – Tanford 1961).

The classical Svedberg equation (2-12 Svedberg and Pedersen, 1940) combines  $s^0_{20,w}$  and  $D^0_{20,w}$ . The concentration dependency of sedimentation  $k_s$  can also be used to give information on molecular weight (equation 2-11 Rowe, 1977), conformation through combination with  $[\eta]$  (see *e.g.* Wales and Van Holde, 1954; Rowe, 1977).  $k_s$  can however be used to give an indication of swollen volume,  $v_s$  and of hydration,  $\delta$ .

$$k_s = 2 \bar{v} \left\{ \frac{v_s}{\bar{v}} + \left[ \frac{f}{f_0} \right]^3 \right\} \quad (2-76)$$

where

$$v_s = \bar{v} + \frac{\delta}{\rho_0} \quad (2-77)$$

and for spherical molecules,  $k_s = 4v_s$  (Rowe, 1992).

There are many other functions that can be used to estimate gross conformation; the  $\Pi$  function is the result of the combination of the weight average molecular weight,  $M_w$ , the 2<sup>nd</sup> virial coefficient, B and the intrinsic viscosity,  $[\eta]$ .

$$\Pi = \frac{2BM_w}{[\eta]} \quad (2-78)$$

A further combined hydrodynamic parameter is the Scheraga-Mandelkern function,  $\beta$  which combines,  $[\eta]$ ,  $s_{20,w}^0$ ,  $M_w$  and can be related to  $v$  and P.

$$\beta = \frac{[\eta]^{1/3} \eta_0 N_A s_{20,w}^0}{M_w^{2/3} (1 - \bar{v} \rho_0) 100^{1/3}} = \frac{N_A^{1/3}}{(16200\pi^2)^{1/3}} \frac{v^{1/3}}{P} \quad (2-79)$$

According to Rowe (Rowe, 1977, 1992) the concentration dependencies of viscosity,  $k_\eta$  and sedimentation,  $k_s$  can be combined to give an indication of  $v_s$  and therefore hydration.

$$\frac{k_\eta}{k_s} \sim \frac{v_s}{v} \quad (2-80)$$

All of these shape functions R, P,  $v$ ,  $\Pi$ ,  $\beta$  and  $f/f_0$  can be used to estimate an axial ratio and therefore gross ellipsoidal conformation (see *e.g.* Schachman, 1959; Harding and Cölfen, 1995, *etc.*). Macromolecules can in general be represented as spheres, rods or

coils or a conformation somewhere between these extremes, this can be represented graphically as the Haug triangle (Tombs and Harding, 1998) (**Figure 2-22**).

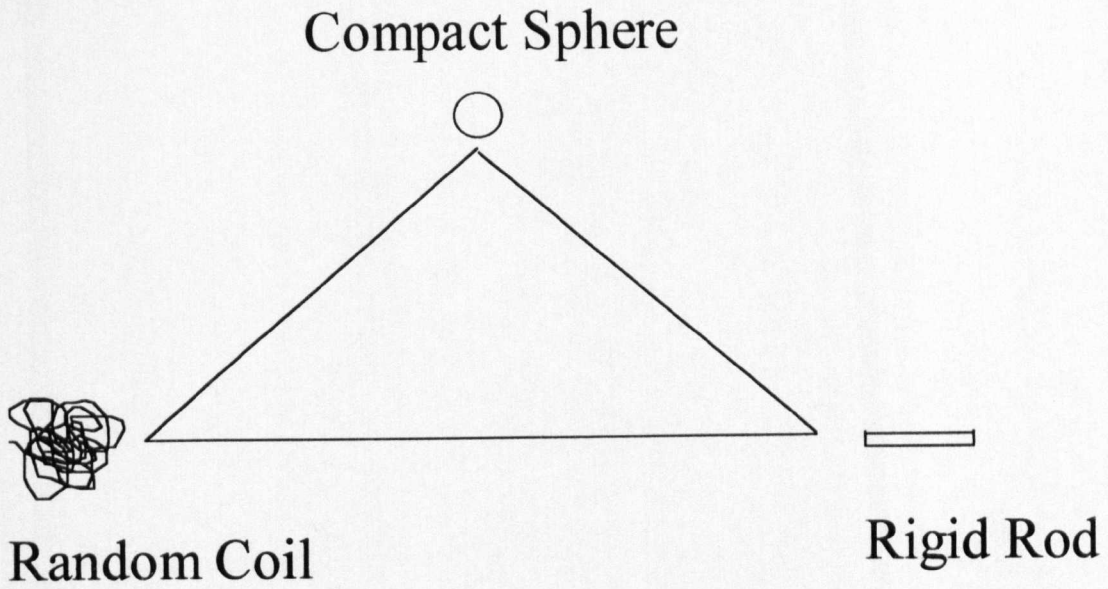


**Figure 2-22** The Haug triangle (adapted from Tombs and Harding, 1998)

Linear chain flexibility can also be modelled in terms of worm-like coils (see for example Bohdanecky, 1983 and Harding, 1997). This is based on the persistence length of the macromolecule *i.e.* the average linear projection of a polymer chain (Figure 2-23).

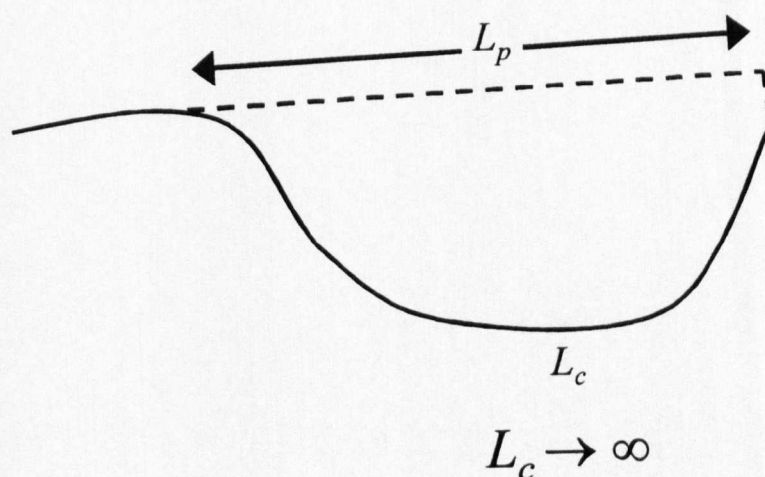


**Figure 2-23** The persistence and contour lengths for a linear macromolecule in the limits of  $L_c \rightarrow \infty$ . Where  $L_p$  corresponds to the average projection (onto a line of the initial direction projected from one end of the macromolecule) that  $L_c$  would have in the hypothetical limit that  $L_c \rightarrow \infty$ . Adapted from Harding, 1997.

It is therefore clear that the persistence length  $L_p$  is related to chain flexibility and in general  $L_c/L_p \rightarrow \infty$  and  $L_c/L_p \rightarrow 1$  are the limits of perfect random coil and a perfect rigid rod respectively. In an alternative nomenclature the “Kuhn statistical chain length”,  $\lambda^{-1}$  is used ( $\lambda^{-1} = 2L_p$ ). There are various combined methods for calculating the contour and persistence lengths (or the Kuhn statistical chain length), the most useful of which is method developed by Bohdanecky (1983) which also yields the mass per unit length,  $M_L$  and diameter of the chain,  $d$ .

$$\left(\frac{M^2}{[\eta]_0}\right)^{1/3} = A_\eta + B_\eta M^{1/2} \quad (2-81)$$

$$A_\eta = A_0 M_L \Phi_{0,\infty}^{-1/3} \quad (2-82)$$

$$B_\eta = B_0 \Phi_{0,\infty}^{-1/3} \left(\frac{\langle R_0^2 \rangle}{M}\right)_\infty^{-1/2} \quad (2-83)$$

where  $\Phi_{0,\infty} = 2.86 \times 10^{23}$  and is the limiting form of the Flory-Fox parameter,  $\Phi$ .

$A_\eta$  and  $B_\eta$  are functions of  $d/\lambda^{-1}$ . Therefore from a plot of  $\left(\frac{M^2}{[\eta]}\right)^{1/3}$  vs.  $M^{1/2}$  one can

obtain the relevant parameters. This theory of Bohdanecky and others is general known as “the theory of worm-like coils” (see for a more detailed explanations Bohdanecky, 1983 and Harding, 1997). Recently (Dondos, 2001) has developed this theory one step further with what he calls the “blob model” in which  $N_c$  the number of Kuhn statistical segments per “blob” need not equal 1 as is implied in the Bohdanecky treatment.

The adapted “blob” theory Dondos (2001) relates the unperturbed chain dimensions to the intrinsic viscosity and Kuhn statistical length as follows –

$$a_\eta^3 = C \left(\frac{N}{N_c}\right)^{3\nu-1} \quad (2-84)$$

where  $\nu$  is the excluded volume index and is related to the Mark-Houwink-Kuhn-Sakurada viscosity exponent,  $a$  as follows –

$$3\nu - 1 = a \quad (2-85)$$

$N$  is the number of Kuhn statistical segments per chain and  $N_c$  is the number of Kuhn statistical segments per “blob”,

$$N = \frac{M}{\lambda^{-1}M_L} \quad (2-86)$$

$$N_c = 0.3a^{-8} \quad (2-87)$$

and

$$C = \frac{[4(1-\nu)(2-\nu)]}{[(2+\nu)(1+\nu)]} \quad (2-88)$$

Therefore,

$$\frac{[\eta]}{M^{0.5}} = \frac{(\lambda^{-1})^{3\nu-1} \Phi C}{M_L^{3\nu} N_c^{3\nu-1.5}} M^{3\nu-1.5} \quad (2-89)$$

and

$$\frac{[\eta]}{M^{0.5}} = K_\theta + 0.51B\Phi M^{0.5} \quad (2-90)$$

where  $\Phi = 2.6 \times 10^{23}$  and  $K_\theta$  in the Stockmayer-Fixman-Burchard equation is equal to

$$K_\theta = \frac{(\lambda^{-1})^{1.5} \Phi}{M_L^{1.5}} \quad (2-91)$$

Therefore by plotting graphs of  $\frac{[\eta]}{M^{0.5}}$  vs.  $M^{3\nu-1.5}$  and  $\frac{[\eta]}{M^{0.5}}$  vs.  $M^{0.5}$  one can calculate the Kuhn statistical length, the mass per unit length and the persistence length by solving simultaneous equations. [Note – in the “blob” theory of Dondos the Kuhn statistical length is denoted as  $A$ , and not  $\lambda^{-1}$  as preferred by others].

It is therefore apparent that the hydrodynamic probes discussed in this chapter have great potential in the characterisation of macromolecular systems. This is particularly true for polydisperse systems *e.g.* polysaccharides (Chapter 3), milk proteins (Chapter 4) and mixed systems (Chapter 5).

## 2.9 REFERENCES

- Abel-Azim A-A A, Atta AM, Farahat MS and Boutros W (1998) Determination of the Intrinsic Viscosity of Polymeric Compounds Through a Single Specific Viscosity Measurement. *Polymer*, **39**, 6827-6833.
- Arias C, Yague A, Rueda C and Garcia Blanco F (submitted). Intrinsic Viscosity Calculated Out of a Single Point Measurement for Chondroitin-4-Sulfate and Chondroitin-6-Sulfate.
- Beckman (1996) *Optima<sup>TM</sup> XL-I Analytical Ultracentrifuge with Integrated Scanning UV/ Visible and Rayleigh Inference – Instruction Manual*. Beckman Inc., Palo Alta, USA.
- Bohdanecky M (1983) New Method for Estimating the Parameters of the Wormlike Chain Model from the Intrinsic Viscosity of Stiff-Chain Polymers. *Macromolecules*, **16**, 1483-1492.
- Burchard W (1992) Static and Dynamic Light Scattering Approaches to Structure Determination of Biomolecules. In: Harding SE, Sattelle DB and Bloomfield VA (Eds.) *Laser Light Scattering in Biochemistry*, pp. 3-23. Royal Society of Chemistry, Cambridge.
- Casassa EF and Eisenberg, H. (1961) Partial Specific Volumes and Refractive Index Increments in Multi-Component Systems. *Journal of Physical Chemistry*, **65** 427-433.
- Cölfen H and Harding SE (1997) MSTAR and MSTAR: Interactive PC Algorithms for Simple, Model Independent Evaluation of Sedimentation Equilibrium Data. *European Biophysics Journal*, **25**, 333-346.

- Creeth JM and Harding SE (1982) Some Observations on a New Type of Point Average Molecular Weight. *Journal of Biochemical and Biophysical Methods*, **7**, 25-34.
- Creeth JM and Pain RH (1967) The Determination of Molecular Weights of Biological Macromolecules by Ultracentrifuge Methods. *Progress in Biophysics and Molecular Biology*, **17**, 217-287.
- Cross M.M (1965) Rheology of Non-Newtonian Fluids: A New Flow Equation for Pseudoplastic Systems. *Journal of Colloid Science.*, **20**, 417-437.
- Dhami R, Harding SE, Jones T, Hughes T, Mitchell JR and To K-M (1995) Physico-Chemical Studies on a Commercial Food Grade Xanthan - I. Characterisation by Sedimentation Velocity, Sedimentation Equilibrium and Viscometry. *Carbohydrate Polymers*, **27**, 93-99.
- Dondos A (2001) A New Relationship Between the Intrinsic Viscosity and the Molecular Mass of Polymers Derived from the Blob Model: Determination of the Statistical Length of Flexible Polymers. *Polymer*, **42**, 897-901.
- Einstein A (1906) A New Determination of Molecular Dimensions Eine neue Bestimmung der Molekuldimensionen. *Annalen der Physik*, **19**, 289-306.
- Einstein A (1911) Correction to My Paper: "A New Determination of Molecular Dimensions" Berichtigung zu meiner Arbeit: "Eine neue Bestimmung der Molekuldimensionen". *Annalen der Physik*, **34**, 591-593.
- Errington N (1993) Hydrodynamic Characterisation of Novel Polysaccharides for Pharmaceutical and Food Use. University of Nottingham. Ph.D.
- Hall DR, Harding SE and Winzor DJ (1999) The Correct Analysis of Low-Speed Sedimentation Equilibrium Recorded by Rayleigh Interference Optical

System in a Beckman XLI Ultracentrifuge. *Trends in Analytical Chemistry*, **113**, 62-68.

Harding SE (1992) Sedimentation Analysis of Polysaccharides. In: Harding SE, Rowe AJ, and Horton JC (Eds.) *Analytical Ultracentrifugation in Biochemistry and Polymer Science*, pp. 495-516. Royal Society of Chemistry, Cambridge.

Harding SE (1994) Shapes and Sizes of Food Polysaccharides by Sedimentation Analysis - Recent Developments. In: Phillips GO, Williams PA and Wedlock DJ (Eds.) *Gums and Stabilisers for the Food Industry 7*, pp. 55-68. IRL Press, Oxford.

Harding SE (1995a) On the Hydrodynamic Analysis of Macromolecular Conformation. *Biophysical Chemistry*, **55**, 69-93.

Harding SE (1995b) Some Recent Developments in the Size and Shape Analysis of Industrial Polysaccharides in Solution Using Sedimentation Analysis in the Analytical Ultracentrifuge. *Carbohydrate Polymers*, **28**, 227-237.

Harding SE (1997) The Intrinsic Viscosity of Biological Macromolecules. Progress in Measurement, Interpretation and Application to Structure in Dilute Solution. *Progress in Biophysics and Molecular Biology*, **68**, 207-262.

Harding SE (1999a) Photon Correlation Spectroscopy. In: Creighton TE (Ed.) *Encyclopaedia of Molecular Biology*, pp. 1847-1849. John Wiley and Sons, New York.

Harding SE (1999b) Protein Hydrodynamics. *Trends in Food Science and Technology*, **2**, 271-305.

- Harding SE, Berth G, Ball A and Mitchell JR (1990) Hydrodynamic Evidence for an Extended Conformation for Citrus Pectin in Dilute Solution. In: Phillips GO, Williams PA and Wedlock DJ (Eds.) *Gums and Stabilisers for the Food Industry 5*, pp. 267-272. IRL Press, Oxford.
- Harding SE and Cölfen H (1995) Inversion Formulae for Ellipsoid of Revolution Macromolecular Shape Functions. *Analytical Biochemistry*, **228**, 131-142.
- Harding SE and Johnson P (1985) The Concentration-Dependence of Macromolecular Parameters. *Biochemical Journal*, **231**, 543-547.
- Harding SE, Vårum KM, Stokke BT and Smidsrød, O (1991) Molecular Weight Determination of Polysaccharides. *Advances in Carbohydrate Analysis*, **1**, 63-144.
- Hecht E and Lujac A (1973) *Optics*. Addison-Wesley, Reading, MA.
- Huggins ML (1942) The Viscosity of Long Chain Molecules IV: Dependence on Concentration. *Journal of the American Chemical Society*, **64**, 2716-2718.
- Huglin MB (1972) Specific Refractive Index Increments. In: Huglin MB (Ed.) *Light Scattering from Polymer Solutions*, pp. 165-332. Academic Press, New York.
- Gralén N (1944) Sedimentation and Diffusion Measurements on Cellulose and Cellulose Derivatives. PhD Dissertation, University of Uppsala, Sweden.
- Jumel K (1994) Molecular Size of Interacting and Degrading Polysaccharides. Ph.D. Thesis, University of Nottingham.

- Kratky O, Leopold H and Stabinger H. (1973) The Determination of the Partial Specific Volume of Proteins by the Mechanical Oscillator Technique. *Methods in Enzymology*, **27D**, 98-110.
- Kratochvil P (1972) Particle Scattering Function. In: Huglin MB (Ed.) *Light Scattering from Polymer Solutions*, pp. 333-384. Academic Press, New York.
- Kratochvil P (1987) *Classical Light Scattering from Polymer Solutions*. Elsevier Science, Amsterdam.
- Kravtchenko TP and Pilnik W (1990) A Simplified Method for the Determination of the Intrinsic Viscosity of Pectin Solutions by Classical Viscometry. In: Phillips GO, Williams PA and Wedlock DJ (Eds.) *Gums and Stabilisers for the Food Industry 5*, pp. 281-286. IRL Press, Oxford.
- Laue TM and Stafford III WF (1999) Modern Applications of Analytical Ultracentrifugation. *Annual Reviews in Biophysics and Biomolecular Structure*, **28**, 75-100.
- McRorie DK and Voelker PJ (1993) *Self-Associating Systems in the Analytical Ultracentrifugation*. Beckman Instruments Inc., California.
- Morris ER, Cutler AN, Ross-Murphy SB and Rees DA (1981) Concentration and Shear rate Dependence of Viscosity in Random Coil Polysaccharide Solutions. *Carbohydrate Polymers*, **1**, 5-21.
- Morris GA, Foster TJ and Harding SE (2000) The Effect of Degree of Esterification on the Hydrodynamic Properties of Citrus Pectin. *Food Hydrocolloids*, **14**, 227-235.

- Pavlov GM (1997) The Concentration Dependence of Sedimentation for Polysaccharides. *European Biophysics Journal*, **25**, 385-398.
- Ralston G (1993) *Introduction to Analytical Ultracentrifugation*. Beckman Instruments Inc., California.
- Rowe AJ (1977) Concentration-Dependence of Transport Processes – General Description Applicable to Sedimentation, Translational Diffusion, and Viscosity Coefficients of Macromolecular Solutes. *Biopolymers*, **16**, 2595-2611.
- Rowe AJ (1992) The Concentration Dependence of Sedimentation. In: Harding SE, Rowe AJ, and Horton JC (Eds.) *Analytical Ultracentrifugation in Biochemistry and Polymer Science*. Royal Society of Chemistry, Cambridge.
- Schachman HK (1959) *Ultracentrifugation in Biochemistry*. Academic Press, New York.
- Stafford III WF (1992a) Boundary Analysis in Sedimentation Transport Experiments: A Procedure for Obtaining Sedimentation Coefficient Distributions Using the Time Derivative of the Concentration Profile. *Analytical Biochemistry*, **203**, 295-301.
- Stafford III WF (1992b) Methods for Obtaining Sedimentation Coefficient Distributions. In: Harding SE, Rowe AJ and Horton JC (Eds.) *Analytical Ultracentrifugation in Biochemistry and Polymer Science*, pp. 359-393. Royal Society of Chemistry, Cambridge
- Štěpánek P (1993) Data Analysis in Dynamic Light Scattering. In: Brown W (Ed.) *Dynamic Light Scattering The Method and Some Applications*. Oxford Science Publications, Oxford.

- Svedberg T and Pedersen KO (1940) *The Ultracentrifuge*. In: Fowler RH and Kapitza P (Eds.) Clarendon Press, Oxford.
- Tanford C (1961) *Physical Chemistry of Macromolecules*, Chapter 6. John Wiley and Sons, New York.
- Teller DC (1973) Characterisation of Proteins by Sedimentation Equilibrium in the Analytical Ultracentrifuge. *Methods in Enzymology*, **27**, 346-441.
- Tombs MP and Harding SE (1998) *An Introduction to Polysaccharide Biotechnology*. Chapter 2. Taylor and Francis, London.
- van der Hulst (1957) *Light Scattering by Particles*. John Wiley and Sons, New York.
- van Holde KE (1985) *Physical Biochemistry*. Second Edition. Prentice-Hall, New Jersey.
- Wales M and van Holde KE (1954) The Concentration Dependence of the Sedimentation Constants of Flexible Macromolecules. *Journal of Polymer Science*, **14**, 81-86.
- Wyatt PJ (1992) Combined Differential Light Scattering with Various Liquid Chromatography Separation Techniques. In: Harding SE, Sattelle DB, Bloomfield VA (Eds.) *Laser Light Scattering in Biochemistry*. Royal Society of Chemistry, Cambridge, Chapter 3.
- Zimm BH (1948) The Scattering of Light and the Radial Distribution Function of High Polymer Systems. *Journal of Chemical Physics*, **16**, 1099.

### 3 CHAPTER 3 – DETAILED CHARACTERISATION OF THE POLYSACCHARIDE SUBSTRATES

Polysaccharides are a group of biopolymers based on saccharide (hexose or pentose) backbones; in general the repeating unit is quite simple (usually less than 4 types of residue). This does not however inhibit the diversity of structural and functional properties of the family (see *e.g.* Tombs & Harding, 1998). Chemical and functional diversity is derived from the types of saccharides present and their linkages to one another. As with other biopolymers *e.g.* proteins, polysaccharides are enantiomeric and the D-form is most common (see *e.g.* Lehninger *et al.*, 1990; Tombs and Harding, 1998). Saccharide monomers (Figure 3-1) cyclise via a hemiacetal linkage to form pyranose (6-member) or furanose (5-member) rings (Rose, 1966; Lehninger *et al.*, 1990 and Tombs and Harding, 1998) (Figure 3-2). The orientation of the pyranose hydroxyl group C1 (Figure 3-2) (C2 for furanoses) is the distinguishing feature of  $\alpha$  and  $\beta$  forms.

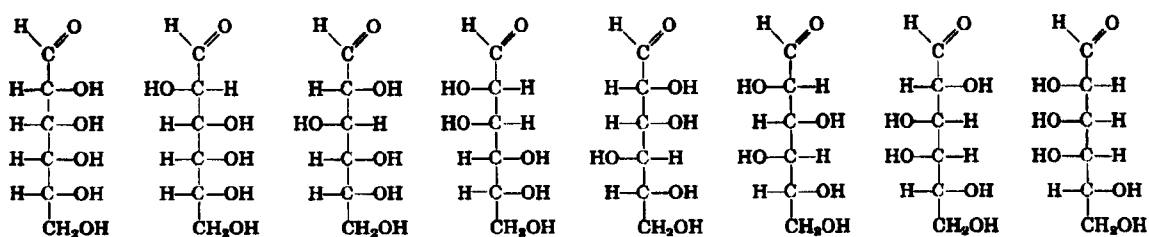


**Figure 3-1** The Fischer projection for the D-hexoses with the chiral carbons labelled in red they are from left to right D-Allose, D-Altrose, D-Glucose, D-Mannose, D-Gulose, D-Idose, D-Galactose and D-Talose (adapted from Lehninger *et al.*, 1990).

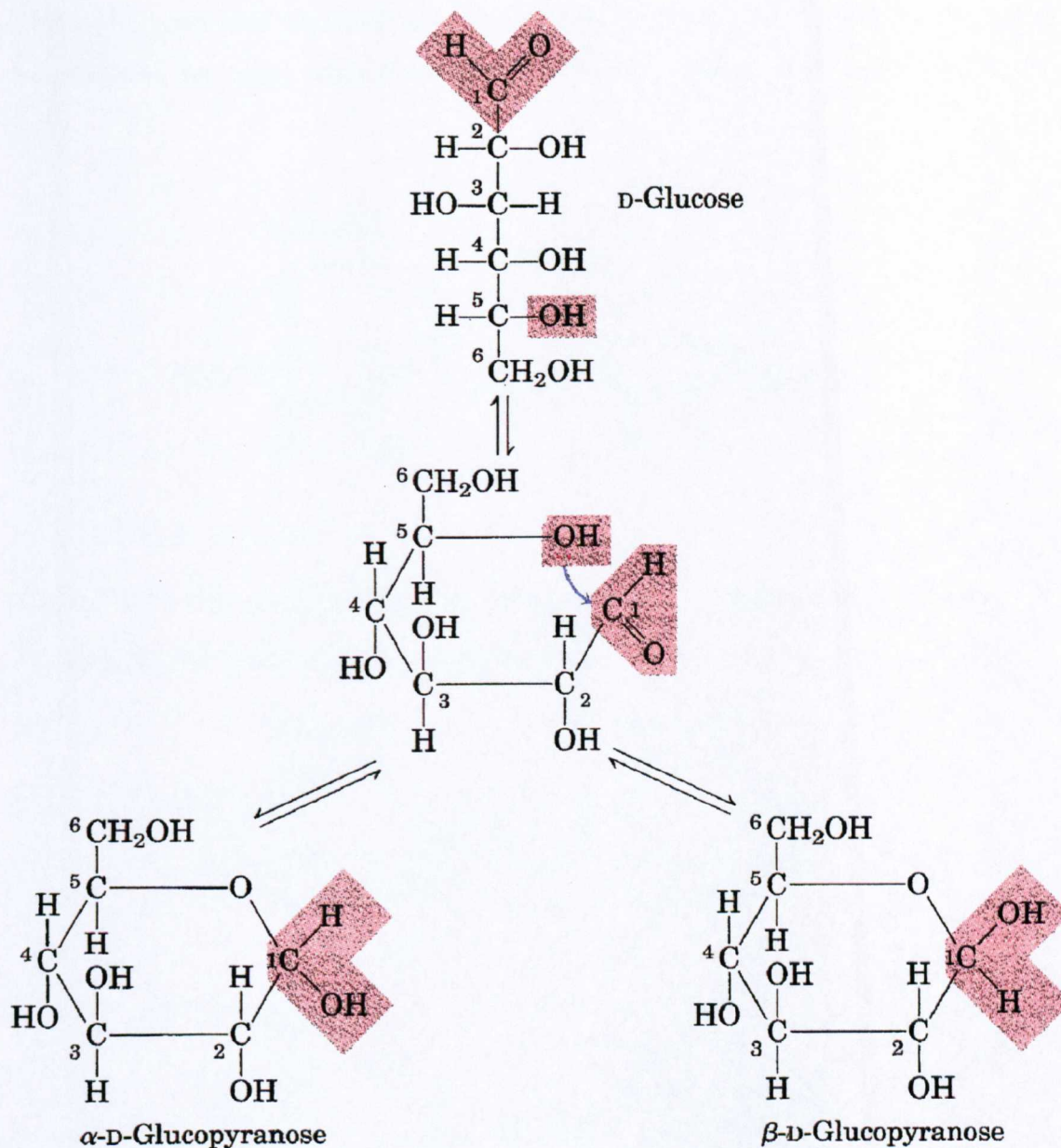


**Figure 3-2** Formation of the two cyclic forms of D-glucopyranose (adapted from Lehninger *et. al.*, 1990).

Therefore saccharide linkages can be designated as follows  $\alpha$ -D-glucopyranosyl (1 $\rightarrow$ 2)  $\beta$ -D-fructofuranoside, where 1 and 2 are the carbon atoms involved in the glycosidic linkage.

This is the systematic chemical name for Sucrose (**Figure 3-3**). Similar structures can be produced for many other disaccharides including Lactose and Trehalose (**Figure 3-4**).

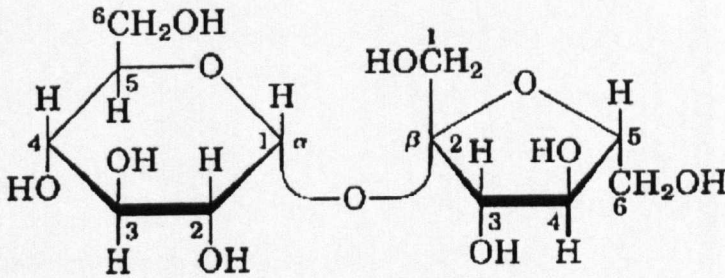


**Figure 3-3** The chemical structure of sucrose -  $\alpha$ -D-glucopyranosyl (1 $\rightarrow$ 2)  $\beta$ -D-fructofuranoside (adapted from Lehninger *et. al.*, 1990).

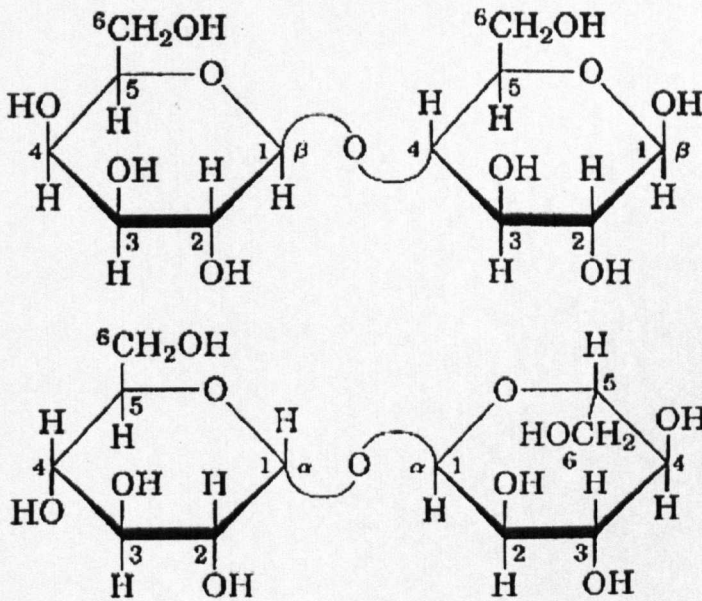


**Figure 3-4** Chemical structures for lactose and trehalose -  $\beta$ -D-galactopyranosyl (1 $\rightarrow$ 4)  $\beta$ -D-glucopyranorose and  $\alpha$ -D-glucopyranosyl (1 $\rightarrow$ 1)  $\alpha$ -D-glucopyranorose respectively (from Lehninger *et. al.*, 1990).

It is therefore clear that by varying the saccharide units, the type of linkage or  $\alpha/\beta$  forms the possibilities for polysaccharide structures are very large.

There are additional problems associated with the hydrodynamic characterisation of polysaccharides due to one or more of the following properties (Oakenfull, 1991; Harding *et. al.*, 1991a) -

- (i) they are polydisperse
- (ii) they give thermodynamically non-ideal solutions
- (iii) unlike globular proteins their solution structure is difficult to determine with any precision
- (iv) in some they have a tendency to self-associate especially at higher concentrations

Detailed knowledge of the hydrodynamic properties of polysaccharides can give fundamental understanding of their biotechnological applications in for example the food, oil, pharmaceutical, and medical industries (Harding *et. al.*, 1991a). It should however be noted that the method for preparing polysaccharide solutions is critical as solution preparation (filtration, heating and purification) can have a strong influence on molecular parameters (see *e.g.* Bongaerts *et. al.*, 2000).

This chapter will therefore give a detailed account of the characterisation of a variety of commercially available polysaccharides including pectin, carrageenan, guar, locust bean gum, xanthan, xylans and some novel polysaccharides *e.g.* chemically modified pectins, xylans and a bacterial exopolysaccharide (AH-EPS).

### 3.1 CHARACTERISATION OF CITRUS PECTINS

#### 3.1.1 Characterisation of Pectin 7000 Series

##### 3.1.1.1 Background

Pectin is the family of complex polysaccharides, which constitute approximately one third of the dry weight of higher primary plant cell walls (Walter, 1991; Tombs and Harding, 1998). Pectins are particularly prevalent in fruit cell walls, especially citrus fruits and apple pommace. The main pectin chain is composed of  $\alpha(1\rightarrow4)$  linked D-galacturonic acid residues.

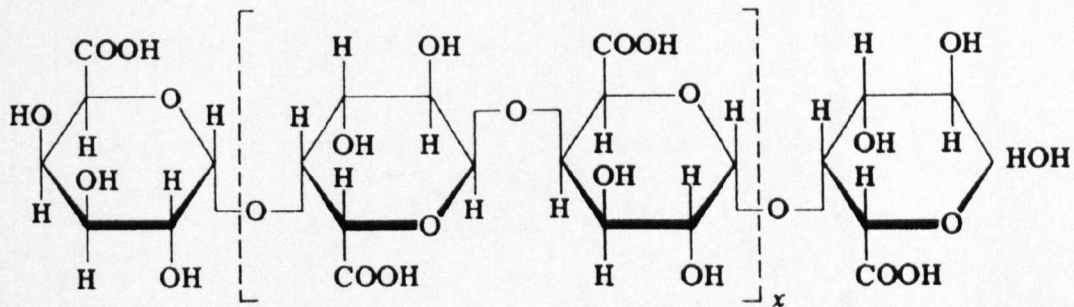


**Figure 3-5** Idealised structure of pectic acid *i.e.* pectin of DE 0% (adapted from Glicksman, 1969).

Many of the galacturonic acid residues have been esterified to form methyl esters. Theoretically the degree of esterification (DE) can range from 0-100%. Pectins with a degree of esterification (DE) > 50% are known as high methoxyl (HM) pectins and consequently low methoxyl (LM) pectins have a DE < 50% (Walter, 1991). Rhamnose residues are incorporated into the main chain at random intervals, which results in a kink in the otherwise linear chain. Side chains of arabinoses and galactans, are also present, either randomly dispersed or in localised “hairy” regions. The degree of esterification and therefore the charge on a pectin molecule is important to the functional properties in the plant cell wall. It also significantly affects their commercial use as gelling and thickening agents (Lapasin and Pricl, 1995; Tombs and Harding, 1998). HM pectins (low charge) form gels at low pH (<4.0) and in the presence of a high amount of soluble solids, usually sucrose (>55%) (Oakenfull, 1991). HM pectin gels are stabilised by hydrogen-bonding and hydrophobic interactions of individually weak but cumulatively strong junction zones (Oakenfull,

1991; Lopes da Silva and Gonçalves 1994; Pilnik, 1990 and Morris, 1979). Conversely, LM pectins (high charge) form electrostatically stabilised gel networks with/ or without sugar and with divalent metal cations, usually calcium in the so-called “egg-box” model (Morris *et al.*, 1982; Pilnik, 1990; Morris, 1980; Oakenfull and Scott, 1998 and Axelos and Thibault, 1991), which also depends on the distribution of negative carboxylate groups and structure breaking rhamnose side chains (Powell *et al.*, 1982; Axelos and Thibault, 1991). A similar “egg-box” model has been proposed for alginate gels (Wang *et al.*, 1994; Morris, 1980) from the results of circular dichroism, small angle X-ray scattering (SAXS) and X-ray fibre diffraction respectively, it is thought that in both pectin and alginate the “egg-box” is formed in a two-step process – dimerisation followed by aggregation of the preformed “egg-boxes” (Thibault and Rinaudo, 1986).

Solution properties such as viscosity also depend on degree of esterification, solvent environment (*i.e.* salt concentration, sugar concentration and pH) together with temperature (Oakenfull, 1991). However the effect of degree of esterification on dilute solution properties such as intrinsic viscosity, sedimentation and weight average molecular weight has not been widely studied, therefore a detailed study on the molecular hydrodynamics of pectins of different DE is clearly called for.

### 3.1.1.2 *Materials*

Pectin samples 7000-7004 were obtained from CP Kelco ex. Citrus Colloids Ltd., (Hereford, UK). The parent pectin 7000 DE 77.8% was systematically de-esterified to 27.9% pectin 7004. All samples were prepared and solubilised for approximately 24 hours in standard pH 6.8, I=0.1 “Paley” buffer, of the following composition Na<sub>2</sub>HPO<sub>4</sub>.12H<sub>2</sub>O - 4.595g; KH<sub>2</sub>PO<sub>4</sub> - 1.561g and NaCl - 2.923g all made up to 1 litre (Green, 1933). [Note – standard phosphate buffer has over time become known as “Paley” buffer after Paley Johnston].

### 3.1.1.3 Methods

#### Densimetry

The buoyancy factor  $(1 - \bar{v}\rho_0) = \Delta\rho/\Delta c$  and hence the partial specific volume,  $\bar{v}$  of the high methoxy pectin molecule was measured with an Anton Paar (Graz, Austria) precision density meter at  $(25.0 \pm 0.1)^\circ\text{C}$  according to the procedure of Kratky, *et. al.*, (1973) (and see also Pavlov, *et. al.*, 1998). Where  $(1 - \bar{v}\rho_0)$  is slope of  $\rho - \rho_0$  versus concentration (where  $\rho$  and  $\rho_0$  are the densities of the pectin solution and the buffer respectively).

#### Capillary Viscometry

Solutions and reference solvents were analysed using a 2ml automatic Schott-Geräte Oswald viscometer, under precise temperature control  $(25.04 \pm 0.01^\circ\text{C})$ . The relative,  $\eta_{\text{rel}}$ , specific,  $\eta_{\text{sp}}$  and intrinsic viscosities were calculated from Equations 2-34, 2-35 and 2-41 respectively.

#### Sedimentation Velocity in the Analytical Ultracentrifuge

The Optima XLI (Beckman Instruments, Palo Alto, USA) equipped with Rayleigh interference optics was used to determine the sedimentation behaviour of the pectin samples. Rotor speeds of 40,000rpm and a 4mm column length in 12mm optical path length double sector cells were used together with an accurately controlled temperature of  $20.0^\circ\text{C}$ . A weighted average partial specific volume,  $\bar{v}$  of  $(0.63 \pm 0.01)\text{ml/g}$  was measured (see section 3.1.1.4) using the method of Kratky *et. al.*, 1973 (see above). The  $g^*(s)$  (sedimentation time derivative) method was used to determine apparent sedimentation coefficients at each concentration. As the sedimenting boundary moves towards the cell base the change in concentration (of the sedimenting species) over time  $(dc/dt)$  across the radial distribution is calculated from the subtraction of multiple pairs of scans (maximum 20 pairs), an apparent sedimentation coefficient distribution  $g^*(s)$  can in this way be produced (Stafford, 1992a,b and Laue & Stafford, 1999). The apparent weight average sedimentation coefficient,  $s^*$  is then calculated.  $s_{20,w}$  values can then be generated according to the

standard equation (see *e.g.* Ralston, 1993; Pavlov, 1997) (Equation 2-10). Apparent sedimentation coefficients,  $s_{20,w}$  were calculated at various concentrations from 0.5 to 2.5mg/ml and extrapolated to zero concentration using the standard conversion equation 2-8 (Ralston, 1993).

### *Sedimentation Equilibrium in the Analytical Ultracentrifuge*

The Beckman Optima XLI ultracentrifuge was also used to determinate the weight average molecular weight,  $M_w$  using low speed sedimentation equilibrium. A rotor speed of 10,000rpm and a 1mm solution column length again in 12mm path length double sector cells were employed at 20.0°C. Equilibrium was reached after approximately 24 hours. Rayleigh interference optics were used to record the solute distributions at sedimentation equilibrium and data subsequently analysed using the QUICKBASIC algorithm MSTARI (Cölfen and Harding, 1997). See section 2.2.2.

### *SEC-MALLS*

SEC-MALLS (size exclusion chromatography coupled to multi-angle laser light scattering) allows on-line light scattering of a heterogeneous solute fractionated by size exclusion chromatography, permitting the extraction of absolute molecular weights and molecular weight distributions (van Holde, 1985; Jumel *et. al.*, 1992; Jumel, 1994). The Wyatt Technology (Santa Barbara, USA) Dawn F multi-angle laser light scattering photometer (Wyatt, 1992) was coupled to TSK Gel 4000, TSK Gel 5000 and TSK Gel 6000 columns protected by a similarly packed guard column (Anachem Ltd., Luton, UK). The eluent was the standard pH 6.8 I=0.1 “Paley” buffer and the injection volume was 100 $\mu$ l. A value for the refractive index increment of 0.146ml/g was used (Chapman *et. al.*, 1987). Solutions were filtered prior to injection to remove any micro-particles in solution (Oakenfull, 1991; Fishman *et. al.*, 2000; Jordan and Brant, 1978).

## 3.1.1.4 Results and Discussion

Densimetry

A partial specific volume,  $\bar{v}$  of  $(0.63 \pm 0.01)$  ml/g was calculated from the slope of  $\rho - \rho_0$  versus concentration (**Figure 3-6**). This value is similar to the value of 0.57 ml/g (Harding, *et al.*, 1991a,b) for citrus pectin.

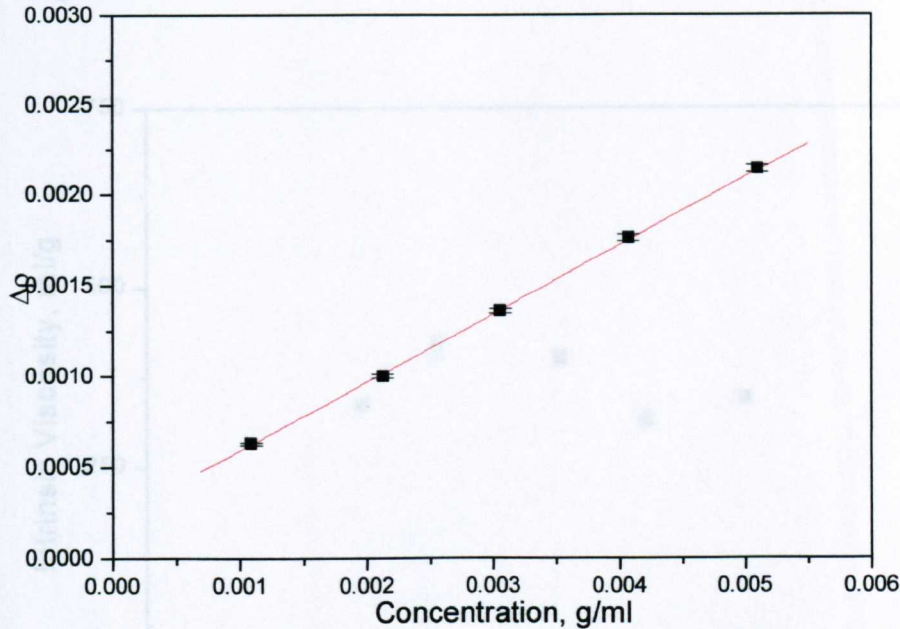


**Figure 3-6** Dependence of density increment  $\Delta\rho = \rho - \rho_0$  (where  $\rho$  and  $\rho_0$  are the densities of the pectin solution and the buffer respectively in g/ml) for a high methoxy pectin in pH 6.8, I=0.1M phosphate/ chloride buffer.

Capillary Viscometry

The sinusoidal relationship between intrinsic viscosity and DE suggests that both charge and steric effects are important in pectin conformation (**Figure 3-7**). We will now show that this, trend is now supported by other data. This would therefore indicate a change in the weight average molecular weight and/ or a change in pectin conformation as DE is reduced. This is perhaps also influenced by the charge screening effect of added salt.

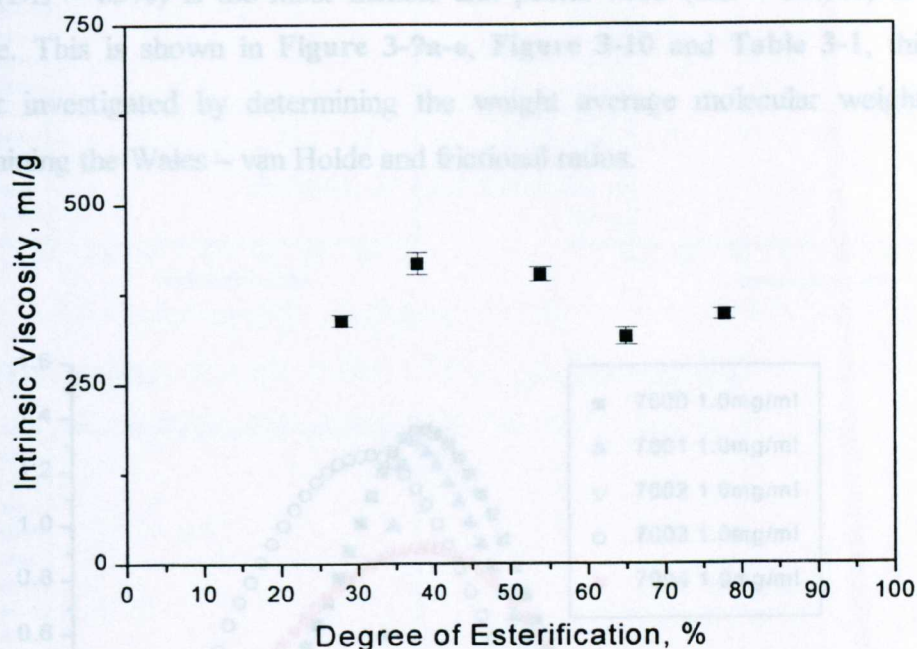


**Figure 3-7** Intrinsic viscosity vs. DE for Pectin 7000 Series in pH 6.8, I=0.1M phosphate/ chloride buffer. Where the DEs are 77.8, 65.0, 53.9, 37.8 and 27.9% for pectins 7000, 7001, 7002, 7003 and 7004 respectively.

According to previous studies (Kravtchenko and Pilnik, 1990; Kravtchenko *et. al.* 1994; Harding *et. al.*, 1991b; Berth, 1988; Berth and Lexow, 1991; Fishman *et. al.*, 2000; Cros, *et. al.* 1995; Lopes da Silva and Gonçalves, 1994 and Berth, 1992) the intrinsic viscosity of pectin typically lies within the range 100-1100ml/g with the majority in the range 300-800ml/g, which is consistent with the results above.

Sedimentation Velocity

The  $g(s^*)$  plots for each pectin sample appear to show homogenous sample (**Figure 3-8**). The trend between sedimentation coefficient and DE is the inverse of intrinsic viscosity and DE. The same is true for the Gralén (1944) concentration dependence,  $k_s$ . This therefore confirms that there is a conformational change upon lowering the degree of esterification (intrinsic viscosity *increases* with *increasing* axial ratio and sedimentation coefficient will *decrease* and vice versa (see *e.g.* Tanford, 1961)). That is the chain rigidity is dependent on both charge and steric factors and that pectin 7001 (DE – 65%) is the most flexible and pectin 7003 (DE – 37.8%) is the least flexible. This is shown in **Figure 3-9a-e**, **Figure 3-10** and **Table 3-1**, this will be further investigated by determining the weight average molecular weight and by determining the Wales – van Holde and frictional ratios.

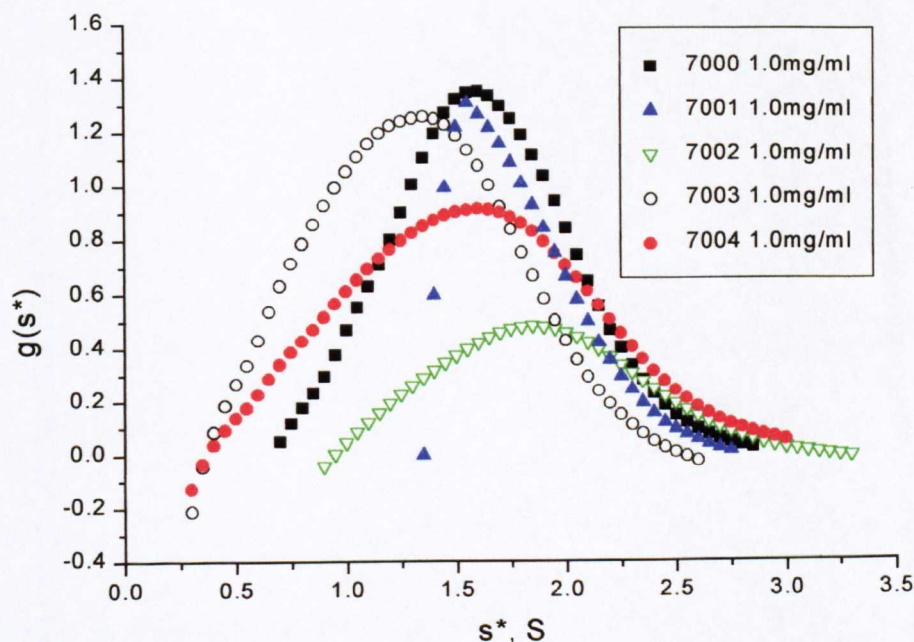
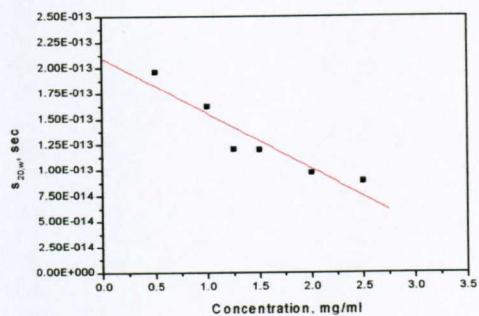
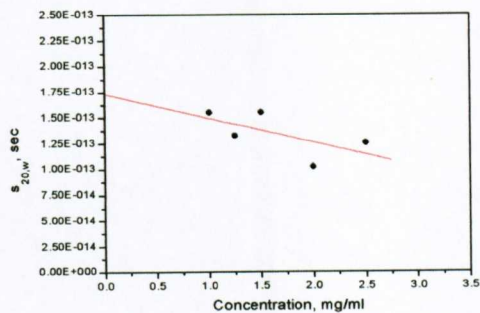


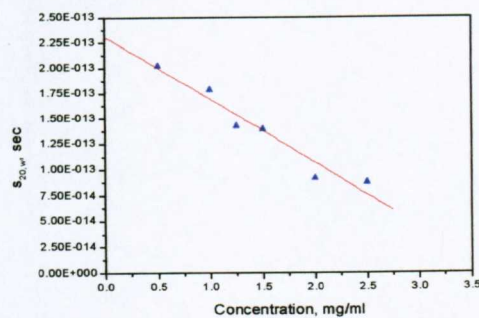
**Figure 3-8**  $g(s^*)$  profiles for pectin samples in pH 6.8,  $I=0.1M$  phosphate/ chloride buffer. Where the DEs are 77.8, 65.0, 53.9, 37.8 and 27.9% for pectins 7000, 7001, 7002, 7003 and 7004 respectively.



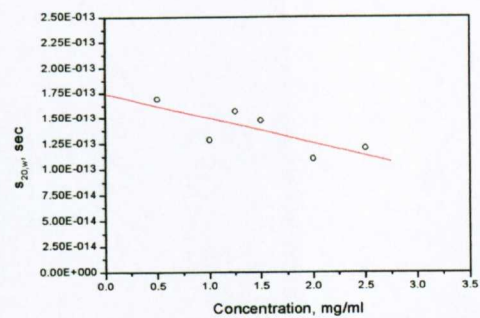
a – DE = 77.8%



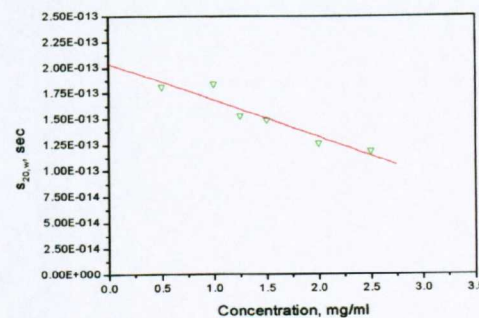
d – DE = 37.8%



b – DE = 65.0%



e – DE = 27.9%



c – DE = 53.9%

**Figure 3-9** Sedimentation coefficient vs. concentration for Pectin 7000 series in pH 6.8, I=0.1M phosphate/ chloride buffer. **a** – Pectin 7000, **b** – Pectin 7001, **c** – Pectin 7002, **d** – Pectin 7003, **e** – Pectin 7004

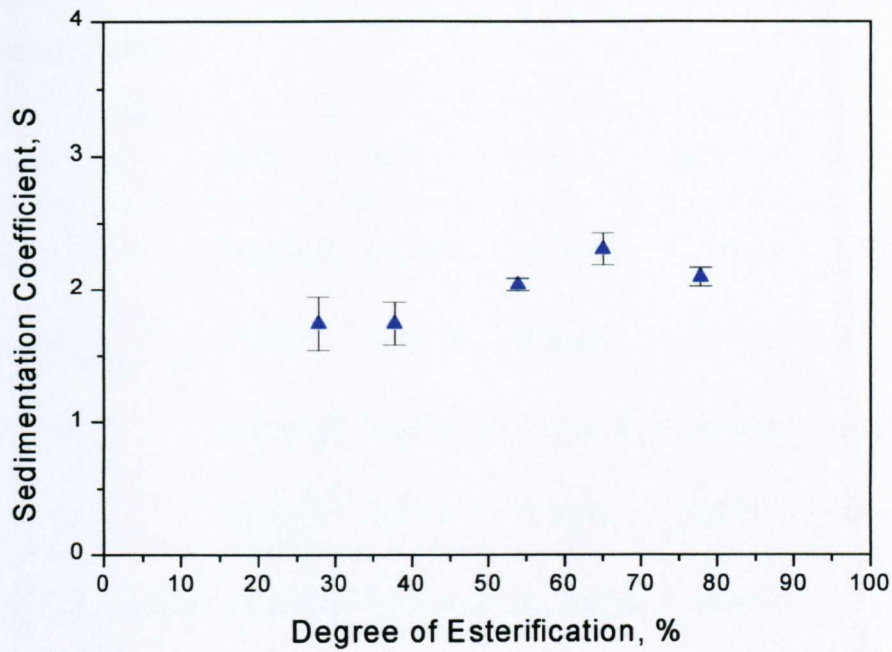


**Figure 3-10** Sedimentation coefficient vs. DE for Pectin 7000 series in pH 6.8, I=0.1M phosphate/ chloride buffer. Where the DEs are 77.8, 65.0, 53.9, 37.8 and 27.9% for pectins 7000, 7001, 7002, 7003 and 7004 respectively.

**Table 3-1** Hydrodynamic data for pectin 7000 series in pH 6.8, I=0.1M phosphate/chloride buffer.

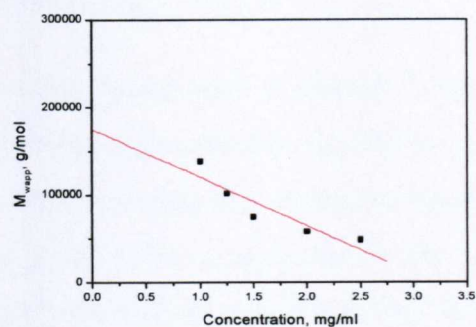
Pectin	7000	7001	7002	7003	7004
DE, %	77.8±0.2	65.0±0.2	53.9±0.2	37.8±0.2	27.9±0.2
[ $\eta$ ], ml/g	345±7	315±12	402±10	417±15	338±8
$s_{20,w}^0$ , S	2.10±0.07	2.31±0.12	2.04±0.05	1.74±0.16	1.74±0.20
$k_s$ , ml/g	257±20	270±30	175±30	140±30	137±20
$^a 10^{-5} \times M_w$ , g/mol	1.76±0.20	1.99±0.09	2.17±0.02	1.65±0.17	1.65±0.20
$^b 10^{-5} \times M_w$ , g/mol	1.86±0.09	2.11±0.10	2.11±0.10	1.88±0.09	1.87±0.09
$k_s/[\eta]$	0.75±0.07	0.85±0.10	0.44±0.08	0.34±0.08	0.41±0.07
$f/f_0$	7.9±0.4	7.8±0.4	8.9±0.4	9.6±0.5	9.6±0.5

a - sedimentation equilibrium

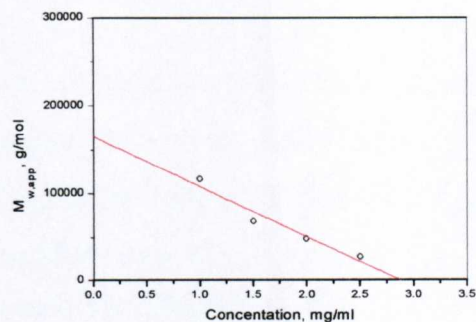
b - SEC-MALLS

### Sedimentation Equilibrium

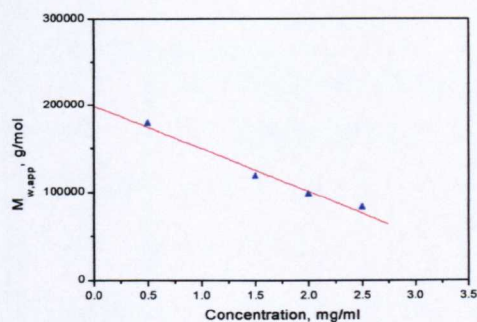
Apparent weight average molecular weights were calculated over the concentration range 0.5 - 2.5mg/ml and extrapolated to zero concentration to obtain “ideal” molecular weights (Figure 3-11a-e). It is seen that there is very little difference in the “ideal” molecular weight for each pectin sample.



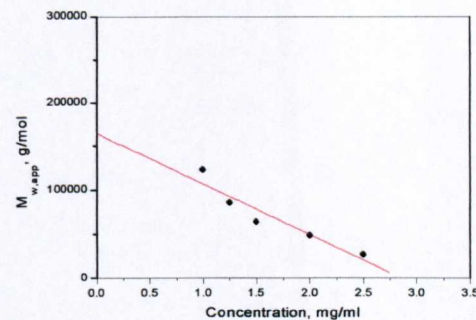
**a** – DE = 77.8%



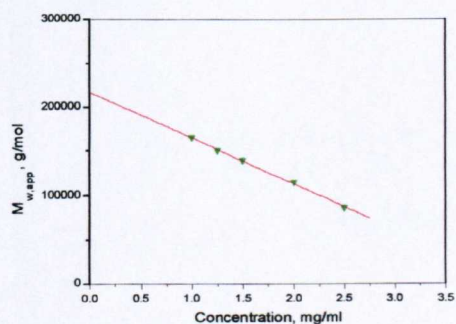
**d** – DE = 37.8%



**b** – DE = 65.0%



**e** – DE = 27.9%



**c** – DE = 53.9%

**Figure 3-11** Apparent weight average molecular weight vs. concentration in pH 6.8, I=0.1M phosphate/ chloride buffer. **a** – Pectin 7000, **b** – Pectin 7001, **c** – Pectin 7002, **d** – Pectin 7003, **e** – Pectin 7004

SEC-MALLS

A single, broad peak at elution volume between ~16-30ml is evident for all samples. As with sedimentation equilibrium, there appears to be very little difference in molecular weight and molecular weight distribution for each pectin sample (**Figure 3-11a-e**). The consistency of the two independent sets of measurements is well illustrated in (**Figure 3-12**), giving high confidence in the reliability of the data.

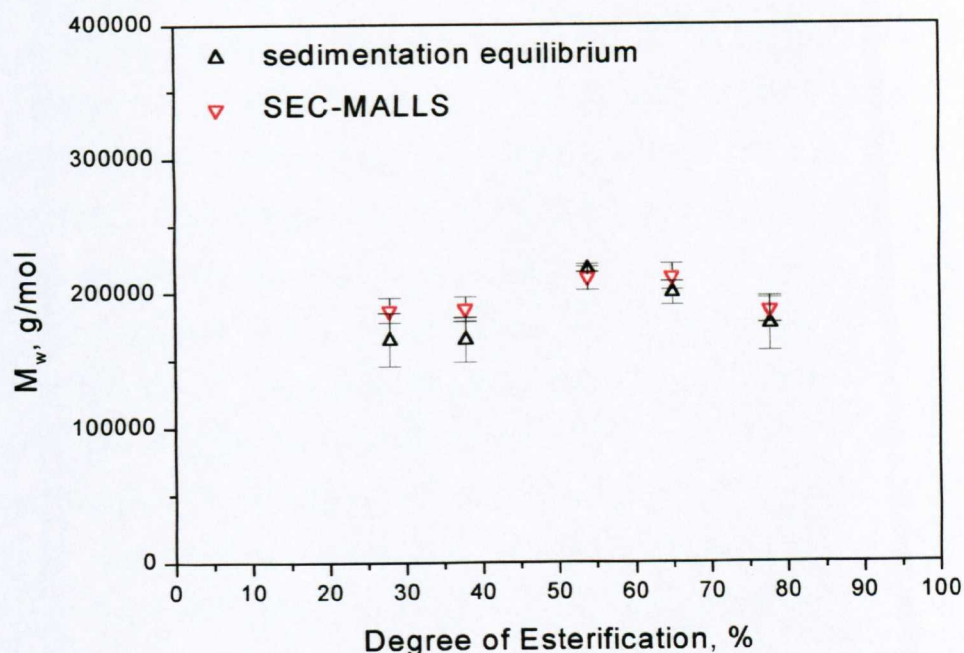


**Figure 3-12** Molecular weight vs. DE for Pectin 7000 Series, from two independent techniques: sedimentation equilibrium and SEC-MALLS in pH 6.8, I=0.1M phosphate/ chloride buffer. Where the DEs are 77.8, 65.0, 53.9, 37.8 and 27.9% for pectins 7000, 7001, 7002, 7003 and 7004 respectively.

The weight average molecular weight of all five pectin samples is approximately constant in the range  $(190000 \pm 30000)$ g/mol which is typical of many pectin molecular weight previously quoted (Harding *et. al.*, 1991b; Cros *et. al.* 1995; Corredig *et. al.*, 2000 and Berth, 1992).

### 3.1.1.5 Concluding Remarks

It would appear from intrinsic viscosity and sedimentation velocity data that there are slight conformation differences between pectins with different degrees of esterification. Both data sets suggest that pectin 7001 (DE 65.0%) is the most flexible (highest sedimentation coefficient, lowest intrinsic viscosity) and that pectin 7003 (DE 37.8%) is least flexible (lowest sedimentation coefficient, highest intrinsic viscosity). This appears to make logical sense since the higher the DE, the lower the charge and lower intra-chain electrostatic repulsions, which are reflected in a more flexible structure even at 0.1M phosphate – chloride buffer, this situation would therefore be expected to be more pronounced in the absence of salt. The more asymmetric a structure is the larger the intrinsic viscosity and the smaller the sedimentation coefficient (see *e.g.* Tanford, 1961). We can however be more quantitative. For example, the Wales-van Holde ratio,  $R = k_s/[\eta]$  is a good indication of chain flexibility (see *e.g.* Harding, 1998), having a value of  $\sim 1.6$  for spheres and random coils and  $< 1.6$  for asymmetric structures, approaching a lower limit of  $\sim 0.2$  for a rigid rod. It can thus be seen from **Table 3-1** and **Figure 3-13** that pectin 7001 is the most flexible ( $R = 0.85 \pm 0.10$ ) and 7003 the least ( $R = 0.34 \pm 0.08$ ). A further manifestation of the effect of DE on chain flexibility is the translational frictional ratio,  $f/f_0$  (Tanford, 1961) (Equation 2-13) a parameter which depends on conformation and (molecular hydration). The clear decrease with decreasing DE is again consistent with a more flexible, less asymmetric structure at higher DE's.

It is worth stressing also that these changes in rigidity of the pectin with change in DE cannot be explained in terms of change in molecular weight increase, since the weight average molecular weight of all five pectin samples is approximately constant in the range  $(190000 \pm 30000)$ g/mol, *and* confirmed by two independent absolute techniques.

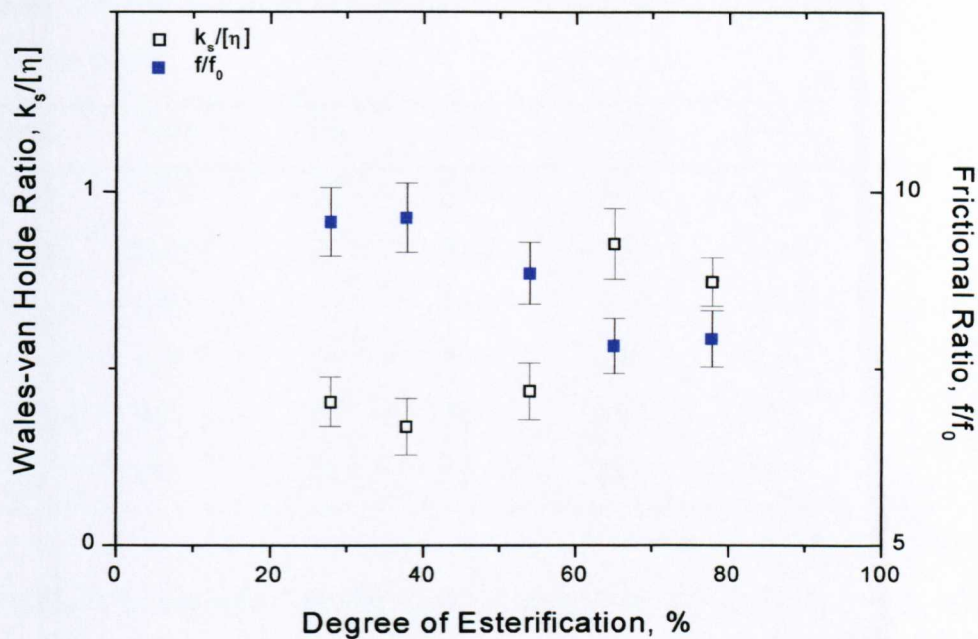


**Figure 3-13** Wales-van Holde and frictional ratios vs. DE for the Pectin 7000 Series in pH 6.8,  $I=0.1M$  phosphate/ chloride buffer. Where the DEs are 77.8, 65.0, 53.9, 37.8 and 27.9% for pectins 7000, 7001, 7002, 7003 and 7004 respectively.

We can take the analysis one step further based on rigid particle hydrodynamics to estimate relative molecular hydration using the premise that  $R$  is a hydration independent function (Rowe, 1977; Creeth and Knight, 1965) whereas  $(f/f_0)$  depends on hydration *and* conformation. The Wales-van Holde ratio allows us to calculate the axial ratio (Harding and Cölfen, 1995), using the ELLIPS1 program (Harding *et. al.*, 1997a). The Perrin function (frictional ratio due to shape),  $P$  and hydration,  $\delta$  can then be estimated from equations 2-14 and 2-78 (Harding *et. al.*, 1997b).

**Table 3-2** Calculated parameters for pectin 7000 series in pH 6.8, I=0.1M phosphate/chloride buffer.

Pectin	7000	7001	7002	7003	7004
DE, %	77.8	65.0	53.9	37.8	27.9
$k_s/[\eta]$	0.75	0.85	0.44	0.34	0.41
a/b	8.6	6.9	21.0	37.0	23.8
P	1.5	1.4	2.0	2.6	2.1
$V_s$ , ml/g	99	117	52	33	58
$\delta$	99	117	52	33	58

It should be stressed that this type of analysis is applicable to quasi-rigid types of molecules (*e.g.* proteins and highly charged or helical polysaccharides). However trends can be discerned and we can see that (in general) the pectins become more flexible (less asymmetric) and more hydrated as DE increases.

### 3.1.2 Effect of High Temperature

#### 3.1.2.1 Background

Relatively little has been published on the ultracentrifuge behaviour of macromolecular solutions at elevated temperature ( $>40^{\circ}\text{C}$ ). This is surprising considering that in many food or pharmaceutical processes macromolecules are exposed to elevated temperatures: Attempts to increase our knowledge of the behaviour of these molecules, in terms of structural integrity and state of oligomerisation would therefore be useful.

#### 3.1.2.2 LM Pectin

##### Materials

The low methoxy pectin (degree of esterification  $\sim 30\%$ ) of high degree of purity was a gift from CP Kelco ex. Citrus Colloids Ltd. (Hereford, UK). The material was solubilised for 24 hours in pH 6.8, ionic strength 0.1, standard phosphate/ chloride buffer (Green, 1933), of the following composition  $\text{Na}_2\text{HPO}_4 \cdot 12\text{H}_2\text{O}$  - 4.595g;  $\text{KH}_2\text{PO}_4$  - 1.561g and  $\text{NaCl}$  - 2.923g all made up to 1litre and then dialysed against this buffer.

##### Methods

##### Viscometry

Solutions and reference solvents were analysed using a 2ml Ostwald viscometer (Schott-Geräte, Mainz, Germany) under precise temperature control ( $\pm 0.01^{\circ}\text{C}$ ) and  $\eta_{\text{rel}}$ ,  $\eta_{\text{sp}}$  and  $\eta_{\text{red}}$  were calculated according to equations 2-34, 2-35 and 2-36.

### Elevated temperature sedimentation velocity

The high temperature unit for the Beckman Model E analytical ultracentrifuge allows centrifugation at temperatures up to 125°C, however for aqueous solutions temperatures > 80°C are impractical. Since parallel measurements were being made with SEC/MALLS, and the latter set-up has a high temperature limit of 60°C, we restricted our ultracentrifuge studies to this upper limit for temperature. Both the rotor and sample cells are pre-heated to the required temperature prior to sample injection. Samples were run at 52640rpm and Schlieren images were captured semi-automatically onto photographic film.  $s_{T,b}$  values were calculated from Schlieren images using a graphics digitising tablet.  $s_{20,w}$  values were then calculated from  $s_{T,b}$  values (sedimentation coefficients at temperature, T and in buffer, b) using the standard equation 2-10 [see for example, Ralston, 1993; Pavlov, 1997]. A partial specific volume (for the macromolecular component),  $\bar{v}$  of (0.63±0.01) was used and assumed to be constant with temperature (see section 3.1.1.4).

There are many additional problems in the use of elevated temperature analytical ultracentrifugation. At higher temperatures the maximum rotor speed must be reduced by ~ 1% per 10°C above 40°C. Care has to be taken in the choice of gaskets, centrepieces and windows: centrepieces used of the KEL-F type. Oil condensation on the chamber lenses is a major problem, which results in poor image resolution. For more information see Beckman, 1974.

### SEC-MALLS

The eluent was the standard pH 6.8 I=0.1 buffer and the injection volume was 100µl. The pectin refractive increment (dn/dc) of 0.15ml/g (Theisen *et. al.*, 2000) was assumed to independent of temperature.

Results and Discussion

**Table 3-3** The effect of temperature on the sedimentation coefficient, reduced viscosity and weight average molecular weight for LM pectin HL7192 in pH 6.8, I=0.1M phosphate/ chloride buffer.

Temperature, °C	$s_{T,b}$ , S	$s_{20,w}$ , S	$\eta_{red}$ , ml/g	$M_w$ , g/mol
20	1.57±0.03	1.59±0.03	268±1	-
30	2.05±0.03	1.62±0.03	263±2	107900±10000
40	2.54±0.04	1.64±0.04	257±2	113900±10000
50	3.31±0.04	1.78±0.04	243±1	112100±10000
60	4.22±0.05	1.92±0.05	241±5	124800±10000

From **Figure 3-14** we see that increase in temperature does not affect the unimodality of the sedimenting boundary as seen in earlier studies (Harding *et. al.*, 1991b). Although  $s_{T,b}$  shows a marked increase with increase in temperature (1.57S to 4.22S from 20°C to 60°C respectively), after correction to standard conditions of solvent viscosity and density the change is not spectacular: 1.57S to 1.92S (**Figure 3-15**). This agrees with the small decrease in reduced specific viscosity  $\eta_{red}$  from (268±1)ml/g to (241±5)ml/g (**Figure 3-16**). An increase in sedimentation coefficient together with a decrease in  $\eta_{red}$  would suggest a slight change in conformation to a more compact form (Tanford, 1961).

It is important also to establish the state of degradation/ association of the material before conclusions over conformation can be drawn, since both the sedimentation coefficient and intrinsic viscosity will be affected by mass as well as shape/hydration considerations: SEC/MALLS provided this. Over the temperature range 30°C to 60°C the molar mass as studied by SEC-MALLS remains relatively constant at approximately (115000±15000)g/mol (**Figure 3-17**), with no sign of dissociation.

This suggests that molecular breakdown is not occurring and therefore any changes in sedimentation coefficient and reduced specific viscosity are the result of conformational changes.

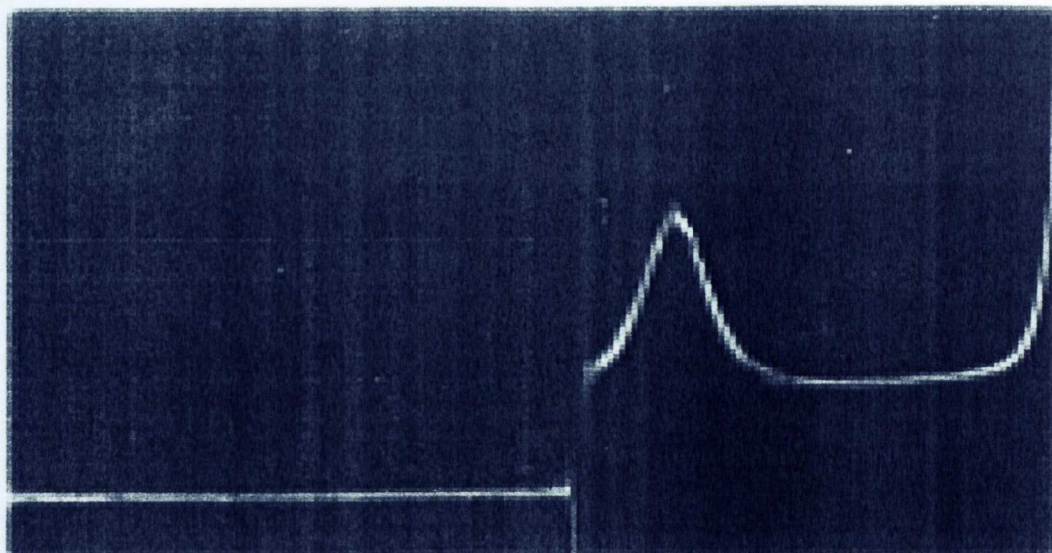


**Figure 3-14** Schlieren peak for LM Pectin HL7192 in pH 6.8, I=0.1M phosphate/chloride buffer, Temperature = 60°C; Concentration 2.3mg/ml; Rotor Speed 52640rpm; t = 3240sec,  $s_{obs} = 4.22S$  and  $s_{20,w} = 1.92S$ . Direction of sedimentation is from left to right.

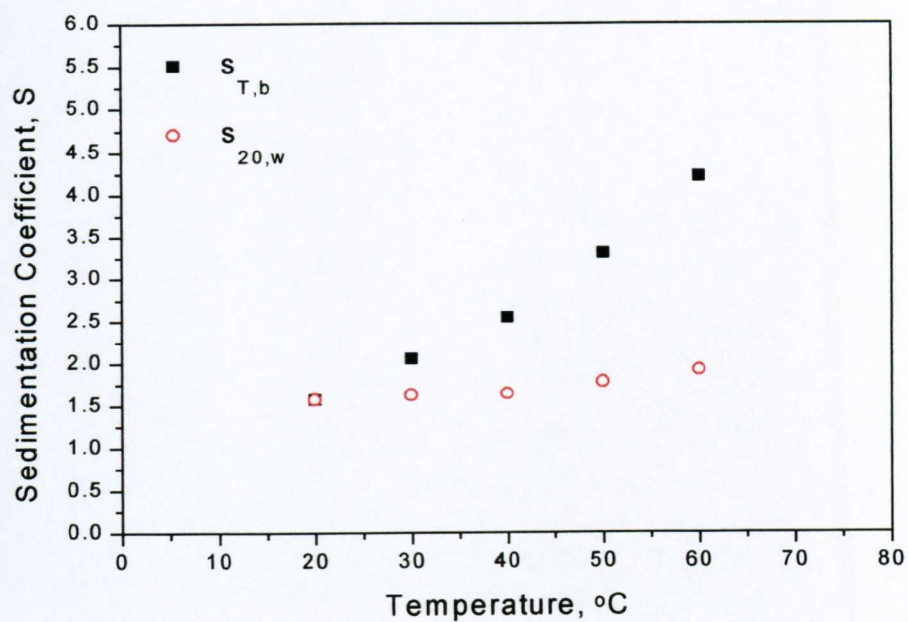


**Figure 3-15** The effect of increased temperature on  $S_{obs}$  and  $S_{20,w}$  for LM Pectin HL7192 in pH 6.8,  $I=0.1M$  phosphate/ chloride buffer.

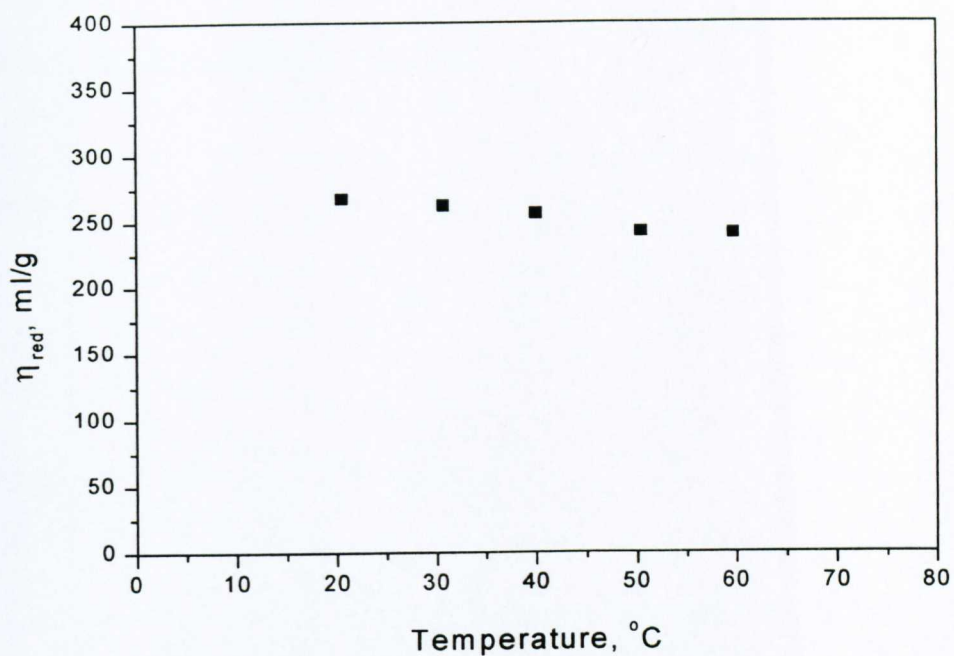


**Figure 3-16** The effect of increased temperature on the reduced viscosity for LM Pectin HL7192 in pH 6.8, I=0.1M phosphate/ chloride buffer.

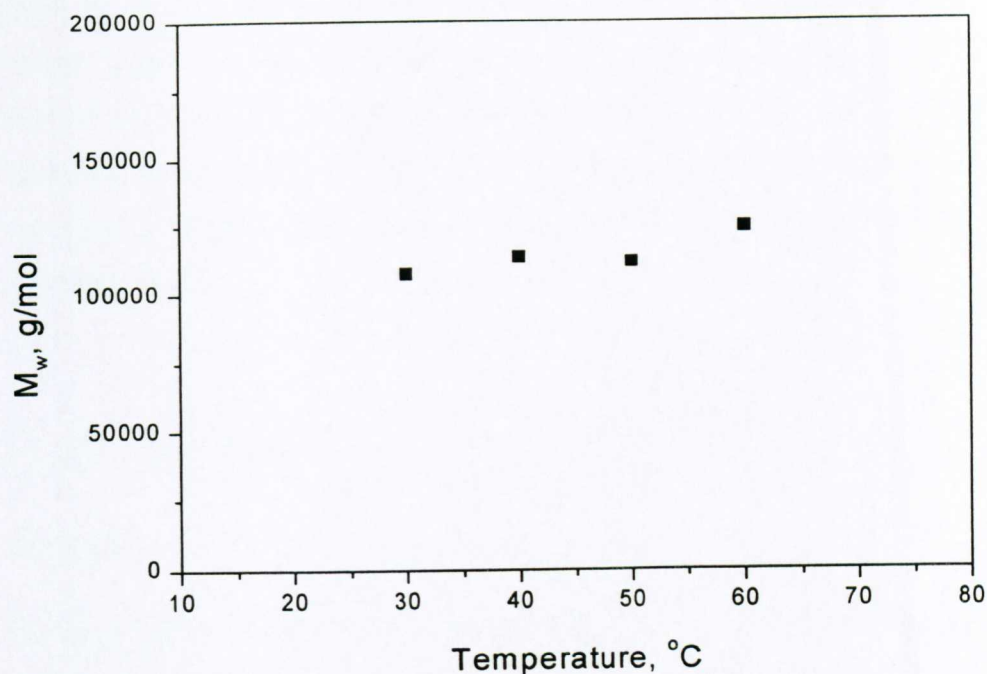


**Figure 3-17** The effect of increased temperature on the weight average molecular weight for LM Pectin HL7192 in pH 6.8,  $I=0.1\text{M}$  phosphate/ chloride buffer.

The apparent uniformity in molar mass over the temperature range together with the slight increase of  $s_{20,w}$  and the small decrease in reduced specific viscosity at increased temperatures suggests only a small conformational change. [Because measurements were made at only a single concentration, there is the possibility that this conclusion may be coloured by the fact we have assumed that

- (i) changes in reduced viscosity reflect changes in intrinsic viscosity
- (ii) the change in  $s_{20,w}$  at this concentration reflects changes in  $s_{20,w}^0$  (i.e. at  $c=0$ ).

As noted above, we have also assumed the partial specific volume has not significantly changed at elevated temperature.]

A low-methoxy pectin molecule at room temperature can be thought of as a rod/ semi-flexible rod type molecule. At elevated temperatures increased chain flexibility is apparent, this is most likely due to increased mobility with the input of thermal energy, together with the partial breakdown of inter- and intra-molecular forces. The fact pectin undergoes a partial transition, but in general terms remains intact at increased temperatures is important as pectin is often used as a stabiliser in heat treatment processes and can therefore give some greater insight into the complex chemistry involved.

### 3.1.2.3 *HM Pectin*

#### Materials

The high methoxy pectin (degree of esterification ~70%) of high degree of purity was a gift from CP Kelco ex. Citrus Colloids Ltd. (Hereford, UK). The material was solubilised for 24 hours in pH 6.8, ionic strength 0.1M, standard phosphate/ chloride buffer (Green, 1933), of the following composition  $\text{Na}_2\text{HPO}_4 \cdot 12\text{H}_2\text{O}$  - 4.595g;  $\text{KH}_2\text{PO}_4$  - 1.561g and  $\text{NaCl}$  - 2.923g all made up to 1litre (Green, 1933) and then dialysed against this buffer.

#### Methods

##### Viscometry

Solutions and reference solvents were analysed using a 2ml automatic Schott-Geräte Oswald viscometer (Schott-Geräte, Mainz, Germany), under precise temperature control ( $\pm 0.01^\circ\text{C}$ ). The relative,  $\eta_{\text{rel}}$  and specific,  $\eta_{\text{sp}}$  viscosities were calculated from equations 2-35 and 2-36.

A common method for measuring intrinsic viscosity (IUPAC - limiting viscosity number) is to calculate the relative and specific viscosity at one concentration (in this case 2.5 mg/ml) and employ the Solomon/ Ciuta approximation (Equation 2-41)

(Harding, 1997, Morris *et. al* 2000, Abel-Azim *et. al*, 1999, Kravtchenko and Pilnik, 1990). According to Kravtchenko and Pilnik (1990), the intrinsic viscosity can be accurately estimated (error 1%) by a single measurement at low concentration. In the same article they achieved good agreement between single point measurements and traditional multi-point extrapolations (see *e.g.* Harding, 1997, Kravtchenko and Pilnik, 1990, Morris *et. al*, 2000) for pectin solutions up to 5mg/ml.

#### Elevated temperature sedimentation velocity

The experimental procedure was identical to that previously described in the previous section for low methoxy pectin (see also Morris *et al.*, 1999), except apparent sedimentation coefficients,  $s_{20,w}$  were calculated at various concentrations from 0.5 to 2.5mg/ml and extrapolated to zero concentration using the standard equation 2-8 (see *e.g.* Ralston, 1993).

#### SEC-MALLS

The eluent was the standard pH 6.8 I=0.1 buffer and the injection volume was 100 $\mu$ l. The pectin refractive increment (dn/dc) of 0.15ml/g (Theisen *et. al.*, 2000) was assumed to independent of temperature.

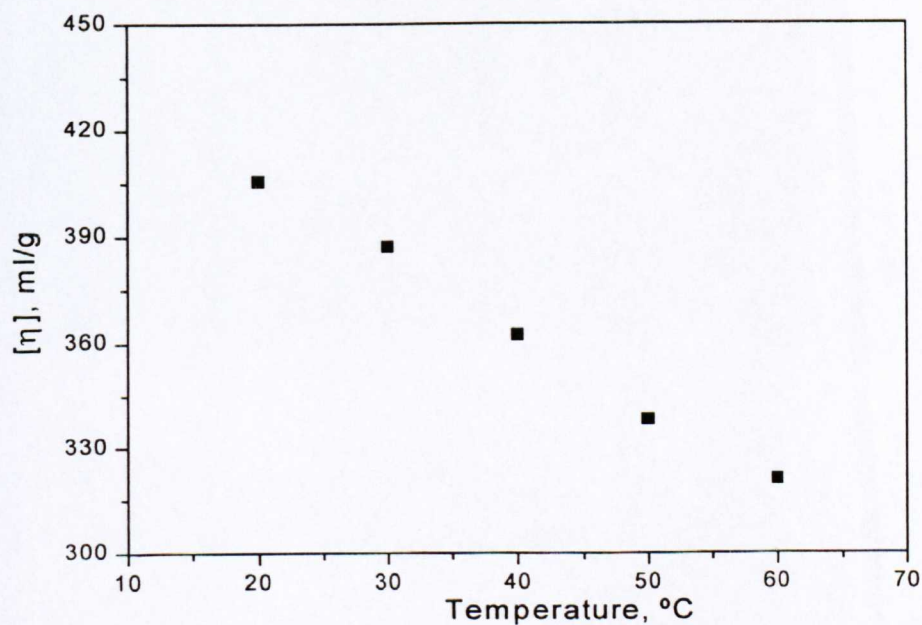
### Results and Discussion

#### Viscometry

There is a clear decrease in intrinsic viscosity,  $[\eta]$  with temperature up to 60°C (Table 3-4 and Figure 3-18), this would be indicative of molecular breakdown and/or a conformational change to a more compact shape, as observed by Morris *et. al.*, 1999 in the case of a low methoxy pectin under the same conditions.

**Table 3-4** Effect of temperature on a high methoxy pectin

Temperature, °C	$[\eta]$ , ml/g	$s_{20,w}^0$ , S	$M_w$ , g/mol	$f/f_0$
20	406±2	1.83±0.01	156000±10000	8.2±0.4
30	387±4	1.81±0.02	144500±10000	7.9±0.3
40	362±4	1.79±0.01	133000±10000	7.5±0.3
50	338±3	1.77±0.02	126500±10000	7.4±0.5
60	321±8	1.76±0.01	116700±10000	6.9±0.4

**Figure 3-18** Effect of increased temperature on the intrinsic viscosity,  $[\eta]$  for a high-methoxy pectin in standard phosphate chloride buffer (pH = 6.8, I=0.1M).

Elevated temperature sedimentation velocity

From **Figure 3-19** we see that increase in temperature does not affect the unimodality of the sedimenting boundary as seen in earlier studies (Harding *et. al.*, 1991b). As the temperature is increased there is a slight decrease in sedimentation coefficient,  $s_{20,w}^0$  (**Table 3-4** and **Figure 3-20**). This is again indicative of a decrease in molecular weight. Although this decrease in sedimentation coefficient does not rule out the possibility of a conformational change, it does suggest that any conformational change is minor in comparison to the decrease in molecular weight.

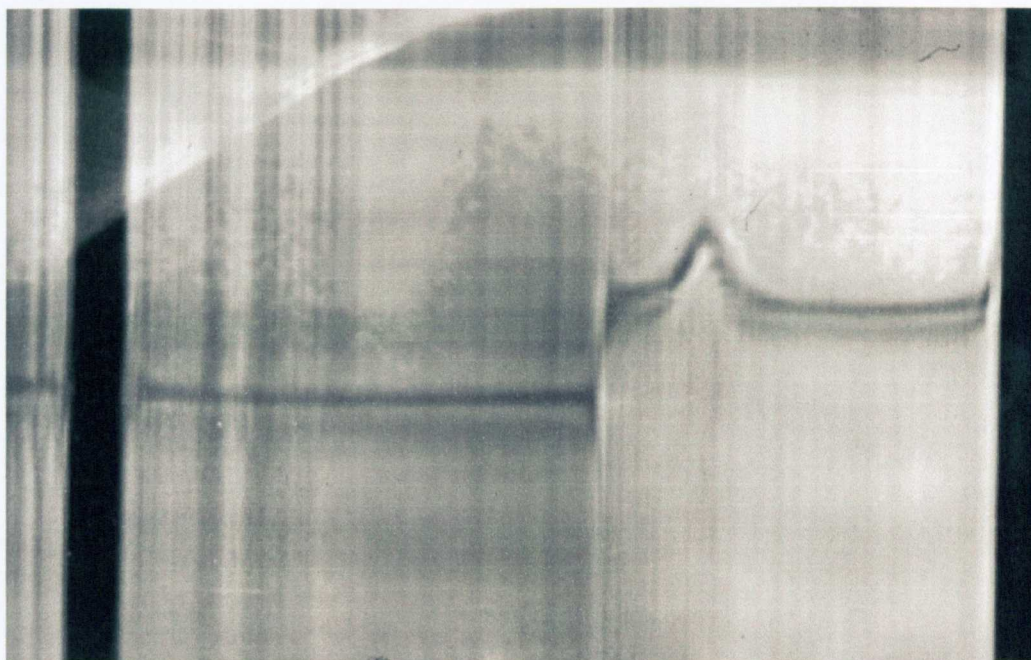


**Figure 3-19** Schlieren peak for a high methoxy pectin in standard phosphate chloride buffer (pH = 6.8, I=0.1M), direction of sedimentation left to right.

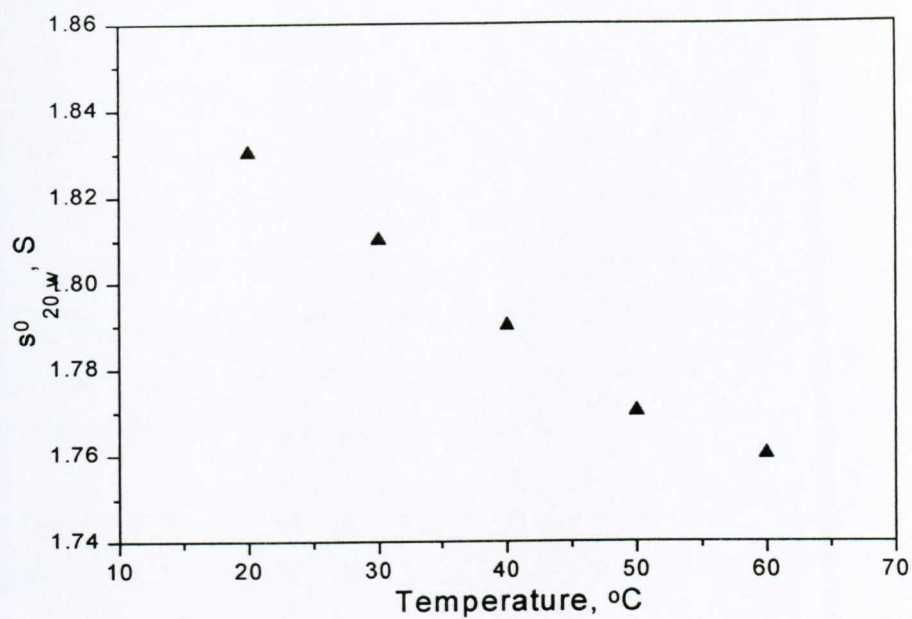


**Figure 3-20** Effect of increased temperature on sedimentation coefficient,  $s_{20,w}^0$  for a high-methoxy pectin in standard phosphate chloride buffer (pH = 6.8, I=0.1M).

## SEC-MALLS

It is clear from **Table 3-4** and **Figure 3-21** that there is a distinct decrease in molecular weight with increasing temperature. This is the contrary to the observations of Morris, *et. al.*, 1999 in the study of a low methoxy pectin. The molecular weight at 20°C is in good agreement with the molecular weight of 160,000g/mol obtained previously for this HM pectin from sedimentation equilibrium (extrapolated to zero concentration to account for thermodynamic non-ideality) in the analytical ultracentrifuge (Morris, unpublished).

Knowledge of both molecular weight and sedimentation coefficient allows the calculation of the translational frictional ratio,  $f/f_0$  (Equation 2-13) (Tanford, 1961). The decrease in  $f/f_0$  (**Table 3-4 & Figure 3-22**) would indicate a reduction of the polymer chain length, consistent with a reduction in molecular integrity.

The linear relationship between  $\log M_w$  and  $\log [\eta]$  at each temperature (**Figure 3-23**) virtually confirms that no major change in conformation was accompanying the change in molecular weight. The Mark Houwink (MHKS) exponent of 0.84 is consistent with the expected pectin value of 0.79, calculated by Berth *et. al.*, 1977.

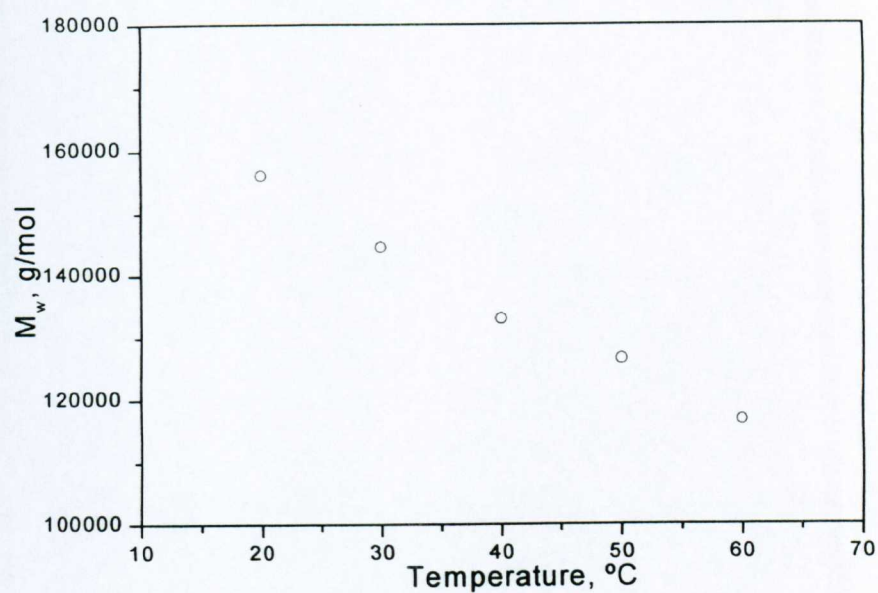


**Figure 3-21** Effect of increased temperature on the weight average molecular weight,  $M_w$  for a high-methoxy pectin in standard phosphate chloride buffer (pH = 6.8, I=0.1M).

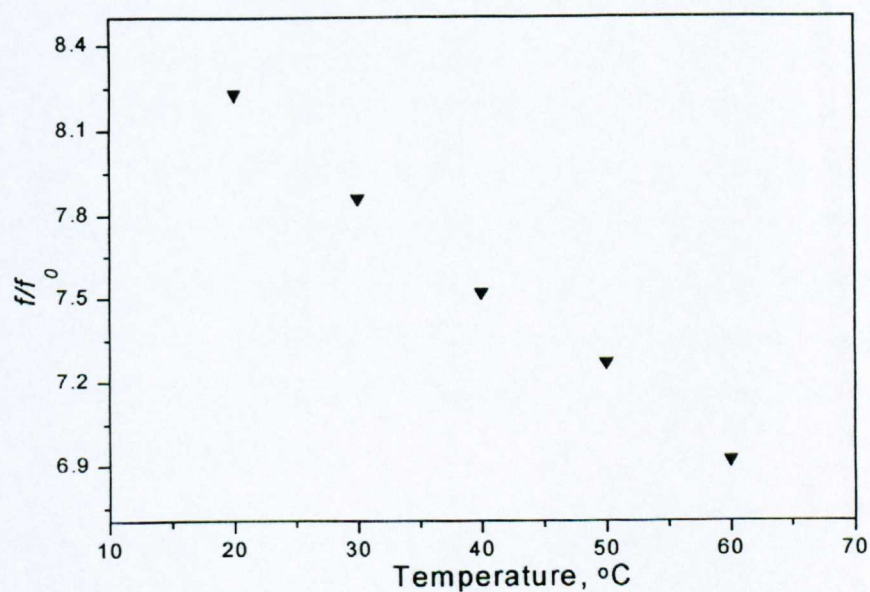


**Figure 3-22** Effect of increased temperature on the translation frictional ratio,  $f/f_0$  for a high-methoxy pectin in standard phosphate chloride buffer (pH = 6.8, I=0.1M).

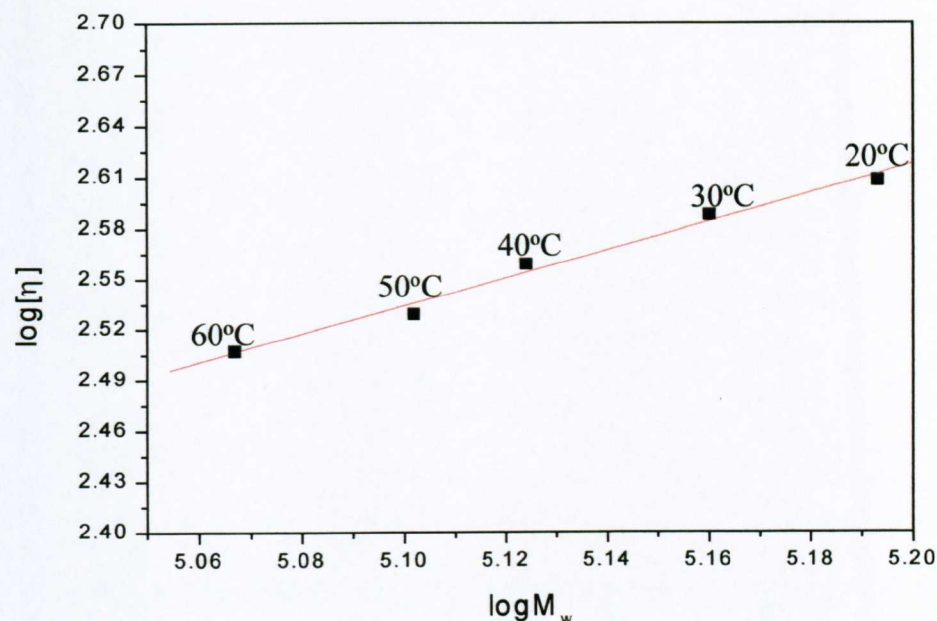


**Figure 3-23** Mark-Houwink (MHKS) plot for a high-methoxy pectin at different temperatures in standard phosphate chloride buffer (pH = 6.8, I=0.1M).

The results obtained clearly indicate that HM pectins, unlike LM pectins (Morris *et al.*, 1999) undergo a loss of structural integrity at elevated temperatures (up to 60°C). HM pectins are susceptible to  $\beta$ -elimination at  $\text{pH} \geq 7$ , even at room temperature (Pilgrim *et al.*, 1991). According to Pilgrim and co-workers, a combination of elevated temperature and long holding times increases the likelihood that aqueous pectin solutions will lose viscosity (molecular weight) through  $\beta$ -elimination of water. It is also likely that partial de-esterification is at least partly responsible for the loss of molecular integrity. It is therefore probable that we are observing (using capillary viscometry, sedimentation velocity and SEC-MALLS) an increase in the rates of these reactions at elevated temperatures.

It possible to quantify this depolymerisation using the “blob” model approach of Dondos (2001) However due to small reductions in molecular weight and intrinsic viscosity the extrapolation procedure is not as reliable as that discussed in section 3.3 concerning guar samples. This is especially true for the Stockmayer-Fixman-Burchard plot (**Figure 3-25**).

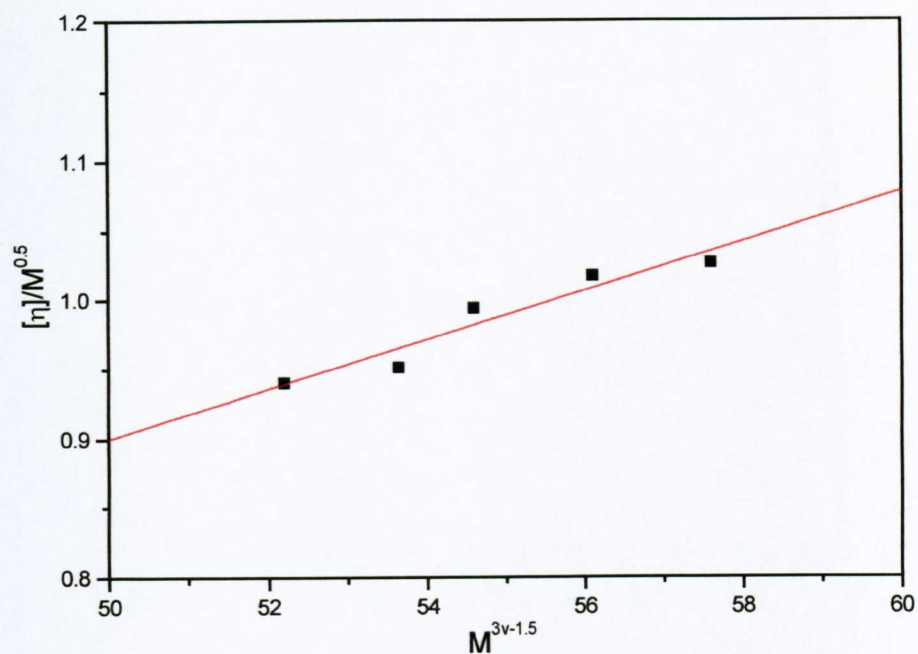


**Figure 3-24** “Blob” model plot of  $\frac{[\eta]}{M^{0.5}}$  vs.  $M^{3v-1.5}$  for a high methoxy pectin sample at elevated temperatures in standard phosphate chloride buffer (pH = 6.8, I=0.1M) (as explained in section 2.7 and Dondos, 2001).

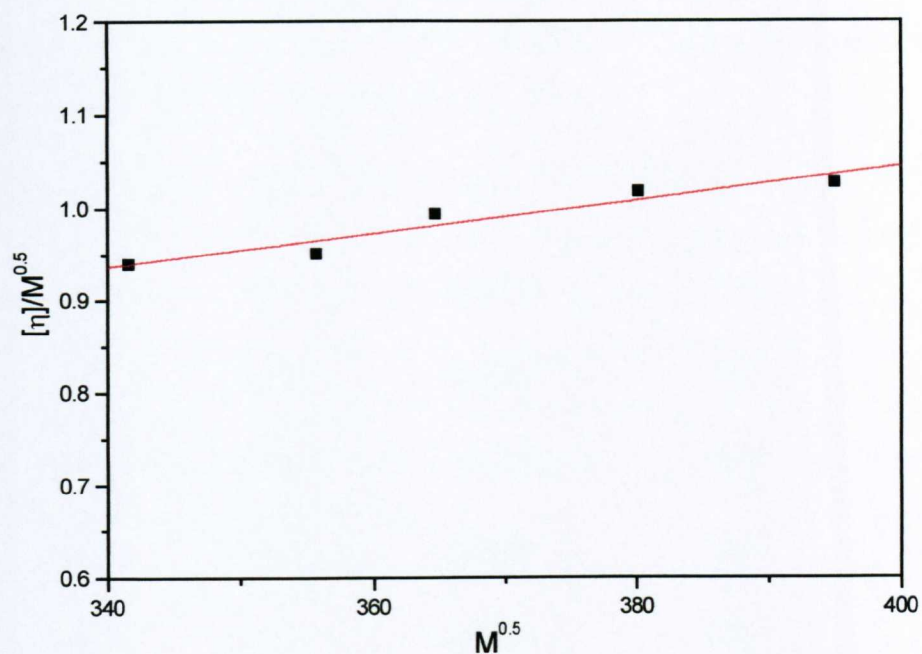


**Figure 3-25** Stockmayer-Fixman-Burchard plot of  $\frac{[\eta]}{M^{0.5}}$  vs.  $M^{0.5}$  for a high methoxy pectin sample at elevated temperatures in standard phosphate chloride buffer (pH = 6.8, I=0.1M).

**Table 3-5** Results of the “blob” model approach for calculating the number of Kuhn statistical segments per chain for a high methyl pectin sample at elevated temperature, from the equations 2-84 - 2-91 and the plots above.

Temperature, °C	$[\eta]$	$M_w$	N
20	406	156000	168
30	387	144500	155
40	362	133000	143
50	338	126500	136
60	321	116700	125

where  $M_L = 2.83 \times 10^9$  g/cm;  $\lambda^{-1} = 3.29 \times 10^{-7}$  cm;  $L_p = 1.65 \times 10^{-7}$  cm;  $\nu = 0.61$ ;  $C = 0.60$ ;  $N_c = 1.21$  and  $K_\theta = 0.33$  (as explained in section 2.7 and Dondos, 2001)

Although it appears from (Table 3-5) that there is a decrease in segment length with increasing temperature, an average decrease of ten segments per chain is on or near the limit of sensitivity of this modelling technique.

This decrease in molecular weight (probably due to  $\beta$ -elimination) is clearly important in the processing of products containing HM pectins, as many food and pharmaceutical processes involve at least one heat treatment stage.

#### 3.1.2.4 Concluding Remarks

Clearly there is a significant effect of high temperature on the hydrodynamic properties of the high methoxy pectin. The effect on the low methoxy pectin is less pronounced and can be regarded as a minor conformational change to that of a more compact molecule. This set of experiments demonstrates quite clearly the susceptibility of high methoxy pectin toward  $\beta$ -elimination as compared to low methoxy pectin. This is important in processing.

### 3.1.3 Effect of Carboxybenzyl Derivatisation

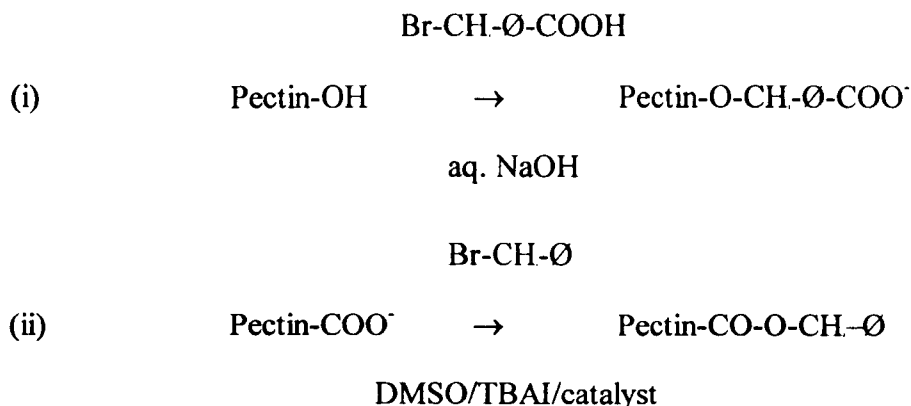
#### 3.1.3.1 Background

Partially hydrophobised pectin derivatives can give rise to new products of industrial importance. Recently, higher alkyl esters of pectin and pectic acid were reported to have improved hydrophobic binding to bile acids and soy proteins what may be useful in medicine and food industries (Klavons and Bennet, 1995). It is therefore of interest to determine the analytical and physical properties of substituted pectins, in order to determine the effect of chemical modification on molecular structure. The effect of two derivatisation methods on two pectin samples has been studied using a variety of hydrodynamic and structural techniques.

#### 3.1.3.2 Materials

Two pectin samples KP and LMP were converted to the carboxybenzyl derivative via

- (i) alkylation of the hydroxyl groups with *p*-carboxybenzyl bromide in alkaline medium (Ebringerova *et. al.*, 1996) and
- (ii) transformation of the tetrabutylammonium salt (TBA) into the benzyl ester by reaction with benzyl bromide in dimethyl sulphoxide (DMSO) (Crescenzi and Della Valle, 1991).



where  $\emptyset$  represents a phenyl group

### 3.1.3.3 Methods

Degrees of substitution and sugar compositions were calculated by the group of Dr. Anna Ebringerova at the Institute of Chemistry, Slovak Academy of Sciences from  $^{13}\text{C}$  NMR spectra.

The water-soluble fraction of parent pectins (KP and LMP) and modified pectins (CB-KP, LMPG2 - alkaline modification and LMPG3 - TBA modification) were then hydrodynamically characterised using sedimentation velocity (sedimentation time derivative see for example Stafford, 1992a,b and Laue and Stafford, 1999), size exclusion chromatography coupled to multi-angle laser light scattering and capillary viscometry.

#### Capillary Viscometry

Solutions and reference solvents were analysed using a 2ml automatic Schott-Geräte Oswald viscometer, under precise temperature control ( $25.33 \pm 0.01$ )°C. The relative,  $\eta_{\text{rel}}$ , specific,  $\eta_{\text{sp}}$  and intrinsic viscosities were calculated from Equations 2-34, 2-35 and 2-41 respectively.

### Sedimentation Velocity in the Analytical Ultracentrifuge

The Optima XLI (Beckman Instruments, Palo Alto, USA) equipped with Rayleigh interference optics was used to determine the sedimentation behaviour of the pectin samples. Rotor speeds of 50,000rpm and a 4mm column length in 12mm optical path length double sector cells were used together with an accurately controlled temperature of 20.0°C. A weighted average partial specific volume,  $\bar{v}$  of (0.63±0.01)ml/g was assumed for both native and substituted pectins (see section 3.1.1.4). The  $g^*(s)$  (sedimentation time derivative) method was used to determine apparent sedimentation coefficients at each concentration. As the sedimenting boundary moves towards the cell base the change in concentration (of the sedimenting species) over time ( $dc/dt$ ) is calculated from the subtraction of multiple pairs of scans (maximum 20 pairs), an apparent sedimentation coefficient distribution  $g^*(s)$  can in this way be produced (Stafford, 1992a,b and Laue & Stafford, 1999). The apparent weight average sedimentation coefficient,  $s^*$  is then calculated.  $s_{20,w}$  values can then be generated according to the standard equation (see *e.g.* Ralston, 1993; Pavlov, 1997) (Equation 2-10). Apparent sedimentation coefficients,  $s_{20,w}$  were calculated at various concentrations from 0.5 to 2.5mg/ml and extrapolated to zero concentration using the standard equation 2-8 (Ralston, 1993). In addition the concentration of the water-soluble fraction was estimated from the areas under the  $g^*(s^*)$  curve.

### SEC-MALLS

The eluent was the standard pH 6.8 I=0.1 “Paley” buffer and the injection volume was 100µl. A value for the refractive index increment of 0.146ml/g was used (Chapman *et. al.*, 1987). The area under the refractive index vs. elution volume curve gave an additional estimation of concentration.

## 3.1.3.4 Results and Discussion

The structural and analytical analyses from the Slovak Academy of Sciences suggested that the pectins had been derivatised by approximately 5% (Table 3-6); this was further indicated by shoulders at 1545 cm<sup>-1</sup> and 1500 cm<sup>-1</sup> in the infrared spectra of carboxybenzyl and benzyl derivatives respectively (Figure 3-26).

**Table 3-6** Analytical data for parent and derivatised pectins

Sample	Sugar Composition, % <sup>a</sup>			DS, %	UV <sub>max</sub> , nm
	Ara	Gal	GalA		
KP	1	11	88	-	198
CB-KP	1	10	89	5 <sup>b</sup>	202, 241
LMP	-	-	91	-	210
LMPG2	5	6	89	4 <sup>b</sup>	197, 236
LMPG3	6	11	84	7 <sup>b</sup>	199, 284

a) calculated from the <sup>13</sup>C signal areas of the corresponding anomeric carbon atoms

b) calculated from the <sup>13</sup>C signal areas of the aromatic protons on C-1 of GalA

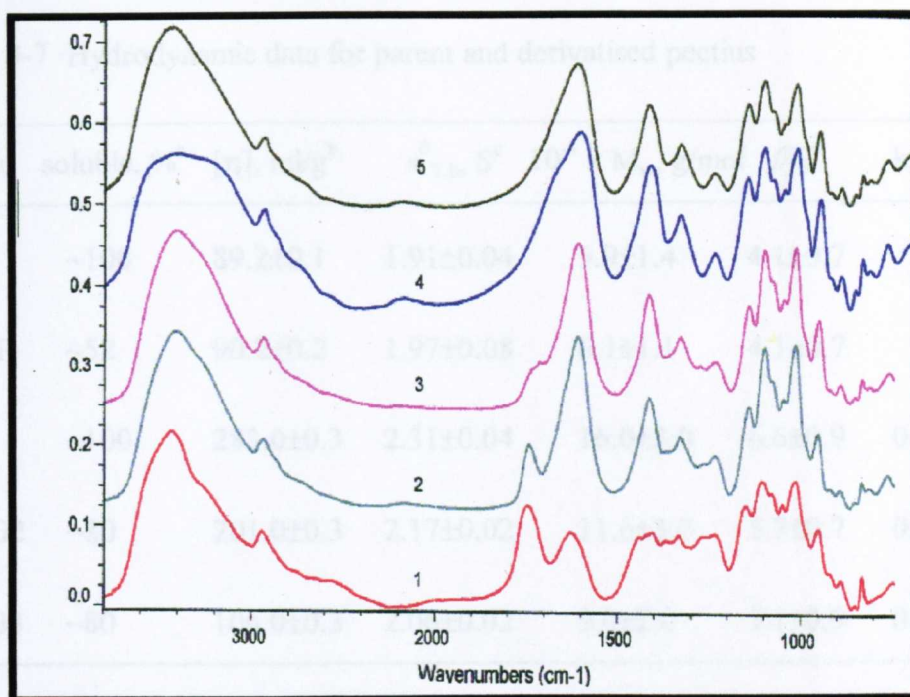


**Figure 3-26** FT-IR spectra for parent and derivatised pectin samples 1) LMP, 2) LMPG3, 3) LMPG2, 4) KP and 5) CB-KP.

### Capillary Viscometry

There are significant differences in the intrinsic viscosities of the two native pectins KP and LMP, 89 and 283 ml/g respectively. However in the case of KP there is little or no difference between the intrinsic viscosities of the native and derivatised samples. This is very different for the LMP sample, for which there is approximately a 30% decrease in viscosity during alkaline derivatisation and a 65% decrease in viscosity during (neutral) DMSO modification (**Table 3-7**). [Note – concentrations were recalculated from the respective  $g^*(s^*)$  curves].

**Table 3-7** Hydrodynamic data for parent and derivatised pectins

Sample	soluble, % <sup>a</sup>	$[\eta]$ , ml/g <sup>b</sup>	$s_{T,b}^0$ , S <sup>c</sup>	$10^{-4} \times M_w$ , g/mol	$f/f_0$ <sup>d</sup>	$k_s/[\eta]$ <sup>e</sup>
KP	~100	89.2±0.1	1.91±0.04	5.9±1.4	4.1±0.7	-
CB-KP	~52	90.2±0.2	1.97±0.08	6.1±1.1	4.1±0.7	-
LMP	~100	283.0±0.3	2.31±0.04	16.0±3.0	6.6±0.9	0.51±0.04
LMPG2	~80	201.0±0.3	2.17±0.02	11.6±3.0	5.7±0.7	0.63±0.06
LMPG3	~80	106.0±0.3	2.06±0.02	9.0±2.0	5.1±0.9	0.85±0.09

a) from the area under the  $g^*(s^*)$  curve

b) calculated from the single point Solomon-Ciuta approximation, (see *e.g.* Kravtchenko and Pilnik, 1990; Harding, 1997; Abel-Azim *et. al.*, 1998)

c) weight average sedimentation coefficient

d) the translational frictional ratio,  $f/f_0$  (Tanford, 1961)

e) Wales-van Holde ratio,  $k_s/[\eta]$  (where  $k_s$  is the concentration dependency of sedimentation, Gralén, 1944)

### Sedimentation Velocity in the Analytical Ultracentrifuge

It is clear from Table 3-7 that a large amount of material remains insoluble after both alkaline and neutral derivitisation. This can be seen by the decrease in area of the  $g^*(s^*)$  curve (Figure 3-27).

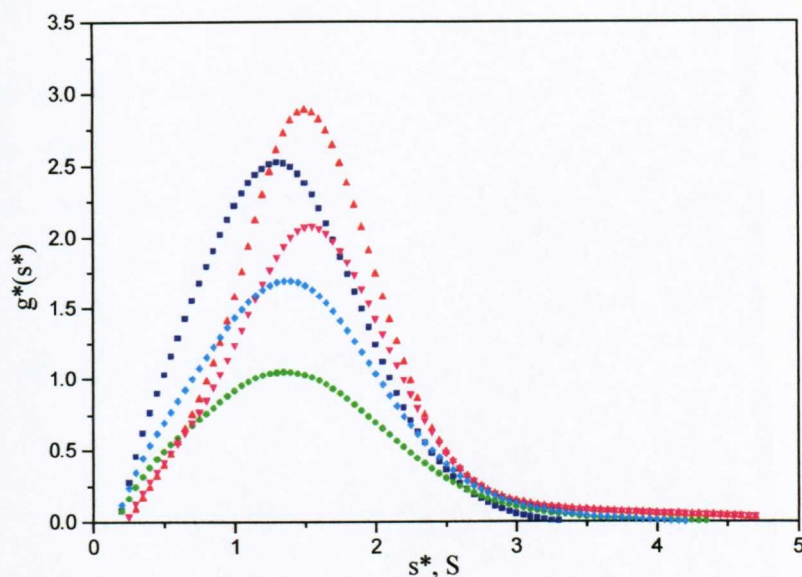


**Figure 3-27**  $g^*(s^*)$  profiles for parent and substituted pectins. Legend – KP – navy squares, CB-KP – green circles, LMP – orange up-triangle, LMPG2 – pink down-triangle and LMPG3 – cyan diamond.

When sedimentation coefficients are extrapolated to infinite dilution we see a similar trend to that of intrinsic viscosity, *i.e.* there is a significant difference between the sedimentation coefficients of the native pectins (**Table 3-7**) and that in the case of LMP there is a decrease in sedimentation coefficient upon derivitisation (**Table 3-7**). This together with a decrease in intrinsic viscosity would indicate molecular degradation, which is supported by the corresponding increase in the Wales – van Holde ratio, suggesting a decrease in axial ratio. It should be noted that the sedimentation coefficient is less sensitive to a decrease in molecular weight for a rigid or semi-rigid molecule such as low methoxy pectin than intrinsic viscosity, the converse is true for a compact molecule.

SEC-MALLS

The weight average molecular weight for KP is significantly lower than for LMP, this is consistent with both viscosity and sedimentation data (Table 3-7). Again it can be seen that the derivatives LMPG2 and LMPG3 (Figure 3-28) are of significantly lower molecular weight than the native pectin LMP and that there is little or no difference between the molecular weights for KP and CB-KP (Figure 3-28), this is again consistent with other techniques (Table 3-7).

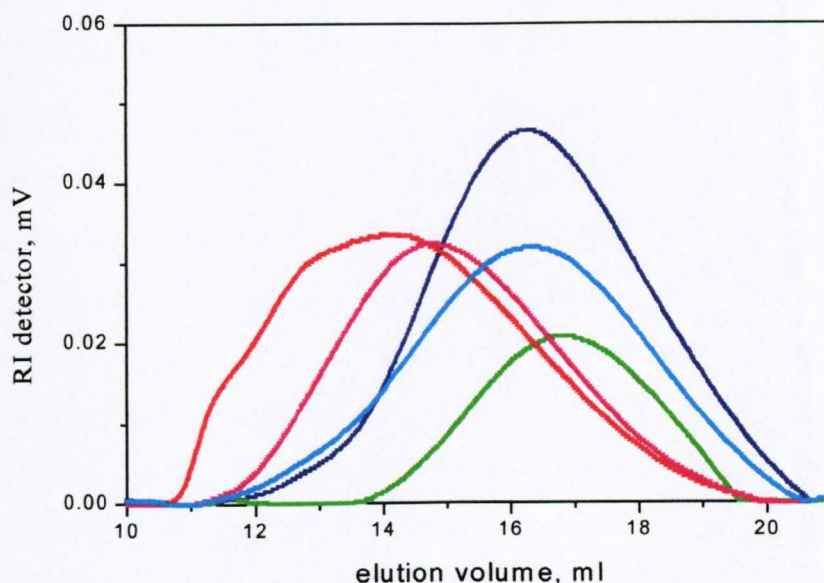


**Figure 3-28** Elution profiles for parent and substituted pectins. Legend – KP – navy squares, CB-KP – green circles, LMP – orange up-triangle, LMPG2 – pink down-triangle and LMPG3 – cyan diamond.

One can again see the loss in soluble material for the derivatised samples; this is especially noticeable for CB-KP (green circles).

### 3.1.3.5 Concluding Remarks

Modification of KP and LMP under mild conditions yielded water soluble derivatives exhibiting low DS (Table 3-6) indicated by the signal areas of the aromatic protons on C-1 of galacturonic acid using  $^{13}\text{C}$  NMR, this was further supported by FT-IR (Figure 3-26).

The introduction of small amounts of *p*-carboxybenzyl (CB) ether groups had practically no effect on the hydrodynamic properties in the case of KP. The soluble fraction (~52%) of CB-KP has similar hydrodynamic properties to the parent pectin KP (Table 3-7, Figure 3-27 and Figure 3-28).

However, the CB-derivative of LMP, LMPG2 as well as the benzyl ester LMPG3 show significantly reduced weight average molecular weight,  $M_w$ , weight average sedimentation coefficient,  $s_{T,b}^0$  and intrinsic viscosity,  $[\eta]$  when compared to the native pectin (Table 3-7, Figure 3-27 and Figure 3-28). These data can be further interpreted in terms a decrease in translational frictional ratio (Tanford, 1961) and an increase in the Wales – van Holde ratio (Table 3-7). We suggest that the decrease in molecular weight is due to chain cleavage from  $\beta$ -elimination and that the increased reaction time for the neutral (benzylation of the carboxylate groups in DMSO) protocol results in increased cleavage. KP appears to more tolerant to reaction conditions this is perhaps due to the fact that a large amount of the native methyl esters had been removed prior to derivatisation, as the methyl esters are the primary driving force in  $\beta$ -elimination reactions this should at least partially explain the increased tolerance and the low molecular weight of the native pectin, KP.

As derivatised polysaccharides are increasingly finding uses in both medical and food industries it may be of considerable interest to try to determine which physical changes (if any) modification has on polysaccharide moiety. This will be further investigated for another plant cell-wall polysaccharide arabinoxylan in section 3.5.

## 3.2 CHARACTERISATION OF CARRAGEENANS

### 3.2.1 Background

Carrageenans are a group of industrially important water-soluble polysaccharides extracted from red seaweed (Vreeman *et. al.*, 1980; Harding *et. al.*, 1997; Myslabodski *et. al.*, 1996; Quemener *et. al.*, 2000; Bongaerts *et. al.*, 2000; Viebke *et. al.*, 1995 and Viebke and Williams, 2000). The carrageenans consist of alternating 4-linked  $\alpha$ -D-galactosyl and 3-linked  $\beta$ -D galactosyl residues, the main commercial carrageenans –  $\kappa$ ,  $\iota$  and  $\lambda$ , differ from each other by the amount and location of ester sulphate (Myslabodski *et. al.*, 1996)  $\kappa$  has one sulphate group per disaccharide,  $\iota$  has two and  $\lambda$  has three (Langendorff *et. al.*, 2000a,b)(Figure 3-29).

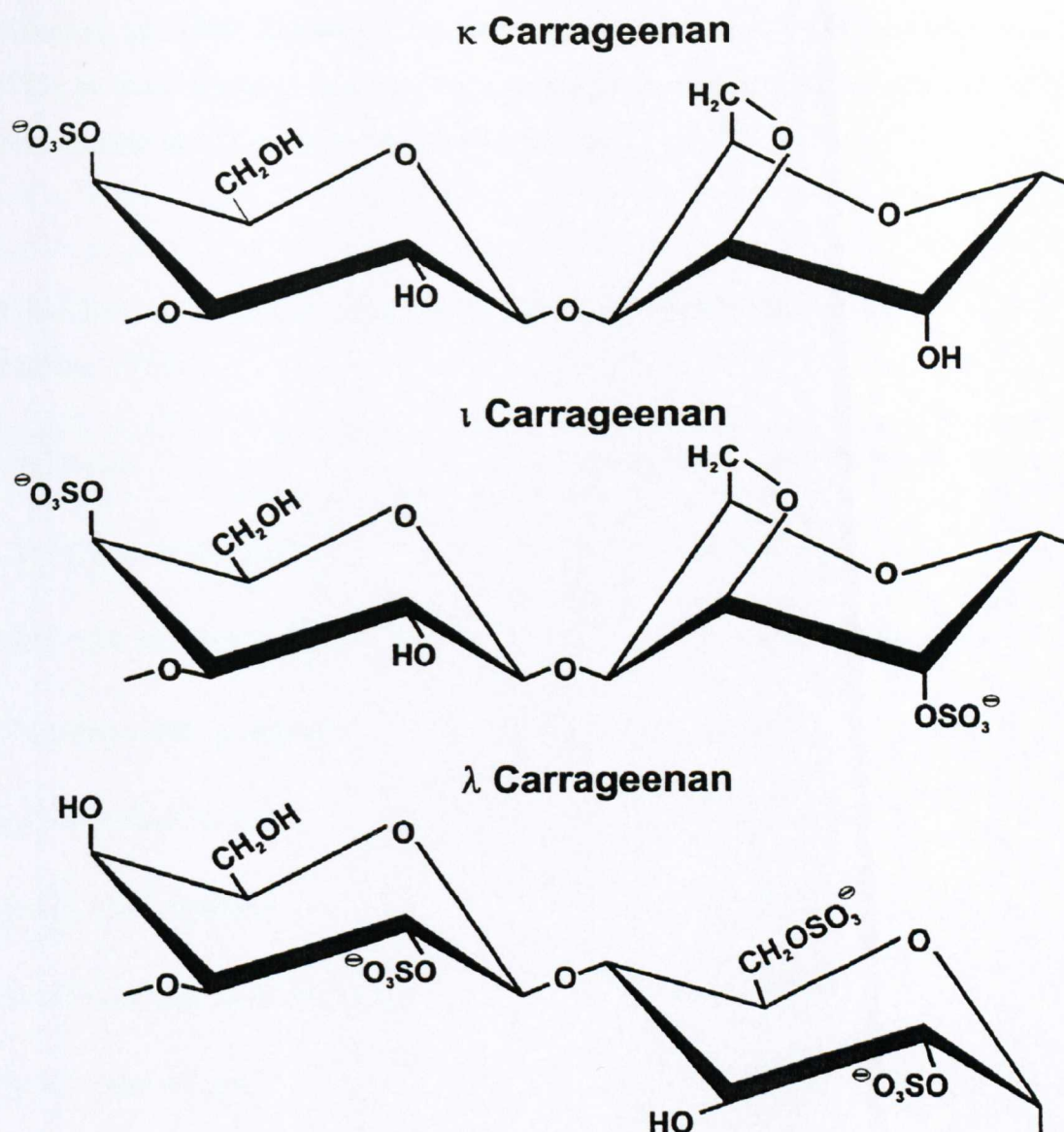


**Figure 3-29** Idealised structure for the commercial carrageenans (adapted from Tombs and Harding, 1998).

Carrageenans are widely used in the food industry for their gelling and thickening properties (Quemener *et al.*, 2000; Viebke *et al.*, 1995 and Tombs and Harding, 1998) (Table 3-8). Both  $\kappa$  and  $\iota$ -carrageenans in aqueous solution undergo temperature dependent transitions from an ordered helical state at low temperature to a disordered random coil state at higher temperature (Morris, 1979, 1980; Chambers *et al.*, 1994; Viebke *et al.*, 1995; Schorsch *et al.*, 2000; Langendorff *et al.*, 2000a,b; Viebke *et al.*, 1995 and Bongaerts *et al.*, 2000). The helical form is required for gelation. The coil – helix – gel mechanism (Norton *et al.*, 1978; Morris, 1979, 1980;

Morris *et al.*, 1980; Rochas and Rinaudo, 1984; Chambers *et al.*, 1994; Viebke *et al.*, 1995) is most favoured however as  $\lambda$ -carrageenan cannot form a helix due to the steric hindrance it is therefore unable to form gels.

**Table 3-8** Major uses of carrageenans in the food industry (adapted from Tombs and Harding, 1998)

Application	carrageenan type and content, %
Chocolate milk stabilisation	$\kappa$ , 0.02-0.03
Filled milk stabilisation	$\kappa$ or $\iota$ , 0.02-0.04
Evaporated milk stabilisation	$\kappa$ , 0.0005
Ice cream stabilisation	$\kappa$ , 0.02-0.03
Coffee-white stabiliser	$\lambda$ , 0.1-0.3
Instant pie filling cream thickener	mixed, 0.1-3
Gelled water dessert	$\kappa$ , $\iota$ , 0.5-1
Canned food stabilisation	$\kappa$ , 0.5-2
Beer clarification	trace

It is still debatable whether the helical forms of  $\kappa$ - and  $\iota$ -carrageenan are single or double helices, although the main body of evidence would support a double helical structure - Bongaerts *et al.* (2000) report a single helix conformation for  $\iota$ -carrageenan, Ciancia *et al.*, (1997) reports a single helix for  $\kappa$ -carrageenan; Morris (1980, 1990) claims  $\iota$ - and  $\kappa$ -carrageenan form double helices; as does Viebke *et al.* (1995) and Viebke and Williams (2000) for  $\kappa$ -carrageenan. The ionic environment is also important in helical stability; in the case of both  $\kappa$ - and  $\iota$ -carrageenan the

stabilising effect of counterions follows the lyotropic (Hofmeister) series (*i.e.*  $\text{Li}^+$ ,  $\text{Na}^+$ ,  $\text{NR}_4^+ \ll \text{NH}_4^+ < \text{K}^+ < \text{Cs}^+ < \text{Rb}^+$ ) (Norton *et al.*, 1983; Rochas and Rinaudo, 1984; Austen *et al.*, 1988; Ciancia, *et al.*, 1997; Norton, 1990; Morris, 1990; Augustin *et al.* 1999) although this is less pronounced in the case of iota-carrageenan (which also forms stable helices with divalent cations), Morris (1990) suggests that counterion binding is non-specific “atmospheric” attraction: due to the high charge density of the polymer, although in the case of  $\kappa$ -carrageenan there may be site specific binding in the case of the larger group 1 cations ( $\text{K}^+$ ,  $\text{Cs}^+$ ,  $\text{Rb}^+$ ) and hence the greater sensitivity to the lyotropic (Hofmeister) series (Morris, 1990; Oakenfull and Scott, 1990). The co-ion also has an effect on helical stability in the case of  $\kappa$ -carrageenan (Ciancia *et al.*, 1997; Oakenfull and Scott, 1990) and it is reported that  $\text{I}^-$  anions stabilise the helical form but inhibit helix aggregation and hence gelation (Ciancia *et al.*, 1997). Furthermore the behaviour of mixed carrageenan systems can be predicted from knowledge of the behaviour of the pure components (Norton, 1990).

At first glance it would appear quite simple to differentiate between a single and double helix using molecular measurements from light scattering or sedimentation equilibrium. This has proved elusive due to the concentration dependency of hydrodynamic parameters and it is very likely that the way in which concentration dependency is dealt with in data analysis has a great influence upon the calculated molecular weight (Harding *et al.*, 1997 and Bongaerts *et al.*, 2000) and therefore the helical conformation estimated (Bongaerts *et al.*, 2000)

Carrageenans have further applications in the food industry as a stabiliser in milk systems such as ice cream and chocolate milk (Glicksman, 1969; Tombs and Harding, 1998 and Langendorff *et al.*, 2000a,b) (Table 3-8), several studies into the exact nature of milk/ carrageenan interactions have been investigated (Snoeren, 1976; Dalgleish and Morris, 1988; Mleko *et al.*, 1997; Langendorff *et al.*, 1997; Mora-Gutierrez *et al.*, 1998; Langendorff *et al.*, 1999; Langendorff *et al.*, 2000a,b; Tziboula and Horne, 2000; Schorsch *et al.*, 2000; Bourriot *et al.*, 1999 and Bourriot *et al.*, 2000). It seems to be the consensus that the carrageenan molecule binds onto the positively charged  $\kappa$ -casein on the exterior of the casein micelle and stabilises the micelle against flocculation at low carrageenan concentration. In order for the

interaction to take place the carrageenan must have a sufficiently high charge density and in the case of  $\kappa$ - and  $\iota$ -carrageenan it must therefore be in the helical form (Langendorff *et. al.*, 2000a,b). The mean distance between sulphate groups is 0.5nm (coil) to 0.2nm (helix) for  $\iota$ -carrageenan; 1.0nm (coil) to 0.4nm (helix)  $\kappa$ -carrageenan and 0.3nm for  $\lambda$ -carrageenan, and it is speculated that no interaction will take place when the distance between sulphate groups is greater than 0.5nm (Langendorff *et. al.*, 2000b).

The molecular masses of the carrageenans have been extensively estimated using light scattering (Vreeman *et. al.*, 1980; Myslabodski *et. al.*, 1996; Viebke *et. al.*, 1995 and Viebke and Williams, 2000 and references therein) the latter using asymmetric flow field-flow fractionation (AF4) as the separation media rather than traditional chromatography. Surprisingly carrageenan molecular masses have only been measured rarely using sedimentation equilibrium (Harding *et. al.*, 1997).

In this section, we will try to determine the fundamental hydrodynamic parameters for both  $\kappa$ - and  $\iota$ -carrageenan (intrinsic viscosity,  $[\eta]$ , sedimentation coefficient,  $s_{20,w}^0$  and weight average molecular weight,  $M_w$ ) in aqueous solution and try to equate this to their three-dimensional solution state.

### 3.2.2 $\kappa$ -carrageenan

A  $\kappa$ -carrageenan sample was kindly supplied from SKW Bio-Systems (France) and was used without further purification.  $\kappa$ -carrageenan powder was dissolved in pH 6.8, I=0.1M buffer (Green, 1933) or in 0.1M lithium chloride buffer. The resulting solutions were heated to approximately 80°C for 30mins to obtain a true solution (Viebke *et. al.*, 1995 and Viebke and Williams, 2000) and allowed to cool to room temperature prior to measurements.

### 3.2.3 $\iota$ -carrageenan

An  $\iota$ -carrageenan sample was also kindly supplied from SKW Bio-systems (France) and was used without further purification and was treated in an identical manner to  $\kappa$ -carrageenan as has been described previously in 3.2.3 and by Viebke *et. al.* (1995) and Viebke and Williams (2000). [Note – both  $\kappa$ -carrageenan and  $\iota$ -carrageenan samples contain minor contamination of the other].

### 3.2.4 Methods

#### 3.2.4.1 *Capillary Viscometry*

Solutions and reference solvents were analysed using a 2ml automatic Schott-Geräte Oswald viscometer, under precise temperature control (24.85±0.01)°C. The relative,  $\eta_{rel}$ , specific,  $\eta_{sp}$  and intrinsic viscosities were calculated from Equations 2-35, 2-36 and 2-41 respectively.

#### 3.2.4.2 *Sedimentation Velocity in the Analytical Ultracentrifuge*

The Optima XLI (Beckman Instruments, Palo Alto, USA) equipped with Rayleigh interference optics was used to determine the sedimentation behaviour of the saccharide samples. Rotor speeds of 50,000rpm and a 4mm column length in 12mm

optical path length double sector cells were used together with an accurately controlled temperature of 20.0°C. A typical carrageenan weighted average partial specific volume,  $\bar{v}$  of (0.510±0.005)ml/g was used for both samples (Vreeman *et. al.*, 1980 and Harding *et. al.*, 1997). Sedimenting boundaries were analysed using the sedimentation time derivative method,  $s_{20,w}$  values were evaluated at various concentrations from 0.5 to 3.0mg/ml and extrapolated to zero concentration (to remove the effects of non-ideality) using the standard equation (Equation) (see *e.g.*, Ralston, 1993).

#### 3.2.4.3 *Sedimentation Equilibrium in the Analytical Ultracentrifuge*

The Beckman Optima XLI ultracentrifuge was also used to determinate the weight average molecular weight,  $M_w$  using low speed sedimentation equilibrium. A rotor speed of 5,000rpm and a 1mm solution column length again in 12mm path length double sector cells were employed at 25.0°C. Equilibrium was reached after approximately 24 hours. Rayleigh interference optics were used to record the solute distributions at sedimentation equilibrium and data subsequently analysed using the QUICKBASIC algorithm MSTARI (Cölfen and Harding, 1997 - see section 2.2.2) and Origin Equilibrium (Microcal Software Inc., Northampton, MA).

#### 3.2.4.4 *SEC-MALLS*

The eluent was I=0.1M LiCl and the injection volumes were 100µl. A value for the refractive index increment of 0.126ml/g was used (Theisen *et. al.*, 2000).

### 3.2.5 Results and Discussion

#### 3.2.5.1 Capillary Viscometry

##### *κ-carrageenan*

An intrinsic viscosity of  $(420 \pm 10)$  ml/g estimated from the Solomon-Ciuta approximation (Equation 2-41) is lower than previous intrinsic viscosity estimates 870 ml/g – Lecacheux *et. al.*, (1985) and  $(630 \pm 60)$  ml/g – Harding *et. al.*, (1997), which is probably due to a lower weight average molecular weight.

##### *ι-carrageenan*

An intrinsic viscosity of  $(1270 \pm 20)$  ml/g estimated from the Solomon-Ciuta approximation (Equation 2-41) is indicative of a high molecular weight rigid or semi-rigid polysaccharide, which would be expected for a helical structure (single or double) such as *ι*-carrageenan.

#### 3.2.5.2 Sedimentation Velocity in the Analytical Ultracentrifuge

##### *κ-carrageenan*

*κ*-carrageenan samples show a classical concentration dependency in sedimentation velocity experiments (Figure 3-30 and Figure 3-31). The infinite dilution sedimentation coefficient (Figure 3-31),  $s_{20,w}^0 = (3.58 \pm 0.07)$  S is slightly less than those calculated of  $(4.19 \pm 0.20)$  S and 4.82 S calculated by Harding *et. al.*, 1997 and Vreeman *et. al.*, 1980 respectively: this would indicate either a lower molecular weight, a more asymmetric/ hydrated structure (or both).

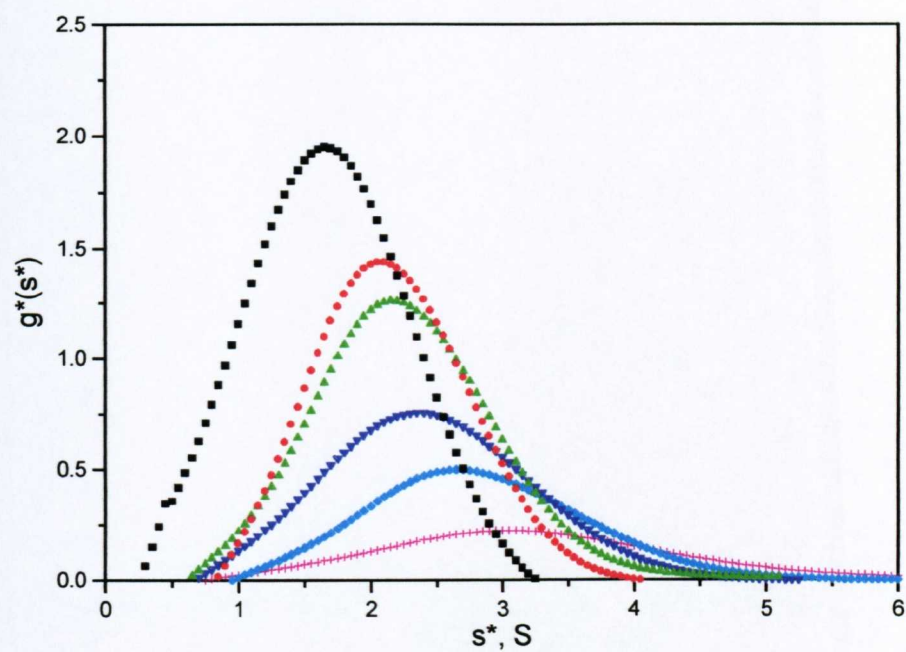


**Figure 3-30** The sedimentation distributions for  $\kappa$ -carrageenan at different concentrations. Legend – 3.0mg/ml (black squares); 2.5mg/ml (red circles); 2.0mg/ml (green up-triangle); 1.5mg/ml (blue down-triangle); 1.0mg/ml (cyan diamonds) and 0.5mg/ml (magenta crosses).

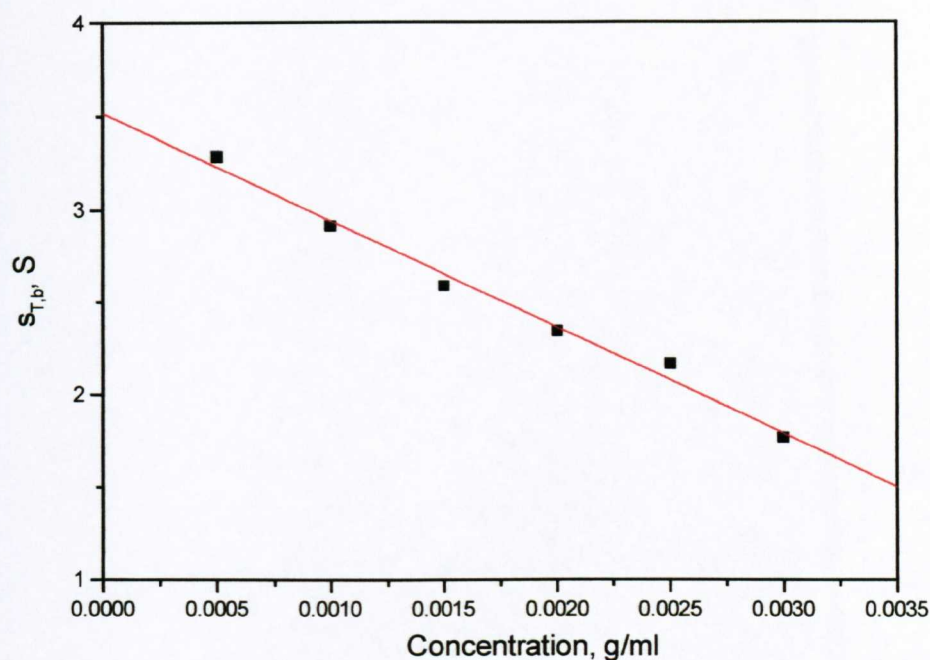


**Figure 3-31** The concentration dependency of sedimentation for  $\kappa$ -carrageenan in standard phosphate buffer at 20°C.

Furthermore the calculated value of  $k_s$  ( $163 \pm 9 \text{ ml/g}$ ) is significantly lower than the value of  $590 \pm 40 \text{ ml/g}$  quoted by (Harding *et. al.*, 1997), under the same buffer conditions.

#### *$\iota$ -carrageenan*

$\iota$ -carrageenan also shows a strong concentration dependency (**Figure 3-32**), the infinite dilution sedimentation coefficient,  $s_{20,w}^0 = (6.91 \pm 0.22)S$  is larger than calculated from  $\kappa$ -carrageenan. This would indicate that  $\iota$ -carrageenan has either higher molecular weight or a more compact structure than  $\kappa$ -carrageenan (or both – which I think is more likely). This can be investigated further by the calculation of the weight average molecular weight from either sedimentation equilibrium or SEC-MALLS. The calculated value of Gralén coefficient,  $k_s$  ( $198 \pm 20 \text{ ml/g}$ ) is slightly higher.

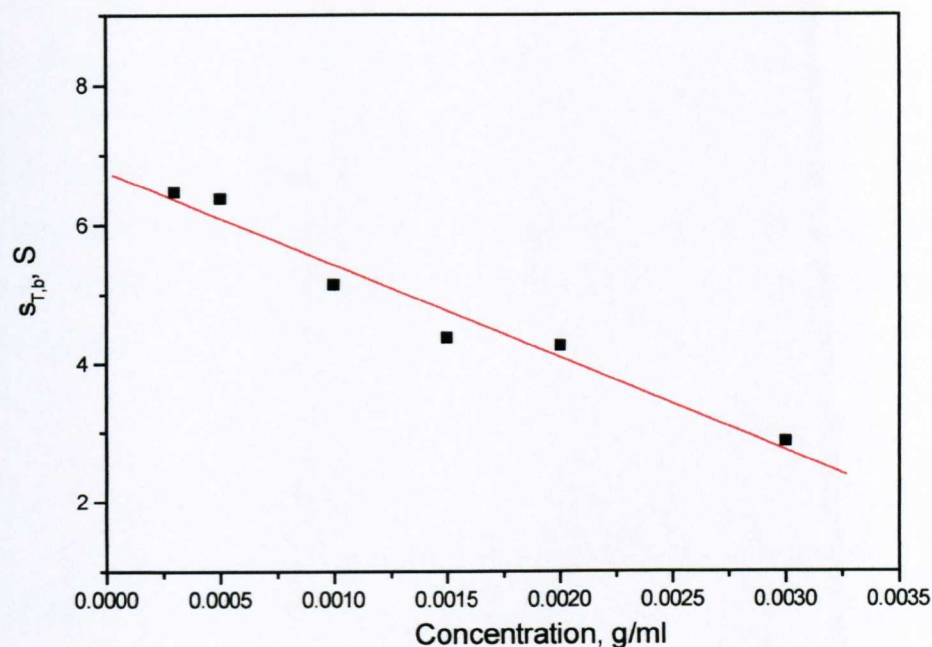


**Figure 3-32** The concentration dependency of sedimentation for  $\iota$ -carrageenan in standard phosphate buffer at 20°C.

### 3.2.5.3 Sedimentation Equilibrium in the Analytical Ultracentrifuge

#### $\kappa$ -carrageenan

Due to the thermodynamic non-ideality and the concentration dependency of chain aggregation (Bongaerts *et. al.*, 2000) it was impossible to get information on the molecular weights over a large concentration range. It was only possible to calculate a molecular weight at low concentration (0.25mg/ml) at this concentration these effects are probably small and hence it is reasonable to approximate  $M_{w,app} = M_w$ . The calculated molecular weight at 0.25mg/ml for  $\kappa$ -carrageenan was thus  $(280,000 \pm 30,000)$ g/mol (from MSTAR). This is in good agreement with the value  $(300,000 \pm 40,000)$ g/mol calculated earlier by Harding *et. al.*, (1997).

### *ι-carrageenan*

It would appear that under the conditions studied that aggregation is a more serious problem for *ι*-carrageenan and it was therefore impossible to gain any molecular weight information from sedimentation equilibrium. [Note – sedimentation equilibrium is strictly speaking unaffected by intermolecular aggregation, however the presence of “gel” like material at the cell base makes it difficult to analyse the radial distribution].

#### 3.2.5.4 SEC-MALLS

### *κ-carrageenan*

Unfortunately in standard phosphate buffer at ambient temperatures it was not possible to obtain molecular weight measurements with any degree of reliability. However it has been reported that the use of lithium chloride buffer at 50°C should favour the coil form of carrageenan and hence prevent chain aggregation (Lecacheux *et. al.*, 1985). Under these conditions we were able to calculate weight average molecular weights for *κ*-carrageenan samples. All *κ*-carrageenan samples produced unimodal distributions and calculated weight average molecular weights, of  $M_w$  were in the range of (268,000±36000)g/mol. This appears to be in reasonable agreement with sedimentation equilibrium and is not too different from the (300,000±40,000)g/mol calculated by Harding *et. al.*, (1997). This value is also in excellent agreement with the predicted value of 252,000 g/mol found by substituting our value for intrinsic viscosity (420 ml/g) into the MHKS equation of Rochas *et. al.*, (1990) ( $[\eta] = 3.1 \times 10^{-3} M_w^{0.95}$ ). Assuming our data from both independent methods to be reliable (*i.e.* molecular weights in both the ordered and random state are approximately the same (280,000±30000)g/mol and (268,000±36000)g/mol respectively) this would suggest a single helix in the ordered state as measured by sedimentation equilibrium (Table 3-9), which is agreement with the findings of Ciancia *et. al.*, (1997).

*ι-carrageenan*

The situation in the case of  $\iota$ -carrageenan was virtually identical and an average molecular weight of  $298,000 \pm 40,000$  was estimated. Although the errors are quite large approximately 13% in both cases, I think we can say that the molecular weight of  $\iota$ -carrageenan is slightly higher than that of  $\kappa$ -carrageenan. As we were unable to calculate molecular masses in the ordered helical state we are unable to estimate the helical order (single or double) (Table 3-9).

**Table 3-9** Hydrodynamic data for  $\kappa$ - and  $\iota$ -carrageenan in dilute solution

Carrageenan	$[\eta]$ , ml/g	$s_{20,w}^0$ , S	$k_s$ , ml/g	$k_s/[\eta]$	$M_w$ , g/mol	$f/f_0$
Kappa	$420 \pm 10$	$3.58 \pm 0.07$	$163 \pm 9$	$0.39 \pm 0.03$	$275000 \pm 35000^a$	$8.7 \pm 0.9$
Iota	$1270 \pm 20$	$6.91 \pm 0.22$	$198 \pm 20$	$0.16 \pm 0.02$	$298000 \pm 40000^b$	$4.7 \pm 0.6$

a – average of molecular weights from sedimentation equilibrium and SEC-MALLS

b – molecular weight from SEC-MALLS

### 3.2.6 Concluding Remarks

As with all polysaccharide samples sample preparation is very important, this is especially true for carrageenan samples, which undergo concentration dependent aggregation (Bongaerts *et. al.*, 2000). This concentration dependency of molecular weight has according to Bongaerts and co-workers (2000) lead to the overestimation of molecular masses in light scattering measurements, this will then in the opinion of Bongaerts result in the erroneous prediction of double helical structure. Neither  $g^*(s)$ ,  $s$  vs.  $c$  from sedimentation velocity nor  $M_w$ , from sedimentation equilibrium (the latter estimated at 0.25mg/ml) are consistent for a double helical formation for  $\kappa$ -carrageenan.

The intrinsic viscosity and sedimentation coefficient of  $\iota$ -carrageenan are significantly larger than those of  $\kappa$ -carrageenan, but their molecular weights are essentially the same (within the margins of the errors).

One should take care when calculating molecular weights and assigning oligomeric states to carrageenan molecules due to the concentration dependency of aggregation, this is further complicated by thermodynamic non-ideality in centrifugal analyses. Clearly the speculation on  $\kappa$ - and  $\iota$ -carrageenan conformation are open to debate, but this study has only gone to prove the difficulty in estimating molecular weights in self-associating polysaccharide systems.

Clearly when gathering molecular weight information it is important to consider the concentration at which measurements are quoted, it may therefore be possible to calculate carrageenan molecular weights from combined sedimentation – diffusion experiments via the Svedberg equation (2.12), this would however require extrapolation to infinite dilution in the case of both sedimentation coefficient and diffusion coefficient and also to zero angle for diffusion measurements, due to the angular dependency of dynamic light scattering for asymmetric particle, this however also very sensitive to aggregated material.

### 3.3 CHARACTERISATION OF GALACTOMANNANS

#### 3.3.1 Background

The “mannans” or “galactomannans” are commonly known as “gums” as they have been traditionally used as adhesives however they have recently found use in the food industry as thickeners and stabilisers (Tombs and Harding, 1998). The main repeat unit is  $\beta$  (1  $\rightarrow$  4) linked mannose, which is  $\alpha$  (1 $\rightarrow$  6) linked with galactose to varying degrees. The “G : M ratio”, is approximately 1 : 2 for guar gum and 1 : 4 for locust bean gum (LGB) (Figure 3-33). Both guar and LBG are neutral water-soluble polysaccharides of relatively high molecular weight (Sharman *et. al.*, 1978; Robinson *et. al.*, 1982; Jumel, 1994 and Tombs and Harding, 1998). In this section we will look at one LBG sample M175 and the effect of hydrolysis on the guar gum sample M150.

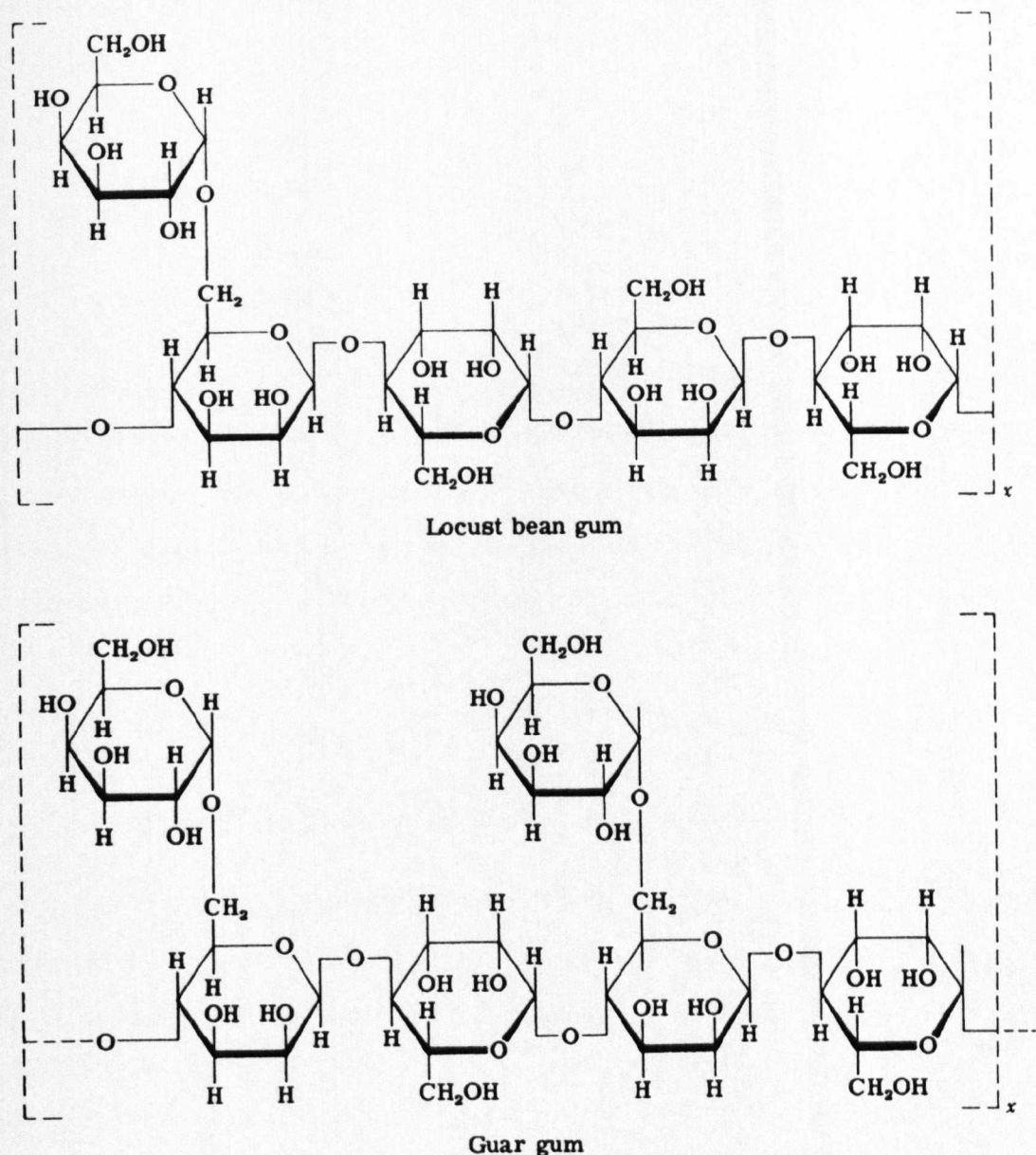


**Figure 3-33** Idealised structures for locust bean and guar gums (adapted from Glicksman, 1969).

### 3.3.2 Materials

#### 3.3.2.1 *Guar M150, Guar M90, Guar M30 and LBG M175*

Drs. Simon Ross-Murphy and David Picout (King's College, London - KCL) provided all the galactomannan samples. Guars M90 and M30 were produced from

the native M150 by hydrolysis. All samples were dissolved overnight in hot water with stirring.

### 3.3.3 Methods

#### 3.3.3.1 *Capillary Viscometry*

Solutions and reference solvents were analysed using a 2ml automatic Schott-Geräte Oswald viscometer, under precise temperature control ( $25.02 \pm 0.01$ )°C. The relative,  $\eta_{rel}$  specific,  $\eta_{sp}$  and reduced,  $\eta_{red}$  viscosities were calculated from Equations 2-34, 2-35 and 2-36 respectively, the intrinsic viscosities were estimated from the Huggins plot (Equation 2-38). Independent viscosity experiments were also carried out at KCL.

#### 3.3.3.2 *Sedimentation Velocity in the Analytical Ultracentrifuge*

The Optima XLI (Beckman Instruments, Palo Alto, USA) equipped with Rayleigh interference optics was used to determine the sedimentation behaviour of the saccharide samples. Rotor speeds of 50,000rpm and a 4mm column length in 12mm optical path length double sector cells were used together with an accurately controlled temperature of 20.0°C. A typical polysaccharide weighted average partial specific volume,  $\bar{v}$  of  $(0.600 \pm 0.005)$ ml/g was used for both galactomannan samples. Sedimenting boundaries were analysed using the sedimentation time derivative method,  $s_{20,w}$  values were evaluated at various concentrations from 0.5 to 2.0mg/ml and extrapolated to zero concentration (to remove the effects of non-ideality) using the standard equation (see *e.g.* Ralston, 1993).

### 3.3.3.3 SEC-MALLS

The eluent was the standard pH 6.8 I=0.1 "Paley" buffer and the injection volume was 100 $\mu$ l. A value for the refractive index increment of 0.146ml/g was used (Jumel, 1994).

## 3.3.4 Results and Discussion

### 3.3.4.1 Capillary Viscometry

The intrinsic viscosity for the guar samples decreased with increasing degradation from 1750ml/g for M150 to 399ml/g for M30 (Table 3-10). The results for each of the guar samples were the same as had been previously reported at KCL (Pioucot, personal communication). The intrinsic viscosity for LBG M175 was not determined. It has been noted previously (Goycoolea *et. al.*, 1995) that galactomannan solution viscosities can be very sensitive to pH and therefore, one must be careful when comparing results between different studies and as the viscosity can be at least partially regained this is not entirely a depolymerisation effect.

### 3.3.4.2 Sedimentation Velocity in the Analytical Ultracentrifuge

A hyper-sharp boundary typical for elongated polysaccharides was obtained for each polysaccharide, the steepness of the boundary correlated very well with molecular weight (Figure 3-34). The slopes of the sedimenting boundaries for M90 and M30 are smaller than for M150 due to lower viscosity and greater diffusion of the lower molecular weight species. After  $g^*(s^*)$  analyses one obtained relatively narrow sedimentation distributions (Figure 3-35). As would be expected the sedimentation coefficient also decreased with increased degradation from 7.8S for M150 to 3.3S for M30, however due to the large concentration dependency a 2<sup>nd</sup> order concentration dependency extrapolation was needed and therefore the values for  $k_s$  are quite unreliable (Figure 3-36). The value  $s_{20,w}^0$  for LBG M175 lies somewhere between that of guar M30 and M90 (Table 3-10).

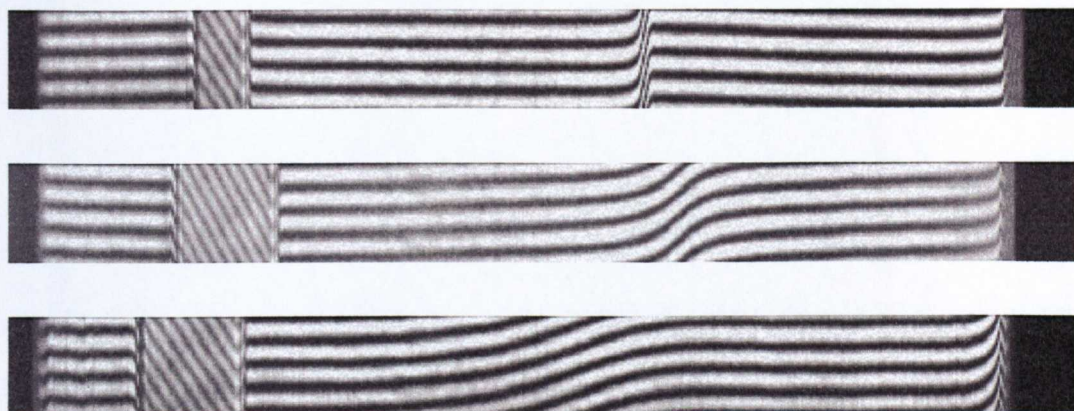


**Figure 3-34** The sedimenting boundaries for from top to bottom guar M150, M90 and M30, recorded using the XLI interference optical system on the XLI. Speed = 50,000rpm; temperature = 20°C; solvent = water and concentration 1.5mg/ml.

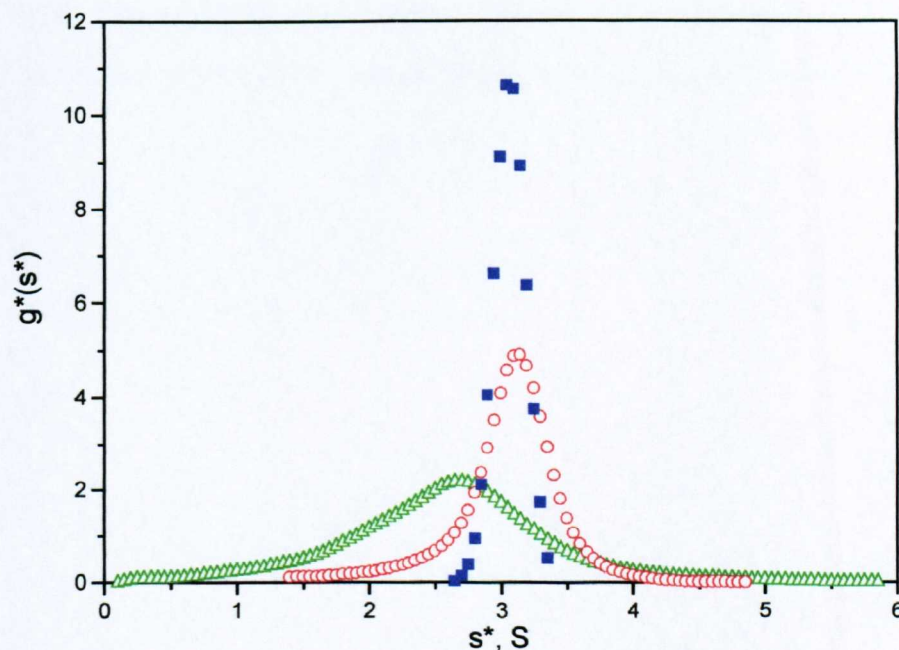


**Figure 3-35**  $g^*(s^*)$  peaks for guar samples. Legend guar M150 – blue squares, M90 – red open circles and M30 – green open triangles under same conditions described in **Figure 3-34**. [Note – due to concentration dependency the apparent sedimentation coefficient of M90 is greater than that of M150, however the sedimentation coefficient for M150 is greater when extrapolated to infinite dilution (**Figure 3-36**)].

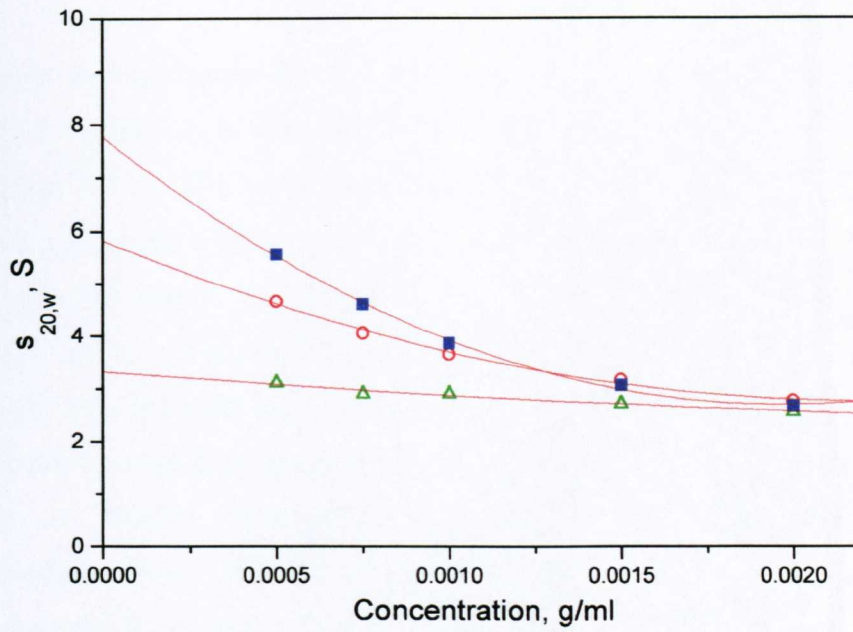


**Figure 3-36** Concentration dependency of sedimentation for guar samples. Legend guar M150 – blue squares, M90 – red open circles and M30 – green open triangles.

### 3.3.4.3 SEC-MALLS

Weight average molecular weights calculated from SEC-MALLS were as expected ( $M_{150} > M_{90} > M_{30}$ ), with LBG M175 falling between guar samples M90 and M150 (**Figure 3-37**). The molecular weight of  $1.8 \times 10^6$  g/mol for LBG M175 is in very good agreement with the value of  $1.7 \times 10^6$  g/mol previously measured for same sample; this result was calculated from intrinsic viscosity measurements (Wielinga, 1990). [Note – it has also been reported (Richardson *et. al.*, 1998) that the molecular weight of LBG solutions are very sensitive to solvent conditions]. The molecular weights for each guar sample were the same as had been previously reported at KCL from a MHKS relationship for viscosity measurements (Picout, personal communication). Plots of log RMS radius versus log  $M_w$  yielded slopes of approximately 0.5 for each guar sample, indicating that there is little or no difference in conformation between the guar samples (**Figure 3-38**). The same is true for a plot of log  $[\eta]$  vs. log  $M_w$ , which also validates the previous work at KCL (**Figure 3-39**). A slope of 0.69 for the plot of log  $[\eta]$  vs. log  $M_w$  is in reasonable agreement with the results of Sharman *et. al.*, 1978 (0.64); Robinson *et. al.*, 1982 (0.72) and Jumel, 1994 (0.60).

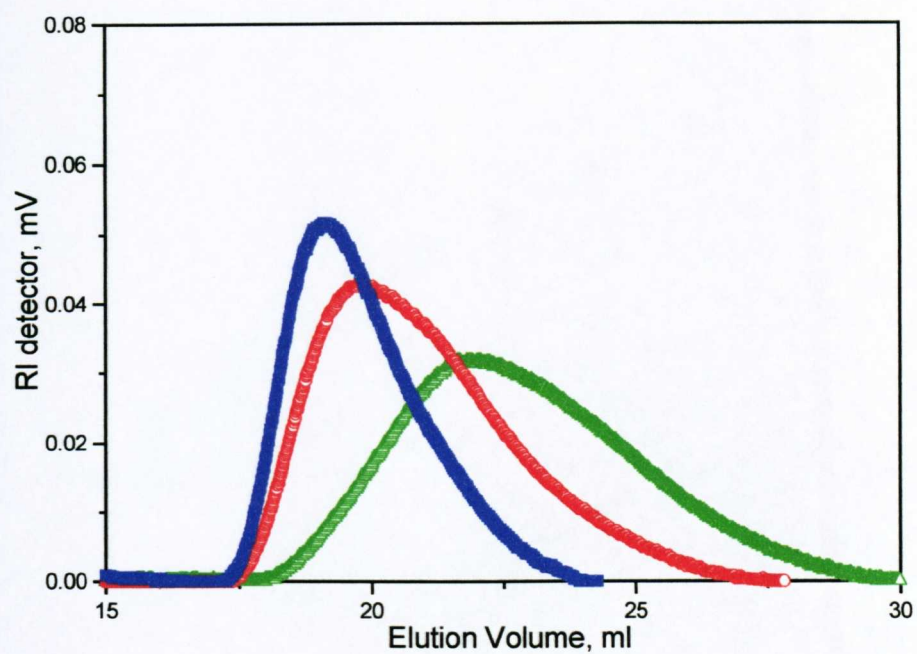


**Figure 3-37** Elution profiles for guar samples in standard “Paley” buffer. Legend guar M150 – blue squares, M90 – red open circles and M30 – green open triangles.

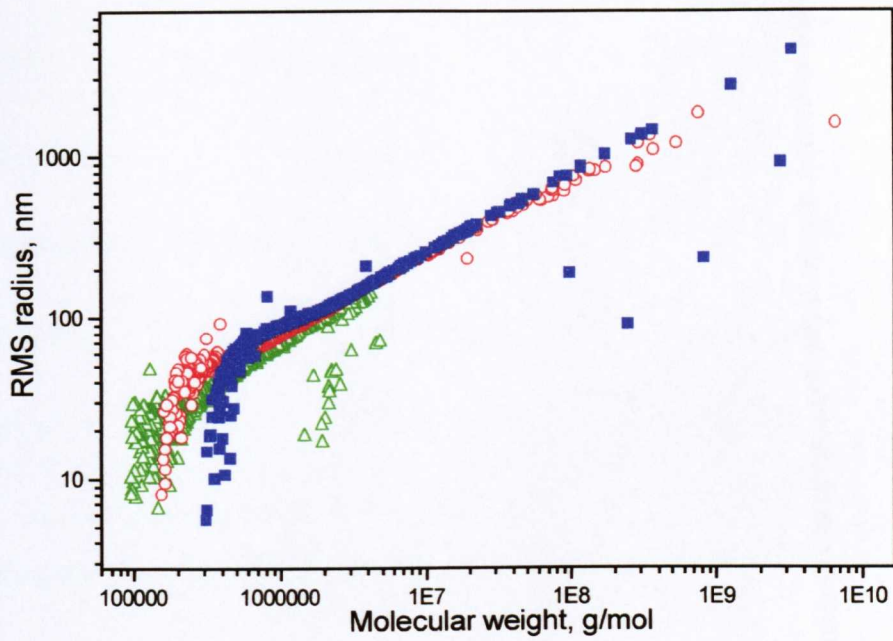


**Figure 3-38** Plots of log RMS radius vs. log  $M_w$  for guar samples. The average slope is  $0.51 \pm 0.04$ . Legend guar M150 – blue squares, M90 – red open circles and M30 – green open triangles.

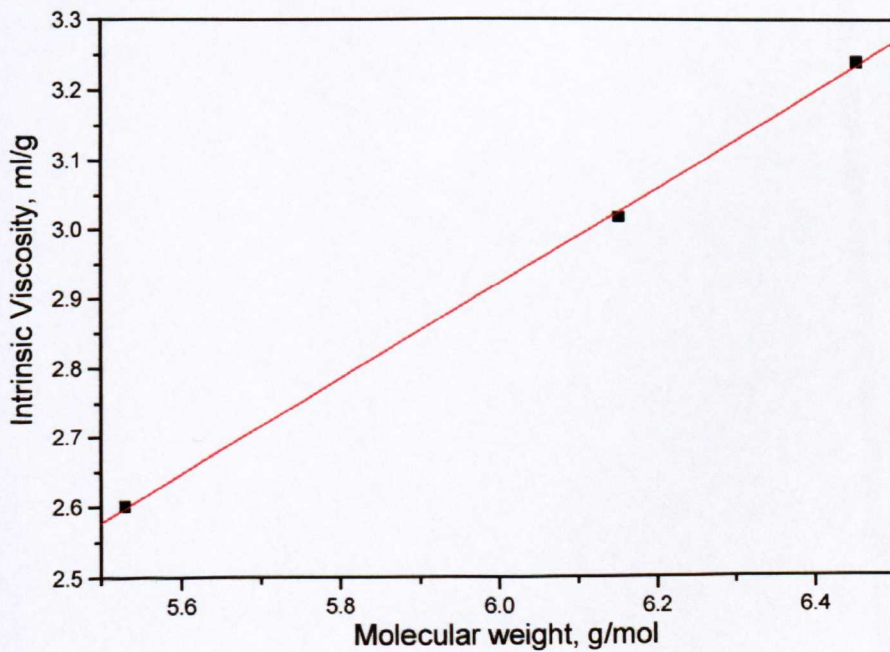


**Figure 3-39** The MHKS viscosity plot for guar samples. Slope is  $0.69 \pm 0.01$ .

**Table 3-10** The hydrodynamic data for guar M150, M90, M30 and LBG M175

Sample	$[\eta]$ , ml/g	$s_{20,w}^0$ , S	$10^{-5} \times M_w$ , g/mol	$f/f_0$	G : M <sup>1</sup>
LGB M175	-	5.1±0.1	18±5	17±3	-
Guar M150	1750±25	7.8±0.2	28±4	15±2	1 : 1.52
Guar M90	1050±20	5.8±0.2	14±2	12±1	1 : 1.52
Guar M30	400±10	3.3±0.2	3.4±0.3	8.4±1.0	1 : 1.56

1) Courtesy of Gill West, Plant Biochemistry, University of Nottingham, Sutton Bonington. Samples also contain about 1% arabinose.

### 3.3.5 Concluding Remarks

The results all indicate that the 3 guar samples and LBG M175 are rigid polysaccharides of high molecular weight (**Table 3-10**). Furthermore, the degradation procedure does not change the conformation as indicated by the linearity of the MHKS plot for viscosity and RMS radius. The viscosity ( $a$ ) and light scattering ( $\epsilon$ ) MHKS parameters can approximately related very simply –

$$\epsilon = \frac{(a + 1)}{3} \quad (3-1)$$

where  $\epsilon$  is the MHKS coefficient for RMS radius and  $a$  is the viscosity coefficient.

This is also consistent with the slope ( $b$ ) of approximately 0.4 for the sedimentation MHKS plot (**Figure 3-40**). The slopes of the three MHKS plots: **Figure 3-38**, **Figure 3-39** and **Figure 3-40** are consistent with a semi-rigid coil type conformation (see **Table 2-2**, see also Jumel, 1994 and Tombs and Harding, 1998). It is therefore clear that the results are in general agreement that the guar samples are semi-rigid coils.

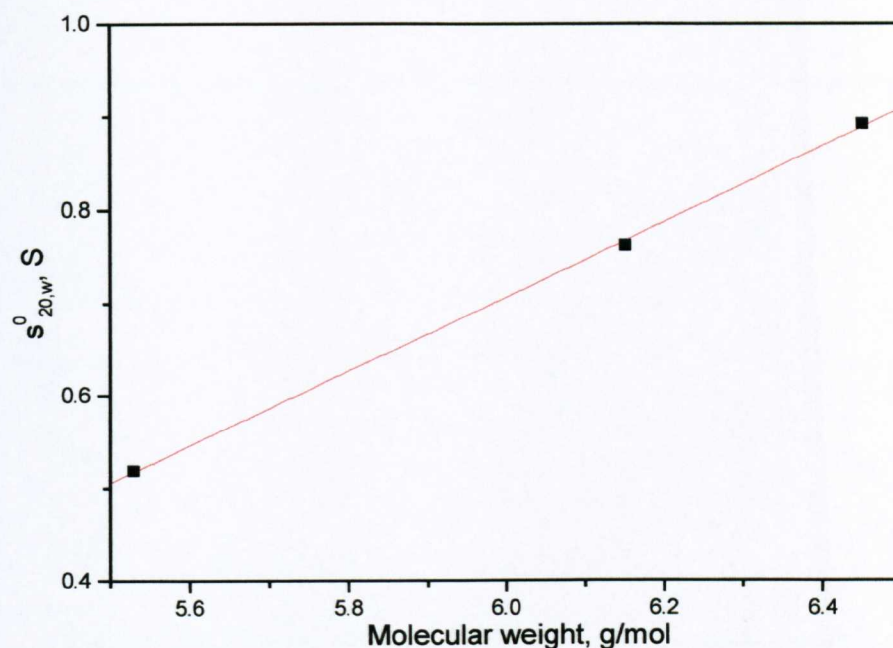


**Figure 3-40** The MHKS sedimentation plot for guar samples. Slope is  $0.40 \pm 0.01$ .

One can at least semi-quantify the degree of depolymerisation by using the translational frictional ratio (Tanford, 1961). There is a decrease in  $f/f_0$  upon degradation  $M_{150} > M_{90} > M_{30}$  (Table 3-10). The translational frictional ratio for LBG M175 is significantly larger indicating a more rigid structure, which is due to the lower G : M ratio.

As we have good estimates of the intrinsic viscosities, weight average molecular weights and the MHKS viscosity exponent it should be possible to calculate the mass per unit length,  $M_L$ , the persistence length  $L_p$ , the Kuhn statistical segment length,  $\lambda^{-1}$  and the number of segment lengths per chain,  $N$  using the “worm-like coil” (Bohdanecky, 1983 and Harding, 1997) or “blob” model (Dondos, 2001) by plotting graphs of  $\frac{[\eta]}{M^{0.5}}$  vs.  $M^{3\nu-1.5}$  (Figure 3-41) and  $\frac{[\eta]}{M^{0.5}}$  vs.  $M^{0.5}$  (Figure 3-42) respectively.

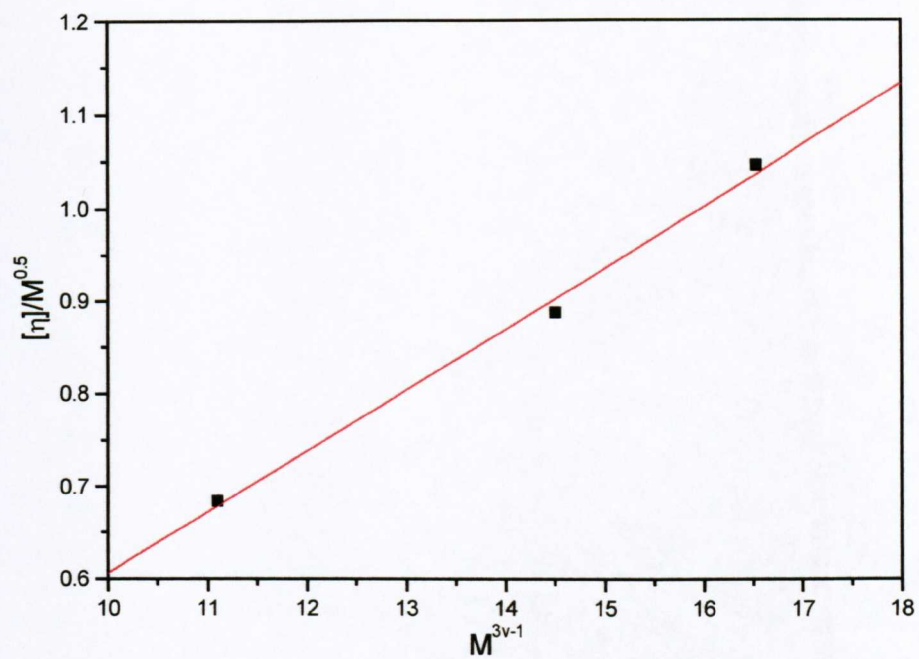
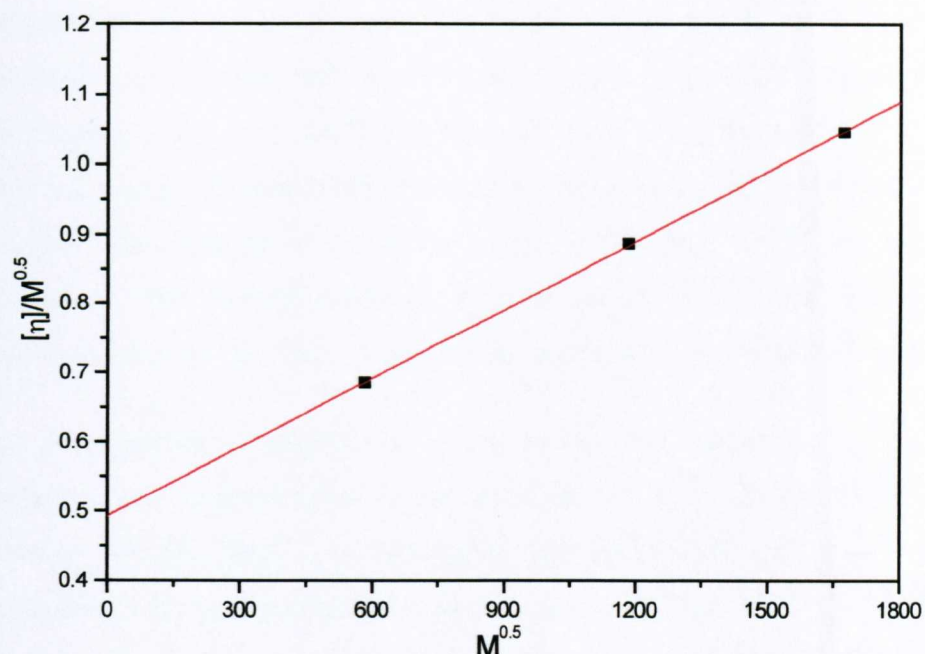


Figure 3-41 “Blob” model plot of  $\frac{[\eta]}{M^{0.5}}$  vs.  $M^{3v-1.5}$  for guar samples.



**Figure 3-42** Stockmayer-Fixman-Burchard plot  $\frac{[\eta]}{M^{0.5}}$  vs.  $M^{0.5}$  for guar samples.

**Table 3-11** Results of the “blob” model approach for calculating the number of Kuhn statistical segments per chain for the three guar samples, from the equations 2-84 - 2-91 and the graphs above.

Sample	$[\eta]$	$M_w$	N
Guar M150	1750	2800000	1958
Guar M90	1050	1400000	979
Guar M30	399	340000	238

where  $M_L = 3.06 \times 10^9$  g/cm;  $\lambda^{-1} = 4.68 \times 10^{-7}$  cm;  $L_p = 2.34 \times 10^{-7}$  cm;  $\nu = 0.56$ ;  $C = 0.76$ ;  $N_c = 5.84$  and  $K_\theta = 0.49$ . For the explanation of terms see section 2.7 or Dondos (2001).

This clearly gives a good quantitative estimate of the change in chain length due to depolymerisation. As there appears to be no change in molecular conformation all Kuhn statistical segments will be of the same length ( $4.68 \times 10^{-7}$  cm) and of the same mass ( $3.06 \times 10^9$  g.mol<sup>-1</sup>.cm<sup>-1</sup>) and therefore it is only the number of segments  $N$ , which will change (Table 3-11), the linearity of (Figure 3-41 and Figure 3-42) seem to support this hypothesis. The data suggests that guar M150 has twice as many segments as M90 and approximately 8 times that of M30, which can be seen in the decrease in intrinsic viscosity, sedimentation coefficient and molecular weight.

This investigation demonstrates quite nicely the importance of hyper-sharp boundaries and concentration dependency in the hydrodynamic analysis of high molecular weight rigid or semi-rigid polysaccharides and the usefulness of quantitative and semi-quantitative models *i.e.* the “blob” model and translational frictional ratio in the estimation of the molecular parameters of flexible and semi-flexible polymers.

### 3.4 CHARACTERISATION OF TWO BACTERIAL POLYSACCHARIDES - *APHANOTHECE HALOPHYTICA* AND XANTHAN

#### 3.4.1 Background

The two bacterial polysaccharides chosen were, a previously well studied polysaccharide (xanthan) and a not so well characterised cyanobacterial polysaccharide. It has been known, for a long time that Cyanobacteria, the most widely distributed photosynthetic prokaryotes in nature produce large amounts of exopolysaccharides (see *e.g.* Drews and Weckesser, 1982). These exopolysaccharides have potential biotechnological importance as conditioners of soils for the improvement of their water-holding capacity, emulsifiers, viscosifiers, medicines and bioflocculants (Bar-or and Shilo, 1987; Falchini *et al.*, 1996; Mazor *et al.*, 1996; Bar and Visnovsky 1997; Choi *et al.*, 1998; De Philippis and Vincenzini, 1998).

Although the monosaccharidic compositions of exopolysaccharides present in a number of species of cyanobacteria have been determined (De Philippis and Vincenzini, 1998; Nicolaus *et al.*, 1999), further studies are necessary to understand and assess the biotechnological potential of cyanobacterial exopolysaccharide. Indeed, only a few papers have dealt with the physico-chemical and structural studies. Their data has suggested that the solution conformation of exopolysaccharide from *Cyanospira capsulata* (CC-EPS) is a random coil (Cesaro *et al.*, 1990; Navarini *et al.*, 1992). Aqueous solutions of CC-EPS show good rheological properties, just about equivalent to those of xanthan (Cesaro *et al.*, 1990; Navarini *et al.*, 1990). CC-EPS is a regular branched acidic polysaccharide with an decasaccharide (Marra *et al.*, 1990) or octasaccharide repeating unit (Garozzo *et al.*, 1998).

*Aphanothece halophytica* is one of the few halophilic cyanobacteria (Brock, 1976). *Aphanothece halophytica* GR02, usually a benthic cyanobacterium in the Guangrao saltworks, which often forms surface water blooms. After the bloom formation, the brine of the saltworks gradually becomes viscous due to of the release of large amounts of exopolysaccharide from *A. halophytica* GR02 (AH-EPS) (Liu and Lin 1993). AH-EPS consists mainly of glucose, fucose, mannose, arabinose and glucuronic acid. A possible backbone of AH-EPS contains glucose, arabinose, fucose, mannose and glucuronic acid with branch points at mannose, and the

remaining glucose and glucuronic acids are at terminal positions. No proteins and sulphate residues were detected (Li *et. al.*, in press).

Xanthan, an exopolysaccharide from *Xanthomonas campestris*, has been extensively studied and similarly to carrageenan the exact nature of the helical structure (single or double) is open to debate. Various authors (Yevlampieva *et. al.*, 1999; Kitamura *et. al.*, 1990) promote the double helix whereas Milas and Rinaudo (1979) together with Milas *et. al.* (1996) advocate a single helix and has been reported to have two independent coil overlap concentrations,  $c^*$  and  $c^{**}$  (Launay *et. al.*, 1997).

Xanthan has gained widespread use as a viscosifier and stabiliser in a number of different commercial applications (Sanderson, 1990; Gordon, 1990; Millane *et. al.*, 1990 and Dhami *et. al.*, 1995b), including many food applications, where it was approved in the EC in 1980 under the name E415.

In this section we report a comparative hydrodynamic study on the dilute solution and rheological properties of the exopolysaccharide produced by the halophilic cyanobacterium *A. halophytica* GR02 and xanthan in guanidine hydrochloride, GuHCl solvent. To our knowledge, this is the first report on the hydrodynamic characterisation of the exopolysaccharide from the cyanobacterium.

### 3.4.2 Materials

*Aphanothece halophytica* GR02 was isolated from the Guangrao saltwork in the Shandong province of P. R. China. After 20 days growth, the cells were removed by centrifugation, and the supernatant filtered through a 0.45 $\mu$ m porous membrane, and then concentrated under reduced pressure at 40°C. Sodium azide was added to prevent bacterial growth, this concentrated medium was then dialysed against tap water (60 hours) and distilled water (18 hours) and then concentrated again. The exopolysaccharides were then precipitated by the addition of four volumes of 95% ethanol at 4°C overnight (Li *et. al.*, submitted).

The resulting dried exopolysaccharide sample then proved difficult to dissolve. Many typical aqueous solvents used in hydrodynamic characterisations were tested for their

effectiveness as a solvating agent, including “Paley” buffers of differing pHs (Green, 1933), DMSO and ethanol. These solvents however proved ineffective. It was found that only after several days stirring at room temperature in 1M guanidine hydrochloride, GuHCl was a reasonably homogeneous solution formed. Therefore all subsequent analyses were carried out in this medium. 1M GuHCl also suppresses any microbiological growth.

### 3.4.3 Methods

#### 3.4.3.1 Capillary Viscometry

Solutions and reference solvents were analysed using a 2ml automatic Schott-Geräte Oswald viscometer, under precise temperature control ( $24.96 \pm 0.01$ )°C. The relative,  $\eta_{rel}$  specific,  $\eta_{sp}$  and reduced,  $\eta_{red}$  viscosities were calculated from Equations 2-34, 2-35 and 2-36 respectively, and intrinsic viscosities were estimated from the Huggins and Kraemer plots (Equations 2-38 and 2-40 respectively).

#### 3.4.3.2 Rotational Viscometry

AH-EPS and xanthan samples of various concentrations (0.1-1.5mg/ml and 0.1-1.2mg/ml respectively) were prepared in 1M GuHCl. The viscosity at 25°C was measured using a controlled stress rheometer (CS10, Bohlin) with double gap geometry (DG40/50). The shear rate used was in the range 0.5-160s<sup>-1</sup>. The set of data was then fitted with the Cross, (1965) equation (2-47).

The four fitting parameters in this equation were optimised to minimise the value of

$$\Sigma(\log(\eta_f) - \log(\eta))^2 \quad (3-2)$$

where  $\eta_f$  is the fitted value for each point. Typically for xanthan or xanthan-like molecules the exponent ( $m$ ) of the Cross-equation will tend towards a slope of -1 at low concentrations (Launay *et. al.*, 1984), this diagnostic of a “weak gel-like” response rather than the classical random coil response of ( $m \sim 0.75$  at low concentrations) for a solution such as guar gum (Richardson and Ross-Murphy, 1987a,b). The intrinsic viscosity can then be obtained via the Huggins and Kraemer equations.

### 3.4.3.3 *Sedimentation Velocity in the Analytical Ultracentrifuge*

The Optima XLI (Beckman Instruments, Palo Alto, USA) equipped with Rayleigh interference optics was used to determine the sedimentation behaviour of the saccharide samples. Rotor speeds of 40,000rpm and a 4mm column length in 12mm optical path length double sector cells were used together with an accurately controlled temperature of 25.0°C. A value of the partial specific volume,  $\bar{v}$  of (0.600±0.005)ml/g was taken for xanthan (Dhami *et. al.*, 1995b, Sato *et. al.* 1984) a similar value was taken for AH-EPS as 0.6ml/g is a good estimate for the partial specific volume of most polysaccharides. Sedimenting boundaries were analysed using the sedimentation time derivative method,  $s_{20,w}$  values were evaluated at various concentrations from 0.5 to 3.0mg/ml and extrapolated to zero concentration (to remove the effects of non-ideality) using the standard equations (see e.g., Ralston, 1993). [Note - both conventional ( $s$  vs.  $c$ ) and reciprocal ( $1/s$  vs.  $c$ ) extrapolations were used].

### 3.4.3.4 *Sedimentation Equilibrium in the Analytical Ultracentrifuge*

The Beckman Optima XLI ultracentrifuge was also used also to determinate the weight average molecular weight,  $M_w$  using low speed sedimentation equilibrium. A rotor speed of 3,000rpm and a 1mm solution column length in 12mm path length double sector cells were employed at a running temperature of 25.0°C. Equilibrium was reached after approximately 72 hours. Rayleigh interference optics were used to record the solute distributions at sedimentation equilibrium and data subsequently

analysed using the QUICKBASIC algorithm MSTARI (Cölfen and Harding, 1997) (see section 2.2.2).

### 3.4.4 Results and Discussion

#### 3.4.4.1 Capillary Viscometry for AH-EPS

There appears to be a discontinuity in the graph at concentrations approximately 1mg/ml, it is likely that this is a result of the effect of shear thinning on polysaccharide solutions, especially at low concentrations (Launay *et al.*, 1997). Similar inconsistencies have been observed for xanthan (Dhami *et al.*, 1995b). It is also probable that an increase in viscosity is due to the transition from the dilute to the semi-dilute regimes *i.e.*  $c^*$ , the critical coil overlap concentration effect (Figure 3-43). It was therefore considered best to use the low concentration data for the zero concentration extrapolations (Dhami *et al.*, 1995b). In order to investigate the effect of shear rate on our AH-EPS sample we repeated viscosity measurements using a Bohlin CS10 with double gap geometry.

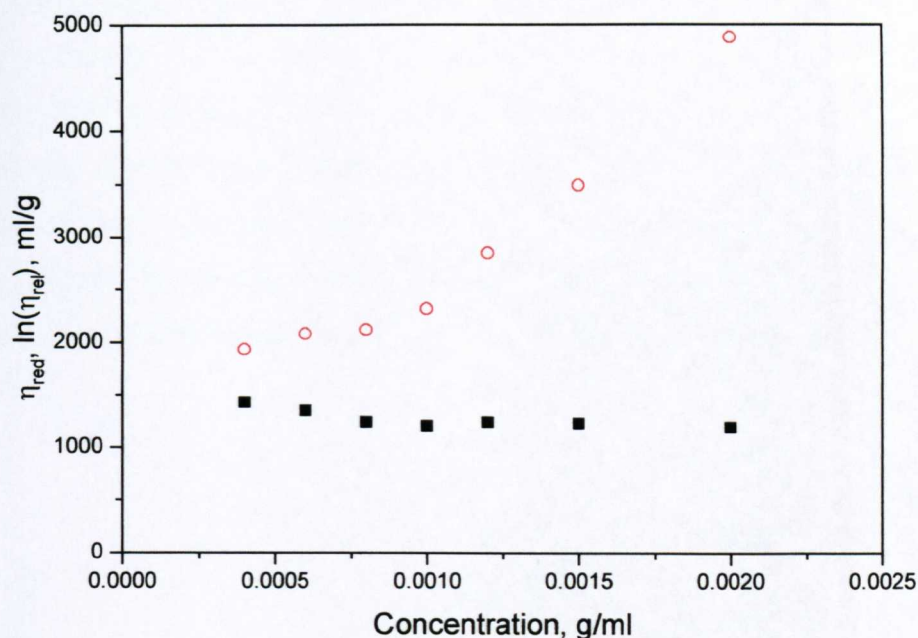


**Figure 3-43** Huggins (red) and Kraemer (black) plots for AH-EPS from capillary viscometry.

#### 3.4.4.2 Capillary Viscometry for Xanthan

The experiment above was repeated using a well characterised (in water) bacterial polysaccharide - xanthan. Due to the large shear thinning effect in the capillary no meaningful results can be inferred. It could however be observed that AH-EPS shear-thinned in the capillary in a similar manner to that of xanthan. This is consistent with the findings of Cesaro *et. al.*, (1990); and Navarini *et. al.*, (1990) in their studies of the chemically similar exopolysaccharide CC-EPS.

#### 3.4.4.3 Rotational Viscometry for AH-EPS

The data obtained at low shear rate and low concentrations were discarded due to the noise level. The viscosities obtained at high shear rate and low concentrations were also discarded due to turbulence (**Figure 3-44**). Although the raw data does not reach a higher Newtonian plateau, the zero shear viscosity value obtained by the fitting of

the Cross-equation was remarkably reliable. We were however unable to clarify the situation regarding the exponent of the Cross-equation (which should be approximately  $-1$  at low concentrations for a xanthan-like solution) this is due concentration or solvent effects. Extrapolation to zero concentration gives an intrinsic viscosity of 8200 and 7900ml/g respectively from the Kraemer and Huggins plots (Figure 3-45). An estimation of the coil overlap concentration,  $c^*$  is independent of the intrinsic viscosity and can therefore be measured without creating a bias, a  $c^*$  of 0.67mg/ml was found for AH-EPS (Figure 3-46).

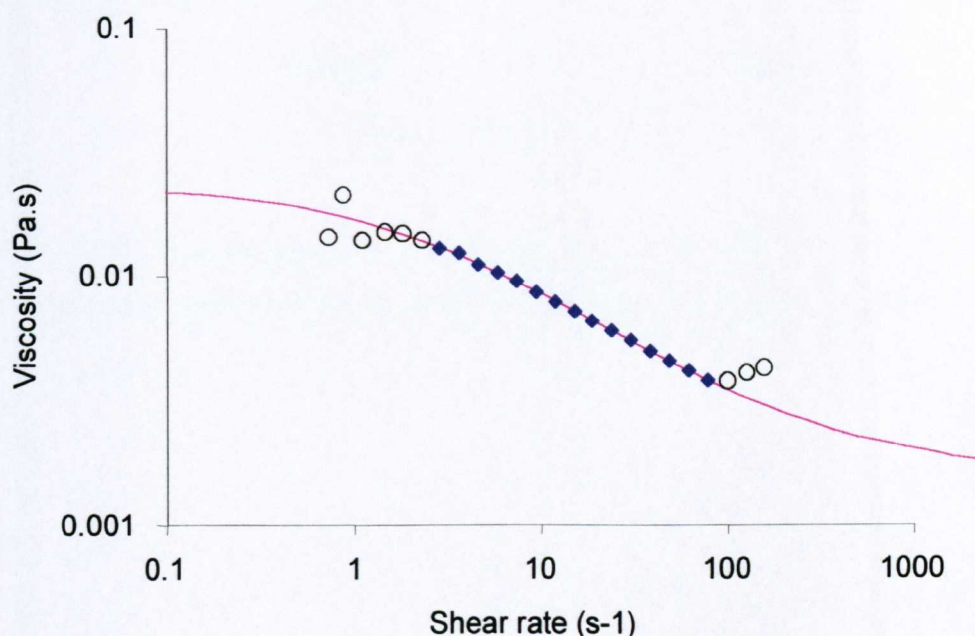


**Figure 3-44** Viscosity and fitting of AH-EPS at 0.6g/l measured at 25°C. Circles: points not used for fitting. Square: points used for fitting. Line: fitted curve.

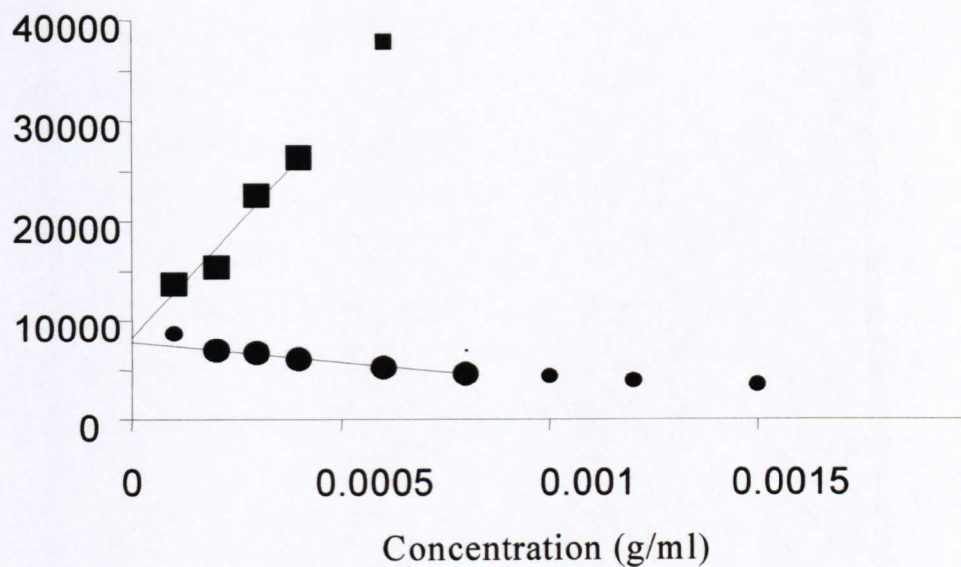


**Figure 3-45** Huggins (square) and Kraemer (circle) plots for AH-EPS. Extrapolation towards zero concentration was performed on the points with a large marker.

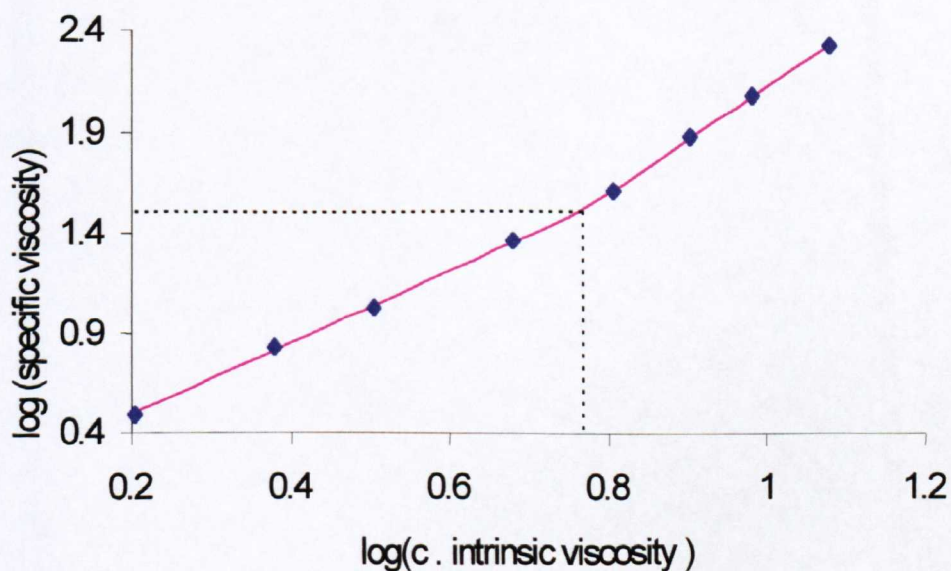


**Figure 3-46** Coil overlap plot obtained with an intrinsic viscosity value of 8000 ml/g (see text for explanation).

#### 3.4.4.4 Rotational Viscometry for Xanthan

No curvature was observed at low shear rates for the xanthan sample. It was therefore impossible to fit the data via the Cross-equation and calculate an intrinsic viscosity under the experimental conditions. Previous studies (Shatwell *et al.*, 1990; Launay *et al.*, 1997; Capron *et al.*, 1997; Milas *et al.*, 1996 and Dhami *et al.*, 1995b) calculate the intrinsic viscosity to be in the range of 3000-9000ml/g. This we know is unusual as rotational viscometry is the standard technique for measuring the viscosity of xanthan, we can only surmise it is an artefact of the guanidine hydrochloride solvent system or of the sample concentration.

#### 3.4.4.5 Sedimentation Velocity for AH-EPS

The analysis of the sedimenting boundary indicated that the solution was almost entirely homogeneous with only a small amount of aggregated material (**Figure 3-47**). As with the viscometry results an apparent discontinuity can be seen below 1mg/ml (**Figure 3-48** and **Figure 3-49**): this is fairly consistent with the  $c^*$  of 0.7mg/ml calculated from zero-shear viscosity estimates using the Cross-equation. Therefore only the lowest three concentrations were used to estimate the infinite dilution sedimentation coefficient,  $s_{20,w}^0$  and the concentration dependency,  $k_s$ . Although the sedimentation coefficients are in reasonable agreement the concentration dependencies are quite different. In general  $k_s$  values from the reciprocal plot ( $1/s$  vs.  $c$ ) (**Figure 3-49**) are more reliable in non-ideal systems (see *e.g.* Harding, 1995). The results from sedimentation velocity indicate that AH-EPS is a large non-ideal, rigid/extra-rigid rod-like polysaccharide. This was also supported by the formation of classical hyper-sharp boundaries. This is quite different with observations that the solution conformation of the related cyanobacterial exopolysaccharide from *Cyanospora capsulata* (CC-EPS) is a random coil (Cesaro *et al.*, 1990; Navarini *et al.*, 1992).

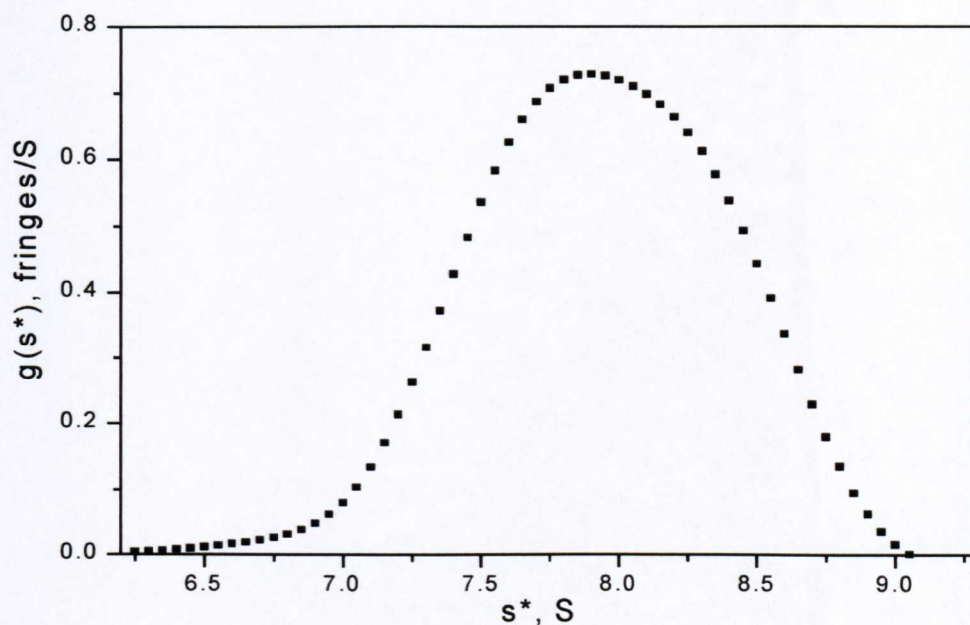


**Figure 3-47**  $g(s^*)$  profile for AH-EPS at 40,000 rpm at 25°C in 1M guanidine hydrochloride and concentration 1.0mg/ml.

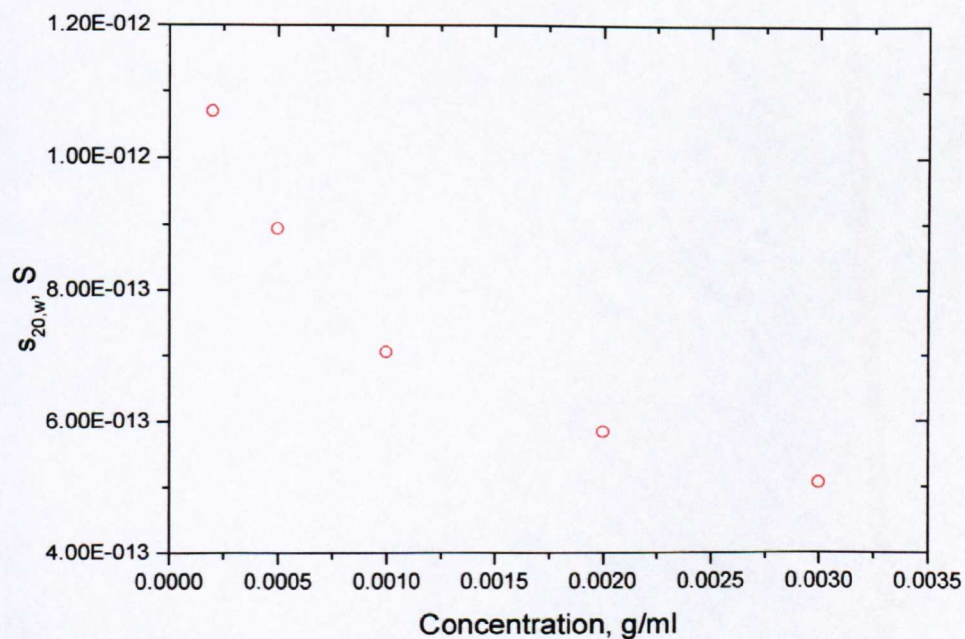


**Figure 3-48** Concentration dependency of sedimentation of AH-EPS – conventional plot at 25°C in 1M guanidine hydrochloride.

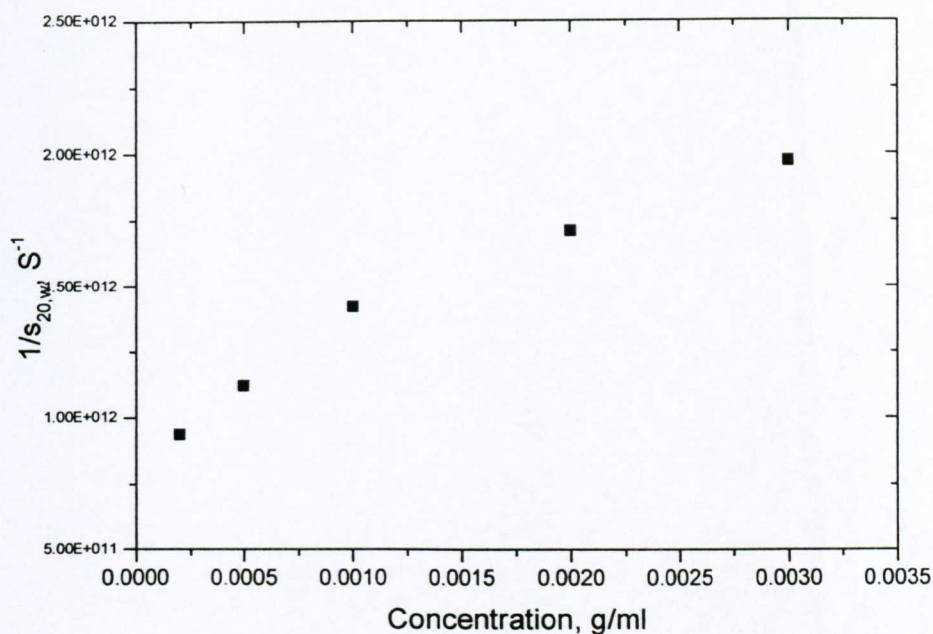


**Figure 3-49** Concentration dependency of sedimentation of AH-EPS – reciprocal plot at 25°C in 1M guanidine hydrochloride.

#### 3.4.4.6 Sedimentation Velocity for Xanthan

Similar shaped hyper-sharp boundaries to those of AH-EPS (see *e.g.* **Figure 3-34**) were observed indicating that AH-EPS and xanthan have similar rigid conformations. A sedimentation coefficient,  $s_{20,w}^0$  of 11.4S is quite similar to those observed in pH 6.5 I=0.3 buffer (Dhami *et. al.*, 1995b) and only slightly smaller than that of AH-EPS. (**Table 3-12**)

#### 3.4.4.7 Sedimentation Equilibrium for AH-EPS

Unlike the viscometry and sedimentation velocity, there appears to be no effect of  $c^*$  on sedimentation equilibrium. Molecular weights were therefore extrapolated over the entire concentration range (**Figure 3-50** and **Figure 3-51**). Results are again consistent with a non-ideal system.

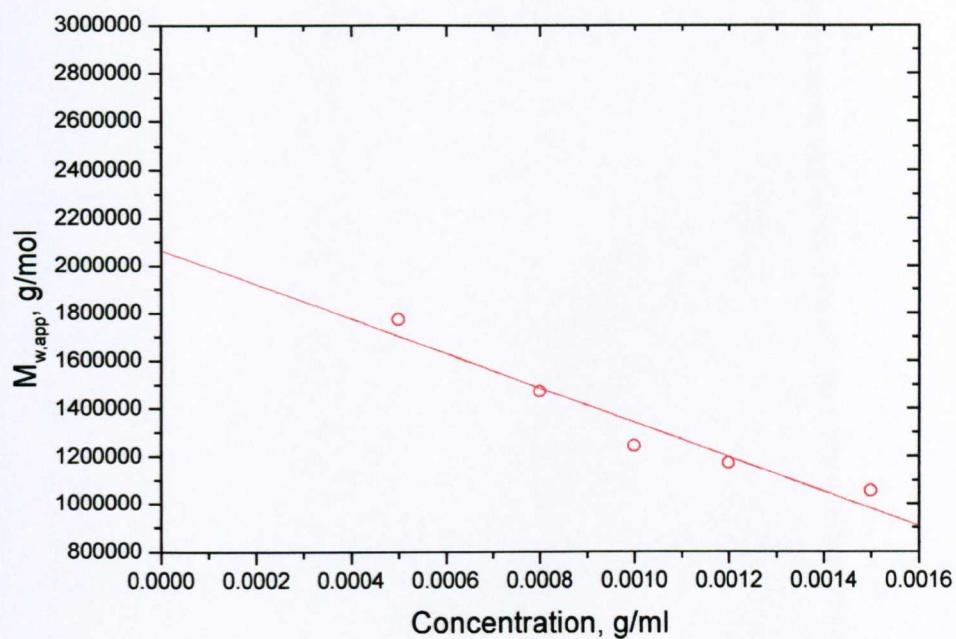


**Figure 3-50** Concentration dependency of apparent molecular weight of AH-EPS – conventional plot at 25°C in 1M guanidine hydrochloride.

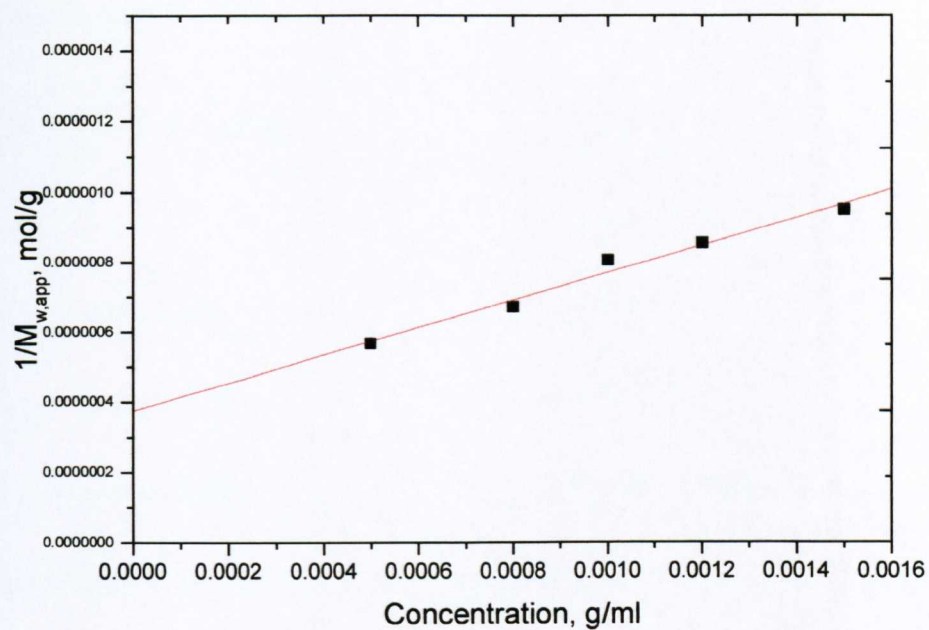


**Figure 3-51** Concentration dependency of apparent molecular weight of AH-EPS – reciprocal plot at 25°C in 1M guanidine hydrochloride.

**Table 3-12** Experimental and calculated parameters for AH-EPS and xanthan in 1M guanidine hydrochloride

Hydrodynamic Parameter	AH-EPS	xanthan
$\bar{v}$ , ml/g	0.600±0.005	0.600±0.005
$[\eta]$ , (from capillary), ml/g	1630±100	-
$[\eta]$ , (from rotational), ml/g	8000±200	-
$c^*$ , (from rotational), g/ml	0.00067±0.00004	-
$S_{20,w}^0$ (from plot of $s$ vs. $c$ ), S	11.4±0.4	10.9±0.3
$S_{20,w}^0$ (from plot of $1/s$ vs. $c$ ), S	12.2±0.1	11.8±0.8
$k_s$ (from plot of $1/s$ vs. $c$ ), ml/g	743±5	540±30
$10^{-6} \times M_w$ (from $M_{wapp}$ vs. $c$ ), g/mol	2.1±0.2	4.8±0.2
$10^{-6} \times M_w$ (from $1/M_{wapp}$ vs. $c$ ), g/mol	2.7±0.2	6.9±0.6
$10^4 \times B$ (from $1/M_{wapp}$ vs. $c$ ), ml.mol/g <sup>2</sup>	2.0±0.1	1.0±0.1
2BM (from $1/M_{wapp}$ vs. $c$ ), ml/g	1100±150	1400±250
$f/f_0$ (from plot of $s$ vs. $c$ and $1/M_{wapp}$ vs. $c$ )	9.7±0.8	19.0±2.0
$R=k_s/[\eta]$ , (from Bohlin and plot of $1/s$ vs. $c$ )	0.10±0.01	-
$\Pi=2BM/[\eta]$ , (from Bohlin and $1/M_{wapp}$ vs. $c$ )	0.14±0.02	-

### 3.4.4.8 Sedimentation Equilibrium for Xanthan

There appears to be no effect of  $c^*$  on the molecular weight calculated from sedimentation equilibrium. Molecular weights are again consistent with those of (Milas *et al.*, 1996; Milas and Rinaudo, 1979; Capron *et al.*, 1997; Dhimi *et al.*, 1995b)  $5.6 \times 10^6$ ;  $3.6 \times 10^6$ ;  $9 \times 10^6$  and  $(5.9 \pm 0.6) \times 10^6$  g/mol respectively. However the 2<sup>nd</sup> thermodynamic virial coefficient, B for AH-EPS is twice that of xanthan, but the product 2BM for xanthan larger than that of AH-EPS.

### 3.4.5 Concluding Remarks

Our data would suggest that AH-EPS, though chemically different is physically similar in its properties to xanthan. This is particularly true of the results from viscometry (both capillary and double gap) and for sedimentation velocity. Both samples show classic shear thinning behaviour over a large concentration range, as well as the existence of a critical coil overlap concentration,  $c^*$ . This together with the formation of hyper-sharp boundaries during sedimentation velocity indicates that both AH-EPS and xanthan are large extra rigid or rigid rod polysaccharides (Pavlov *et al.*, 1997). The greater molecular weight of xanthan would indicate a greater degree of extension than AH-EPS due to the larger translational frictional ratio,  $f/f_0$  (Tanford, 1961) a parameter that depends on conformation and molecular hydration (Equation 2-13).

Due to the unreliability of intrinsic viscosity measurements from capillary viscometry it is only possible to estimate the Wales-van Holde ratio,  $R = k_s / [\eta]$  or the  $\Pi$  function,  $2BM / [\eta]$  from the Bohlin measurements. [Note – as  $k_s$  is quite sensitive to ionic strength, R only gives reliable conformation if charge effects are suppressed, in 1M guanidine hydrochloride charge effects should be negligible, charge effects were probably sufficiently suppressed at  $I = 0.3M$  in the case of Dhimi *et al.*, 1995b]. The small values for each function therefore indicate that AH-EPS is an extended rod-like molecule (Dhimi *et al.*, 1995b and Harding *et al.*, 1991 and Harding and Cölfen, 1995) of the zone A type (Pavlov *et al.*, 1997) of axial ratio,  $a/b$  greater than 100.

The data suggests that like many exobacterial polysaccharides AH-EPS does exhibit xanthan-like properties (at least in the solvent system studied) and could be industrially useful, this is however dependent on the cost effectiveness of extraction and purification.

### 3.5 CHARACTERISATION OF NATIVE AND MODIFIED ARABINOXYLANS

The final set of polysaccharides chosen was an arabinoxylan (AGX), which, like pectin, is derived from plant cell walls and its carboxybenzyl derivative (CB-AGX).

#### 3.5.1 Background

Xylan, a structural polysaccharide of the hemicellulose class is the second most abundant naturally occurring organic compound. Xylan is a major component of plant cell walls and can be found at levels up to 30% in some hardwoods. Xylan is often covalently linked to other cell wall components, such as lignin, and is thought to form an interface between cellulose and lignin in the plant cell wall. The arabinoxylans of wheat grains compose approximately 70% of the endosperm cell wall and are therefore the principle source of fibre in flour. Water-soluble arabinoxylans leached from the endosperm form high viscosity solutions able to hold 10 times their weight in water.

The xylan backbone is essentially  $\beta(1\rightarrow4)$  linked pentose D-xylose units.

...  $\rightarrow4)$   $\beta$ -D-Xylp- (1 $\rightarrow$ ...

This backbone is heavily branched with glucuronyl ( $\alpha$ -D-GlcpA) and/ or arbinosyl ( $\alpha$ -L-Araf) residues, although additional polysaccharide side chains are found. Xylans with ( $\alpha$ 1 $\rightarrow$ 2 linked) glucuronic acid or methyl glucuronic acid side chains are common in hard woods. O-acetyl groups substitute many of the OH- groups at C2 and C3 of the xylans. The average degree of polymerisation of the xylan backbone varies between about 100 and 200 depending on the wood species and the mode of isolation. Softwoods differ from hardwoods by the lack of acetyl groups and the presence of arbinofuranose units  $\alpha$ 1 $\rightarrow$ 3 linked to the xylan backbone.

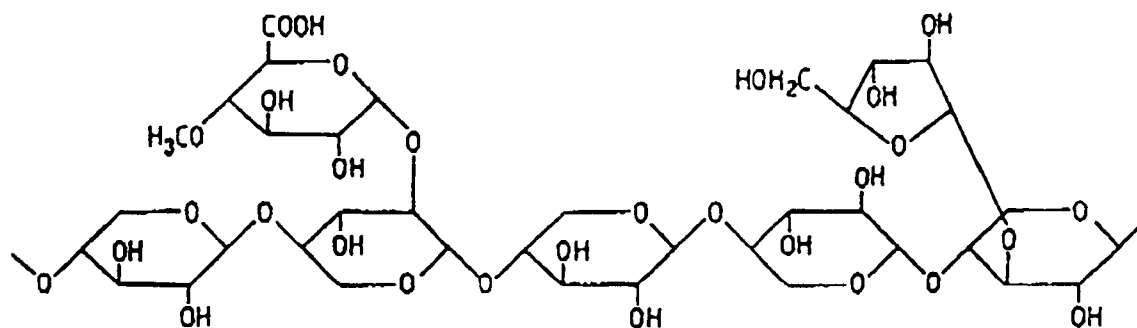


**Figure 3-52** Partial chemical structure of arabino-4-O-methylglucuronoxylan from softwood (adapted from de Gruyter, 1984).

As hydrolysis of xylans releases xylose and arabinose as the predominant sugars they are often referred to as pentosans. Although only partially soluble in water the hydrodynamic properties of xylans have been previously characterised (Dhami *et al.*, 1995a). The chemical modification of xylans has been pioneered by the group led by Dr. Anna Ebringerova at the Slovak Academy of Sciences in Bratislava. The process of chemical modification has been found to give rise to novel molecular functions applicable to many chemical disciplines (Ebringerova *et al.*, 1996). The introduction of a carboxy-benzyl (CB) group onto a native xylan changes the chemical properties significantly. Very significant changes can be seen in both the UV spectra.

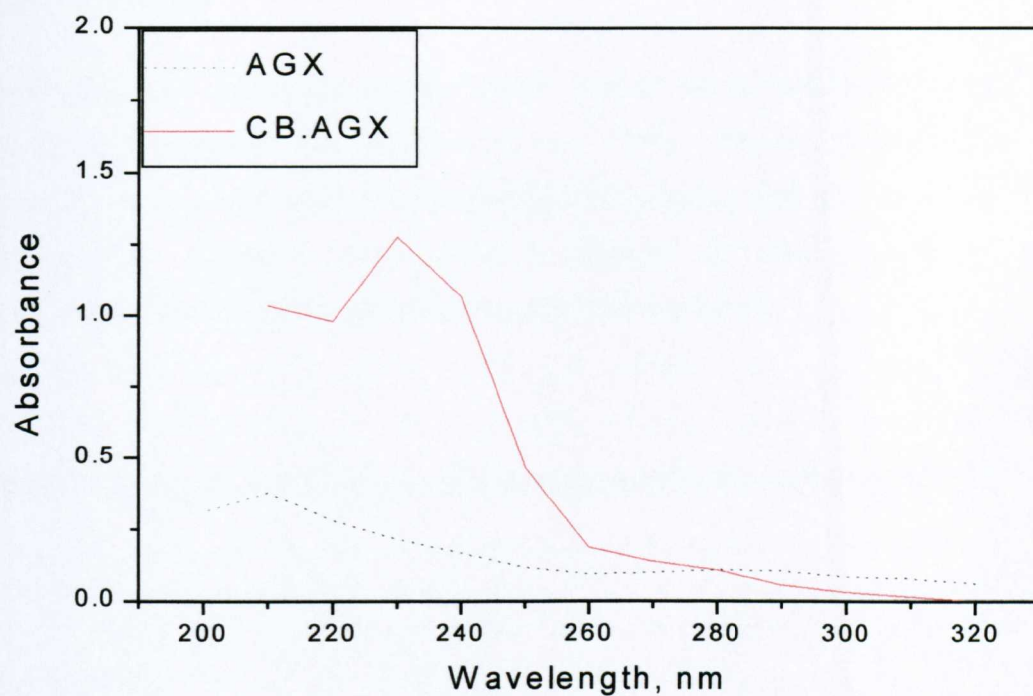


**Figure 3-53** UV absorption data for modified and native arabinoxylans.

The introduction of the absorbing chromophore is of great interest to the users of the analytical ultracentrifuge, as it enables the use of UV optics to study solute distributions.

### 3.5.2 Materials

Both native and chemically modified arabino-xylans were prepared by the group of Dr. Anna Ebringerova (Ebringerova *et. al.*, 1996). Native xylan AGX is from corncob and is of the arabino-4-O-methylglucuronoxylan type typical of soft woods and cereals. Chemical modification is achieved by reaction with excess *p*-bromomethylbenzoic acid in the presence of sodium hydroxide.

**Table 3-13** Typical composition and physical properties for arabinoxylan AGX

Property	
Moisture (%)	~10
D-Xylose (wt.%)	73.6
D-Glucose (wt.%)	2.5
D-Mannose (wt.%)	5.1
L-Arabinose (wt.%)	18.8
Uronic acid (wt.%)	8.7

Information courtesy of Dr. Anna Ebringerova.

Prior to hydrodynamic analysis it is necessary that both the sample and the buffer be in identical ionic environments, it is therefore imperative that the sample is dialyzed against the appropriate buffer. This process of dialysis against a large excess of buffer allows the sample to be treated as a simple two-component system and therefore simplifies calculations accordingly (Cassassa and Eisenberg, 1964). In general 24 hours is considered to be a long enough for the sample and diazylate to reach iso-ionic equilibrium. All samples discussed in this report have been dialyzed

for approximately 24 hours against an ionic strength 0.1, pH 7.5 phosphate chloride buffer.

### 3.5.3 Methods

#### 3.5.3.1 *UV Absorption*

Both modified and native arabinoxylans were studied using UV Absorption in the range 200 - 320nm using the LKB Biochrom Ultraspec 4050 (Figure 3-53). 1 cm quartz cells were used, and the respective diazylates were used as blanks.

#### 3.5.3.2 *Capillary Viscometry*

Solutions and reference solvents were analysed using a 2ml automatic Schott-Geräte Oswald viscometer, under precise temperature control ( $25.02 \pm 0.01$ )°C. The relative,  $\eta_{rel}$  specific,  $\eta_{sp}$  and reduced,  $\eta_{red}$  viscosities were calculated from Equations 2-34, 2-35 and 2-36 respectively, the intrinsic viscosities were estimated from the Huggins plot (Equation 2-38).

#### 3.5.3.3 *Sedimentation Velocity in the Analytical Ultracentrifuge*

Arabinoxylan samples of different concentrations were prepared for use in both the Beckman XLA and XLI analytical ultracentrifuges (Beckman Inc. Palo Alto, CA). A rotor speed of 50,000 rpm was chosen and cells were scanned at 30-minute intervals for up to 15 scans. A typical polysaccharide weighted average partial specific volume,  $\bar{v}$  of ( $0.600 \pm 0.005$ )ml/g. Data was analysed using the Beckman Origin Transport program (Microcal Software Inc. Northampton, MA).

#### 3.5.3.4 *Sedimentation Equilibrium in the Analytical Ultracentrifuge*

Cells were scanned every 4 hours at 18,000 rpm until two consecutive scans give identical absorption/ interference profiles. The centrifuge is then accelerated to 55,000 rpm in order to obtain the baseline absorbance required for data analysis. All absorbance data sets were analysed using the MSTAR and MSTAR programs for absorption and interference data respectively (Cölfen and Harding, 1997) see section 2.2.2.

### 3.5.4 Results and Discussion

#### 3.5.4.1 *UV Absorption*

The UV absorption profiles (**Figure 3-53**) show that both native and modified samples appear to be free from any peptide contaminants (or at least those containing aromatic groups). It is also clear that the introduction of the CB group causes a marked change in the spectrophotometric properties of the samples.

#### 3.5.4.2 *Capillary Viscometry*

Reduced viscosity vs. concentration plots shown in **Figure 3-54** reveal only a small decrease (~6%) in intrinsic viscosity, from  $(82.8 \pm 0.4)$  ml/g to  $(77.6 \pm 0.6)$  ml/g, caused by the chemical substitution. It is worth pointing out that these values may be partially affected by possible systematic dilution errors caused by dialysis, although it should be stressed that both samples received identical dialysis protocols.

[Note – such dialysis errors would not affect  $s_{20,w}^0$  nor  $M_w$  discussed below, since concentration is not an integral part of the function (unlike reduced viscosity) and if solutions are serially diluted, concentration errors do not affect the extrapolated  $c=0$  values].

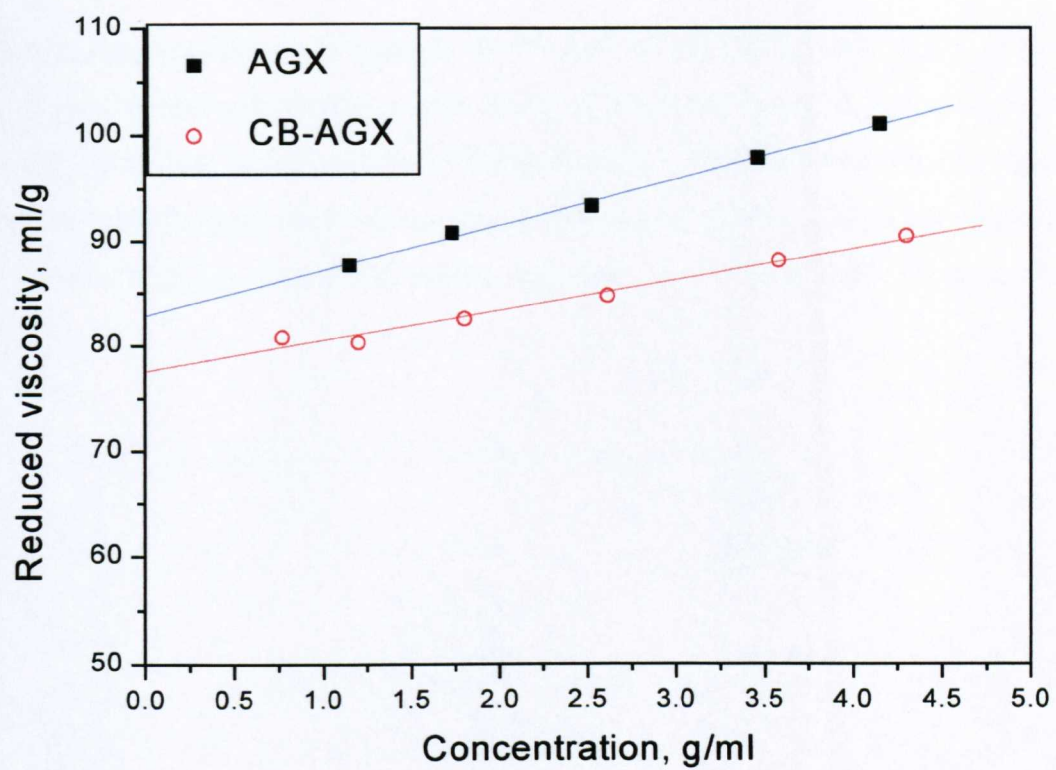


**Figure 3-54** Reduced viscosity vs. concentration for AGX and CB-AGX in I= 0.1, pH 7.5 phosphate chloride buffer.

## 3.5.4.3 Sedimentation Velocity in the Analytical Ultracentrifuge

Sedimentation coefficients (**Figure 3-55**) for both native “AGX” and “CB-AGX” do not show any dramatic decrease with increase in concentration, and follow almost identical behaviour, with  $s_{20,w}^0 = (1.72 \pm 0.06)S$  and  $(1.77 \pm 0.06)S$  respectively. [Note – sedimentation experiments were performed at significantly lower concentrations for the substituted xylan due to the greater sensitivity of the substituted UV-absorbing group].

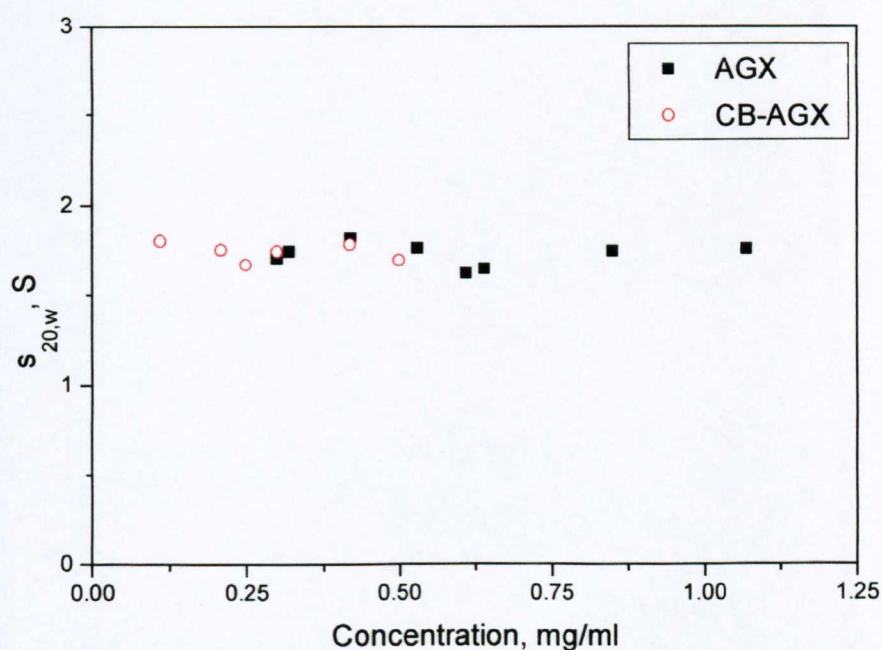


**Figure 3-55** Apparent sedimentation coefficient vs. sedimenting concentration for AGX and CB-AGX in  $I=0.1$ , pH 7.5 phosphate chloride buffer.

## 3.5.4.4 Sedimentation Equilibrium in the Analytical Ultracentrifuge

Molecular weight behaviour (**Figure 3-56**) is also indistinguishable between the native and substituted xylans, showing the same decrease in  $M_{w,app}$  with concentration through non-ideality. Extrapolated “ideal” values are also very similar  $M_w = (37000 \pm 1500) \text{g/mol}$  and  $(40000 \pm 3000) \text{g/mol}$  respectively.

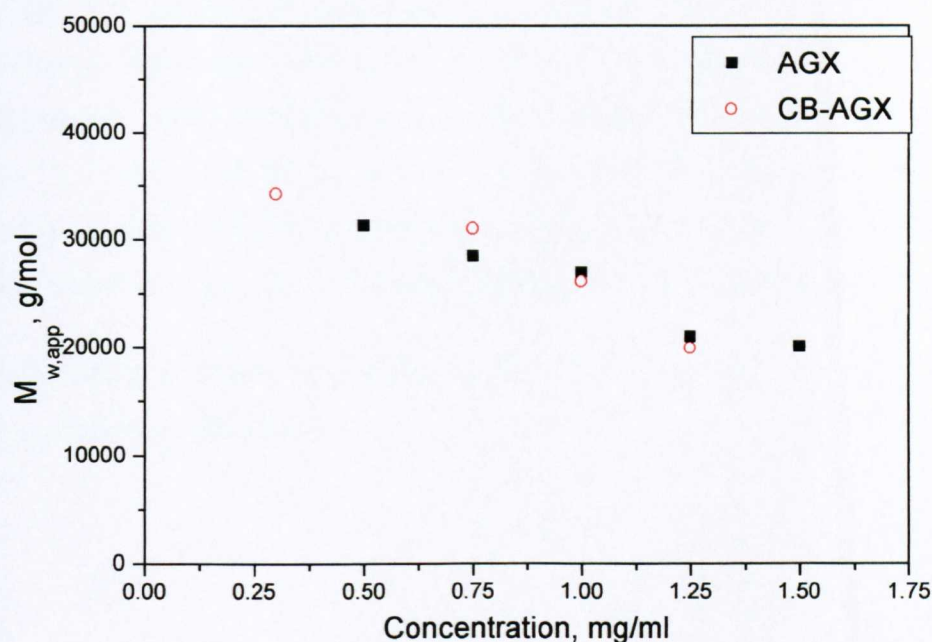


**Figure 3-56** Apparent molecular weight (from low speed sedimentation equilibrium) vs. cell loading concentration for AGX and CB-AGX in  $I= 0.1$ , pH 7.5 phosphate chloride buffer.

### 3.5.5 Concluding Remarks

As there appears to be no significant differences in the sedimentation coefficients nor molecular weights on chemical substitution it would appear that the chemical substitution by the aromatic tag CB has no effect on the physical integrity of the arabinoxylan “AGX”, with no conformational change or no induced self-association. The small decrease in intrinsic viscosity may indicate possibly a slight conformational change. It is possible of course that increasing the degree of substitution, DS, could accentuate this minor affect (or conversely, reducing the DS could remove it completely). Our conclusions are nonetheless similar to that observed previously for “blue dextran” (Errington *et al.*, 1992b) and di-iodotyrosine labelled dextran (Errington *et al.*, 1992a), viz.: labelling of polysaccharides for visualisation purposes does at least in these cases not seriously affect their structural integrity.

Having characterised all the polysaccharide reactants for the casein interaction work, we now turn to casein itself.

### 3.6 REFERENCES

- Abel-Azim A-A A, Atta AM, Farahat MS and Boutros W (1998) Determination of the Intrinsic Viscosity of Polymeric Compounds Through a Single Specific Viscosity Measurement. *Polymer*, **39**, 6827-6833.
- Augustin MA, Puvanenthiran A and McKinnon IR (1999) The Effect of  $\kappa$ -Carrageenan Conformation on its Interaction with Casein Micelles. *International Dairy Journal*, **9**, 413-414.
- Austen KJR, Goodall DM and Norton IT (1988) Anion Effects on Equilibria and Kinetics of the Disorder-Order Transition in  $\kappa$ -Carrageenan. *Biopolymers*, **27**, 139-155.
- Axelos MAV and Thibault J-F (1991) The Chemistry of Low-Methoxyl Pectin Gelation. In: Walter RH (Ed.) *The Chemistry and Technology of Pectin*. Academic Press, San Diego, California. Chapter 5, pp109-118.
- Bar E and Visnovsky S (1997). Development of an Algal Biomatrix as a Natural Solution for Improving Soil Characteristics and for Land Stabilization. *Phycologia*, (Suppl.), **36**, 5.
- Bar-or Y and Shilo M (1987) Characterization of Macromolecular Flocculants Produced by *Phormidium* sp. Strain J-1 and by *Anabaenopsis circularis* PCC6720. *Applied Environmental Microbiology*, **53**, 2226-2230.
- Beckman (1974) *Beckman Spinco Service Manual*. Beckman Instruments, Palo Alto, California.
- Berth G (1988) Studies on the Heterogeneity of Citrus Pectin by Gel Permeation Chromatography on Sepharose 2B/ Sepharose 4B. *Carbohydrate Polymers*, **8**, 105-117.

- Berth G (1992) Methodical Aspects of Characterisation of Alginate and Pectate by Light Scattering and Viscometry Coupled with GPC. *Carbohydrate Polymers*, **19**, 1-9.
- Berth G, Anger H and Linow F (1977) Light-Scattering and Viscometric Studies for Molecular Weight Determination of Pectin in Aqueous Solutions. *Nahrung*, **21**, 939-950.
- Berth G and Lexow D (1991) The Determination of the Molecular Weight Distribution of Pectins by Calibrated GPC Part II. The Universal Calibration. *Carbohydrate Polymers*, **15**, 51-65.
- Bohdanecky M (1983) New Method for Estimating the Parameters of the Wormlike Chain Model from the Intrinsic Viscosity of Stiff-Chain Polymers. *Macromolecules*, **16**, 1483-1492.
- Bongaerts K, Paoletti S, Deneff B, Vanneste K, Cuppo F and Raynaers H (2000) Light Scattering Investigation of  $\iota$ -Carrageenan Aqueous Solutions. Concentration Dependence of Association. *Macromolecules*, Web Edition, 23/10/00, <http://dx.dio.org/10.1021/ma000996y>.
- Brock TD (1976). Halophilic Blue-Green Algae. *Archives in Microbiology*, **107**, 109-111.
- Capron I, Brigand G and Muller G (1997) About the Native and Re-Natured Conformation of Xanthan Exopolysaccharide. *Polymer*, **38**, 5289-5295.
- Cassassa EF and Eisenberg H (1964). Thermodynamic Analysis of Multicomponent Systems. *Advances in Protein Chemistry*, **19**, 287-395.

- Cesaro A, Liut G, Bertocchi C, Navarini L and Urbani R. (1990). Physicochemical Properties of the Exocellular Polysaccharide from *Cyanospira capsulata*. *International Journal of Biological Macromolecules*, **12**, 79-84.
- Chapman HD, Morris VJ, Selvendran RR and O'Neill MA (1987). Static and Dynamic Light Scattering Studies of Pectic Polysaccharides from the Middle Lamellae and Primary Cell Walls of Cider Apples. *Carbohydrate Research*, **165**, 53-68.
- Ciancia M, Milas M and Rinaudo M (1997) On the Specific Role of Coions and Counterions on  $\kappa$ -Carrageenan Conformation. *International Journal of Biological Macromolecules*, **20**, 35-41.
- Choi WC, Yoo S, Oh I and Park SH (1998). Characterization of an Extracellular flocculating substance produced by a Planktonic Cyanobacterium, *Anabaena sp.* *Biotechnology Letters*, **20**, 643-646.
- Cölfen H and Harding SE (1997) MSTARA and MSTARI : Interactive PC Algorithms for Simple, Model Independent Evaluation of Sedimentation Equilibrium Data. *European Biophysics Journal*, **25**, 333-346.
- Corredig M, Kerr W and Wicker L (2000) Molecular Characterisation of Commercial Pectins by Separation with Linear Mix Gel Permeation Columns In-Line with Multi-Angle Light Scattering Detection. *Food Hydrocolloids*, **14**, 41-47.
- Creeth JM and Knight CG (1965) On the Estimation of the Shape of Macromolecules from Sedimentation and Viscosity Measurements. *Biochimica et Biophysica Acta*, **102**, 549-558.
- Crescenzi V and Della Valle F (1991). *Italian Patent. Application*, PD 91A00033.

- Cros S, Garnier C, Axelos MAV, Imberty A and Perez S (1995) Solution Conformations of Pectin Polysaccharides: Determination of Chain Characteristics by Small Angle Neutron Scattering, Viscometry and Molecular Modeling. *Biopolymers*, **39**, 339-352.
- Cross MM (1965) Rheology of Non-Newtonian Fluids: A New Flow Equation for Pseudoplastic Systems. *Journal of Colloid Science*, **20**, 417-437.
- de Gruyter G (Editor) (1984). *Wood Chemistry, Ultrastructure, Reaction*. Berlin, New York. Pages 106-131.
- De Philippis R and Vincenzini M (1998). Exocellular Polysaccharides from Cyanobacteria and their Possible Applications. *FEMS Microbiology Reviews*, **22**, 151-175.
- Dhami R, Harding SE, Elizabeth NJ and Ebringerova A (1995a). Hydrodynamic Characterization of the Molar Mass and Gross Conformation of Corn Cob Hetroxylan AGX. *Carbohydrate Polymers*, **28**, 113-119.
- Dhami R, Harding SE, Jones T, Hughes T, Mitchell JR, and To K (1995b). Physico-Chemical Studies on a Commercial Food Grade Xanthan-I. Characterisation by Sedimentation Velocity, Sedimentation Equilibrium and Viscometry. *Carbohydrate Polymers*, **27**, 93-99.
- Dondos A (2001) A New Relationship Between the Intrinsic Viscosity and the Molecular Mass of Polymers Derived from the Blob Model: Determination of the Statistical Length of Flexible Polymers. *Polymer*, **42**, 897-901.
- Drews G and Weckesser J (1982). Function, Structure and Composition of Cell Walls and External Layers. In: Carr NG and Whitton BA (Eds.) *The Biology of Cyanobacteria*. Vol 19. pp.333-357. Blackwell Scientific Publications, Oxford.

- Ebringerova A, Novotna M, Kucurakova M and Machova E (1996) Chemical Modification of Beechwood Xylan with *p*-Carboxybenzyl Bromide. *Journal of Applied Polymer Science*, **6**, 1043-1047.
- Errington NC, Harding SE, Illum E and Schact EH (1992a) Physico-Chemical Studies on Di-Iodotyrosine Dextran. *Carbohydrate Polymers*, **18**, 289-294.
- Errington NC, Harding SE, Rowe AJ (1992b) Use of Scanning Absorption Optics for Sedimentation Equilibrium Analysis of Labelled Polysaccharides: Molecular Weight of Blue Dextran. *Carbohydrate Polymers*, **17**, 151-154.
- Falchini L, Sparvoli E and Tomaselli L (1996) Effect of *Nostoc* (Cyanobacteria) Inoculation on the Structure and Stability of Clay Soils. *Biol. Fertil. Soils*, **23**, 346-352.
- Fishman ML, Chau HK, Hoagland HD and Ayyad K (2000) Characterization of Pectin, Flash-Extracted from Orange Albedo by Microwave Heating, Under Pressure. *Carbohydrate Research*, **323**, 126-138.
- Garozzo D, Impallomeni G, Spina E and Sturiale L (1998). The Structure of the Exopolysaccharide from the Cyanobacterium *Cyanospira capsulata*. *Carbohydrate Research*, **307**, 113-124.
- Glicksman M (1969) *Gum Technology in the Food Industry*. Academic Press, San Diego.
- Gordon CM (1990) The Use of Xanthan Gum in Salad Dressings and Other Products – the User’s Viewpoint. In: Phillips GO, Williams PA and Wedlock DJ (Eds.) *Gums and Stabilisers for the Food Industry 5*, pp. 351-358. IRL Press, Oxford.

- Goycoolea FM, Morris ER and Gidley MJ (1995) Viscosity of Galactomannans at Alkaline and Neutral pH: Evidence of “Hyperentangulation” in Solution. *Carbohydrate Polymers*, **27**, 69-71.
- Gralén N (1944) Sedimentation and Diffusion Measurements on Cellulose and Cellulose Derivatives. PhD Dissertation, University of Uppsala, Sweden.
- Green AA (1933) The Preparation of Acetate and Phosphate Buffer Solutions of Known pH and Ionic Strength. *Journal of the American Chemical Society*, **55**, 2331-2336.
- Harding SE (1995) Some Recent Developments in the Size and Shape Analysis of Industrial Polysaccharides in Solution Using Sedimentation Analysis in the Analytical Ultracentrifuge. *Carbohydrate Polymers*, **28**, 227-237.
- Harding SE (1997) The Intrinsic Viscosity of Biological Macromolecules. Progress in Measurement, Interpretation and Application to Structure in Dilute Solutions. *Progress in Biophysics and Molecular Biology*, **68**, 207-262. Elsevier, Amsterdam.
- Harding SE, Berth G, Ball A, Mitchell JR and Garcia de la Torre J (1991b) The Molecular-Weight Distribution and Conformation of Citrus Pectins in Solutions Studied by Hydrodynamics. *Carbohydrate Polymers*, **16**, 1-15.
- Harding SE and Cölfen H (1995) Inversion Formulae for Ellipsoid of Revolution Macromolecular Shape Functions. *Analytical Biochemistry*, **228**, 131-142.
- Harding SE, Day K, Dhimi R and Lowe PM (1997a). Further Observations on the Size, Shape and Hydration of Kappa-Carrageenan in Dilute Solution. *Carbohydrate Polymers*, **32**, 81-87.

- Harding SE, Horton JC and Cölfen H (1997b). The ELLIPS Suite of Macromolecular Conformation Algorithms. *European Biophysics Journal*, **25**, 347-359.
- Harding SE, Vårum KM, Stokke BT and Smidsrød, O (1991a) Molecular Weight Determination of Polysaccharides. *Advances in Carbohydrate Analysis*, **1**, 63-144.
- Jordan RC and Brant DA (1978) An Investigation of Pectin and Pectic Acid in Dilute Aqueous Solution. *Biopolymer*, **17**, 2885-2895.
- Jumel K (1994) Molecular Size of Interacting and Degrading Polysaccharides. Ph.D. Thesis, University of Nottingham.
- Jumel K, Browne P and Kennedy JF (1992). In: Harding SE, Sattelle DB and Bloomfield VA (Eds.). *Laser Light Scattering in Biochemistry*. Royal Society of Chemistry, Cambridge, Chapter 2.
- Kitamura S, Kuge T and Stokke BT (1990) A Differential Scanning Calorimetric Study on the Conformation of Xanthan in Aqueous NaCl. In: Phillips GO, Williams PA and Wedlock DJ (Eds.) *Gums and Stabilisers for the Food Industry 5*, pp. 329-332. IRL Press, Oxford.
- Klavons JA and Bennet RD (1995). Preparation of Alkyl Esters of Pectin and Pectic Acid. *Journal of Food Science*, **60**, 513-515.
- Kratky O, Leopold H and Stabinger H. (1973) The Determination of the Partial Specific Volume of Proteins by the Mechanical Oscillator Technique. *Methods in Enzymology*, **27D**, 98-110.
- Kravtchenko TP and Pilnik W (1990) A Simplified Method for the Determination of the Intrinsic Viscosity of Pectin Solutions by Classical Viscometry. In:

Phillips GO, Williams PA and Wedlock DJ (Eds.) *Gums and Stabilisers for the Food Industry 5*, pp. 281-286. IRL Press, Oxford.

Kravtchenko TP., Voragen AGJ and Pilnik W. (1994) Characterisation of Industrial High Methoxy Pectin. In: Phillips GO Williams PA and Wedlock DJ (Eds.) *Gums and Stabilisers for the Food Industry 7*, pp. 27-36. IRL Press, Oxford.

Lapasin R and Prici S (1995). *Rheology of Industrial Polysaccharides, Theory and Applications*. Blackie, London, UK.

Laue TM and Stafford III WF (1999) Modern Applications of Analytical Ultracentrifugation. *Annual Reviews in Biophysics and Biomolecular Structure*, **28**, 75-100.

Launay B, Cuvelier G and Martinez-Reyes S (1997) Viscosity of Locust Bean, Guar and Xanthan Gum Solutions in the Newtonian Domain: a Critical Examination of the  $\log(\eta_{sp})_0 - \log C[\eta]_0$  Master Curves. *Carbohydrate Polymers*, **34**, 385-395

Launay B, Cuvelier G and Martinez-Reyes S (1984) Xanthan Gum in Various Solvent Conditions: Intrinsic Viscosity and Flow Properties. In: Philips GO, Wedlock DJ and Williams PA (Eds.) *Gums and Stabilisers for the Food Industry 2*, pp. 79-98. Pergamon Press, Oxford.

Lecacheux D, Panaras R, Brigand G and Martin G (1985) Molecular Weight Distributions of Carrageenans by Size Exclusion Chromatography and Low Angle Laser Light Scattering. *Carbohydrate Polymers*, **5**, 423-440.

Lehninger AL, Nelson DL and Cox MM (1990). *Principles of Biochemistry*. Second Edition. Worth, New York.

- Li P, Liu Z and Xu R (in press). Chemical Characterization of the Released Polysaccharide from the Cyanobacterium *Aphanothece halophytica* GR02. *Journal of Applied Phycology*.
- Liu Z and Lin H (1993). A Species of Microalga with Useful and Developable Prospects - *Aphanothece halophytica*. *Sea-lake Salt and Chemical Industry*, **22**, 16-19 (in Chinese).
- Lopes da Silva JA and Goncalves MP (1994) Rheological Study into the Ageing Process of High Methoxyl Pectin/ Sucrose Gels. *Carbohydrate Polymers*, **24**, 235-245.
- Marra M, Palmeri A, Ballio A, Segre A and Slodki ME (1990). Structural Characterisation of the Exopolysaccharide from *Cyanospira capsulata*. *Carbohydrate Research*, **197**, 338-344.
- Mazor G, Kidron GJ, Vonshak A and Abeliovich A (1996). The Role of Cyanobacterial Exopolysaccharides in Structuring Desert Microbial Crusts. *FEMS Microbiological Ecology*, **21**, 121-130.
- Milas M, Reed WF and Printz S (1996) Conformation and Flexibility of Native and Re-Natured Xanthan in Aqueous Solutions. *International Journal of Biological Macromolecules*, **18**, 211-221.
- Milas M and Rinaudo M (1979) Conformational Investigation on the Bacterial Polysaccharide Xanthan. *Carbohydrate Research*, **76**, 189-196.
- Millane RP, Narasaiah TV and Wang B (1990) Molecular Structures of Variants of Xanthan Gum with Truncated Sidechains. In: Phillips GO, Williams PA and Wedlock DJ (Eds.) *Gums and Stabilisers for the Food Industry 5*, pp. 365-372. IRL Press, Oxford.

- Morris ER (1979) Polysaccharide Structure and Conformation in Solutions and Gels. In: Blanshard JMV and Mitchell JR (Eds.) *Polysaccharides in Food*, pp. 15-31. J Wiley and Sons, London.
- Morris ER (1980) Physical Probes of Polysaccharide Conformation and Interactions. *Food Chemistry*, **6**, 15-39.
- Morris ER (1990) Comparison of the Properties and Function of Alginate and Carrageenans. In: Phillips GO, Williams PA and Wedlock DJ (Eds.) *Gums and Stabilisers for the Food Industry 5*, pp. 483-496. IRL Press, Oxford.
- Morris ER, Powell DA, Gidley MJ and Rees DA (1982) Conformation and Interactions of Pectins I. Polymorphism Between Gel and Solid States of Calcium Polygalacturonate. *Journal of Molecular Biology*, **155**, 507-516.
- Morris ER, Rees DA and Robinson G (1980) Cation-Specific Aggregation of Carrageenan Helices: Domain Model of Polymer Gel Structure. *Journal of Molecular Biology*, **138**, 349-362.
- Morris GA, Butler SNG, Foster TJ, Jumel K and Harding SE (1999). Elevated Temperature Analytical Ultracentrifugation of a Low-Methoxy Polyuronide. *Progress in Colloid and Polymer Science*, **113**, 205-208.
- Morris GA, Foster TJ and Harding SE (2000) The Effect of Degree of Esterification on the Hydrodynamic Properties of Citrus Pectin. *Food Hydrocolloids*, **14**, 227-235.
- Navarini L, Bertocchi C, Cesaro A, Lapasin R. and Crescenzi V (1990). Rheology of Aqueous Solutions of an Extracellular Polysaccharide from *Cyanospira capsulata*. *Carbohydrate Polymers*, **122**, 169-187.

- Navarini L, Cesaro L and Ross-Murphy SB (1992). Viscoelastic Properties of Aqueous Solutions of an Exocellular Polysaccharide from Cyanobacteria. *Carbohydrate Polymers*, **18**, 265-272.
- Nicolaus B, Panico A, Lama L, Romano I, Manca MC, De Giulio A. and Gambacorta A (1999). Chemical Composition and Production of Exopolysaccharides from Representative Members of Heterocystous and Non-Heterocystous Cyanobacteria. *Phytochemistry*, **52**, 639-647.
- Norton (1990) The Influence of Ionic Environment and Polymeric Mixing on the Physical Properties of Iota and Kappa Carrageenan Systems. In: Phillips GO, Williams PA and Wedlock DJ (Eds.) *Gums and Stabilisers for the Food Industry 5*, pp. 511-520. IRL Press, Oxford.
- Norton IT, Goodall DM, Morris ER and Rees DA (1978) Dynamics of the Salt-Induced Random Coil to Helix Transition in Segmented ι-Carrageenan. *Journal of the Chemical Society Chemical Communications*, **1978**, 515-517.
- Norton IT, Goodall DM, Morris ER and Rees DA (1983) Role of Cations in the Conformation of Iota and Kappa Carrageenan. *Journal of the Chemical Society Faraday Transactions*, **79**, 2475-2488.
- Oakenfull DG (1991) The Chemistry of High-Methoxyl Pectins. In: Walter RH (Ed.) *The Chemistry and Technology of Pectin*, pp 87-108. Academic Press, San Diego.
- Oakenfull DG and Scott A (1990) The Role of the Cation in the Gelation of Kappa-Carrageenan. In: Phillips GO, Williams PA and Wedlock DJ (Eds.) *Gums and Stabilisers for the Food Industry 5*, pp. 507-510. IRL Press, Oxford.

- Oakenfull DG and Scott A (1998) Milk Gels with Low Methoxy Pectins. In: Phillips GO, Williams PA and Wedlock DJ (Eds.) *Gums and Stabilisers for the Food Industry 9*, pp 212-221. Oxford University Press, Oxford.
- Pavlov GM (1997) The Concentration Dependence of Sedimentation for Polysaccharides. *European Biophysics Journal*, **25**, 385-398.
- Pavlov GM, Rowe AJ and Harding SE (1997). Conformation Zoning of Large Molecules Using the Analytical Ultracentrifuge. *Trends in Analytical Chemistry*, **16**, 401-405.
- Pavlov GM, Korneeva EV, Harding SE and Vichoreva GA (1998) Dilute Solution Properties of Carboxymethylchitins in High Ionic-Strength Solvent. *Polymer*, **39**, 6951-6961.
- Pilgrim GW, Walter RH and Oakenfull DG (1991). Jams, Jellies, and Preserves. In: Walter RH (Ed.) *The Chemistry and Technology of Pectin*, pp23-50. Academic Press, San Diego.
- Pilnik W (1990) Pectin - A Many Splendoured Thing. In: Phillips GO, Williams PA and Wedlock DJ (Eds.) *Gums and Stabilisers for the Food Industry 5*, pp. 209-222. IRL Press, Oxford.
- Powell DA, Morris ER, Gidley MJ and Rees DA (1982) Conformation and Interactions of Pectins II. Influence of Residue Sequence on Chain Association in Calcium Pectate Gels. *Journal of Molecular Biology*, **155**, 317-331.
- Ralston G (1993). *Introduction to Analytical Ultracentrifugation*. Beckman Instruments Inc., California.

- Richardson RK and Ross-Murphy SB (1987a) Non Linear Viscoelasticity of Polysaccharide Solutions. 1 Guar Galactomannan Solution. *International Journal of Biological Macromolecules*, **9**, 250-256.
- Richardson RK and Ross-Murphy SB (1987b) Non Linear Viscoelasticity of Polysaccharide Solutions. 2 Xanthan Polysaccharide Solution. *International Journal of Biological Macromolecules*, **9**, 257-264.
- Richardson PH, Willmer J and Foster TJ (1998) Dilute Solution Properties of Guar and Locust Bean Gum in Sucrose Solutions. *Food Hydrocolloids*, **12**, 339-348.
- Robinson G, Ross-Murphy SB and Morris ER (1982). Viscosity-Molecular Weight Relationships, Intrinsic Chain Flexibility, and Dynamic Solution Properties of Guar Galactomannan. *Carbohydrate Research*, **107**, 17-32.
- Rochas C and Rinaudo M (1984) Mechanism of Gel Formation in  $\kappa$ -Carrageenan. *Biopolymers*, **23**, 735-745.
- Rochas C, Rinaudo M and Landry S (1990) Role of the Molecular Weight on the Mechanical Properties of Kappa Carrageenan Gels. *Carbohydrate Polymers*, **12**, 255-266.
- Rose S (1966) *The Chemistry of Life*. Penguin Books, London.
- Rowe AJ (1977) Concentration-Dependence of Transport Processes – General Description Applicable to Sedimentation, Translational Diffusion, and Viscosity Coefficients of Macromolecular Solutes. *Biopolymers*, **16**, 2595-2611.
- Sanderson GR (1990) The Functional Properties and Applications of Microbial Polysaccharides – A Supplier's View. In: Phillips GO, Williams PA and

Wedlock DJ (Eds.) *Gums and Stabilisers for the Food Industry 5*, pp. 333-344. IRL Press, Oxford.

Sato T, Norisuye T and Fujita H (1984). Double-Stranded Helix of Xanthan in Dilute-Solution - Further Evidence. *Polymer Journal*, **16**, 423-429.

Sharman WR, Richards EL, Malcolm GN (1978). Hydrodynamic Properties of Aqueous Solutions of Galactomannans. *Biopolymers*, **17**, 2817-2833.

Shatwell KP, Sutherland IW and Ross-Murphy SB (1990) Influence of Acetyl and Pyruvate Substituents on Solution Properties of Xanthan Polysaccharide. *International Journal of Biological Macromolecules*, **12**, 71-78.

Snoeren THM, Both P and Schmitt DG (1976) An Electron-Microscopy Study of Carrageenan and its Interaction with  $\kappa$ -Casein. *Netherlands Milk and Dairy Journal*, **30**, 132-141.

Stafford III WF (1992a) Boundary Analysis in Sedimentation Transport Experiments: A Procedure for Obtaining Sedimentation Coefficient Distributions Using the Time Derivative of the Concentration Profile. *Analytical Biochemistry*, **203**, 295-301.

Stafford III WF (1992b). Methods for Obtaining Sedimentation Coefficient Distributions. In: Harding SE, Rowe AJ and Horton JC (Eds.). *Analytical Ultracentrifugation in Biochemistry and Polymer Science* pp. 359-393. Royal Society of Chemistry, Cambridge.

Tanford C (1961). *Physical Chemistry of Macromolecules*. John Wiley and Sons, New York, Chapter 6.

- Theisen A, Johann C, Deacon MP and Harding SE (2000) *Refractive Increment Data-Book for Polymer and Biomolecular Scientists*. Nottingham University Press, Nottingham.
- Thimault JF and Rinaudo M (1986) Chain Association of Pectic Molecules During Calcium-Induced Gelation. *Biopolymer*, **25**, 455-468.
- Tombs MP and Harding SE (1998) *An Introduction to Polysaccharide Biotechnology*. Taylor and Francis, London . Chapter 2.
- van Holde KE (1985) *Physical Chemistry*. Second Edition. Prentice-Hall, New York.
- Walter RH (Editor) (1991) *The Chemistry and Technology of Pectin*. Academic Press, New York.
- Wang Z-Y, White JW, Konno M, Saito S and Nozawa T (1994) A Small-Angle X-Ray Scattering Study of Alginate Solution and its Sol-Gel Transition by Addition of Divalent Cations. *Biopolymer*, **35**, 227-238.
- Wielinga WC (1990) Production and Application of Seed Gums. Millane RP, Narasaiah TV and Wang B (1990) In: Phillips GO, Williams PA and Wedlock DJ (Eds.) *Gums and Stabilisers for the Food Industry 5*, pp. 383-403. IRL Press, Oxford.
- Wyatt PJ (1992) Combined Differential Light Scattering with Various Liquid Chromatography Separation Techniques. In: Harding SE, Sattelle DB, Bloomfield VA (Eds.) *Laser Light Scattering in Biochemistry*. Royal Society of Chemistry, Cambridge, Chapter 3.

Yevlampieva NP, Pavlov GM and Rjuntsev EI (1999) Flow Birefringence of Xanthan and Other Polysaccharide Solutions. *International Journal of Biological Macromolecules*, **26**, 295-301.

## **4 CHAPTER 4 – DETAILED CHARACTERISATION OF THE MILK PROTEIN SUBSTRATES**

Milk proteins have been studied extensively in biochemistry for over 150 years. Milk is itself a complex mixture of water, lactose, fat, minerals and proteins and the protein composition of milk varies greatly from one species to the other, concentrations ranging from 10-200g/l (Jennes, 1970). Bovine milk has generated the most interest, although Caprine, Equine, and Human milks have also been investigated. Bovine milk on average consists of 3.6% protein (Dickinson and Stainsby, 1982). Historically milk proteins have been split into two types depending on their acid solubility

- (i) acid insoluble caseins
- (ii) acid soluble whey proteins

Both the caseins and whey proteins consist of multi-component mixtures.

**Table 4-1** Some properties of the major components of Bovine milk. Adapted from Jennes, 1970. Assumes total protein = 36g/l and ~78% casein.

Protein	Approximate	Genetic	Monomer	
	Concentration, g/l	Variants	$M_w^a$ , g/mol	$s_{20,w}^a$ , S
<b>Caseins</b>	28.0			
$\alpha_s$ -Casein	15.4	A, B, C, D	30,000	1.6
$\beta$ -Casein	7.0	A <sup>1</sup> , A <sup>2</sup> , A <sup>3</sup> , B, B <sub>2</sub> , C, D	24,100	1.4
$\kappa$ -Casein	4.2	A, B	20,000	1.57
$\gamma$ -Casein	1.4	A, B	30,000	1.55
<b>Whey Proteins</b>	8.0			
$\beta$ -lactoglobulin	4.8	A, B, C, D	18,300	1.8
$\alpha$ -lactalbumin	1.1	A, B	14,200	1.75
Bovine serum albumin	0.5		69,000	4.0
Immunoglobulin G	0.9		160,000	7.0

<sup>a</sup>values not necessarily corrected for non-ideality

Although the heterogeneity of milk proteins is in itself a hindrance in any hydrodynamic characterisation, it is by no means the only problem. Under the conditions experienced in milk (pH ~ 6.8, Ionic strength ~ 0.1M) the caseins form supermolecular aggregates called “casein micelles”, and  $\beta$ -lactoglobulin also dimerises. This chapter describes our attempts to characterise milk proteins in various states of association – Native micelles (4.1), sodium caseinate as a model for “casein submicelles” (4.2),  $\beta$ -casein (4.3.1),  $\kappa$ -casein (4.3.2) and the most abundant whey protein  $\beta$ -lactoglobulin (4.4).

## 4.1 CASEIN MICELLES IN SKIM MILK

### 4.1.1 Background

Casein is the major protein component of bovine milk  $\sim 2.8 \pm 0.3\%$  (Dickinson and Stainsby, 1982). The casein component is a complex mixture of the four most common caseins -  $\alpha_{s1}$ ,  $\alpha_{s2}$ ,  $\beta$  and  $\kappa$  in the ratios of approximately 4:1:4:1 respectively (Srinivasan *et. al.*, 1996) (Table 4-2).

**Table 4-2** Major components of bovine milk. Adapted from Dickinson and Stainsby (1982)

Component	Quantity, %
Water	86.5 $\pm$ 1.5
Lactose	4.8 $\pm$ 0.2
Fat	4.2 $\pm$ 1.0
Total Protein	3.6 $\pm$ 0.4
Caseins	2.8 $\pm$ 0.3
Whey Proteins	0.8 $\pm$ 0.1
Salts	0.9 $\pm$ 0.1

A large proportion of casein in milk is in the form of casein micelles, which can be thought of as a complex of calcium caseinate – calcium phosphate (citrate) (Dickinson and Stainsby, 1982). The casein micelle is usually thought of as a hydrated sphere, with the “hydration” -  $\delta$  (*i.e.* the amount of solvent associated with the protein either chemically or physically entrained expressed as mass of water per unit mass of protein) previously estimated on the basis of dynamic light scattering (Dewan *et. al.*,

1973) to be  $(3.7 \pm 0.5)$ . The colloidal calcium phosphate is essential for micellar stability. Removal of  $\text{Ca}^{2+}$  ions results in a smaller complex – the casein “sub-micelle” (**Figure 4-1**).  $\kappa$ -casein is usually found on the exterior of the casein sub-micelle and therefore important to sub-micellular and micellar stability. The  $\kappa$ -casein is thought to coat the hydrophobic core of the sub-micelle and is important in casein/ polysaccharide interactions due to having a positively charged region available for electrostatic bonding (Langendorff *et. al.*, 1999). The size distribution of casein micelles is very broad (20-250nm in diameter) and this is at least partially due to the availability of  $\kappa$ -casein (Sullivan *et. al.* 1955; Rose and Colvin, 1966b; McGann and Pyne, 1970 and Dickinson and Stainsby, 1982).

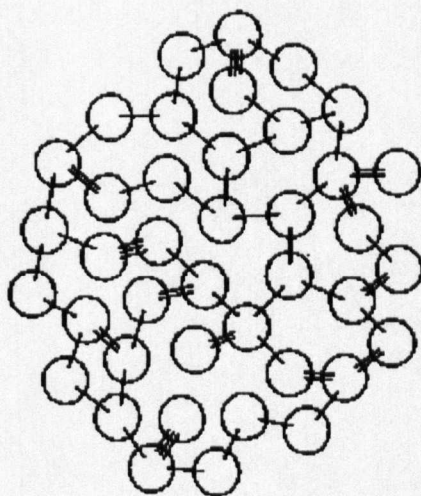


**Figure 4-1** Sub-unit model for the casein micelle. From Dickinson and Stainsby (1982).

In this Chapter we re-examine the question of size, shape and hydration of casein micelles, using a combination of modern analytical ultracentrifugation and capillary viscometry. Advantage will be taken of some recent advances in sedimentation velocity analysis, namely the time-derivative procedure (Stafford, 1992a,b and Laue and Stafford, 1999). The method is particularly useful for quantitatively assaying the heterogeneity of a preparation without the need for a so-called separation medium (as required by chromatographic procedures). The time-derivative or  $g^*(s^*)$  (usually simplified to  $g(s^*)$ ) allows the real time computation of sedimentation coefficient

distributions by the  $dc/dt$  method *i.e.* the change in concentration with time. The subtraction of pairs of data sets allows the averaging of  $g(s^*)$  curves and therefore reduces baseline contributions.

The concentration dependence of the sedimentation coefficient,  $k_s$  (ml/g) is also a very useful parameter (Gralén, 1944). When combined with the intrinsic viscosity,  $[\eta]$  this provides an estimate for particle shape without assumptions over hydration as described in previous articles (see *e.g.* Creeth and Knight, 1965; Rowe, 1977; Rowe, 1992 and Harding, 1997). Once the expected spherical shape has been confirmed for the casein micelles, the intrinsic viscosity data can be re-interpreted to provide a value for the molecular hydration.

#### **4.1.2 Materials**

Skimmed milk powder was dissolved in distilled water 1:10 w/v. The resulting dispersion was of composition – protein 35.6g/l (of which 28.0g/l is casein), sugar (mainly lactose) 50.4g/l, fat 0.6g/l, sodium 0.6g/l and calcium 1.3g/l. (This represents a concentration, typical of some modern food applications). Dilutions were subsequently made for hydrodynamic analyses.

#### **4.1.3 Methods**

##### *4.1.3.1 Sedimentation Velocity in the Analytical Ultracentrifuge*

There are four main optical systems, which can be used, in the analytical ultracentrifuge – Schlieren, absorption, turbidity and interference (see *e.g.* Schachman, 1959 and Ralston, 1993). It was found however that Schlieren and turbidity studies were only valid at high concentrations and absorption at low concentrations (see section 2.2). The Interference system on the Beckman Optima XLI (Beckman Instruments, Palo Alto, USA) was sensitive over the concentration range of interest and was therefore employed. Rotor speeds of 12,600rpm and a 4mm column length in a 12mm path length double sector cell (one sector for solution, the other for solvent) were used together with an accurately controlled temperature of

20.0°C. A weighted average partial specific volume,  $\bar{v}$  of (0.733±0.002)ml/g was calculated from the individual casein amino acid sequences (Perkins, 1986). As casein micelles are 4:1:4:1 mixture of the four main caseins –  $\alpha_{s1}$ ,  $\alpha_{s2}$ ,  $\beta$  and  $\kappa$  (Srinivasan *et. al.*, 1986), the partial specific volume of the casein micelle is therefore the weighted average of individual caseins. The  $g(s^*)$  (sedimentation time-derivative) method was used to determine apparent sedimentation coefficients at each concentration by the procedure described in Stafford, 1992a,b and Laue and Stafford, 1999.

#### 4.1.3.2 Capillary Viscometry

Solutions and reference solvents were analysed using a 2ml automatic Schott-Geräte Ostwald viscometer, under precise temperature control (25.04±0.01°C). The relative viscosity,  $\eta_{rel}$ , was calculated from the standard equation 2-35 (see *e.g.* van Holde, 1985; Harding, 1997).  $t_0$  is the flow time for the solvent (82.63±0.01) seconds. ( $\rho/\rho_0$ ) is assumed to be unity (as the density of the solvent and the sample are approximately equal at low concentrations). A plot of reduced specific viscosity vs. concentration yields the intrinsic viscosity,  $[\eta]$  at the intercept and slope is related to the Huggins constant (Huggins, 1942),  $K_H$  or the related concentration dependence regression coefficient,  $k_\eta$  (Rowe, 1977) (Equations 2-38 and 2-39 respectively see section 2.3).

#### 4.1.4 Results and Discussion

##### 4.1.4.1 Sedimentation Velocity in the Analytical Ultracentrifuge

The sedimentation profile of casein micelles results in a broad peak *i.e.* large size distribution, and shows a large concentration dependency (**Figure 4-2** and **Figure 4-3**). Apparent mode average sedimentation coefficients were calculated at various concentrations and extrapolated to zero concentration using the standard equation 2-8 (see *e.g.* Ralston, 1993; Pavlov, 1997; etc.), where the Gralén parameter,  $k_s$  is a measure of concentration dependence (**Figure 4-3**). The mode average sedimentation coefficient,  $s_{T,b}^0 = (845 \pm 2)S$  and  $k_s = (16.9 \pm 0.1)ml/g$ , this is characteristic of a large extremely hydrated spherical molecule.

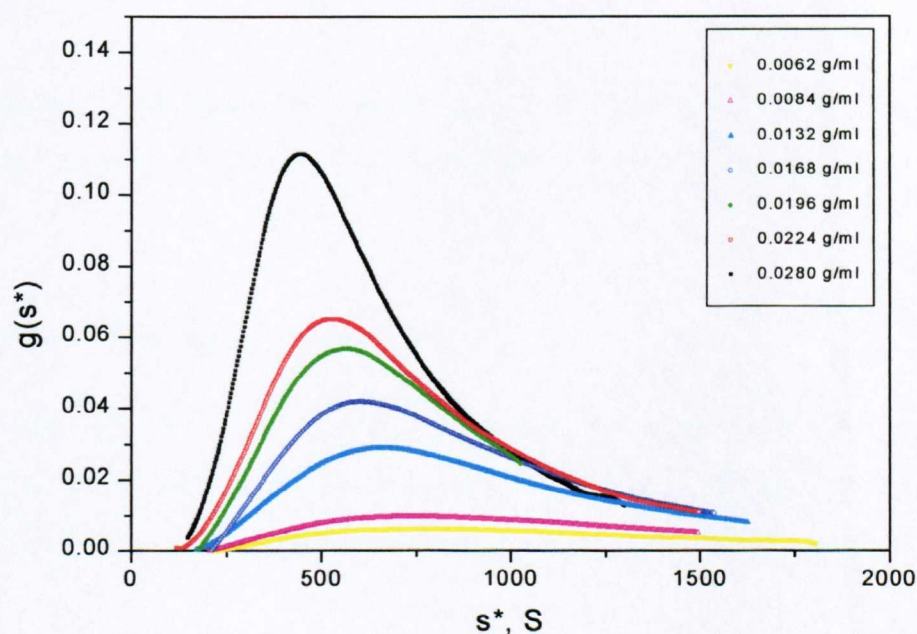


**Figure 4-2**  $g(s^*)$  profiles for casein micelles at differing concentrations in skim milk at 12600rpm.

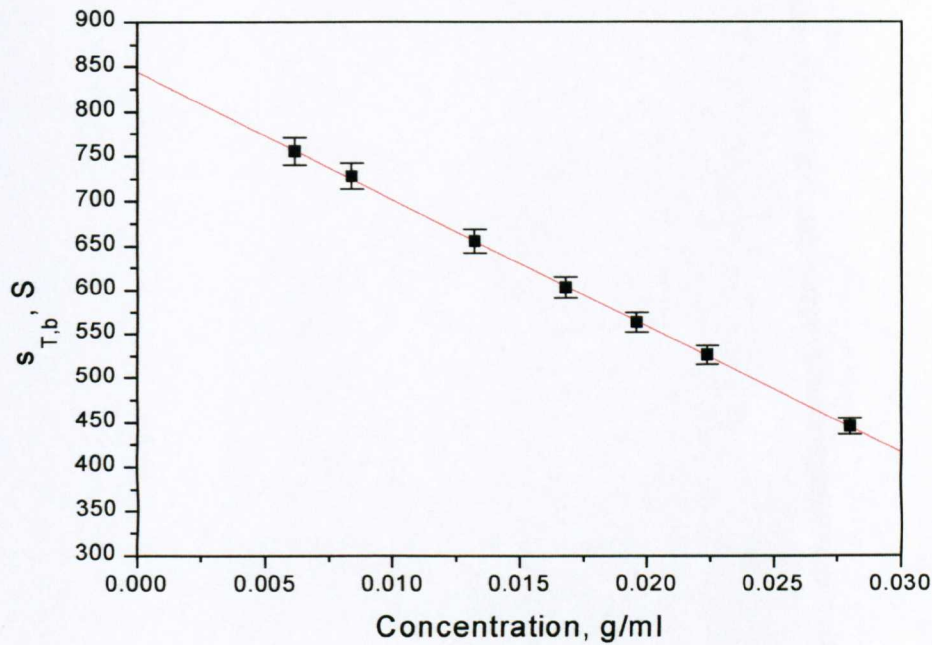


**Figure 4-3** Concentration dependence of sedimentation for casein micelles in skim milk. From the plot above  $s_{T,b}^0 = (845 \pm 2)S$  and  $k_s = (16.9 \pm 0.1)ml/g$ .

#### 4.1.4.2 Capillary Viscometry

Results indicate a classical positive dependence of reduced viscosity on concentration (Huggins) (**Figure 4-4**). The relatively large intrinsic viscosity (for a protein) would also suggest a rather hydrated molecule.

The Wales-van Holde ratio,  $R = k_s/[\eta]$  (see *e.g.* Harding, 1997), a combination of the Gralén parameter,  $k_s$  and the intrinsic viscosity  $[\eta]$  can give an approximate concentration independent indication of macromolecular shape, which is independent of an assumed value of the hydration,  $\delta$ .

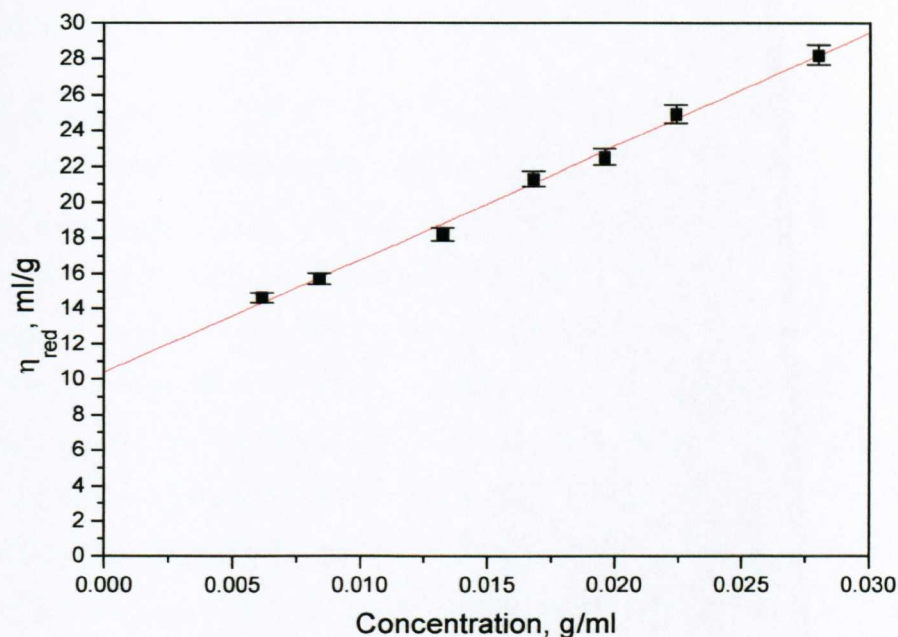


**Figure 4-4** Concentration dependence of reduced viscosity (Huggins plot) of casein micelles in skim milk. From the plot above  $[\eta] = (10.4 \pm 0.4) \text{ ml/g}$  and  $k_{\eta} = (61 \pm 4) \text{ ml/g}$  and  $K_H = 5.9 \pm 0.5$ .

From the data above  $R = 1.63 \pm 0.07$  (Table 4-3). Since the theoretical value for a sphere is 1.6 (see *e.g.* Creeth and Knight, 1965; Rowe, 1977; Rowe, 1992 and Harding, 1997), we can reasonably say that casein micelles are spherical. Having confirmed the spherical shape it is possible to calculate the hydration (Equations 2-43 and 2-77) using the Einstein viscosity increment,  $v$ , where  $v$  is 2.5 for a sphere (Einstein, 1911 and Harding, 1997).

This yields a value of 4.2 ml/g for the swollen specific volume. If we approximate  $\rho_0$  to the density of water, this results in a hydration,  $\delta$  of  $(3.4 \pm 0.5)$  grams of solvent/grams of protein, which is in good agreement with a previously estimated value of  $(3.7 \pm 0.5)$  (Dewan *et al.*, 1973) from dynamic light scattering. A further “ballpark” estimate for the swollen specific volume can be made from the following approximate relationship (Rowe, 1977) (Equation 2-80). This yields a value of  $\sim 3 \text{ ml/g}$  for  $v_s$ ,

which is in general agreement with the previous value. [Note- a typical non-micelles forming protein  $v_s$  is usually of the order of  $\sim 1 \text{ ml/g}$ ].

It is also possible to estimate the molecular weight from the sedimentation coefficient,  $s_{T,b}^0$ , the Gralén parameter,  $k_s$ , and the swollen volume,  $v_s$  (Rowe, 1977) (Equation 2-11). From equation 2-11 a molecular weight,  $M_w$  of  $2.8 \times 10^8 \text{ g/mol}$  can be calculated from the mode average sedimentation coefficient of 845S. The value for molecular weight is in good agreement with the value of  $2.0 \times 10^8 \text{ g/mol}$  (Schorsch *et. al.*, 1999a,b) measured by turbidity. Further simple mathematical manipulation of the data can yield the corresponding diffusion coefficient,  $D_{T,b}^0$  and hydrodynamic radius,  $r_H$ , via rearrangements of the Svedberg and Stokes-Einstein (see *e.g.* Harding, 1999) relationships (Equations 2-12 and 2-62 respectively). The calculated  $D_{T,b}^0 = 2.8 \times 10^{-8} \text{ cm}^2/\text{sec}$  and  $r_H = 78 \text{ nm}$  are also in good agreement with the previously published values (Lin *et. al.*, 1971; Dewan *et. al.*, 1974 and Schorsch *et. al.*, 1999). Having now confirmed the spherical nature of casein micelles, it is now possible to evaluate the diffusion coefficient using the fixed  $90^\circ$  angle Protein Solution Dynopro 801 dynamic light instrument. As with sedimentation experiments measurements were made at a number of concentrations and extrapolated to infinite dilution (Figure 4-5), due the turbid nature of milk the concentration range for diffusion measurements was somewhat smaller. This resulted in a translational diffusion coefficient of  $(2.8 \pm 0.2 \times 10^{-8}) \text{ cm}^2 \text{ sec}^{-1}$ , which is in exact agreement with that previously calculated from sedimentation and viscosity experiments.

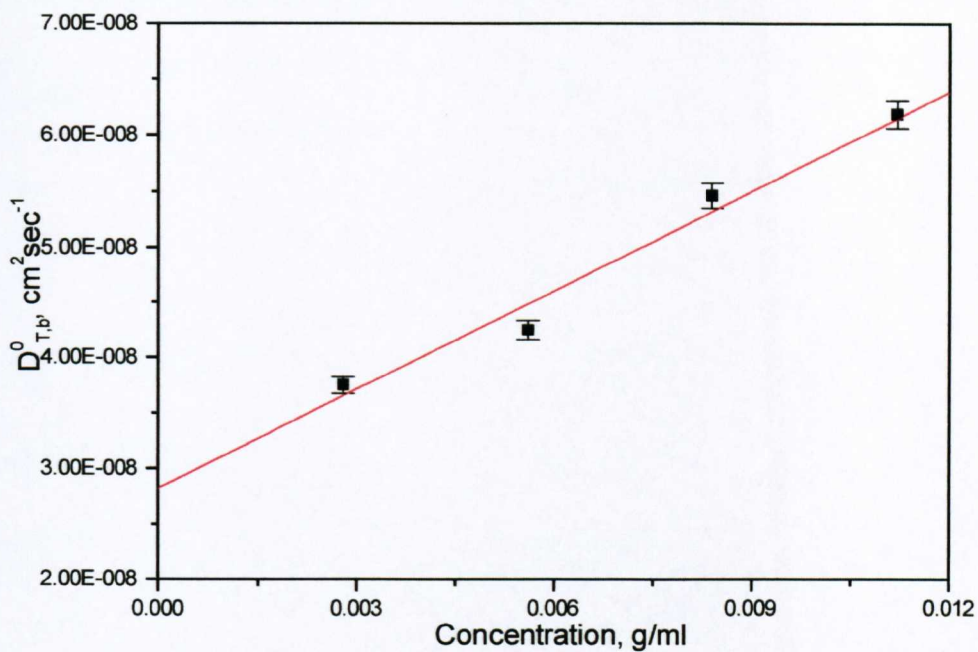


**Figure 4-5** Concentration dependence of diffusion of casein micelles in skim milk. From the graph above  $D_{T,b}^0 = (2.8 \pm 0.2) \times 10^{-8} \text{ cm}^2 \text{ sec}^{-1}$  and  $k_D = (105 \pm 13) \text{ ml/g}$ .

It is also possible to calculate the translational frictional ratio,  $f/f_0$  (Tanford, 1961) from either Equation 2-13 or 2-67 (**Table 4-3**).

**Table 4-3** Experimental hydrodynamic parameters for casein micelles in skim milk

Parameter	Value
$\bar{v}$ , ml/g	0.733±0.002
$s_{T,b}^0$ , S	845±2
$k_s$ , ml/g	16.9±0.1
$[\eta]$ , ml/g	10.4±0.4
$k_\eta$ , ml/g	61.0±2.0
$K_H$	5.9±0.5
$k_s/[\eta]$	1.63±0.07
$k_\eta/k_s$	~3.6
$D_{T,b}^0$ cm <sup>2</sup> /sec	2.8 x 10 <sup>-8</sup>

Table 4-4 Calculated hydrodynamic parameters for casein micelles in skim milk

Parameter	Value
$a/b$	1.0
$\delta$ (Eq. 2-44, 2-77)	3.4
$v_s$ , ml/g (Eq. 2-43)	4.2
$v_s$ , ml/g (Eq. 2-80)	~3.0
$M_w$ , g/mol	$2.8 \times 10^8$
$D_{T,b}^0$ cm <sup>2</sup> /sec	$2.8 \times 10^{-8}$
$r_H$ , nm	78
$f/f_0$	1.8

#### 4.1.5 Concluding Remarks

The results obtained using the novel sedimentation velocity (time-derivative) – capillary viscometry approach are clearly in good agreement with the results of the more widely used methods, for example dynamic light scattering (Lin *et al.*, 1971; Dewan *et al.*, 1973 and Dewan *et al.*, 1974) and can be regarded as being good estimates for the hydrodynamic properties of casein micelles, as demonstrated by the agreement of calculated and measured values of the translational diffusion coefficient. If we continue to presume that casein micelles are spherical (*i.e.* the MHKS exponent from sedimentation,  $b = 0.666$ ) we can formulate the following MHKS relationship -  $s_{T,b} = 2.0 \times 10^{-3} M_w^{0.666}$ , which is almost identical to the MHKS equation calculated by Dewan *et al.*, (1974) -  $s_{T,b} = 1.8 \times 10^{-3} M_w^{0.665}$ .

Furthermore, the qualitative estimation of shape from the Wales-van Holde ratio (see *e.g.* Creeth and Knight, 1965; Rowe, 1977; Rowe, 1992 and Harding, 1997) requires no prior knowledge of hydration and is model independent. The parameters discussed are all average values, which will have a broad distribution, as in **Figure 4-2**.

It is therefore clear that this combined hydrodynamic approach could in the future be used to define the state of the casein micelle under a variety of physiological conditions such as pH, ionic strength and soluble solid concentration, and could be of particular use in mixed biopolymer systems. The effect of sugar (sucrose) on casein molecular weight has also been discussed recently (Schorsch *et al.*, 1999).

## 4.2 SODIUM CASEINATE

### 4.2.1 Background

The mixed milk protein, sodium caseinate is widely used in the food industry. The most common applications are water binding, gelling and thickening agents and most importantly as an emulsifier (Euston *et. al.*, 1995). Sodium caseinate can be found in coffee whiteners, cream liqueurs and whipped toppings.

Sodium caseinate is a mixture of four most common caseins -  $\alpha_{s1}$ ,  $\alpha_{s2}$ ,  $\beta$  and  $\kappa$  and are generally in the ratios of 4:1:4:1 (Srinivasan *et. al.*, 1996). Caseins are amphoteric and have well defined hydrophobic and hydrophilic regions. Individual caseins are random coils, which results in a flexible structure susceptible to proteolysis (Guo, *et. al.*, 1995), however the amphoteric nature of the molecules allows for both steric and electrostatic interactions (Euston *et. al.*, 1996). This promotes the formation of aggregates, due to entropy driven hydrophobic interactions (Fang and Dalgleish, 1996; Dickinson and Golding, 1997). This leads to the formation of the casein “sub-micelle” (Figure 4-6). As most of the calcium ions are removed in processing supermolecular casein micelles are not formed.

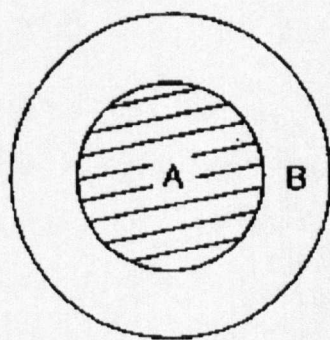


**Figure 4-6** The proposed structure of the casein “sub-micelle”. (A is the hydrophobic core and B is the  $\kappa$ -casein rich exterior). From Dickinson and Stainsby (1982).

There is growing interest in mixed biopolymer-caseinate systems coupled with a growing need for a molecular understanding of potential interaction phenomena. However, a rigorous undertaking of the behaviour of such mixed systems can be properly attempted it is important to establish the oligomeric properties of sodium

caseinate in dilute solution conditions. In this study we use a combination of capillary viscometry, sedimentation velocity and sedimentation equilibrium analytical ultracentrifugation to probe the state of self-association of caseinate at 20°C.

#### 4.2.2 Materials

Sodium caseinate was obtained from Unilever Research, Colworth House and was found to be 88% casein (Nandi, personal communication).

##### 4.2.2.1 Solutions

All samples were prepared in standard pH 6.8, I=0.1 Paley buffer (Green, 1933), of the following composition  $\text{Na}_2\text{HPO}_4 \cdot 12\text{H}_2\text{O}$  - 4.595g;  $\text{KH}_2\text{PO}_4$  - 1.561g and NaCl - 2.923g all made upto 1 litre.

#### 4.2.3 Methods

##### 4.2.3.1 Capillary Viscometry

Solutions and reference solvents were analysed using a 2ml automatic Schott-Geräte Oswald viscometer, under precise temperature control ( $25.03 \pm 0.05$ )°C. The relative,  $\eta_{\text{rel}}$  specific,  $\eta_{\text{sp}}$  and reduced,  $\eta_{\text{red}}$  viscosities were calculated from Equations 2-34, 2-35 and 2-36 respectively, and intrinsic viscosities were estimated from the Huggins and Kraemer plots (Equations 2-38 and 2-40 respectively).

##### 4.2.3.2 Sedimentation Velocity in the Analytical Ultracentrifuge

Two types of analytical ultracentrifuges were used for the determination of sedimentation velocity behaviour: a Beckman Optima XLA equipped with UV absorption optics together with the Beckman Optima XLI equipped with both UV absorption and Rayleigh interference optics. Rotor speeds of 40,000rpm and a 4mm

column length were used together with an accurately controlled temperature of 20.0°C. The weighted average partial specific volume,  $\bar{v}$  of (0.733±0.002)ml/g was calculated from the amino acid sequences of the individual caseins (Perkins, 1986).  $s_{20,w}$  values were then calculated according to the standard equation 2-10 (see e.g. Ralston, 1993; Pavlov, 1997).

#### 4.2.3.3 *Sedimentation Equilibrium in the Analytical Ultracentrifuge*

The Beckman Optima XLA and XLI ultracentrifuge were also used in the determination of the weight average molecular weight,  $M_w$ . A rotor speed of 10,000rpm and a 1mm column length were employed at 20.0°C. Equilibrium was reached after approximately 24 hours. An overspeed of 55,000rpm is required at the end of the experiment in order to give a baseline for UV absorption data. Data was analysed using the PC programs MSTAR and MSTAR1 for absorption and interference data respectively. See section 2.2.2.

### 4.2.4 **Results and Discussion**

#### 4.2.4.1 *Capillary Viscometry*

As sodium caseinate is used as a viscosifier it is not surprising that a relatively high (compared to other proteins) intrinsic viscosity (13±3)ml/g and (14±2)ml/g from the Huggins and Kraemer plots respectively (**Figure 4-7**). The positive slope of the Kraemer plot is perhaps the most interesting aspect of this investigation. This is probably due to concentration dependent self-association (Mitchell, personal communication).

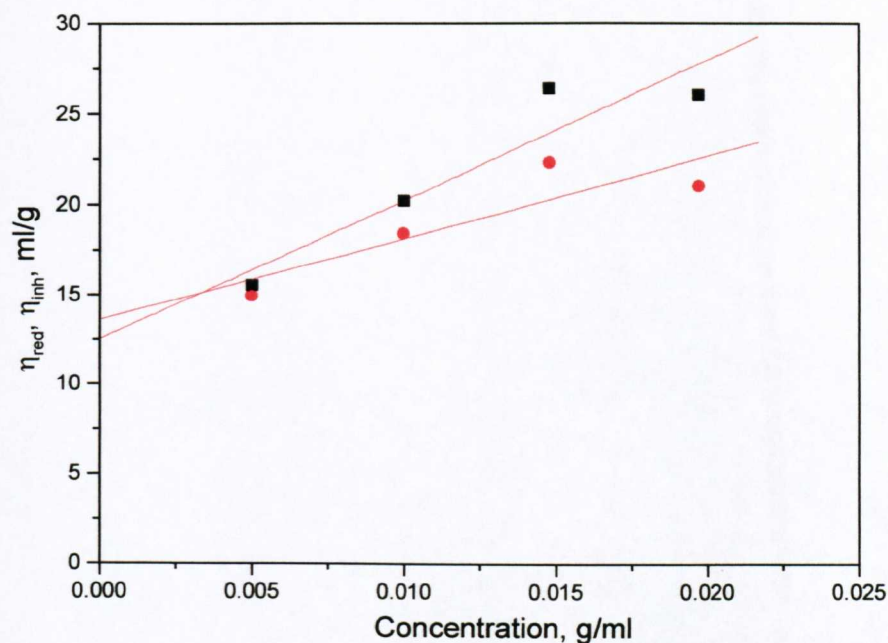


**Figure 4-7** The Huggins (squares) and Kraemer (circles) plots for sodium caseinate in standard pH 6.8,  $I=0.1\text{M}$  “Paley” buffer.

#### 4.2.4.2 Sedimentation Velocity

The sedimenting boundary was followed at 280nm (**Figure 4-8**) and apparent sedimentation coefficients were obtained at different concentrations. From the sedimentation coefficient vs. concentration plot there is clear evidence that aggregation is taking place (**Figure 4-9**). This is consistent with the findings from intrinsic viscosity measurements (see above).

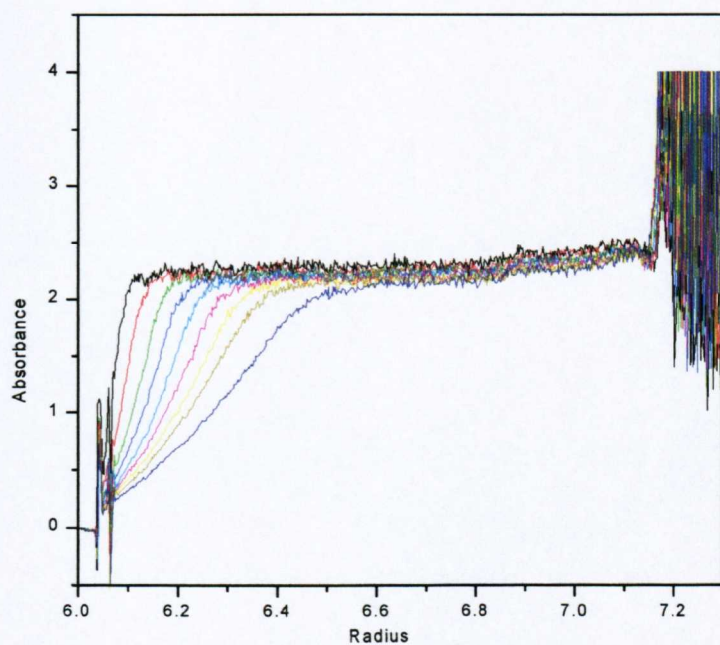


**Figure 4-8** Sedimentation velocity diagram for sodium caseinate at 40,000rpm, 20.0°C at 280nm, boundary concentration, initial  $c = 3.5\text{mg/ml}$ , scanned every 5 minutes in standard pH 6.8,  $I=0.1\text{M}$  "Paley" buffer.

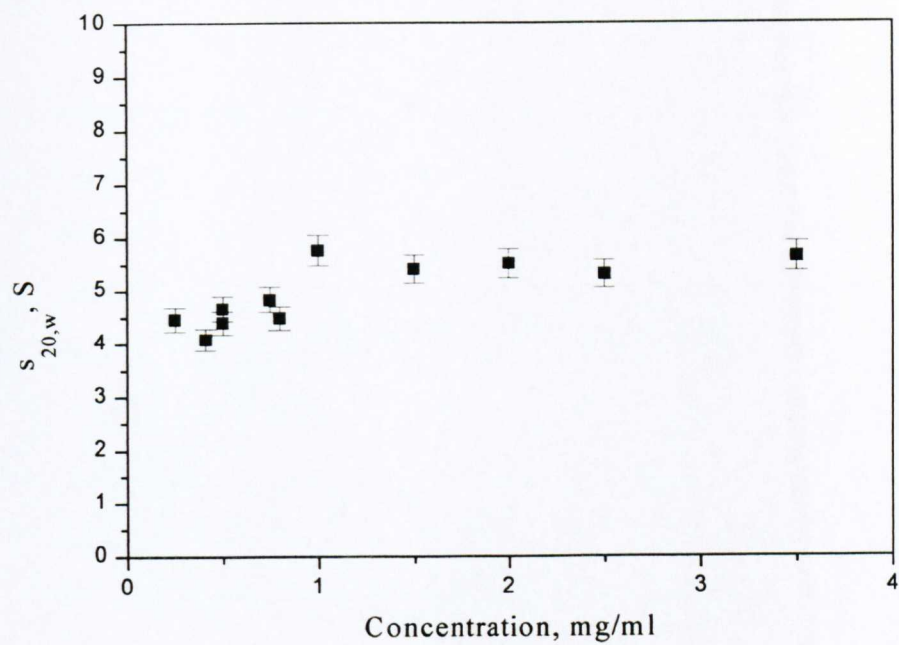


**Figure 4-9**  $s_{20,w}$  vs. concentration for sodium caseinate in standard pH 6.8,  $I=0.1M$  "Paley" buffer.

## 4.2.4.3 Sedimentation Equilibrium

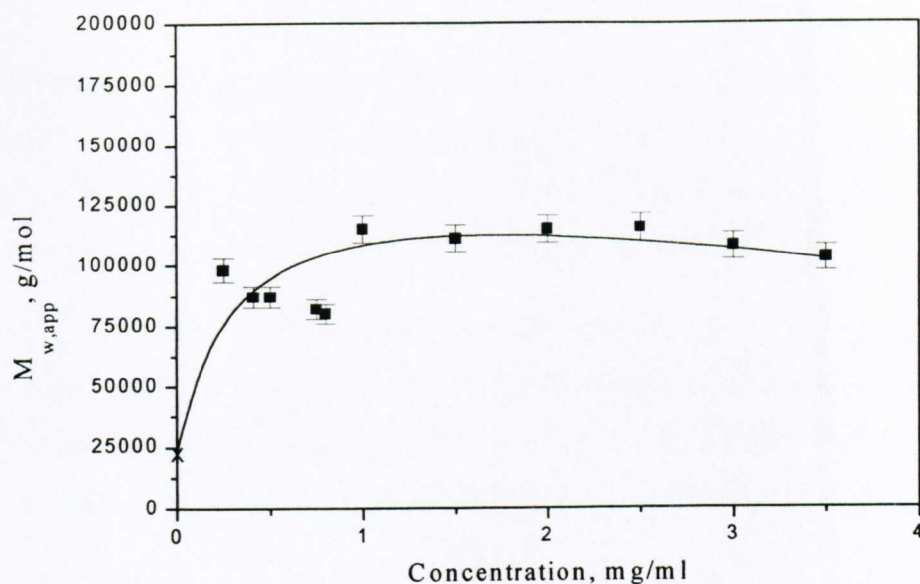


**Figure 4-10**  $M_{w,app}$  vs. concentration for sodium caseinate. Where “X” marks the “monomer” molecular weight in standard pH 6.8, I=0.1M “Paley” buffer. Line fitted manually.

The sedimentation equilibrium data also suggests aggregation (**Figure 4-10**). [Note – no monomer was indicated on the sedimentation coefficient vs. concentration plot as I did not try to fit monomer – n-mer models to sedimentation velocity data]. From this data it is also possible to calculate the hydrodynamic shape of the caseinate species, by calculating frictional ratios or plotting a pseudo Mark-Houwink relationship. The frictional ratios were calculated using the following equation 2-13. A frictional ratio of  $\sim 1.5$  indicates an approximately spherical species at all concentrations and suggests that there are no conformational changes upon aggregation. Having calculated an average ( $f/f_0$ ) of  $\sim 1.5$  (**Table 4-5**) we then calculated the Perrin function, P (from Equation 2-14) in order to determine the axial ratio of prolate ellipsoid of revolution. As the hydration of sodium caseinate is difficult to estimate we considered the two extreme conditions (i) where hydration value,  $\delta = 0.35\text{g/g}$  which is a typical protein value and (ii)  $P = 1$ , which is equivalent to a perfect sphere (Cölfen *et. al.*, 1997).

(i) assuming  $\delta = 0.35\text{g/g}$  then  $P = 1.32$ , which corresponds to a prolate ellipsoid of axial ratio 6:1 (Harding and Cölfen, 1995).

(ii) when  $P = 1$ , we can then calculate  $\delta = 1.7\text{g/g}$ .

As sodium caseinate is commercially available as a water binding agent it appears plausible that a relatively large hydration value (1.7) is possible, this value is somewhat smaller than the value of 3.4 obtained for the intact micelle, but is however a great deal higher than the typical globular protein value of 0.35.

The MHKS plot was calculated according to equation 2-15 and the value for the exponent,  $b$  was estimated to be 0.63, clearly indicating a spherical conformation (for spheres, rods and coils  $b = 0.667$ , 0.15 and 0.4-0.5 respectively see **Table 2-2** and see also Jumel, 1994 and Tombs and Harding, 1998). (**Figure 4-11**)

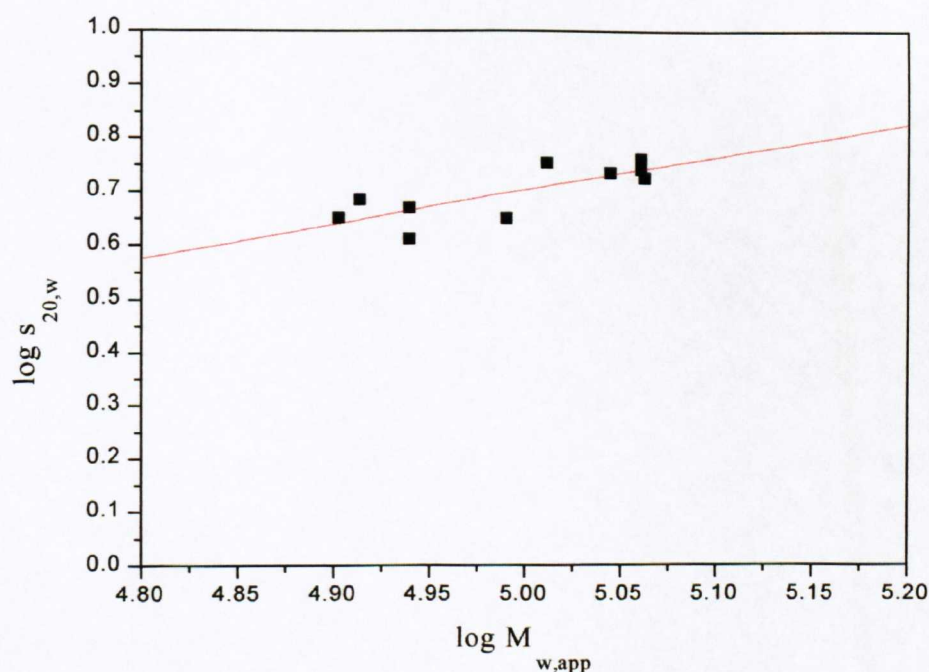


**Figure 4-11** MHKS sedimentation plot for sodium caseinate in standard pH 6.8,  $I=0.1\text{M}$  "Paley" buffer. The line fitted corresponds to  $s=0.0035M^{0.63}$ .

Therefore, it is reasonable to presume that

- (i) the sodium caseinate aggregates are spherical independent of their size.
- (ii) sodium caseinate aggregate is very hydrated.

In an attempt to quantify the oligomeric species present, and if possible any association constants for aggregation, subsidiary plots were calculated for monomer-tetramer ( $n=4$ ), monomer-pentamer ( $n=5$ ), monomer-hexamer ( $n=6$ ) and trimer-hexamer ( $n=2$ ) systems (Nichol *et al.*, 1972). Since all values of  $n$  gave poor correlation with the data, it is clear that several oligomers must co-exist in dynamic equilibrium. It is also likely that thermodynamic non-ideality and the hydration properties of caseinate aggregates may affect the validity of this procedure (Winzor, personal communication).

#### 4.2.5 Concluding Remarks

Casein aggregates at all concentrations appear to be approximately spherical, as frictional ratios at all concentrations are  $\sim 1.5$ . This implies that there are no conformational changes upon further aggregation.

In this section we can see the problems, which can arise due to the opposing effects of aggregation and concentration dependency (Figure 4-9 and Figure 4-10) and unfortunately in this case we were unable to fit a suitable model to the molecular weight data. It is likely that this is due the presence of multiple components (perhaps  $n = 1-12$ ) and this is further complicated by the thermodynamic non-ideality (the 2<sup>nd</sup> virial coefficient,  $B$ ) in molecular mass measurements. If more information were available about sodium caseinate structure, *e.g.* triaxial shape from X-Ray measurements, one could estimate the contribution of thermodynamic non-ideality using the Fortran program COVOL (Harding *et al.*, 1999) and the modelling of molecular mass data may then be simplified.

**Table 4-5** Hydrodynamic parameters for sodium caseinate in standard pH 6.8, I=0.1M “Paley” buffer

Concentration mg/ml	$s_{20,w}$ S	$M_{w,app}$ g/mol	$(f/f_0)_{app}$
3.50	5.65±0.10	103000±15000	1.4±0.2
3.00	-	108000±15000	-
2.50	5.31±0.10	116000±10000	1.6±0.2
2.00	5.51±0.10	115000±28000	1.5±0.3
1.50	5.41±0.05	111000±31000	1.5±0.3
1.00	5.76±0.05	115000±30000	1.5±0.3
0.80	4.48±0.05	-	-
0.75	4.83±0.10	82000±15000	1.4±0.2
0.50	4.66±0.10	87000±15000	1.5±0.2
0.50	4.39±0.10	-	1.6±0.2
0.41	4.08±0.20	87000±15000	1.7±0.3
0.25	4.45±0.20	98000±21000	1.7±0.3

[Note - the large errors in molecular masses are due to sample heterogeneity, sedimentation coefficient errors are larger at low concentration due to the increased difficulty in determining the boundary second moment].

## 4.3 INDIVIDUAL CASEINS

### 4.3.1 $\beta$ -casein

#### 4.3.1.1 *Background*

$\beta$ -casein is the 2<sup>nd</sup> most abundant casein at approximately 35% of the total casein content in bovine milk. As with the other caseins  $\alpha$  and  $\kappa$  it has a strong tendency to self-associate. In the case of  $\beta$ -casein self-association is concentration, temperature and ionic strength dependant (Sullivan *et. al.*, 1955; Payens and van Markwijk, 1963; Payens *et. al.*, 1969; Buchheim and Schmitt, 1979 and Arima *et. al.*, 1979). Most studies have been undertaken at lower temperatures *e.g.* 8.5 and 13.5°C (Payens and van Markwijk, 1963) in order to determine the monomer molecular weight and sedimentation coefficient (24,000g/mol and 1.6S respectively). Although significant aggregation takes place at 20°C (Hoagland, 1966; Payens *et. al.*, 1969; Arima *et. al.*, 1979) there is still a large amount of monomer present, especially at low concentration.

A typical sedimentation velocity experiment shows two distinct peaks (**Figure 4-12**) – one for the monomer and the other for a larger polymer. The sedimentation coefficient for the “fast” moving species has been reported to have a strong concentration dependency (Payens and van Markwijk, 1963, Payens *et. al.*, 1969 and Thompson, 1971) at the concentrations required (~ 2-3mg/ml) for the Schlieren optical system.

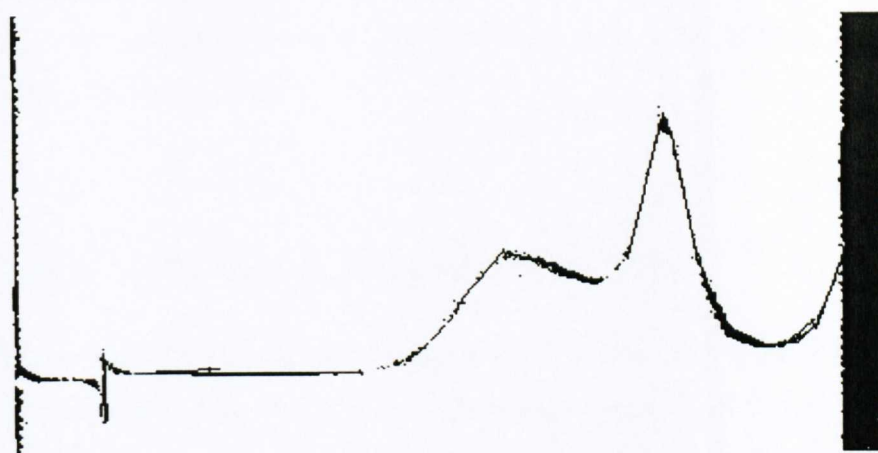


**Figure 4-12** Typical sedimenting boundary for  $\beta$ -casein at 8.5°C in barbiturate buffer pH 7.5,  $I = 0.2M$  (adapted from Payens and van Markwijk, 1963).

However modern applications of the analytical ultracentrifuge for example the new Beckman XLI and sedimentation time derivative analyses ( $dc/dt$ ) (Stafford, 1992a,b and Laue and Stafford, 1999) allow determinations of sedimentation coefficient and heterogeneity at lower concentrations. This therefore allows the estimation of the relative amounts of each component from the areas under the  $g^*(s^*)$  (or  $dc/dt$ ) curves.

#### 4.3.1.2 Methods

##### Sedimentation Velocity in the Analytical Ultracentrifuge

The Beckman Optima XLI equipped with both UV absorption and Rayleigh interference optics. Rotor speeds of 50,000rpm and a 4mm column length were used together with an accurately controlled temperature of 20.0°C. The partial specific volume,  $\bar{v}$  of (0.741±0.002)ml/g was calculated from the amino acid sequence of  $\beta$ -casein (Perkins, 1986). As all sedimentation coefficients are apparent due to non-ideality and will decrease with increasing concentration (assuming no self-association) and hence an extrapolation to zero concentration is required (Gralén, 1944; Creeth and Pain, 1967; van Holde, 1985; Ralston, 1993; Harding, 1994; Jumel, 1994; Pavlov, 1997; and Morris *et. al.*, 2000) (Equation 2-8). The Gralén (1944) parameter,  $k_s$  is a measure of concentration dependence. As sedimentation coefficients are also temperature and solvent sensitive, it is the convention that all sedimentation coefficient values are quoted at the standard conditions of 20°C and

water,  $s_{20,w}$  were calculated according to the standard equation (see *e.g.* Ralston, 1993; Pavlov, 1997) Equation (2-10).

### Sedimentation Equilibrium in the Analytical Ultracentrifuge

The Beckman Optima XLI ultracentrifuge was also used in the determination of the weight average molecular weight,  $M_w$ . A rotor speed of 10,000rpm and a 1mm column length were employed at 20.0°C in multi-channel cells (as described in Yphantis, 1964). Equilibrium was reached after approximately 24 hours. An overspeed of 55,000rpm is required at the end of the experiment in order to give a baseline for UV absorption data. As the meniscus region was significantly reduced in solute the low-speed equilibrium algorithm MSTARI was not appropriate and the data was therefore analysed using the Beckman (Beckman Inc., Palo Alto, CA) PC program “Origin Equilibrium” (Microcal Software Inc., Northampton, MA, USA).

#### 4.3.1.3 Results and Discussion

### Sedimentation Velocity in the Analytical Ultracentrifuge

Sedimenting boundaries show 2 species. The “slow” component has a sedimentation coefficient of 1.6S, which is typical of a  $\beta$ -casein monomer; the larger species (~12.0S) is a significantly larger polymer (Figure 4-13). This is typical of previous studies on  $\beta$ -casein (Sullivan *et. al.*, 1955; Payens and van Markwijk, 1963; Hoagland, 1966; Thompson, 1971 and Arima *et. al.*, 1979). The relative amount of the aggregate (%) decreased with decreasing concentration (Table 4-6), which is in agreement with results of Payens and van Markwijk (1963); this is further quantified by a decrease in the weight average sedimentation coefficient (Figure 4-14). At such low concentrations, the concentration dependency of the “fast” species (Payens and van Markwijk, 1963) was not apparent; however at 0.5mg/ml there is a slight decrease possibly indicating a slightly lower molecular weight.

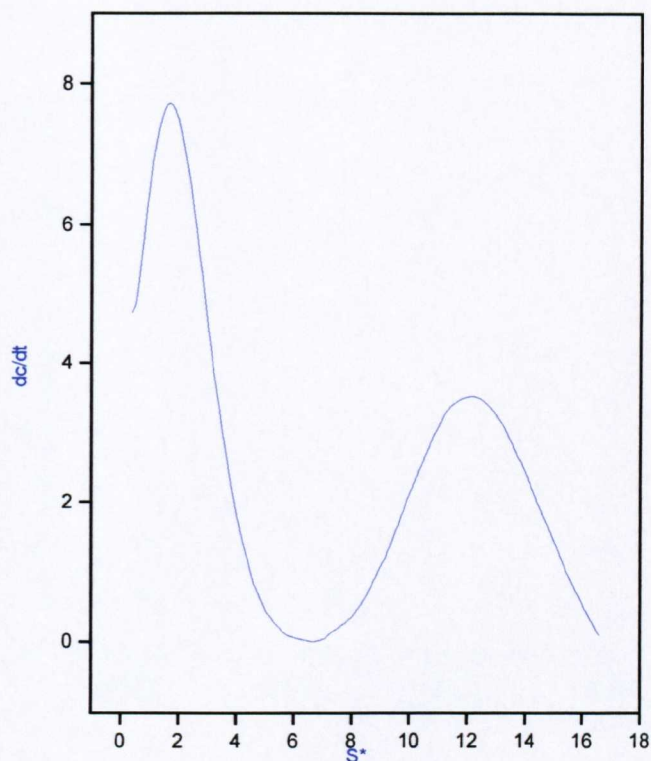


**Figure 4-13** Sedimentation coefficient distribution for  $\beta$ -casein at concentration 2mg/ml in standard "Paley" buffer at 20°C.

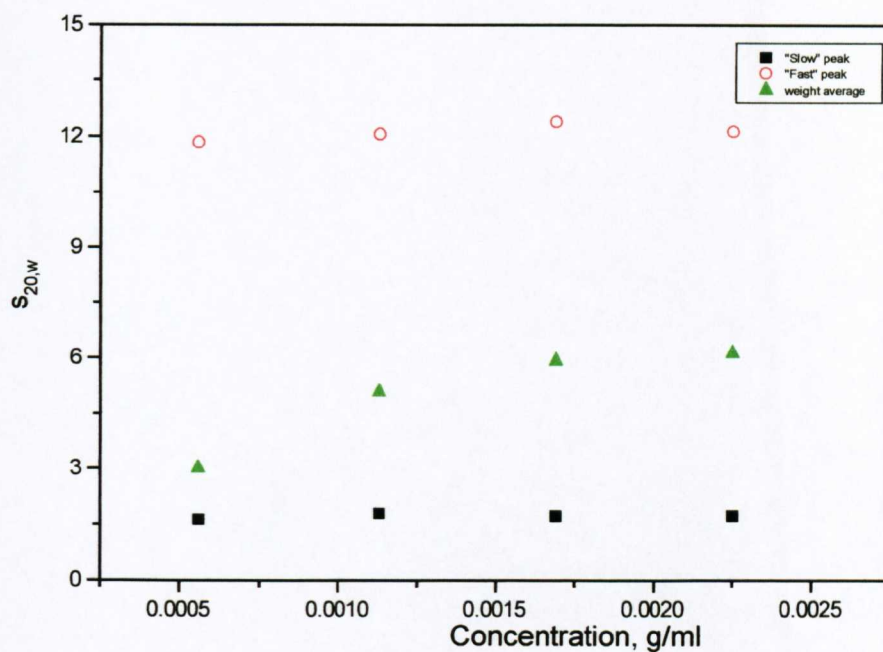


**Figure 4-14** Change in sedimentation coefficient with concentration for  $\beta$ -casein in standard “Paley” buffer at 20°C. Legend – black squares (slow peak); red circles (fast peak) and green triangles (weight average).

#### Sedimentation Equilibrium in the Analytical Ultracentrifuge

Sedimentation equilibrium allowed the estimation of weight average molecular weights,  $M_w$ . The weight average molecular weight shows a similar increase with increasing concentration (**Figure 4-15**) (**Table 4-6**).

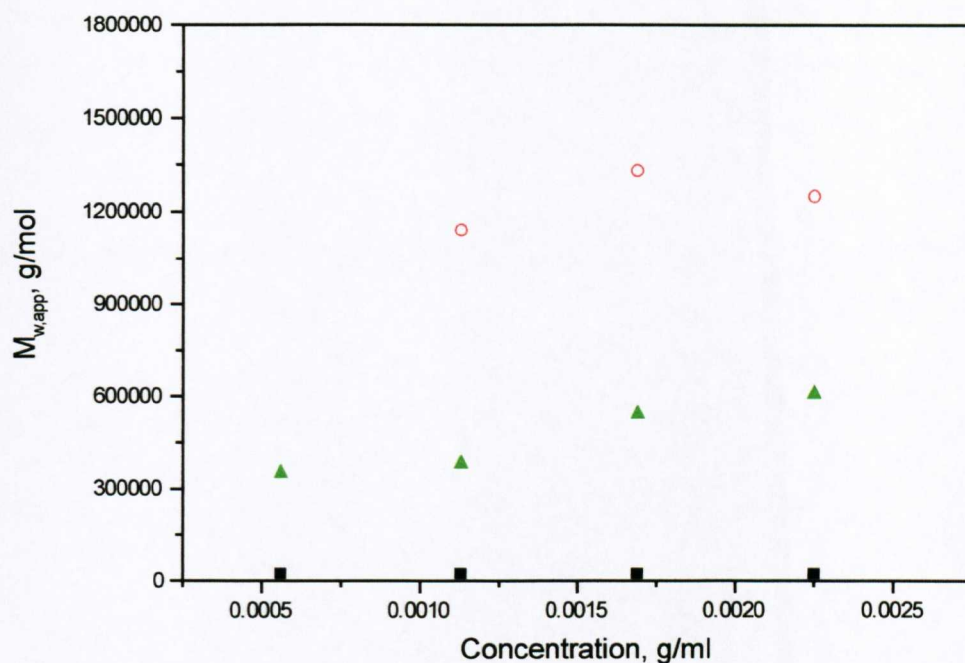


**Figure 4-15** Change in molecular weight with concentration for  $\beta$ -casein in standard “Paley” buffer at 20°C. Legend – black squares (monomer), red circles (polymer) and green triangles (weight average).

It is therefore possible to calculate the molecular weight of the “fast” sedimenting species (assuming the relative amounts of monomer and polymer are the same in sedimentation velocity and sedimentation equilibrium experiments and the monomer mass is 24,100g/mol) and hence the degree of polymerisation.

$$M_w(\text{polymer}) = \frac{[M_w(\text{average}) - (\text{fraction monomer} \times M_w \text{ monomer})]}{\text{fraction polymer}}$$

where  $M_w$  (average) is the weight average molecular weight of all species as measured by sedimentation equilibrium. The polymer molecular weight was estimated at all concentrations and at 1.1, 1.7 and 2.2mg/ml this resulted in reasonable agreement  $(1.25 \pm 0.1) \times 10^6$  g/mol, this is representative of a polymer of degree of

polymerisation, DP of 52. Under similar conditions Payens *et. al.*, 1969; Buchheim and Schmitt, 1979 and Arima *et. al.*, 1979 calculated degrees of polymerisation of 41-50, 38 and 49 respectively. The estimated polymer molecular weight at 0.6mg/ml was significantly different and was therefore not included in the calculations above.

**Table 4-6** Hydrodynamic properties for  $\beta$ -casein in pH 6.8, I=0.1M phosphate buffer at 20°C

Concentration, g/ml	%monomer <sup>1</sup>	$s_w$ , S	$M_w$ , g/mol	average DP <sup>2</sup>
0.0006	86.2	3.00±0.02	350000±100000	15±4
0.0011	68.2	5.06±0.02	380000±150000	16±6
0.0017	60.4	5.92±0.03	540000±80000	22±3
0.0022	57.5	6.12±0.05	610000±25000	25±1

<sup>1</sup>from the area under the  $dc/dt$  curves

<sup>2</sup>assuming monomer molecular weight of 24,100 g/mol

From the table above there is no simple relationship between weight average sedimentation coefficient and weight average molecular weight. This feature is most likely to do with experimental error (there is an approximately a 35% error on weight average molecular weights at the 2 lower concentrations, but less than 15% at the higher concentrations). Minor inconsistencies aside one can see that the general trend is followed for each of the 4 parameters. As concentration increases the relative amount of monomer decreases and hence weight average sedimentation coefficients, molecular weights and degrees of polymerisation increase.

#### 4.3.1.4 Concluding Remarks

Having calculated the molecular weight and sedimentation coefficient it is therefore possible to estimate the translational frictional ratio (Tanford, 1961) (Equation 2-13) for the monomer and polymer (assuming a monomer  $M_w$  of 24,100g/mol and a polymer  $M_w$  of 1,250,000g/mol and sedimentation coefficients of 1.6S and 12.0S respectively). The translational frictional ratio gives a hydration dependent indication of macromolecular conformation (Harding, 1997). Monomer and polymer frictional ratios were calculated to be 1.8 and 3.2 respectively; the monomer  $f/f_0$  is in agreement with previous results (Sullivan *et. al.*, 1955 and Jenness, 1971) and is indicative of a random coil. The polymer is therefore either more extended and/or more hydrated than the monomer, which is consistent with the findings of Payens and van Markwijk, 1963 and Payens *et. al.*, 1969 who claim that  $\beta$ -casein forms “rod-like polymers that are intertwined firmly”. One can also estimate the diffusion coefficient by rearrangement of the Svedberg equation (2-12). This results in diffusion coefficients (not corrected for concentration effects) at 20°C of  $6.2 \times 10^{-7}$  and  $9.2 \times 10^{-8}$  cm<sup>2</sup>/sec for monomers and polymers respectively. The monomer diffusion coefficient is similar to the value of  $6.05 \times 10^{-7}$  cm<sup>2</sup>/sec quoted by Thompson, 1971.

It is clear that when addressing a complex associating system such as  $\beta$ -casein one can never answer all the questions. However it is reasonable to assume that at least some questions have been answered concerning the dilute solution properties of  $\beta$ -casein in pH 6.8, I=0.1M phosphate buffer at 20°C. Clearly this agrees with the results of previous workers (Payens and van Markwijk, 1963 and Payens *et. al.*, 1969) concerning the increase in weight average molecular weight (and weight average sedimentation coefficient) with increasing concentration, although the polymer size does not change a great deal over the concentration range studied. This study is a good example of how modern developments in analytical ultracentrifugation (the XLI and sedimentation time derivative) are able to deal with complex self-associating systems even at low concentrations. This shows that sedimentation velocity can separate multi-component mixtures without the need for separation media such as columns or membranes, which can disrupt the monomer – n-mer equilibria and can enable the quantitative estimation of component concentration within a mixture.

## 4.3.2 $\kappa$ -casein

### 4.3.2.1 Background

Kappa-casein is the least abundant of the three major caseins ( $\alpha_s$ ,  $\beta$  and  $\kappa$ ) and is present at about 10-15% in bovine milk (Srinivasan *et. al.*, 1996). Although  $\kappa$ -casein (and other caseins) can not be crystallised, molecular models based on amino-acid sequence have been proposed (Kumosinski *et. al.*, 1991a,b) (**Figure 4-16**) this structure has been described as the “horse and rider”, the most recent model provides good correlation with  $\kappa$ -casein functional properties.

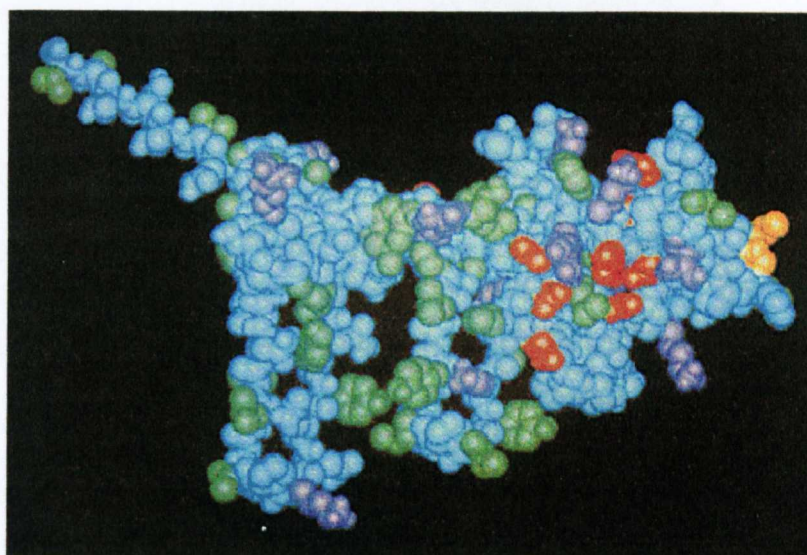


**Figure 4-16** A space filling model of  $\kappa$ -casein. The peptide backbone is coloured cyan, hydrophobic side chains green, acidic side chains red, basic side chains purple and the Phe-Met (105-106) bond in orange (adapted from Kumosinski *et. al.*, 1991a).

The most interesting property is that  $\kappa$ -casein is calcium insensitive (Waugh and von Hippel, 1956) and is therefore suspected to play an important role in micellar stabilisation (Waugh and von Hippel, 1956; Sullivan *et. al.*, 1959; Swaisgood and Brunner, 1962; Thompson and Pepper, 1962; Pepper and Thompson, 1963; Swaisgood and Brunner, 1963; Zittle and Walter, 1963; Swaisgood *et. al.*, 1964; MacKinlay and Wake, 1964; MacKinlay and Wake, 1965; Rose, 1965; Rose and Colvin, 1966a,b; Payens, 1966; MacKinlay *et. al.*, 1966; Thompson *et. al.*, 1967; Waugh *et. al.*, 1970; Farrell Jr., 1973; Dewan *et. al.*, 1974; Carroll and Farrell Jr., 1983; Kumosinski *et. al.*, 1991a; Groves *et. al.*, 1998; Farrell Jr. *et. al.*, 1998 and Lehner *et. al.*, 1999). Evidence that  $\kappa$ -casein is involved in micelle stabilisation is due

to the fact that it is insensitive calcium precipitation in the concentrations normally found in milk (Zittle and Walter, 1963).  $\kappa$ -casein is also the milk component most sensitive to the action of the enzyme chymosin (referred to as rennin in many publications) (MacKinlay and Wake, 1965; MacKinlay *et. al.*, 1966; MacKenzie, 1971; MacKinlay and Wake, 1971; Kumosinski *et. al.*, 1991a; Farrell Jr. *et. al.*, 1998 and Lehner *et. al.*, 1999). Chymosin cleaves the  $\kappa$ -casein molecule at the Phe-Met bond (105-106) and releases the “hairy tail” – casein macropeptide (CMP) and leaving the insoluble para- $\kappa$ -casein (Kumosinski *et. al.*, 1991a; Farrell Jr. *et. al.*, 1998 and Lehner *et. al.*, 1999) this destroys the micelle stabilising ability and results in micelle coagulation. Heat induced coagulation of micelles is due to the interaction of  $\kappa$ -casein with  $\beta$ -lactoglobulin at high temperatures (Zittle *et. al.*, 1962). Various authors have also suggested that the degree of phosphorylation, disulphide bonding and glycosylation of  $\kappa$ -casein also play minor roles in micellular stabilisation. (Thompson and Pepper, 1962; Zittle and Walter, 1963; Pepper and Thompson, 1963; MacKinlay and Wake, 1964; MacKinlay and Wake, 1965; Hoagland, 1966; Farrell Jr., 1973; Kumosinski *et. al.*, 1991a and Farrell Jr. *et. al.*, 1998)

The mechanism of stabilisation is still somewhat vague the classical model suggested by Waugh (Waugh *et. al.*, 1970 and Waugh, 1971) concentrates the  $\kappa$ -casein on the outside of the micelle, the core consisting of a hydrophobic  $\alpha_s$ - $\beta$  complex. Carroll and Farrell Jr. (1983) brought this theory into doubt; they suggest that there may be two different types of micelles

- (i)  $\kappa$ -casein at the periphery
- (ii)  $\kappa$ -casein uniformly distributed throughout micelle.

They further claim that micelles with uniformly distributed  $\kappa$ -casein are smaller than those with  $\kappa$ -casein concentrated on the micellular surface. This may be related to then findings of Sullivan *et. al.*, 1959; Rose, 1965; Rose and Colvin, 1966b and McGann and Pyne, 1970, who all claim that increased  $\kappa$ -casein contents decrease micelle size.

$\kappa$ -casein is known to self-associate and has been characterised in many solvents including phosphate (various concentrations/ pHs), 5M Guanidine Hydrochloride; 7M

Urea, Acetic Acid (33, 66%), NaCl (Swaisgood and Brunner, 1962; Thompson and Pepper, 1962; Zittle and Walter, 1963; Pepper and Thompson, 1963; Swaisgood and Brunner, 1963; Swaisgood *et. al.*, 1964; MacKinlay and Wake, 1964 and Farrell Jr. *et. al.*, 1998). However most authors have been concerned with calculating the molecular weight of monomeric species. The consensus molecular weight and sedimentation coefficient are 23,000g/mol and 1.4S respectively, which are in agreement with the amino-acid composition (Kumosinski *et. al.*, 1991a). Under the conditions similar to those of milk (approximately pH 7 and ionic strength 0.1M) sedimentation coefficients of ~13.5S (Pedersen, 1936; Swaisgood and Brunner, 1962; Thompson and Pepper, 1962; Zittle and Walter, 1963; Pepper and Thompson, 1963; Swaisgood and Brunner, 1963; Swaisgood *et. al.*, 1964; MacKinlay and Wake, 1964) [Note Pedersen, 1936, – the current naming convention for caseins was not in use and therefore the species characterised was not designated  $\kappa$ -casein]. Molecular weight determinations have been somewhat less frequent, Swaisgood *et. al.*, 1964, suggest that a molecular weight of 650,000g/mol for the 13.5S species and Farrell Jr. *et. al.*, 1998 suggests (650,000-1,200,000)g/mol at 25°C and (895,000-2,000,000)g/mol at 37°C, the differences in calculated molecular weights dependent on the analysis program used. This does however show the temperature dependency of aggregation and is also the difficulties in sedimentation equilibrium analyses. It can therefore be estimated (very roughly) that  $\kappa$ -casein molecular weight is between 600,000 and 900,000g/mol at 20°C in phosphate buffer.

Although the associated state of  $\kappa$ -casein in isolation bears little or no resemblance to the state of  $\kappa$ -casein in native casein micelles it is of interest to determine hydrodynamic parameters such as sedimentation coefficient and molecular weight in order to formulate a model for casein-polysaccharide interactions, as the positively charged region on the  $\kappa$ -casein molecule represents the most likely interaction site (Dickinson, 1998). Similar studies on  $\kappa$ -casein- $\alpha_s$ -casein interactions in a simple “model micelle” system (Pepper and Thompson, 1963 and Tessier *et. al.*, 1963) have utilised sedimentation velocity experiments to monitor changes in molecular size. Zittle *et. al.* (1962) used the same principle to follow the interaction of  $\kappa$ -casein and  $\beta$ -lactoglobulin upon heating.

Recent modern developments in analytical ultracentrifugation *i.e.* the advent of the Beckman Optima XLI (Beckman Inc., Palo Alto, CA, USA) and sedimentation time derivative method for sedimentation velocity (Stafford, 1992a,b and Laue and Stafford, 1999) have opened new avenues for research in this field. Therefore sedimentation experiments both velocity and equilibrium have been carried out on purified  $\kappa$ -casein (Sigma, Loughborough, UK) in pH 6.8, I = 0.1M phosphate chloride buffer (Green, 1933) using the Beckman XLI.

#### 4.3.2.2 *Methods*

##### *Sedimentation Velocity in the Analytical Ultracentrifuge*

The Beckman Optima XLI equipped with both UV absorption and Rayleigh interference optics. Rotor speeds of 50,000rpm and a 4mm column length were used together with an accurately controlled temperature of 20.0°C. The partial specific volume,  $\bar{v}$  of (0.739±0.002)ml/g was calculated from the amino acid sequence of  $\kappa$ -caseins (Perkins, 1986). As all sedimentation coefficients are apparent due to non-ideality and will decrease with increasing concentration (assuming no self-association) and hence an extrapolation to zero concentration is required (Gralén, 1944; Creeth and Pain, 1967; van Holde, 1985; Ralston, 1993; Harding, 1994; Jumel, 1994; Pavlov, 1997; and Morris *et. al.*, 2000) (Equation 2-8). The Gralén (1944) parameter,  $k_s$  is a measure of concentration dependence. As sedimentation coefficients are also temperature and solvent sensitive, it is the convention that all sedimentation coefficient values are quoted at the standard conditions of 20°C and water,  $s_{20,w}$  were calculated according to the standard equation (see *e.g.* Ralston, 1993; Pavlov, 1997) Equation (2-10). Values of  $s_{20,w}^0$  and  $k_s$  can be used in the determination of molecular weights (Rowe, 1977) (Equation 2-11). [Note – weight average sedimentation coefficients will yield z-average molecular weights (Rowe – personal communication)].

Sedimentation Equilibrium in the Analytical Ultracentrifuge

The Beckman Optima XLI ultracentrifuge was also used in the determination of the weight average molecular weight,  $M_w$ . A rotor speed of 10,000rpm and a 1mm column length were employed at 20.0°C in multi-channel cells (as described in Yphantis, 1964). Equilibrium was reached after approximately 24 hours. An overspeed of 55,000rpm is required at the end of the experiment in order to give a baseline for UV absorption data. As the meniscus region was free of solute the low-speed equilibrium algorithm MSTAR was not appropriate and the data was therefore analysed using the Beckman (Beckman Inc. Palo Alto, CA) PC program Origin Equilibrium (Microcal Software Inc., Northampton, MA, USA).

4.3.2.3 *Results and Discussion*Sedimentation Velocity in the Analytical Ultracentrifuge

Velocity experiments indicated one sedimenting boundary (**Figure 4-17**– inset); subsequent DCDT analysis resulted in a single peak with a weight average sedimentation coefficient of  $\sim 13.0S$  (**Figure 4-17**) over the entire concentration range ( $s_{20,w}^0 = 13.8S$ ;  $k_s = 16\text{ml/g}$ ) (**Figure 4-18**). Weight average sedimentation coefficients were calculated rather than fitting a series of Gaussian peaks, as Gaussian fitting requires prior knowledge of the types of species present *e.g.* monomers, dimers *etc.* This information was not available and it is also important not to bias any results by making unnecessary assumptions. The value of  $s_{20,w}^0$  (**Table 4-7**) indicates that under the conditions studied  $\kappa$ -casein is in a considerably associated state (monomer  $s_{20,w}^0 \sim 1.4S$  - Swaisgood and Brunner, 1962) is in good agreement with the results of previous work in similar solvents (Swaisgood and Brunner, 1962; Thompson and Pepper, 1962; Zittle and Walter, 1963; Pepper and Thompson, 1963; Swaisgood and Brunner, 1963; Swaisgood *et. al.*, 1964 and MacKinlay and Wake, 1964). This then enables the calculation of  $M_z$  from Equation 2-11, if one knows  $v_s$  (Rowe, 1977),  $v_s$  was estimated using Equation 2-80 (Rowe, 1977 and Rowe, 1992) using the  $K_\eta$  (Equation 2-39) calculated by Swaisgood *et. al.*, 1964. This results in a z-average molecular weight of  $\sim 770,000\text{g/mol}$ , which is consistent with the range of

weight average molecular weights quoted by Swaisgood *et. al.*, 1964, and Farrell Jr. *et. al.*, 1998.

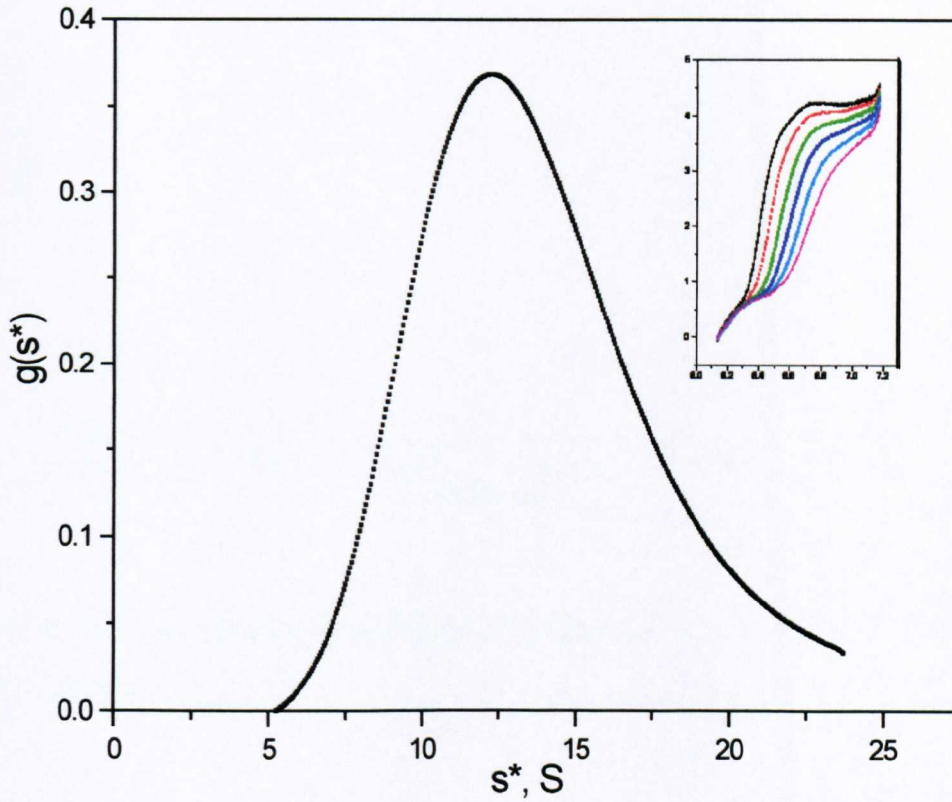


**Figure 4-17** Sedimentation coefficient distribution for  $\kappa$ -casein at 2mg/ml – a typical sedimenting boundary inset in standard “Paley” buffer at 20°C. Sedimenting boundary recorded every 2 minutes at 50,000 rpm.

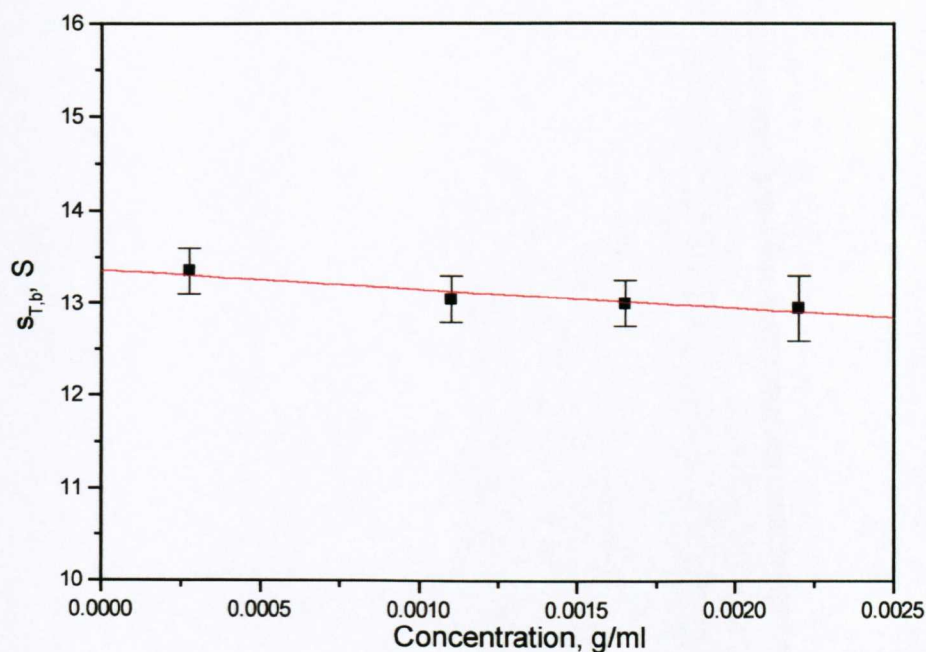


**Figure 4-18** Concentration dependence of sedimentation of  $\kappa$ -casein in standard “Paley” buffer at 20°C.

#### Sedimentation Equilibrium in the Analytical Ultracentrifuge

There is a great deal of variation in molecular weight (**Table 4-7**) with concentration and it is not clear whether this is experimental variation or an inherent property of  $\kappa$ -casein, which may explain the large discrepancies in the molecular weight determinations of Farrell Jr. and co-workers, 1998. However it was possible to estimate the molecular weight at infinite dilution (**Figure 4-19**) to account for thermodynamic non-ideality (see *e.g.* Ralston, 1993) (Equation 2-24). A weight average molecular weight of  $\sim 750,000$ g/mol is in general agreement with the value from sedimentation velocity. Again the values are in reasonable agreement with values of Swaisgood *et. al.*, 1964, and Farrell Jr. *et. al.*, 1998.

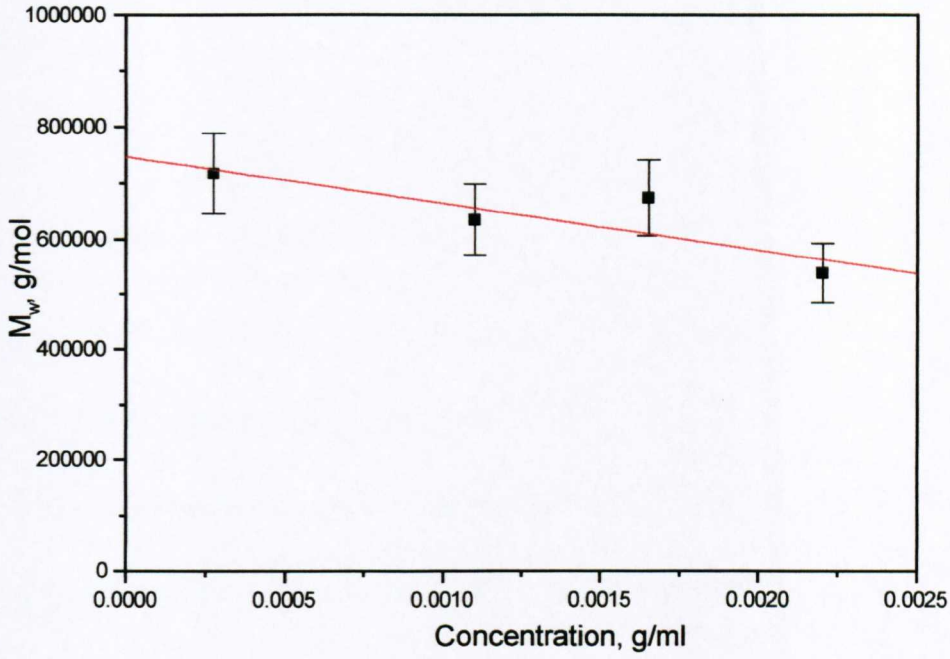


**Figure 4-19** Concentration dependence of molecular weight of  $\kappa$ -casein in standard “Paley” buffer at 20°C.

**Table 4-7** Hydrodynamic properties of  $\kappa$ -casein in pH 6.8, I = 0.1M phosphate buffer at 20°C

$S_{20,w}^0$ <sup>1</sup>	$k_s$ <sup>2</sup>	$M_z$ <sup>3</sup>	$M_w$ <sup>4</sup>	$[\eta]$ <sup>5</sup>	$k_\eta$ <sup>5</sup>	$D_{20,w}^0$ <sup>6</sup>	$f/f_0$ <sup>7</sup>
13.8±0.1	16±4	7.7±0.4	7.5±0.6	9.5	18.3	1.7	2.1±0.2

<sup>1</sup>sedimentation coefficient at infinite dilution in Svedberg units

<sup>2</sup>concentration dependency of sedimentation, ml/g

<sup>3</sup> $10^{-5}$  x z-average molecular weight calculated from 2-80 and 2-11, g/mol

<sup>4</sup> $10^{-5}$  x weight-average molecular weight from Origin Equilibrium, g/mol

<sup>5</sup>intrinsic viscosity and regression coefficient,  $k_\eta$  at 25°C in 0.1M NaCl from Swaisgood *et. al.*, 1964 both in ml/g (no errors quoted)

<sup>6</sup>translational diffusion coefficient at infinite dilution calculated from rearrangement of equation 2-12, F ( $1F = 10^7$  cm<sup>2</sup>/sec)

<sup>7</sup>translational frictional ratio from equation 2-13

#### 4.3.2.4 Concluding Remarks

$\kappa$ -casein has been characterised in phosphate buffer (Green, 1933) and sedimentation coefficients are in good agreement with those calculated previously. The concentration dependency of sedimentation,  $k_s$  allowed the estimation of  $v_s$  and hence the z-average molecular weight from the equation of Rowe (1977, 1992). The z-average molecular weight from sedimentation velocity is at the very least in general agreement with the weight average molecular weight from sedimentation equilibrium, this is important as for non-ideal systems it is essential to obtain complementary evidence from one (or more) independent, absolute techniques. Results for molecular weight also fall well within the limits of the consensus values from various investigations.

Having calculated the molecular weight and sedimentation it is therefore possible to estimate the translational frictional ratio (**Table 4-7**) (Tanford, 1961) (Equation 2-13), which gives a hydration dependent indication of macromolecular conformation (Harding, 1997). One can also estimate the diffusion coefficient by rearrangement of the Svedberg equation (2-12). Results would suggest that  $\kappa$ -casein is a moderately extended molecule compared to globular proteins. This is consistent with a relatively high value for the intrinsic viscosity,  $[\eta]$ , calculated by Swaisgood *et. al.*, (1964) and in agreement with the conclusions of Payens, (1966). This result is not however too surprising considering the high proline content of all the caseins (Farrell Jr., 1973 and Kumosinski *et. al.*, 1991a,b). Proline is a well known as a structure-breaker in polypeptides and therefore favours more open or extended structures. A similar feature has been seen in mucins (Harding, 1989).

## 4.4 $\beta$ -LACTOGLOBULIN

### 4.4.1 Background

Whey proteins are soluble below pH 4.6 (the pH at which caseins are precipitated) and contribute approximately 20% of bovine milk protein. They are a diverse group of proteins consisting of  $\beta$ -lactoglobulin,  $\alpha$ -lactalbumin, blood serum proteins and immunoglobulins (Jennes, 1970; Advani, 1994; Saril, 2000) (**Table 4-1**).  $\beta$ -lactoglobulin is the major whey protein in bovine milk (Jennes, 1970; Dickinson and Stainsby, 1982) and is present at about 4.8g/l on average, however there is no  $\beta$ -lactoglobulin in human milk.

Bovine  $\beta$ -lactoglobulin is known to have 4 genetic variants A, B, C and D (Saril, 2000) and variant B is the most common in western cattle (Advani, 1994). Bovine  $\beta$ -lactoglobulin genetic variant B consists of 162 amino acid residues and has a molecular weight based on amino acid composition of 18,300 g/mol (Advani, 1994; Fox and McSweeney, 1998 and Saril, 2000). One important structural note is that  $\beta$ -lactoglobulin B contains 5 cysteine residues, 4 of which are involved in disulphide bonds. This results in a compact globular protein of diameter 3.6nm (Saril, 2000)

Bovine  $\beta$ -lactoglobulin exists under the normal conditions of milk (pH 6.8, I~0.1M) as a dimer (**Figure 4-20**) (MacKenzie, 1971, Advani, 1994 and Saril, 2000), however it is known that concentration, pH and temperature have a significant affect on the oligomeric state.

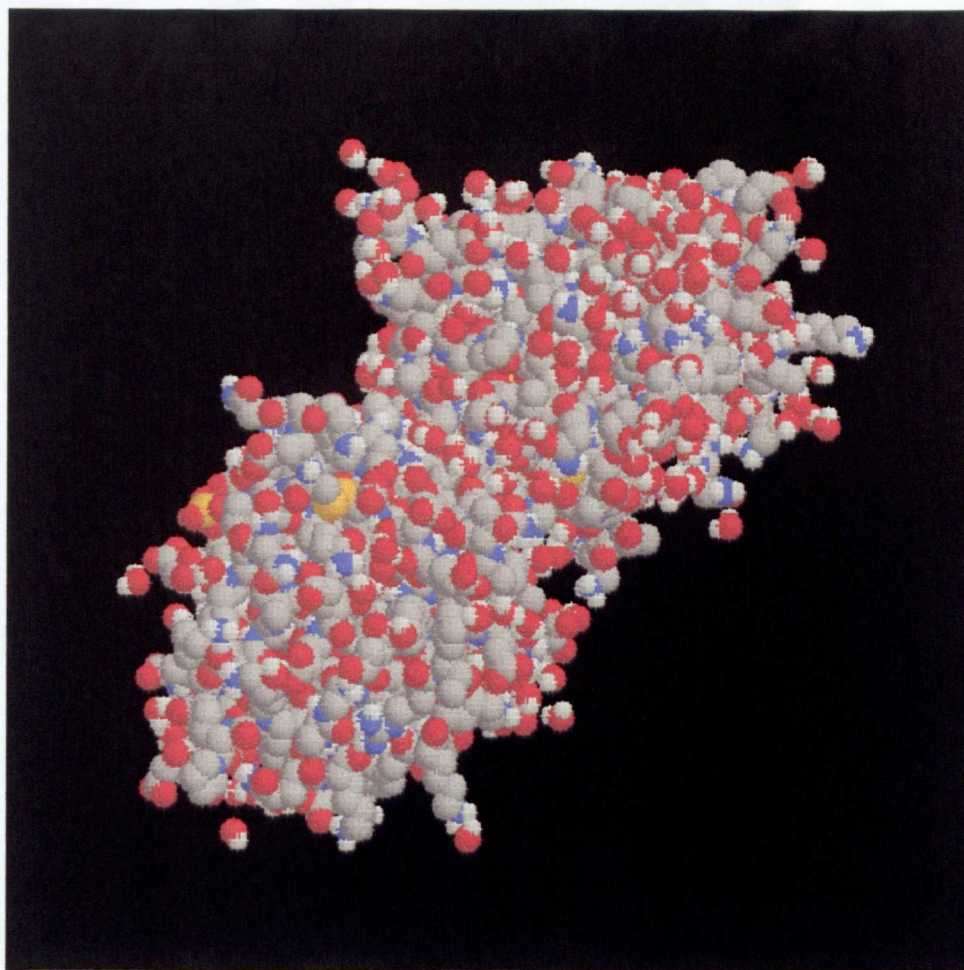


**Figure 4-20** A space filling model of a  $\beta$ -lactoglobulin dimer. Where carbon is grey, hydrogen – white, oxygen – red, nitrogen – blue and sulphur – yellow.

Of most interest in this study is the effect of temperature on the oligomeric state and conformation of  $\beta$ -lactoglobulin at low concentration, and conditions similar to those found in milk. It has been reported that heat denaturation of  $\beta$ -lactoglobulin lactoglobulin is a two-step process (Gough and Jennes, 1962; Advani, 1994 and Saril, 2000)

- (i) loss of globular structure
- (ii) aggregation to octamers ( $M_w \sim 146,000\text{g/mol}$ )

Walstra and Jennes, 1984 claim that (i) is reversible at neutral pH below  $70^\circ\text{C}$ .  $\beta$ -lactoglobulin also reacts with  $\kappa$ -casein at increased temperatures (Zittle *et. al.*, 1962 Advani, 1994 and Saril, 2000), which reduces the ability of  $\kappa$ -casein to stabilise calcium sensitive caseins to calcium induced precipitation (Zittle *et. al.*, 1962).

Therefore an investigation into effect of increased temperature on  $\beta$ -lactoglobulin is of importance when considering the possible changes to milk protein structure during heat treatment. As far as we are aware this will also be the first study on the heat denaturation of  $\beta$ -lactoglobulin in which sedimentation experiments will be performed at high temperatures ( $>40^{\circ}\text{C}$ ).

#### 4.4.2 Materials

Bovine  $\beta$ -lactoglobulin A and B (Sigma Chemicals, Loughborough, UK). A concentration of 10mg/ml was prepared and allowed to rehydrate for 3-4 hours in pH 6.8, ionic strength 0.1M, standard phosphate/ chloride buffer (Green, 1933), of the following composition  $\text{Na}_2\text{HPO}_4 \cdot 12\text{H}_2\text{O}$  - 4.595g;  $\text{KH}_2\text{PO}_4$  - 1.561g and  $\text{NaCl}$  - 2.923g all made up to 1litre.

#### 4.4.3 Methods

##### 4.4.3.1 *Capillary Viscometry*

Solutions and reference solvents were analysed using a 2ml Ostwald viscometer (Schott-Geräte, Mainz, Germany) under precise temperature control ( $\pm 0.01$ ).

##### 4.4.3.2 *Sedimentation Velocity in the Analytical Ultracentrifuge at High Temperature*

The high temperature unit for the Beckman Model E analytical ultracentrifuge allows centrifugation at temperatures up to  $125^{\circ}\text{C}$ , however for aqueous solutions temperatures  $> 80^{\circ}\text{C}$  are impractical. Both the rotor and sample cells are pre-heated to the required temperature prior to sample injection. Samples were run at 52640rpm and Schlieren images were captured semi-automatically onto photographic film.  $s_{T,b}$  values were calculated from Schlieren images using a graphics digitising tablet.  $s_{20,w}$  values were then calculated from  $s_{T,b}$  values (sedimentation coefficients at

temperature, T and in buffer, b) using the standard equation 2-10 [see for example, Ralston, 1993; Pavlov, 1997]. A partial specific volume (for the macromolecular component),  $\bar{v}$  of  $(0.752 \pm 0.002)$  ml/g was calculated from the amino acid composition of genetic variant B (Perkins, 1986) and assumed to be constant with temperature.

#### 4.4.3.3 SEC-MALLS

The eluent was the standard pH 6.8 I=0.1 buffer and the injection volume was 100 $\mu$ l. The pectin refractive increment (dn/dc) of 0.189 ml/g was taken from Theisen *et. al.*, 2000 and assumed to be independent of temperature.

### 4.4.4 Results and Discussion

#### 4.4.4.1 Capillary Viscometry

Capillary viscometry results (Table 4-8) (Figure 4-21) are consistent with the findings that  $\beta$ -lactoglobulin denaturation is reversible below 70°C (Walstra and Jennes, 1984) and that at least one step involves a loss of globular structure (Gough and Jennes, 1962; Advani, 1994 and Saril, 2000). A reduced viscosity of ~4.0 ml/g at 10mg/ml is quite typical for globular proteins and is quite similar to that estimated by Advani (1994) at the same concentration.

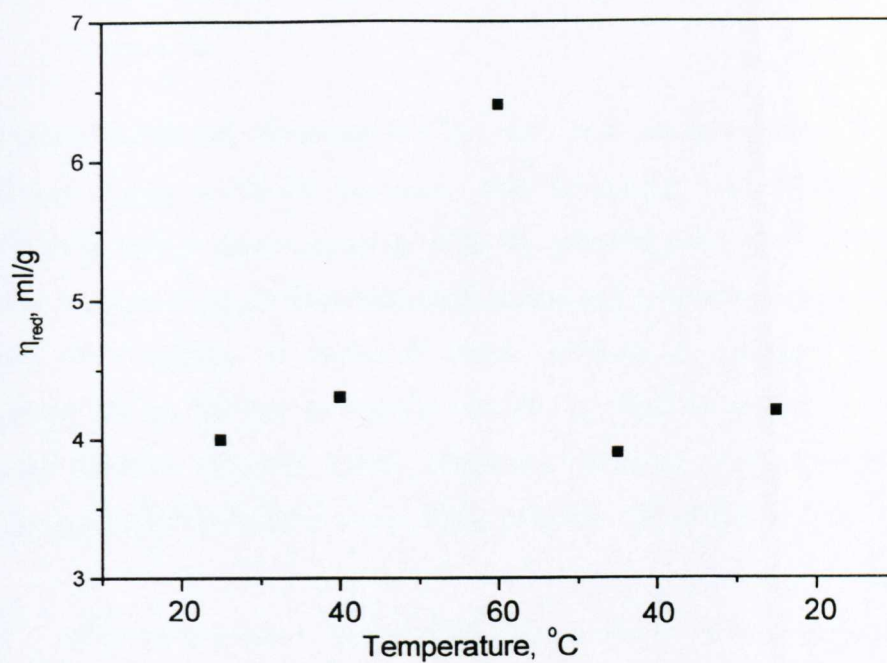


**Figure 4-21** Effect of temperature on reduced viscosity of  $\beta$ -lactoglobulin in pH 6.8, I = 0.1M phosphate/ chloride buffer.

#### 4.4.4.2 Sedimentation Velocity in the Analytical Ultracentrifuge at High Temperature

Sedimentation velocity experiments show one sedimenting species, the sedimentation coefficient ( $s_{20,w}$ ) of which decreases with increasing temperature (**Figure 4-22**) (**Table 4-8**), this is again consistent with the unfolding of a globular structure. It is possible that the changes observed using viscometry and sedimentation velocity could be due to a change in molecular mass, however a decrease in sedimentation coefficient and an increase in reduced viscosity are both indicative of a more open or extended structure (Tanford, 1961). However, before any concrete conclusions can be drawn over conformation it is necessary to calculate the molecular weight.

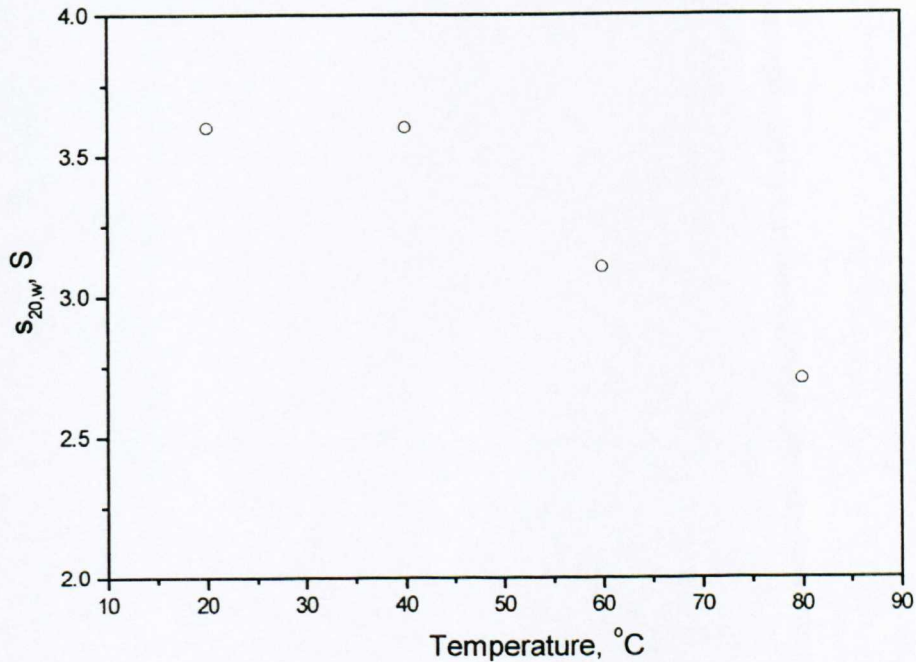


**Figure 4-22** Effect of increased temperature on corrected sedimentation coefficient of  $\beta$ -lactoglobulin in pH 6.8, I = 0.1M phosphate/ chloride buffer.

## 4.4.4.3 SEC-MALLS

The weight average molecular weight is consistent with that of a dimer and it is clear from both **Table 4-8** and **Figure 4-23** that there is not a significant change in molecular weight with increased temperature, as with sedimentation velocity experiments SEC only elutes one component, which would indicate that even at 80°C there are no aggregates formed under the conditions of pH and concentration studied.

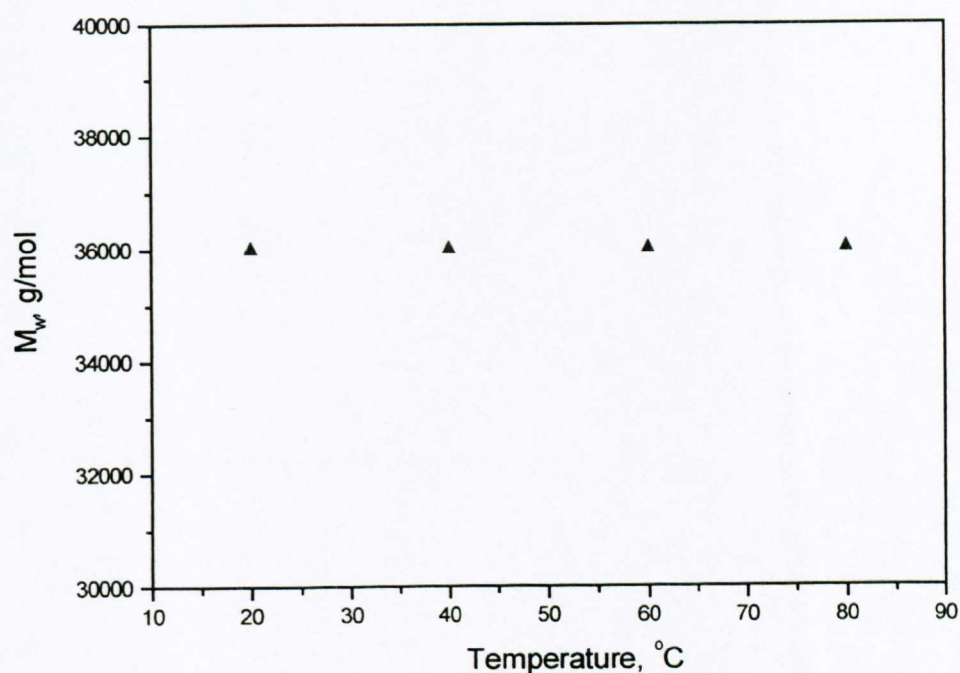


**Figure 4-23** Effect of increased temperature on the weight average molecular weight of  $\beta$ -lactoglobulin in pH 6.8, I = 0.1M phosphate/ chloride buffer.

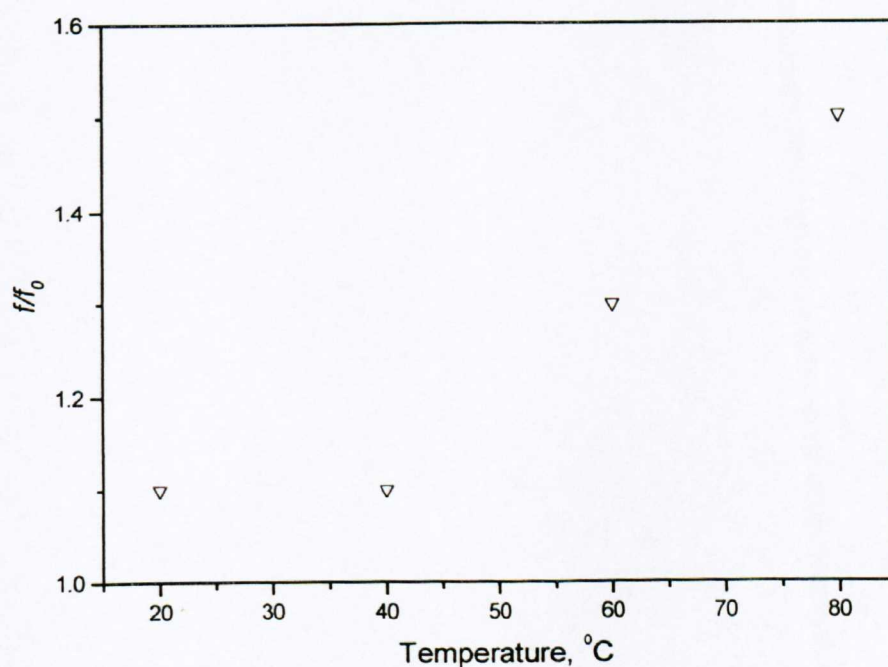
Knowledge of both molecular weight and sedimentation coefficient allows the calculation of the translational frictional ratio,  $f/f_0$  (Equation 2-13) (Tanford, 1961). The clear increase above 40°C (**Figure 4-24**) is a further indication of a more extended structure with a greater axial ratio,  $a/b$ .

**Table 4-8** Effect of elevated temperature on hydrodynamic properties of  $\beta$ -lactoglobulin in pH 6.8, I = 0.1M phosphate/ chloride buffer

Temperature, °C	$M_w$ , g/mol <sup>1</sup>	$s_{20,w}$ , S	$\eta_{red}$ , ml/g <sup>2</sup>	$f/f_0$
20	36000±3000	3.6±0.1	4.0±0.2	1.0±0.1
40	36000±3000	3.6±0.1	4.3±0.2	1.0±0.1
60	36000±3000	3.1±0.1	6.4±0.3	1.2±0.1
80	36000±3000	2.7±0.1	-	1.3±0.1

<sup>1</sup>weight average molecular weight to the nearest 1,000g/mol

<sup>2</sup>viscosity was calculated at 25°C not 20°C

**Figure 4-24** Effect of increased temperature on the translational frictional ratio of  $\beta$ -lactoglobulin in pH 6.8, I = 0.1M phosphate/ chloride buffer.

#### 4.4.5 Concluding Remarks

The thermoreversible denaturation of  $\beta$ -lactoglobulin (at least upto 60°C) is almost definitely the first step in the two-step denaturation process suggested by Gough and Jennes (1962), however unlike previous studies I have measured the sedimentation coefficients at high temperatures. The unimodality of the sedimentation peak and elution profiles even at 80°C would indicate that aggregation does not take place under the conditions studied. These results therefore imply that under the conditions similar to those in milk  $\beta$ -lactoglobulin will undergo a conformation change, but not aggregate at temperatures of less than 80°C. These results appear to be similar to those of Gough and Jennes (1962) who report that under neutral conditions  $\beta$ -lactoglobulin undergoes reversible denaturation upto 70°C, prior to an irreversible aggregation step, perhaps due to the low concentration studied we do not see the subsequent aggregation even at 80°C. This is in contrast to the findings of (Jennes and Gough, 1962); I can only speculate that this is either due to low concentration of  $\beta$ -lactoglobulin or solvent effects.

#### 4.5 REFERENCES

- Advani M (1994) Solution Studies on  $\beta$ -lactoglobulin (Genetic Variant B). University of Nottingham. BSc.
- Arima S, Niki R and Takase K (1979) Structure of  $\beta$ -Casein. *Journal of Dairy Research*, **46**, 281-282.
- Buchheim W and Schmitt DG (1979) On the Monomers and Polymers of  $\beta$ -Casein. *Journal of Dairy Research*, **46**, 277-280.
- Carroll RJ and Farrell Jr HM (1983) Immunological Approach to Location of  $\kappa$ -Casein in the Casein Micelles by Electron Microscopy. *Journal of Dairy Science*, **66**, 679-686.
- Cölfen H, Harding SE, Wilson EK, Scrutton NS and Winzor DJ (1997) Low Temperature Solution Behaviour of *Methylophilus Methylophilus* Electron Transferring Flavoprotein : A Study by Analytical Ultracentrifugation. *European Biophysics Journal*, **25**, 411-416.
- Creeth JM and Pain RH (1967) The Determination of Molecular Weights of Biological Macromolecules by Ultracentrifuge Methods. *Progress in Biophysics and Molecular Biology*, **17**, 217-287.
- Dewan RK, Bloomfield VA, Chudgar A and Morr CV (1973) Viscosity and Voluminosity of Bovine Milk Casein Micelles. *Journal of Dairy Science*, **56**, 699-705.
- Dewan RK, Chudgar A, Mead R, Bloomfield VA and Morr CV (1974) Molecular Weight and Size Distribution of Bovine Milk Casein Micelles. *Biochimica et Biophysica Acta*, **342**, 313-321.

- Dickinson E and Stainsby G (1982) *Colloids in Food*, Chapter 8. Applied Science Publishers, London.
- Dickinson E. and Golding M (1997) Depletion Flocculation of Emulsion Containing Unadsorbed Sodium Caseinate. *Food Hydrocolloids*, **11**, 13-18.
- Einstein A (1911) Correction to My Paper: "A New Determination of Molecular Dimensions" Berichtigung zu meiner Arbeit: "Eine neue Bestimmung der Molekuldimensionen". *Annalen der Physik*, **34**, 591-593.
- Euston SE, Singh H, Munro PA and Dalgleish DG (1995) Adsorption Between Sodium Caseinate and Water Soluble Surfactants in Oil-Water Emulsions. *Journal of Food Science*, **60**, 1124-1131.
- Euston SE, Singh H, Munro PA and Dalgleish DG (1996) Oil in water Emulsions Stabilized by Sodium Caseinate or whey Protein Isolate as Influenced by Glycerol Monostearate. *Journal of Food Science*, **61**, 916-920.
- Fang Y and Dalgleish DG (1996) Competitive Adsorption Between Dioleoylphosphatidylcholine and Sodium Caseinate on Oil-Water Interfaces. *Journal of Agriculture and Food Chemistry*, **44**, 59-64.
- Farrell Jr HM (1973) Models for Casein Micelle Formation. *Journal of Dairy Science*, **56**, 1195-1206.
- Farrell Jr HM, Wickham ED and Groves ML (1998) Environmental Influences on Purified  $\kappa$ -Casein: Disulfide Interactions. *Journal of Dairy Science*, **81**, 2974-2984.
- Fox PF and McSweeney PLH (1998) *Dairy Chemistry and Biochemistry*. pp 188-192. Prentice Hall, New Jersey.

- Gralén N (1944) Sedimentation and Diffusion Measurements on Cellulose and Cellulose Derivatives. PhD Dissertation, University of Uppsala, Sweden.
- Green AA (1933) The Preparation of Acetate and Phosphate Buffer Solutions of Known PH and Ionic Strength. *Journal of the American Chemical Society*, **55**, 2331-2336.
- Groves ML, Wickham ED and Farrell Jr HM (1998) Environmental Effects on Disulfide Bonding Patterns of Bovine  $\kappa$ -Casein. *Protein Chemistry*, **17**, 73-84. (Abstract)
- Guo MR Fow PF, Flynn A and Kindstedt PS (1995) Susceptibility of  $\beta$ -lactoglobulin and Sodium Caseinate to Proteolysis by Pepsin and Trypsin. *Journal of Dairy Science*, **78**, 2336-2344.
- Gough P and Jennes R (1962) Heat Denaturation of  $\beta$ -lactoglobulin A and B *Journal of Dairy Science*, **45**, 1033-1039.
- Harding SE (1989) The Macrostructure of Mucus Glycoprotein in Solution. *Advances in Carbohydrate Chemistry and Biochemistry*, **47**, 345-381.
- Harding SE (1994) Shapes and Sizes of Food Polysaccharides by Sedimentation Analysis - Recent Developments. In: Phillips GO, Williams PA and Wedlock DJ (Eds.) *Gums and Stabilisers for the Food Industry* 7, pp. 55-68. IRL Press, Oxford.
- Harding SE (1997) The Intrinsic Viscosity of Biological Macromolecules. Progress in Measurement, Interpretation and Application to Structure in Dilute Solution. *Progress in Biophysics and Molecular Biology*, **68**, 207-262.
- Harding SE and Cölfen H (1995) Inversion Formulae for Ellipsoid of Revolution Macromolecular Shape Functions. *Analytical Biochemistry*, **228**, 131-142.

- Harding SE, Horton JC, Jones S and Winzor DJ (1999) COVOL: An Interactive Program for Evaluating Second Virial Coefficients from the Triaxial Shape or Dimensions of Rigid Macromolecules. *Biophysical Journal*, **76**, 2432-2438.
- Hoagland PD (1966) Acylated  $\beta$ -Caseins: Electrostatic Interactions and Aggregation. *Journal of Dairy Science*, **49**, 783-787.
- Huggins ML (1942) The Viscosity of Dilute Solutions of Long-chain Molecules. IV. Dependence on Concentration. *Journal of the American Chemical Society*, **64**, 2716-2718.
- Jennes R (1970) Protein Composition of Milk. In: MacKenzie HA (Ed.) *Milk Proteins: Chemistry and Molecular Biology Vol I*, pp. 17-44. Academic Press, New York.
- Jumel K (1994) Molecular Size of Interacting and Degrading Polysaccharides. Ph.D. Thesis, University of Nottingham.
- Jumel K, Browne P and Kennedy JF (1992) In: Harding SE, Sattelle DB, Bloomfield VA Editors). *Laser Light Scattering in Biochemistry*. Royal Society of Chemistry, Cambridge, Chapter 2.
- Kumosinski TF, Brown EM and Farrell Jr HM (1991a) Three Dimensional Modeling of Bovine Caseins:  $\kappa$ -Casein. *Journal of Dairy Science*, **74**, 2879-2887.
- Kumosinski TF, Brown EM and Farrell Jr HM (1991b) Three Dimensional Modeling of Bovine Caseins:  $\alpha_{s1}$ -Casein. *Journal of Dairy Science*, **74**, 2889-2895.
- Langendorff V, Cuvelier G, Launay, B, Michon, C, Parker, A and de Kruif CG (1999) Casein Micelle/ Iota Carrageenan Interactions in Milk: Influence of Temperature. *Food Hydrocolloids*, **13**, 211-218.

- Laue TM and Stafford III WF (1999) Modern Applications of Analytical Ultracentrifugation. *Annual Reviews in Biophysics and Biomolecular Structure*, **28**, 75-100.
- Lehner D, Worning P, Fritz G, Ogendal L, Bauer R and Glatter O (1999) Characterisation of Enzymatically Induced Aggregation of Casein Micelles in Natural Concentration by *in Situ* Static Light Scattering and Ultra Low Shear Viscometry. *Journal of Colloid and Interface Science*, **213**, 445-456.
- Lin SHC, Dewan RK, Bloomfield VA and Morr CV (1971) Inelastic Light Scattering Study of the Size Distribution of Bovine Milk Casein Micelles. *Biochemistry*, **10**, 4788-4793.
- MacKenzie HA (1971) Whole Casein: Isolation, Properties and Zone Electrophoresis. In: MacKenzie HA (Ed.) *Milk Proteins: Chemistry and Molecular Biology Vol II*, pp. 87-116. Academic Press, New York.
- Mackinlay AG, Hill RJ and Wake RG (1966) The Action of Rennin on  $\kappa$ -casein The Heterogeneity and Origin of the Insoluble Products. *Biochimica et Biophysica Acta*, **115**, 103-112.
- Mackinlay AG and Wake RG (1964) The Heterogeneity of  $\kappa$ -Casein. *Biochimica et Biophysica Acta*, **93**, 378-386.
- Mackinlay AG and Wake RG (1965) Fractionation of S-Carboxymethyl- $\kappa$ -Casein and Characterization of the Components. *Biochimica et Biophysica Acta*, **104**, 167-180.
- Mackinlay AG and Wake RG (1971)  $\kappa$ -Casein and its Attack by Rennin (Chymosin). In: MacKenzie HA (Ed.) *Milk Proteins: Chemistry and Molecular Biology Vol II*, pp. 175-216. Academic Press, New York.

- McGann TCA and Pyne GT (1970) The Colloidal Phosphate of Milk III. Nature of its Association with Casein. *Journal of Dairy Research*, **27**, 403-417.
- Morris GA, Foster TJ and Harding SE (2000) The Effect of Degree of Esterification on the Hydrodynamic Properties of Citrus Pectin. *Food Hydrocolloids*, **14**, 227-235.
- Nichol LW, Jackson WJH and Winzor DJ (1972) Preferential Binding of Competitive Inhibitors to the Monomeric Form of  $\alpha$ -Chymotrypsin. *Biochemistry*, **11**, 585-591.
- Pavlov GM (1997) The Concentration Dependence of Sedimentation for Polysaccharides. *European Biophysics Journal*, **25**, 385-398.
- Payens TAJ (1966) Association of Caseins and their Possible Relation to Structure of the Casein Micelle. *Journal of Dairy Science*, **49**, 1317-1324.
- Payens TAJ, Brinkhuis JA and van Markwijk BW (1969) Self-Association in Non-Ideal Systems. Combined Light Scattering and Sedimentation Measurements in  $\beta$ -Casein Solutions. *Biochimica et Biophysica Acta*, **175**, 434-437.
- Payens TAJ and van Markwijk BW (1963) Some Features of the Association of  $\beta$ -Casein. *Biochimica et Biophysica Acta*, **71**, 517-530.
- Pedersen KO (1936) CXXXVIII. Ultracentrifugal and Electrophoretic Studies on Milk Proteins. I. Introduction and Preliminary Results with Fractions from Skim Milk. *Biochemical Journal*, **30**, 948-960.
- Pepper L and Thompson MP (1963) Dephosphorylation of  $\alpha_s$ - and  $\kappa$ -Caseins and its Effect on Micelle Stability in the  $\kappa$ - $\alpha_s$ -Casein System. *Journal of Dairy Science*, **46**, 764-767.

- Perkins SJ (1986) Protein Volumes and Hydration Effects – The Calculation of Partial Specific Volumes, Neutron-Scattering Matchpoints and 280nm Absorption-Coefficients for Proteins and Glycoproteins from amino Acid Sequences. *European Journal of Biochemistry*, **157**, 169-180.
- Ralston G (1993) *Introduction to Analytical Ultracentrifugation*. Beckman Instruments Inc., California.
- Rose D (1965) Protein Stability Problems. *Journal of Dairy Science*, **48**, 139-146.
- Rose D and Colvin JR (1966a) Appearance and Size of Micelles from Bovine Milk. *Journal of Dairy Science*, **49**, 1091-1097.
- Rose D and Colvin JR (1966b) Internal Structure of Casein Micelles from Bovine Milk. *Journal of Dairy Science*, **49**, 351-355.
- Rowe AJ (1977) Concentration-Dependence of Transport Processes – General Description Applicable to Sedimentation, Translational Diffusion, and Viscosity Coefficients of Macromolecular Solutes. *Biopolymers*, **16**, 2595-2611.
- Rowe AJ (1992) The Concentration Dependence of Sedimentation. In: Harding, SE, Rowe AJ and Horton JC (Eds.) *Analytical Ultracentrifugation in Biochemistry and Polymer Science*, pp. 394-407. Royal Society of Chemistry, Cambridge.
- Saril PM (2000) Molecular Weight and Sedimentation Characteristics of Milk Proteins. University of Nottingham. BSc.
- Schorsch C, Clark AH, Jones MG and Norton IT (1999) Behaviour of Milk Protein/ Polysaccharide Systems in High Sucrose. *Colloids and Surfaces B: Biointerfaces*, **12**, 317-329.

Schorsch C, Jones MG and Norton IT (1999) Thermodynamic Incompatibility and Microstructure of Milk Protein/ Locust Bean Gum/ Sucrose Systems. *Food Hydrocolloids*, **13**, 89-99.

Srinivasan M, Singh H and Munro PA (1996) Sodium Caseinate Stabilized Emulsions : Factors Affecting Coverage and Composition of Surface Proteins. *Journal of Agriculture and Food Chemistry*, **44**, 3807-3811.

Stafford III WF (1992a) Boundary Analysis in Sedimentation Transport Experiments: A Procedure for Obtaining Sedimentation Coefficient Distributions Using the Time Derivative of the Concentration Profile. *Analytical Biochemistry*, **203**, 295-301.

Stafford III WF (1992b) Methods for Obtaining Sedimentation Coefficient Distributions. In: Harding SE, Rowe AJ and Horton JC (Eds.) *Analytical Ultracentrifugation in Biochemistry and Polymer Science*, pp. 359-393. Royal Society of Chemistry, Cambridge.

Sullivan RA, Fitzpatrick MM and Stanton EK (1959) Distribution of Kappa-Casein in Skim Milk. *Nature*, **183**, 616-617.

Swaigood HE and Brunner JR (1962) Characterisation of  $\kappa$ -Casein Obtained by Fractionation with Trichloroacetic Acid in a Concentrated Urea Solution. *Journal of Dairy Science*, **45**, 1-11.

Swaigood HE and Brunner JR (1963) Characterisation of Kappa-Casein in the Presence of Various Dissociating Agents. *Biochemical and Biophysical Research Communications*, **12**, 148-151.

Swaigood HE, Brunner JR and Lillevik HA (1964) Physical Parameters of  $\kappa$ -Casein from Cow's Milk. *Biochemistry*, **3**, 1616-1623.

- Tanford C (1961) *Physical Chemistry of Macromolecules*, Chapter 6. John Wiley and Sons, New York.
- Tessier H, Rose D and Marier JR (1963) Tubidimetric Method for Estimating Sum of  $\beta$ - and  $\kappa$ -Caseins in Whole Casein. *Journal of Dairy Science*, **46**, 651-655.
- Theisen A, Johann C, Deacon MP and Harding SE (2000) *Refractive Increment Data-Book for Polymer and Biomolecular Scientists*. Nottingham University Press, Nottingham.
- Thompson MP (1971)  $\alpha_s$  and  $\beta$ -Caseins. In: MacKenzie HA (Ed.) *Milk Proteins: Chemistry and Molecular Biology Vol II*, pp. 117-174. Academic Press, New York.
- Thompson MP, Kalan EB and Greenberg R (1967) Properties of Caseins Modified by Treatment with Carboxypeptidase A. *Journal of Dairy Science*, **50**, 767-769.
- Thompson MP and Pepper L (1962) Effect of Neuraminidase on  $\kappa$ -Casein. *Journal of Dairy Science*, **45**, 794-796.
- Tombs MP and Harding SE (1998) *An Introduction to Polysaccharide Biotechnology*. Chapter 2. Taylor and Francis, London.
- van Holde, K.E. (1985) *Physical Biochemistry*. Second Edition, Chapter 9. Prentice-Hall, New Jersey.
- Walstra P and Jenness R (1984) *Dairy Chemistry and Physics*. Prentice Hall, New Jersey.
- Waugh DF (1971) Formation and Structure of Casein Micelles. In: MacKenzie HA (Ed.) *Milk Proteins: Chemistry and Molecular Biology Vol II*, pp. 3-86. Academic Press, New York.

Waugh DF, Creamer LK, Slattery CW and Dresdner GW (1970) Core Polymers of Casein Micelles. *Biochemistry*, **9**, 787-795.

Wyatt PJ (1992) Combined Differential Light Scattering with Various Liquid Chromatography Separation Techniques. In : Harding SE, Sattelle DB and Bloomfield VA (Eds.). *Laser Light Scattering in Biochemistry*, pp. 35-58. Royal Society of Chemistry, Cambridge.

Yphantis DA (1964) Equilibrium Ultracentrifugation of Dilute Solutions. *Biochemistry*, **3**, 297-317.

Zittle CA, Thompson MP, Custer JH and Cerbulis J (1962)  $\kappa$ -Casein -  $\beta$ -Lactoglobulin Interactions in Solution when Heated. *Journal of Dairy Science*, **45**, 807-810.

Zittle CA and Walter M (1963) Stabilization of  $\beta$ -Casein by  $\kappa$ -Casein Against Precipitation by Calcium Chloride. *Journal of Dairy Science*, **46**, 1189-1191.

## 5 CHAPTER 5 – MIXED CASEIN MICELLE – POLYSACCHARIDE SYSTEMS

“Now we have established a platform having characterised the polysaccharides and casein reactants, we can now probe mixed polysaccharide – protein systems involving these molecules”. Since possible complexes can be large; we added an additional technique to those already considered earlier on in this thesis: the Malvern Mastersizer™.

### 5.1 MALVERN MASTERSIZER™ ANALYSIS OF MIXED SYSTEMS

The Malvern Mastersizer™ allows qualitative and quantitative measurements of particle size and particle size distributions for homogeneous and heterogeneous systems (see section 2.6 for an explanation of the theory of particle size analysis). It is therefore a useful technique for looking at mixed casein micelle – polysaccharide systems. As this allows a quick evaluation of particle size distributions it can be used as a screening method for macromolecular interaction, and therefore any mixtures which appear to be interesting can be further analysed using more quantitative techniques *e.g.* sedimentation velocity.

#### 5.1.1 Experimental considerations of particle size analysis

As with all scattering techniques the concentration of sample is important. The aqueous solvent is placed in a cup with a rotating stirrer; this movement allows the solvent to flow via a plastic tube into the light path. One can then measure the background scattering of the solvent. The species of interest is now added drop-wise until an optimum “obscurance” (or scattering) value is attained; a value of 10-40% is suggested, which equates to about a 100-fold dilution in the case of skim milk. The on-line software then calculates a particle size distribution from the information coming from the 44 angular detectors. It should be noted that as with dynamic light

scattering (photon correlation spectroscopy) the results are from the mathematical manipulation of data rather than a genuine mechanical separation provided by for example chromatographic and sedimentation techniques (Harding *et. al.*, 1999).

## 5.2 ANALYSIS OF MIXED CASEIN MICELLE – POLYSACCHARIDE SYSTEMS

In order to give a crude estimate of macromolecular interaction, skim milk was mixed with various polysaccharides ( $\kappa$ -carrageenan,  $\iota$ -carrageenan, low methoxy pectin, high methoxy pectin, guar gum and locust bean gum) of concentration approximately 1mg/ml [Note – AH-EPS was not used due its poor solubility in aqueous solutions and consequently the xanthan investigation was taken no further]. In all cases except guar and locust bean gum (due to some undissolved aggregates), the polysaccharide alone does not result in sufficient scattering to produce a particle size distribution curve. However the casein micelles in skim milk and skim milk–polysaccharide mixtures did result in measurable particle size distribution curves (**Figure 5-1**). The maxima and areas of these curves can therefore be used as an indicator of whether or not an interaction has taken place, including phase separation and flocculation.

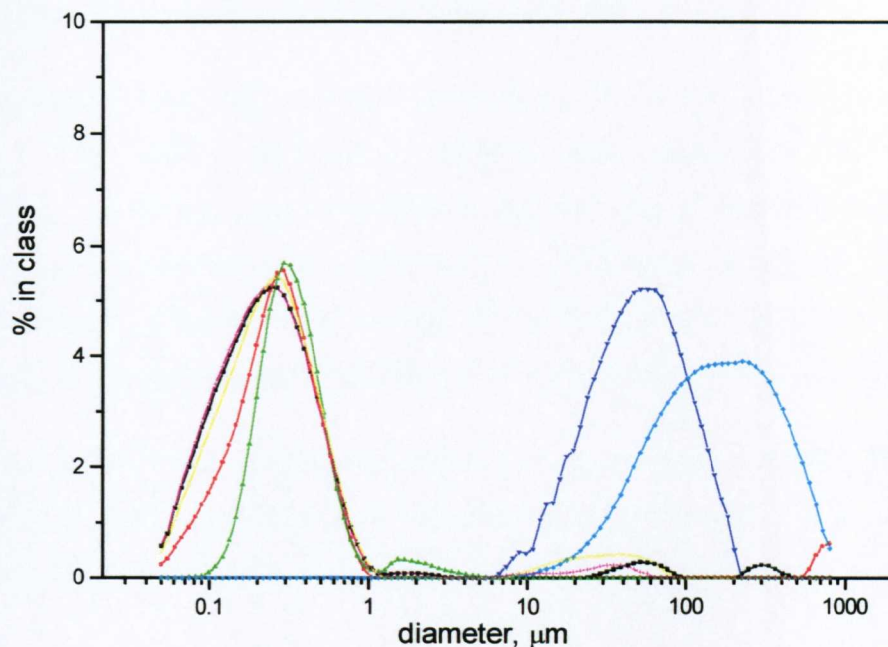


**Figure 5-1** Particle size distribution for skim milk – polysaccharide mixtures. Legend – black – skim milk; red – skim milk + low methoxy pectin; green – skim milk + high methoxy pectin; navy – skim milk +  $\kappa$ -carrageenan; cyan – skim milk +  $\iota$ -carrageenan; magenta – skim milk + guar gum and yellow – skim milk + locust bean gum.

### 5.2.1 Preliminary results of particle size analysis of mixed casein micelle – polysaccharide systems

Results indicate that under the conditions studied (pH  $\sim$  7 and Ionic strength  $\sim$  0.1M)-

- (i) casein micelles are stable to 100-fold dilution
- (ii) casein micelles appear to interact with both  $\kappa$ -carrageenan and  $\iota$ -carrageenan (Dalglish and Morris, 1988; Langendorff *et. al.* 1997, 2000a,b and Michon *et. al.* 2000)
- (iii) casein micelles do not appear to interact with low methoxy pectin, high methoxy pectin, guar gum and locust bean gum. [Note - there are differences in the relative

heights of the peaks, but this is most likely due to temporal fluctuations in sensitivity, which are quite common in my experience of particle size analysis].

In the case of skim milk – carrageenan mixtures the complex was clearly visible to the eye. Skim milk – carrageenan mixtures were reanalysed using sedimentation velocity, but the data was impossible to interpret due to (and as expected) the rapid rate of sedimentation of the casein micelle – carrageenan complexes. This is however in qualitative agreement with particle size analysis, in the sense that there is a large amount of complex present with little or no unaggregated or free micelles present.

As it was now clear which polysaccharides are of particular interest (at least under the conditions studied) a more detailed investigation was carried out into  $\kappa$ -carrageenan interactions.

## **5.2.2 Analysis of mixed casein micelle – $\kappa$ -carrageenan systems**

### *5.2.2.1 Particle size analysis*

In many food applications  $\kappa$ -carrageenan is added to milk products at approximately 0.2mg/ml (0.02%) (see Table 3-8) and therefore this concentration was chosen as the minimum amount of added carrageenan. Further samples of 0.4, 0.6 and 0.8mg/ml  $\kappa$ -carrageenan were also analysed. As 1mg/ml added carrageenan results in complete complexation 0.8mg/ml was considered an appropriate upper limit.

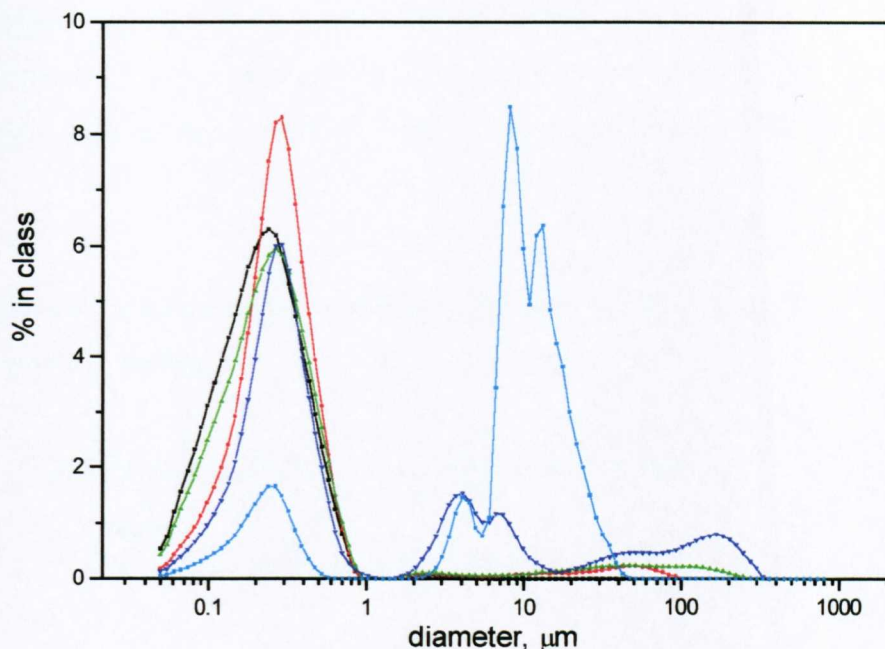


**Figure 5-2** Particle size distribution for skim milk –  $\kappa$ -carrageenan mixtures. Legend – black – skim milk; red – skim milk + 0.2mg/ml  $\kappa$ -carrageenan; green – skim milk + 0.4mg/ml  $\kappa$ -carrageenan; navy – skim milk + 0.6mg/ml  $\kappa$ -carrageenan and cyan – skim milk + 0.8mg/ml  $\kappa$ -carrageenan.

As can be seen from the graph above (**Figure 5-2**), the particle size increases slightly upon addition of 0.2mg/ml  $\kappa$ -carrageenan and the concentration appears to increase as indicated by the area under the curve. There may also be a small amount of aggregated material. However, on addition of larger amounts of  $\kappa$ -carrageenan there is a decrease in the left-hand peak at approximately 250nm, with the appearance of a variety of peaks at larger particle sizes.

#### 5.2.2.2 Sedimentation velocity in the analytical ultracentrifuge

The mixtures used in the particle sizer were then analysed using sedimentation velocity – sedimentation time derivative method. Results were however a little disappointing, as it was impossible to measure the sedimentation coefficient of any aggregated species due to the turbidity of the sample; these larger species could be

seen as a pellet at the base of the centrifuge cell. We could however measure the sedimentation coefficient of the “smaller” species (**Table 5-1**). As with particle size analysis there was a decrease in the area of the first (where first means the peak of smallest particle size) peak with increased carrageenan concentration (**Table 5-1**).

**Table 5-1** Sedimentation coefficient and area of the first peak for skim milk –  $\kappa$ -carrageenan mixtures

Added $\kappa$ -carrageenan, mg/ml	sedimentation coefficient, S	peak area, arbitrary units
0.0	350	57.8
0.2	295	64.8
0.4	335	56.2
0.6	672	18.4
0.8	887	5.6

There is an initial decrease followed by an increase in apparent sedimentation coefficient with increased carrageenan concentration, but it is likely that this is due to the concentration dependency of sedimentation, *i.e.* the lower the concentration of the sedimenting species the greater the apparent sedimentation coefficient. The areas in **Table 5-1** are in qualitative agreement with the results from particle size analysis *i.e.* in general as  $\kappa$ -carrageenan concentration increases the area of the peak decreases (**Figure 5-2**). If we normalise the peak areas in both cases to those of skim milk we can see that the quantitative agreement is excellent except in the case of 0.6mg/ml added  $\kappa$ -carrageenan (**Table 5-2**).

**Table 5-2** Normalised peak areas from particle size and sedimentation time derivative analysis

Added $\kappa$ -carrageenan, ml/g	particle size	sedimentation time derivative
0.0	1.00	1.00
0.2	1.14	1.12
0.4	1.01	0.97
0.6	0.80	0.32
0.8	0.16	0.10

In sedimentation analysis the most common property used for the assignment of a macromolecular interaction is an increase in sedimentation coefficient and therefore molecular weight (see for example Deacon *et al.*, 1998; Deacon, 1999 and Harding *et al.*, 1999) however a change in the concentration of sedimenting species can also be regarded as an indicator of macromolecular interaction (Harding, 1997; Fiebrig, 1995; Deacon, 1999 and Harding *et al.*, 1999). An increase in concentration of sedimenting species at low carrageenan concentration is likely due to a macromolecular interaction (Rowe, personal communication). However it is not easy to qualify the interaction as to our knowledge an increase in concentration of sedimenting species has only previously been used to describe the interaction between chitosan and mucin (Deacon *et al.*, 1999) in sedimentation analysis, however this is fairly common in chromatographic techniques. The decrease in concentration of sedimenting species at higher carrageenan concentrations is typical of systems where the complex (or complexes) formed is too large to be measured using sedimentation velocity ( $M_w > 10^9$  g/mol). The decrease in concentration of reactants (compared to a control) can be used as a so-called “fingerprinting assay”. This has been done previously in mucin/ chitosan interactions (Harding, 1997; Fiebrig, 1995; Deacon, 1999 and Harding *et al.*, 1999).

It is very difficult to ascertain the exact nature of interaction due the concentration dependency of sedimentation. It seems likely that at all carrageenan concentrations there is some form of macromolecular interaction as indicated by a change in the concentration of sedimenting species. The formation of aggregates can be seen clearly in (Figure 5-2) especially at higher carrageenan concentrations and can be implied by the decrease in sedimenting material in sedimentation experiments.

### 5.3 EVIDENCE FOR CASEIN MICELLE – $\kappa$ -CARRAGEENAN INTERACTIONS

(i) formation of large aggregates on addition of approximately 1mg/ml of  $\kappa$ -carrageenan

(ii) increase of sedimenting species at low  $\kappa$ -carrageenan concentrations as indicated by increase in first peak (Figure 5-2), increase in sedimenting material (Table 5-1 and Table 5-2)

(iii) increasing amounts of aggregated material with increasing  $\kappa$ -carrageenan concentration, as indicated by increased particle size (Figure 5-2), decrease in sedimenting material (Table 5-1 and Table 5-2) and the pellet at the base of the centrifuge cell.

It is therefore my opinion that at low  $\kappa$ -carrageenan concentration there is a complexation interaction with the casein micelles probably due to electrostatic interaction with  $\kappa$ -casein on the micelle exterior, as has been indicated previously. At higher  $\kappa$ -carrageenan concentrations this interaction leads to depletion flocculation (Williams and Smith, 1995). The stability of colloidal dispersions is greatly influenced by addition of polyelectrolytes (Williams and Smith, 1995 and Furusawa *et al.*, 1999) at very low  $\kappa$ -carrageenan concentrations the bridging phenomenon is predominant, that is where the polymer is able to adsorb on to the surface of more than one colloidal particle (Figure 5-3).

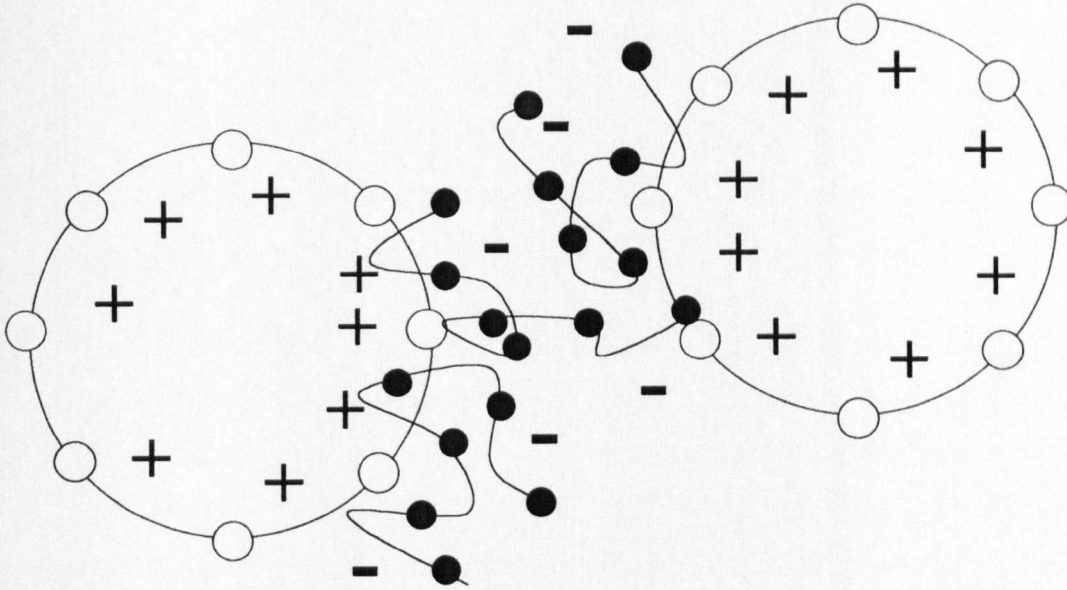


**Figure 5-3** Schematic representation of bridging flocculation in casein micelle -  $\kappa$ -carrageenan systems (adapted from Furusawa *et. al.*, 1999)

When a sufficient  $\kappa$ -carrageenan concentration is reached the colloidal particle will be universally coated this is called steric stabilisation (**Figure 5-4**).

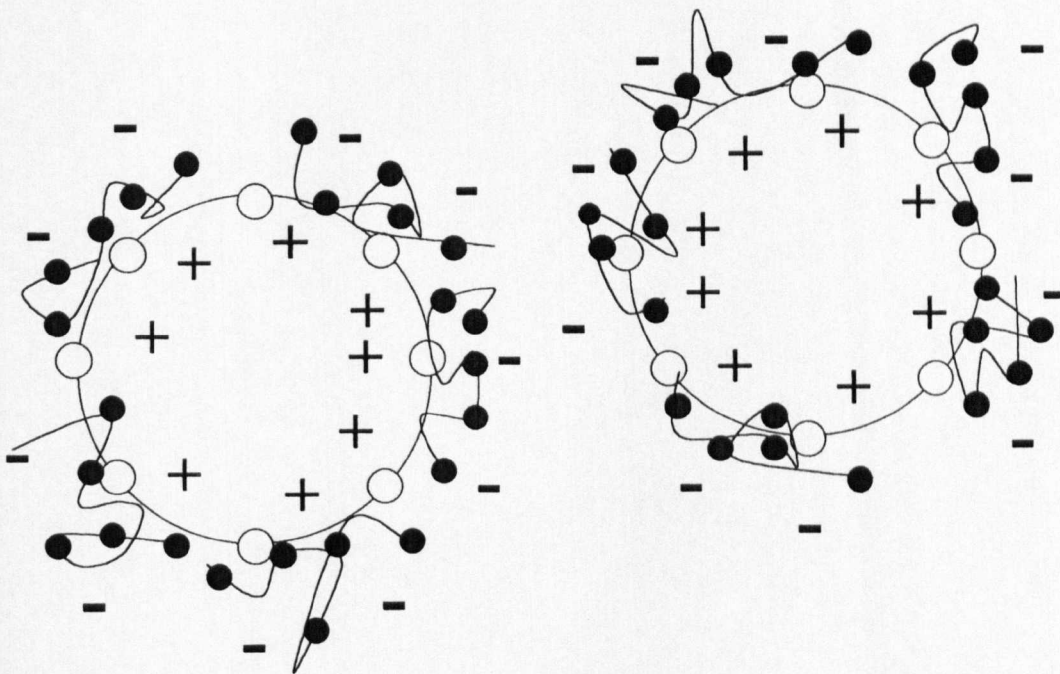


**Figure 5-4** Schematic representation of steric stabilisation in casein micelle -  $\kappa$ -carrageenan systems (adapted from Furusawa *et. al.*, 1999)

This results in a moderate increase micelle diameter, which can be seen using particle size analysis, but is masked in sedimentation analysis due the concentration dependency of sedimentation since as the concentration of sedimenting species decreases the apparent sedimentation coefficient increases. It is likely that a sterically stabilised casein micelle –  $\kappa$ -carrageenan would have a stronger concentration dependency due to increased hydration and possibly greater structural asymmetry.

Finally after the addition of an excess  $\kappa$ -carrageenan a depletion layer ( **Figure 5-5**) is formed where the polymer concentration at the surface is less than that of the bulk, this results in an osmotic pressure difference between the bulk polymer solution and the depleted region containing pure solvent. This in turn results in an attractive force being set up and therefore when two (or more) colloidal particles come close together depletion flocculation will occur (**Figure 5-6**) (Williams and Smith, 1995 and Furusawa *et. al.*, 1999).

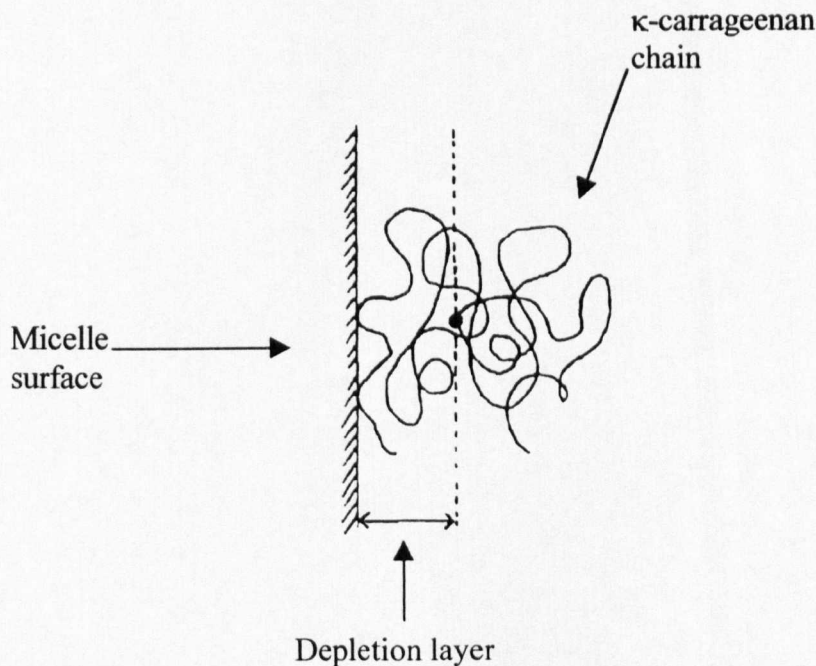


**Figure 5-5** Schematic representation of a  $\kappa$ -carrageenan depletion layer (adapted from Williams and Smith, 1995).

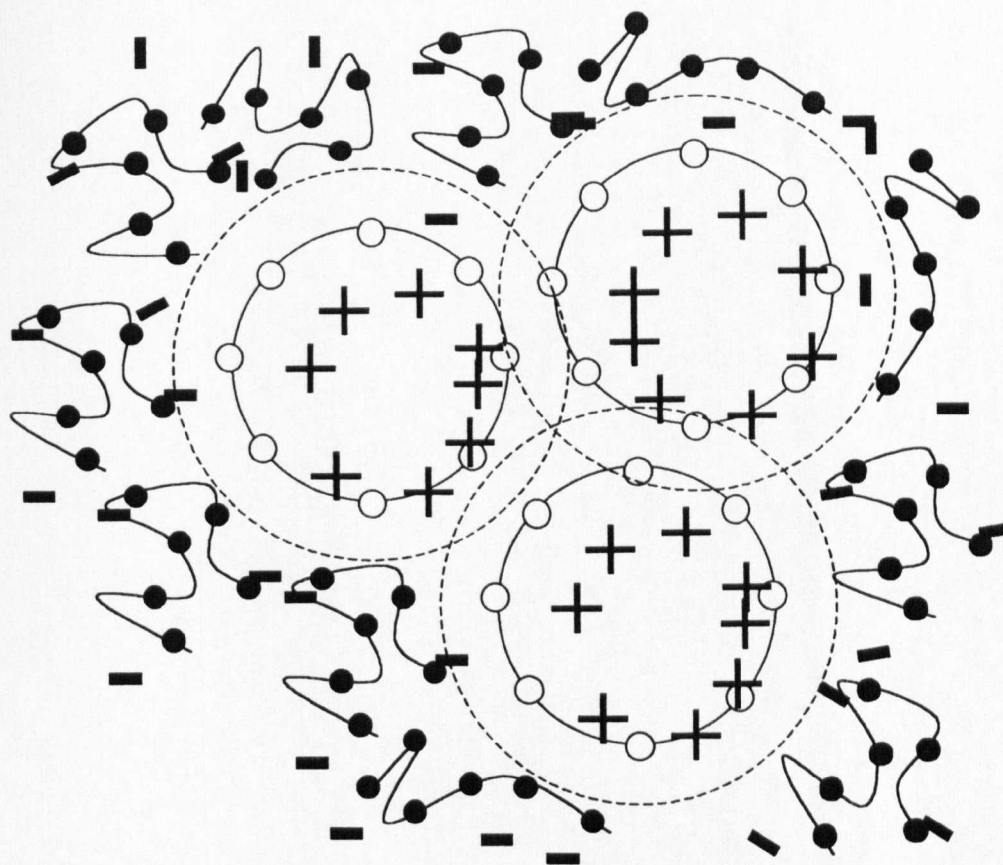


**Figure 5-6** Schematic representation of the exclusion of  $\kappa$ -carrageenan molecules from between casein micelles at close separations leading to depletion flocculation (adapted from Williams and Smith, 1995).

It is my opinion that at low carrageenan concentrations we have an interaction similar to that in (Figure 5-4). At higher carrageenan concentrations we have the situation analogous to (Figure 5-6), where the carrageenan molecules are excluded due to the casein micelle depletion layer (Figure 5-5) and flocculation ensues. [Note – even at lowest  $\kappa$ -carrageenan concentration, bridging flocculation was not observed (Figure 5-3). This is in agreement with the observations of Dalgleish and Morris (1988)].

Recent articles (Schorsch, *et. al.*, 2000 and Langendorff *et. al.*, 2000a,b) report similar interactions between  $\kappa$ -carrageenan and casein micelles in skim milk at high temperatures, using turbidity, particle size and dynamic viscoelastic measurements. In the same articles Langendorff and co-workers also suggests that  $\lambda$ -carrageenan bridges casein micelles at low concentrations.

#### 5.4 REFERENCES

- Dalgleish DG and Morris ER (1988) Interactions Between Carrageenans and Casein Micelles: Electrophoretic and Hydrodynamic Properties of the Particles. *Food Hydrocolloids*, **2**, 311-320.
- Deacon MP, Davis SS, Waite JH and Harding SE (1998) Structure and Mucoadhesion of Mussel Glue Protein in Dilute Solution. *Biochemistry*, **37**, 14108-14112.
- Deacon MP (1999) Polymer Bioadhesives for Drug Delivery. Ph.D. Thesis, University of Nottingham.
- Deacon MP Davis SS, White RJ, Nordman H, Carlstadt I, Errington, N, Rowe AJ and Harding SE (1999) Are Chitosan – Mucin Interactions Specific to Different Regions of the Stomach? Velocity Ultracentrifugation Offers a Clue. *Carbohydrate Polymers*, **38**, 235-238.
- Fiebrig I (1995) Solution Studies on the Mucoadhesive Potential of Various Polymers for Use in Gastrointestinal Drug Delivery Systems. Ph.D. Thesis, University of Nottingham.
- Furusawa K, Ueda M and Nashima T (1999) Bridging and Depletion Flocculation of Synthetic Latices Induced by Polyelectrolytes. *Colloids and Surfaces A: Physicochemical and Engineering Aspects*, **153**, 575-581.
- Harding SE (1997) Characterisation of Chitosan-Mucin Complexes by Sedimentation Velocity Analytical Ultracentrifugation. In: Muzzarelli RAA and Peters MG (Eds.) *Chitin Handbook*, pp 457-466. European Chitin Society, Torrette, Italy.

- Harding SE, Davis SS, Deacon MP and Fiebrig I (1999) Biopolymer Mucoadhesives. *Biotechnology and Genetic Engineering Reviews*, **16**, 41-86.
- Langendorff V, Cuvelier G, Launay B and Parker A (1997) Gelation and Flocculation of Casein Micelles/ Carrageenan Mixtures. *Food Hydrocolloids*, **11**, 35-40.
- Langendorff V, Cuvelier G, Michon C, Launay B, Parker A and de Kruif CG (2000a) Effects of Carrageenan Type on the Behaviour of Carrageenan/ Milk Mixtures. *Food Hydrocolloids*, **14**, 273-280.
- Langendorff V, Cuvelier G, Michon C, Launay B, Parker A and de Kruif CG (2000b) Stability and Gelation of Carrageenan/ Skim Milk Mixtures: Influence of Temperature and Carrageenan Type. POLYMERIX 2000 - Biopolymers for the Food and Cosmetic Industry (Conference Proceeding), pp 147-155. CBB Development, Rennes, France.
- Michon C, Vigouroux F, Boulenguer P, Cuvelier G and Launay B (2000) Gelatin/ Iota Carrageenan Interactions in Non-Gelling Conditions. *Food Hydrocolloids*, **14**, 203-208.
- Schorsch C, Jones MG and Norton IT (2000) Phase Behaviour of Pure Micellar Casein/  $\kappa$ -carrageenan Systems in Milk Salt Ultrafiltrate. *Food Hydrocolloids*, **14**, 347-358.
- Williams PA and Smith NJ (1995) Depletion Flocculation. In: Harding SE, Hill SE. and Mitchell JR (Eds.) *Biopolymer Mixtures*, pp. 161-172. Nottingham University Press, Nottingham.

## 6 CHAPTER 6 – GENERAL DISCUSSION

### 6.1 REVIEW OF RESULTS IN CHAPTER 3 – DETAILED CHARACTERISATION OF POLYSACCHARIDE SUBSTRATES

In general, polysaccharides have not been characterised extensively using the analytical ultracentrifuge, due to the problems of polydispersity and thermodynamic non-ideality. Polydispersity is an inherent property of the building mechanism of polysaccharides and thermodynamic non-ideality is due to asymmetry and polyanion charge affects. It is therefore of utmost importance that measurements are made at a number of concentrations, and extrapolated to infinite dilution [Note – that with many protein samples, where non-ideality is less significant, a single measurement at low concentration can be taken as the intrinsic measurement at infinite dilution].

However, in this laboratory there has been a significant amount of work on for example alginate (Ball *et al.*, 1988, Horton *et al.*, 1991); chitosan (Errington *et al.*, 1993, Cölfen *et al.*, 1996a,b); pectin (Harding *et al.*, 1991); guar (Jumel, 1994); dextran (Ball *et al.*, 1990; Errington, 1993); xanthan (Dhami *et al.*, 1995b); xylan (Dhami *et al.*, 1995a); carrageenan (Harding *et al.*, 1997); locust bean gum (Gaisford *et al.*, 1986); amylose and amylopectin (Tongdang *et al.*, 1999). This “in-house” experience was therefore invaluable in extension of these investigations. For a more detailed review see Harding, (1995).

In chapter 3 the dilute solution hydrodynamic properties were measured for many industrially important polysaccharides *e.g.* pectins, carrageenans, guar, LBG and xanthan, together with some novel polysaccharides *e.g.* CB-pectin, CB-xylan and AH-EPS. Additionally high and low methoxy pectins were characterised at varying temperatures.

### 6.1.1 Effect of DE on hydrodynamic properties of citrus pectin

It is clear that when discussing pectin structures that degree of esterification and hence charge is important not only in dilute solution properties, but also in gelling conditions. It is well known that low methoxy pectins form gels with divalent cations (usually  $\text{Ca}^{2+}$ ) in the so-called “egg-box” model and high methoxy pectins require high soluble solids content, usually sucrose (see *e.g.* Glicksman, 1969).

Intuitively, one would think that the lower the degree of esterification (higher the charge) the more rigid and extended the molecule, due to increased electrostatic repulsions. However, the results in 3.1.1 suggest that there is a balance between electrostatic repulsion of  $\text{COO}^-$  groups and the steric hindrance associated with methyl ester groups. This is clearly demonstrated by the symmetrical relationship between the intrinsic viscosity,  $[\eta]$  and infinite dilution sedimentation coefficient,  $s_{20,w}^0$  and supported by the similar relationship between the translational frictional ratio,  $f/f_0$  and the Wales – van Holde ratio,  $k_s/[\eta]$  (Figure 3-13). All four hydrodynamic parameters indicate that “pectin 7001” (DE = 65%) and “pectin 7003” (DE = 37.8%) is the most flexible and most rigid of the five pectin samples respectively (Table 3-1 and Table 3-2).

It goes without saying that the dilute solution physical properties of a gelling polysaccharide must have an effect on rheological properties such as setting time, gel strength, and melting temperature. Therefore, dilute solution hydrodynamic measurements could be useful in complementing rheological measurements.

### 6.1.2 Effect of elevated temperature on citrus pectin

In many food and pharmaceutical processes polysaccharides are exposed to high temperatures. However high temperature measurement of dilute solution hydrodynamic properties have not, to my knowledge, been widespread. An investigation into the effect of increased temperature on the solution properties of both low and high methoxy pectin allowed also the testing of the “High Temperature Unit” for the Beckman Model E analytical ultracentrifuge (Beckman Inc., Palo Alto, USA), which we believe is the only analytical ultracentrifuge in the world capable of

controlled hydrodynamic studies above 40°C. [Note – in the case of biopolymers we have defined high (or elevated) temperature as being above 40°C, however synthetic polymer chemists may not agree]. The many additional problems that were overcome associated with high temperature analytical ultracentrifugation have been discussed in section 3.1.2.

#### 6.1.2.1 *LM pectin*

When exposed to high temperature there is very little effect on hydrodynamic properties of a low methoxy pectin. There appears to be a very slight conformational change towards a more compact structure as indicated by a decrease in reduced viscosity and increase in sedimentation coefficient and decrease in apparent translation frictional ratio (Tanford, 1961) (Table 3-3).

#### 6.1.2.2 *HM pectin*

The effect of increased temperature on high methoxy pectin is quite dramatic and significantly different to that on low methoxy pectin. There is significant decrease in intrinsic viscosity, sedimentation coefficient, weight average molecular weight and translational frictional ratio with increasing temperature, which all indicates depolymerisation (Table 3-4). This depolymerisation is apparently due to  $\beta$ -elimination, although demethoxylation and loss of “hairy” side groups will also result in a decrease molecular weight. It has been reported previously that high methoxy pectins are susceptible to increased rates of  $\beta$ -elimination at high pH and/ or high temperature. As the  $-\text{CH}_3$  group are the major driving force in the  $\beta$ -elimination reaction this would perhaps go some way to explaining the differences between high and low methoxy pectins when exposed to high temperature.

Although we have demonstrated the capabilities of the high temperature unit in the Beckman Model E for looking at relatively simple biopolymer systems, there are a great deal of possibilities for looking at more complex systems. It should be possible to investigate temperature dependent protein denaturation (see for example section 4.4

on the heat denaturation of  $\beta$ -lactoglobulin) or temperature induced self-association/disassociation. In polysaccharide chemistry it provides an opportunity to study temperature dependent changes in conformational (*e.g.* the coil-helix transition in carrageenan) and temperature dependent macromolecular interactions (*e.g.* carrageenan/ casein interactions). As we have now overcome many of the teething problems associated with high temperature analytical ultracentrifugation, it should open new avenues for future analytical ultracentrifugation research.

### **6.1.3 Effect of chemical substitution on citrus pectin**

The hydrophobisation of polysaccharides has been reported to lead to interesting binding properties in the gut (Klavons and Bennet, 1995) and the addition of an UV absorbing group to a polysaccharide is interesting from visualisation the point of view to the analytical ultracentrifuge user. However, in either case it is important to understand any changes in the structure or physical properties such derivatisation can facilitate.

Pectin samples were derivitised in two ways using the procedures described in Ebringerova *et. al.*, 1996 (KP and LMP) and Crescenzi and Della Valle, 1991 respectively (LMP). Both methods incorporate a form of carboxybenzyl (CB) group into the pectin molecule. Structural characterisation using Fourier Transform Infra-Red (FT-IR) spectroscopy and carbon – 13 Nuclear Magnetic Resonance ( $^{13}\text{C}$  NMR) confirmed that derivitisation had been successful to a degree of substitution (DS) of 5-7% in all three cases.

CB derivatisation of KP (see 3.1.3) had little or no effect on the hydrodynamic properties of the soluble fraction, although ~48% of the sample remained insoluble (Table 3-7). However, the hydrodynamic properties of LMPG2 and LMPG3, the alkaline and neutral derivatives of LMP respectively showed significantly reduced intrinsic viscosity, sedimentation coefficient, weight average molecular weight and translational frictional ratio although 20% remained undissolved (Table 3-7). It is again likely that the depolymerisation is due to  $\beta$ -elimination. The reduction in each of the hydrodynamic parameters was more pronounced in the case of the neutral

reaction conditions (Table 3-7), which is most likely due to the longer reaction time. KP may have been more tolerant to reaction conditions due to the relatively small amount of -CH<sub>3</sub> groups (Ebringerova, personal communication), which results in a more stable pectin under the reaction conditions.

From this investigation it is clear that hydrophobisation of pectin samples does have an effect on the physical properties including solubility. Lower solubility is most likely due to the formation of insoluble aggregates. The loss of molecular integrity of LMP derivatives may also be important in pharmaceutical applications as high molecular weight and therefore viscosity are often a barrier to physiological effectiveness (Furneaux, personal communication).

#### 6.1.4 Carrageenans

##### 6.1.4.1 *κ*-carrageenan

The dilute solution structure of *κ*-carrageenan is still somewhat illusive, in general due to the problems associated with concentration dependent aggregation (Bongaerts *et. al.*, 2000). In hydrodynamic analyses this is further complicated by the opposing force of thermodynamic non-ideality, which can be compensated for by extrapolation to infinite dilution (or by working at low concentrations). It would appear from our observations (*i.e.* almost identical weight average molecular weights in the ordered and random states) that under the conditions studied *κ*-carrageenan is a single helix in the ordered state.

##### 6.1.4.2 *ι*-carrageenan

Many of the problems of *κ*-carrageenan analyses are evident in the study of *ι*-carrageenan. As we were unable to calculate molecular weights in the helical state any interpretation of the helical conformation is difficult. This study does in my opinion demonstrate the difficulties, which can arise in the analysis of polydisperse,

thermodynamically non-ideal, self-associating systems, in this case further complicated by a conformational change.

### 6.1.5 Galactomannans

Guar and locust bean gum (LBG) are primarily polymannans with varying degrees of  $\alpha$  (1 $\rightarrow$ 6) substituted galactose (Tombs and Harding, 1998 and Glicksman, 1969). In section (3.3) we were able to compare

- (i) the effect of galactose substitution on the physical properties of a polymannans
- (ii) the effect of chemical processing on guar galactomannan

Results indicate that LBG is significantly more extended than guar as indicated by a larger translation frictional ratio (Tanford, 1961). This would be consistent with a lesser degree of substitution  $\sim 1 : 4$  (compared with  $1 : 2$  for guar) (Tombs and Harding, 1998 and Glicksman, 1969). In the case of the processed guar there is little or no difference in conformation as indicated by the linearity of the double log Mark – Houwink – Kuhn – Sakurada (MHKS) plots of Root Mean Square (RMS) radius vs.  $M_w$ ;  $[\eta]$  vs.  $M_w$  and  $s_{20,w}^0$  vs.  $M_w$  respectively (Figure 3-38, Figure 3-39 and Figure 3-40). The slope of  $[\eta]$  vs.  $M_w$  is in general agreement with the previous literature values of Jumel, 1994; Sharman *et. al.*, 1978 and Robinson *et. al.*, 1982. Therefore any decrease in intrinsic viscosity, sedimentation coefficient, weight average molecular weight and translational frictional ratio is due to a decrease in chain length and hence axial ratio,  $a/b$ . This clearly demonstrates the usefulness of combined hydrodynamic techniques in estimating the dilute solution conformation of polysaccharides.

### 6.1.6 Bacterial polysaccharides

An interesting property of nature is that when facing similar problems in a similar environment in different species it often comes up with the same (or similar) answers. This is called *convergent evolution*. When bacteria are living under stressed condition

they often secrete exopolysaccharides, which can be chemically *different* to each other, but can have *similar* physical properties.

Therefore when we were characterising a novel bacteria from a Chinese salt marsh, we decided to compare the hydrodynamic properties to those of one of the most popular bacterial polysaccharides in the food industry – xanthan. Unlike xanthan the halophilic bacterial polysaccharide “AH-EPS” is insoluble in water and was difficult to dissolve in any common solvents. It was however soluble in 1M guanidine hydrochloride and therefore all measurements on AH-EPS and xanthan were performed in this solvent. In many ways the properties of AH-EPS were similar to those of xanthan: extreme shear-thinning, high viscosity (**Table 3-12**) [Note – the intrinsic viscosity of xanthan could not be evaluated due to the problems of shear-thinning], hyper-sharp boundaries in sedimentation velocity experiments, and high molecular weight. All of these properties are indicative of a molecule of high axial ratio, *a/b e.g.* of the zone A type (Pavlov *et. al.*, 1997).

Due to the increased acceptability of bacterial polysaccharides in foodstuffs, there is a concerted effort from many laboratories to find new novel bacterial polysaccharides, which may have interesting rheological properties from such diverse environments as Chinese salt marshes (Li *et. al.*, in press) to deep-sea hyper-thermal vents (Gauzenec, 2000). In the case of AH-EPS it seems unlikely that there are any industrial applications due to the solubility problem, but it usefully demonstrates that chemically *different* polysaccharides can have very *similar* properties.

### **6.1.7 Effect of chemical substitution on xylans**

As with pectin samples it is also possible to attach a UV absorbing group to an arabino-xylan (AGX). As with KP there appeared to be little or no difference in the physical properties of the CB derivative. It could be argued that the small decrease in intrinsic viscosity together with an increase in sedimentation coefficient could be indicative of a small conformational change towards a more compact structure (Tanford, 1961), however, such a change (if any) is very mild and may be an artefact

of experimental error (Table 3-13). This study does show however, how chemical derivatisation can have very different effects on different polysaccharides.

## 6.2 REVIEW OF RESULTS IN CHAPTER 4 – DETAILED CHARACTERISATION OF MILK PROTEIN SUBSTRATES

Milk proteins have been extensively studied using the analytical ultracentrifuge over the last 70 years although most researchers have concentrated on  $\beta$ -lactoglobulin (Zittle *et. al.*, 1962; Advani, 1994 and Saril, 2000) fractionated samples (Pedersen, 1936; von Hippel and Waugh, 1955) or on the individual caseins (Swaigood and Brunner, 1962; Swaigood and Brunner, 1963; Swaigood *et. al.*, 1964; Thompson and Pepper, 1962; Pepper and Thompson, 1963; Zittle *et. al.*, 1962; Waugh *et. al.*, 1970; Thompson *et. al.*, 1967; Payens and van Markwijk, 1963; Parry Jnr. and Carroll, 1969; Buchheim and Schmitt, 1979; Payens, 1979; Sullivan *et. al.*, 1955 and Waugh and von Hippel, 1956). During the 1970s Lin *et. al.*, 1971 and Dewan *et. al.*, 1974 had previously made combined sedimentation – diffusion measurements on the intact casein micelle.

In Chapter 4, the solution properties of casein micelles, sodium caseinate (as a model for the casein sub-micelle),  $\beta$ -casein,  $\kappa$ -casein and the major whey protein  $\beta$ -lactoglobulin. Where appropriate results were compared and contrasted with those of previous workers.

### 6.2.1 Casein micelles

The characterisation of casein micelles in the analytical ultracentrifuge initially proved difficult due to the high concentration of sedimenting species (casein ~ 28mg/ml) and therefore turbidity. This did however enable us to compare all four optical systems on the analytical ultracentrifuge (see *e.g.* Figure 2-2 Comparison of the optical records for a sedimenting boundary obtained from the (a) Schlieren, (b) interference, (c) photographic absorbance (Turbidity), and (d) photoelectric absorbance optical systems (adapted from Schachman, 1959, Ralston, 1993). At high

concentration the combined photographic absorption/ Schlieren method was most appropriate and UV absorption at low concentration (as is usual with UV absorption data the  $g^*(s^*)$  plots obtained from this method were fairly noisy). However the interference system on the Beckman Optima XLI (Beckman Inc., Palo Alto, USA) proved reliable over the entire concentration range. We should note that it is likely under all systems that due to polydispersity some information was lost at the cell base and therefore “number” and “weight” average sedimentation coefficients were not obtainable and the “mode” average was the most accessible (Figure 4-2).

The sedimentation-time derivative method (Stafford, 1992a,b and Laue and Stafford, 1999) combined with intrinsic viscosity measurements is perhaps the most simple of the combined hydrodynamic approaches, but this method enabled the confirmation of spherical micelle nature (from  $k_s/[\eta] = 1.6$ ) and the calculation of other hydrodynamic parameters through a series of equations, including the Svedberg, Stokes-Einstein and the concentration dependency of sedimentation (Rowe, 1977) equation. The agreement between calculated and experimental diffusion coefficients not only validates the  $D_{T,b}^0$  calculation, but also molecular weight, translational frictional ratio and hence the “Rowe equation” (at least in the case of casein micelles) (Table 4-3 and Table 4-4).

The characterisation of casein micelles in the analytical ultracentrifuge goes to demonstrate that this powerful solution technique need not be confined to “ideal”, “monodisperse”, and “non-associating” low molecular weight proteins. This has further demonstrated that solution turbidity need not be a problem and in fact in the case of combined photographic absorption/ Schlieren optics it can indeed be beneficial.

### 6.2.2 Sodium Caseinate

Sodium caseinate can be considered to represent the casein “sub-micelle” and has been described as a hydrated spherical aggregate of between 4-10 casein “monomers”. The analysis of complex self-associating systems is not new to the analytical

ultracentrifuge, however in this case we were unable to quantitatively describe the equilibrium species. This could be due to one of two reasons (or both)

(i) that the results are not of sufficient quality to determine whether or not we have for example a monomer – dimer – hexamer equilibrium

(ii) we have in equilibrium all species from monomer to decamer (or even dodecamer) which is too complicated for our simple model.

It is my belief that option (ii) is the most likely, but option (i) can certainly not be ruled out. Nonetheless we did however observe self-association and found good agreement with the hydrated sphere model.

### 6.2.3 Individual caseins

#### 6.2.3.1 $\beta$ -casein

The bimodal nature of  $\beta$ -casein in dilute solution has been reported previously (Payens and van Markwijk, 1963; Payens *et al.*, 1969 and Thompson, 1971) consisting of one “fast” peak of ~12S and a “slow” monomer peak of 1.6S respectively (Figure 4-12). The average molecular weight of the polymeric species has not previously been well characterised.

By assuming that the relative amount of monomers and polymers were the same in sedimentation velocity and sedimentation equilibrium experiments, at similar loading concentrations, one could make an estimate of polymer molecular weight and hence calculate the degree of polymerisation. Results were in reasonable agreement with those quoted in the literature (Payens *et al.*, 1969; Buchheim and Schmitt, 1979 and Arima *et al.*, 1979). One should however be careful with systems such as  $\beta$ -casein, which undergoes concentration, temperature and ionic strength dependant self-association. I can say with reasonable confidence that these results are characteristic of  $\beta$ -casein under these conditions (Table 4-6) (pH 6.8, I=0.1M and temperature = 20°C), but any correlation drawn with previous results should be treated with extreme care, as there are small differences in experimental conditions. Encouragingly

however is the clear agreement with the results of for example Payens and van Markwijk, 1963 using Schlieren optics on the Model E. It shows that there is good agreement between  $dc/dr$  vs.  $r$  (from Schlieren) and  $dc/dt$  vs.  $s^*$  from sedimentation time derivative.

#### 6.2.3.2 $\kappa$ -casein

As with  $\beta$ -casein, sedimentation coefficients for this system have been previously well documented (Perdersen, 1936; Swaisgood and Brunner, 1962; Thompson and Pepper, 1962; Zittle and Walter, 1963; Pepper and Thompson, 1963; Swaisgood and Brunner, 1963; Swaisgood *et. al.*, 1964; MacKinlay and Wake, 1964), but reliable weight average molecular weight for the polymeric species has been less reported. In the present study the measured sedimentation coefficient was in good agreement with other workers. We were also able to calculate the “weight” average and “z” average molecular weights; the values were in the “region of general consensus” (Farrell Jnr. *et. al.*, 1998). As has been described previously for other macromolecular systems we were then able to calculate the translation frictional ratio (Tanford, 1961), which indicates that  $\kappa$ -casein is a fairly extended molecule; the latter finding is in agreement with the viscosity measurements of Swaisgood *et. al.*, 1964 and is not unexpected for a proline-rich molecule (Farrell Jnr., 1973 and Kumosinski *et. al.*, 1991a,b).

#### 6.2.4 $\beta$ -lactoglobulin

When exposed to high temperature  $> 70^\circ\text{C}$  the native  $\beta$ -lactoglobulin dimer is believed to denature and self-associate to form octamers. Our results indicate that  $\beta$ -lactoglobulin does denature at high temperature, but we have no evidence for self-association (or disassociation). Denaturation is indicated by an increase in reduced viscosity, a decrease in sedimentation coefficient and therefore an increase in translational frictional ratio, which is typical of the formation of a more open structure (Tanford, 1961) (Table 4-8). Viscosity measurements are also consistent with reversible denaturation up to  $60^\circ\text{C}$ .

This further highlights the application high temperature analytical ultracentrifugation to protein denaturation and/ or other more complex temperature dependent phenomena.

### 6.3 REVIEW OF RESULTS IN CHAPTER 5 – MIXED CASEIN MICELLE – POLYSACCHARIDE SYSTEMS

In Chapter 5 we investigated the interactions between casein micelle (in skim milk) and some commercially available polysaccharides under the conditions commonly found in milk (pH ~ 6.7 and I ~ 0.1M).

Primary investigations using the Malvern Mastersizer<sup>TM</sup> and sedimentation velocity (sedimentation time derivative, Stafford, 1992a,b and Laue and Stafford, 1999) indicated that only  $\kappa$ - and  $\iota$ -carrageenan showed any significant interaction under the above conditions (**Figure 5-1**). Therefore a more detailed investigation was centred on the concentration dependency of the  $\kappa$ -carrageenan interaction.

Results suggest that at low concentrations  $\kappa$ -carrageenan molecules adhere to the surface of the casein micelle, probably due to an electrostatic interaction with  $\kappa$ -casein on the exterior of casein micelle. However, at higher carrageenan concentrations depletion flocculation is dominant (**Figure 5-2** and **Figure 5-6**).

This study has demonstrated the usefulness of the Mastersizer as an additional hydrodynamic technique in the investigation of mixed systems. It is especially useful in mixed milk – polysaccharide system, due to difficulties in sedimentation analysis of turbid high molecular weight systems. In this type of system the sedimentation coefficient of the high molecular weight aggregates can not be quantitatively estimated using the analytical ultracentrifuge due their rapid rate of sedimentation ( $s^* \sim 2000$ -5000) and perhaps more significantly due to the masking of larger species by the turbidity of the remaining non-complexed casein micelles. There was however a good qualitative agreement between particle size and sedimentation time derivative analyses.

#### 6.4 CONCLUDING REMARKS AND SUGGESTIONS FOR FUTURE WORK

This work has focussed on the solution properties of commercial polysaccharides and their possible interactions with casein micelles. This is however a very complicated system and a great deal of work was required on the individual substrates before the interaction phenomena could be studied.

As a prelude to the study of casein micelle – polysaccharide interactions, a variety of commercial polysaccharides were studied (in order to obtain baseline values) results in general confirmed the hypothesis that polysaccharides are random coils or semi-rigid rods in dilute solution, which is typical of viscous high molecular weight polymers.

It was also necessary to investigate milk proteins of varying degrees of association, it was confirmed to casein micelles are spherical, hydrates super-molecular structures. Concentration dependant self-association together with thermodynamic non-ideality in sodium caseinate systems made it difficult to model the solution species. Concentration dependant self-association proved to be less of a problem in the case of individual caseins ( $\beta$ - and  $\kappa$ -).

Under the conditions studied only the carrageenans appear to interact with casein micelles. At low concentration there is steric stabilisation reaction, but as the  $\kappa$ -carrageenan concentration is increased depletion flocculation is induced.

On the whole this demonstrates the effectiveness of dilution solution hydrodynamics as a tool for the investigation of complex polydisperse, non-ideal, self-associating systems and their interactions.

The possibilities for future work in this field are almost infinite. As both the polysaccharide structures and casein structures (and therefore any complexes) are influenced by charge and temperature, one can therefore change their physical properties by altering the aqueous environment, *i.e.* pH and ionic strength. This would then affect the properties upon mixing. Under the conditions used (pH 6.8, I = 0.1M) pectin does not interact, however in alternative solution conditions we may expect to see both HM and LM pectin interactions with casein as has been indicated by Marozziene and de Kruif (2000) at pH 5.3, however when they increase the pH to

6.7 (approximately the same as we have studied) the pectin molecules desorb, therefore it is clear when considering polysaccharide – protein interactions the solution conditions are very important.

It may also be of interest commercially to compare the dilute solution hydrodynamic properties of polysaccharides with industrially important physical properties such as gel strength, setting time, setting temperature etc.

## 6.5 REFERENCES

- Advani M (1994) Solution Studies on  $\beta$ -lactoglobulin (Genetic Variant B). University of Nottingham. BSc.
- Arima S, Niki R and Takase K (1979) Structure of  $\beta$ -Casein. *Journal of Dairy Research*, **46**, 281-282.
- Ball A, Harding SE, and Mitchell JR (1988) Combined Low Speed Sedimentation Equilibrium/ Gel Permeation Chromatography Approach to Molecular Weight Distribution Analysis. Application to Sodium Alginate. *International Journal of Biological Macromolecules*, **10**, 259-264.
- Ball A, Harding SE and Simpkin NJ (1990) On the Molecular Weight Distribution of Dextran T-500. In: Phillips GO, Williams PA and Wedlock DJ (Eds.) *Gums and Stabilisers for the Food Industry 5*, pp. 447-450. IRL Press, Oxford.
- Bongaerts K, Paoletti S, Deneff B, Vanneste K, Cuppo F and Raynaers H (2000) Light Scattering Investigation of  $\iota$ -Carrageenan Aqueous Solutions. Concentration Dependence of Association. *Macromolecules*, Web Edition, 23/10/00, <http://dx.dio.org/10.1021/ma000996y>.
- Buchheim W and Schmitt DG (1979) On the Monomers and Polymers of  $\beta$ -Casein. *Journal of Dairy Research*, **46**, 277-280.
- Cölfen H, Harding SE and Vårum KM (1996a) Investigation, Using Analytical Ultracentrifugation, of the Effect of the Incorporation of the Fluorophore 9-Anthraldehyde on Two Chitosans of Differing Degrees of Acetylation. *Carbohydrate Polymers*, **30**, 55-60.

- Cölfen H, Harding SE, Vårum KM and Winzor DJ (1996b) A Study by Analytical Ultracentrifugation of the Interaction between Lysozyme and Extensively Deacetylated Chitin. *Carbohydrate Polymers*, **30**, 45-53.
- Crescenzi V and Della Valle F (1991) *Italian Patent. Application*, PD 91A00033.
- Dewan RK, Chudgar A, Mead R, Bloomfield VA and Morr CV (1974) Molecular Weight and Size Distribution of Bovine Milk Casein Micelles. *Biochimica et Biophysica Acta*, **342**, 313-321.
- Dhami R, Harding SE, Elizabeth NJ and Ebringerova A (1995a) Hydrodynamic Characterization of the Molar Mass and Gross Conformation of Corn Cob Hetroxylan AGX. *Carbohydrate Polymers*, **28**, 113-119.
- Dhami R, Harding SE, Jones T, Hughes T, Mitchell JR, and To K (1995b) Physico-Chemical Studies on a Commercial Food Grade Xanthan-I. Characterisation by Sedimentation Velocity, Sedimentation Equilibrium and Viscometry. *Carbohydrate Polymers*, **27**, 93-99.
- Ebringerova A, Novotna M, Kucurakova M and Machova E (1996) Chemical Modification of Beechwood Xylan with *p*-Carboxybenzyl Bromide. *Journal of Applied Polymer Science*, **6**, 1043-1047.
- Errington N (1993) Hydrodynamic Characterisation of Novel Polysaccharides for Pharmaceutical and Food Use. University of Nottingham. Ph.D.
- Errington E, Harding SE, Vårum KM and Illum L (1993) Hydrodynamic Characterisation of Chitosans of Differing Degrees of Acetylation. *International Journal of Biological Macromolecules*, **15**, 113-117.
- Farrell Jr HM (1973) Models for Casein Micelle Formation. *Journal of Dairy Science*, **56**, 1195-1206.

- Farrell Jr HM, Wickham ED and Groves ML (1998) Environmental Influences on Purified  $\kappa$ -Casein: Disulfide Interactions. *Journal of Dairy Science*, **81**, 2974-2984.
- Gaisford SE, Harding SE, Mitchell JR and Bradley TD (1986) A Comparison between the Hot and Cold Water Soluble Fractions of Two Locust Bean Gum Samples. *Carbohydrate Polymers*, **6**, 423-442.
- Gauzennec J (2000) The Deep-Sea Hypothermal Vents: A New Source of Bacterial Exopolysaccharides of Biotechnological Interest? POLYMERIX 2000 Biopolymers for the Food and Cosmetic Industry (Conference Proceeding), pp 187-193. CBB Development, Rennes, France.
- Glicksman M (1969) *Gum Technology in the Food Industry*. Academic Press, San Diego.
- Harding SE, Berth G, Ball A, Mitchell JR and Garcia de la Torre J (1991) The Molecular-Weight Distribution and Conformation of Citrus Pectins in Solutions Studied by Hydrodynamics. *Carbohydrate Polymers*, **16**, 1-15.
- Harding SE (1995) Some Recent Developments in the Size and Shape Analysis of Industrial Polysaccharides in Solution Using Sedimentation Analysis in the Analytical Ultracentrifuge. *Carbohydrate Polymers*, **28**, 227-237.
- Harding SE, Day K, Dhami R and Lowe PM (1997) Further Observations on the Size, Shape and Hydration of Kappa-Carrageenan in Dilute Solution. *Carbohydrate Polymers*, **32**, 81-87.
- Horton JC, Harding SE, Mitchell JR and Morton-Holmes DF (1991) Thermodynamic Non-Ideality of Dilute Solutions of Sodium Alginate Studied by Sedimentation Equilibrium Ultracentrifugation. *Food Hydrocolloids*, **5**, 125-127.

Jumel K (1994) Molecular Size of Interacting and Degrading Polysaccharides. Ph.D. Thesis, University of Nottingham.

Klavons JA and Bennet RD (1995) Preparation of Alkyl Esters of Pectin and Pectic Acid. *Journal of Food Science*, **60**, 513-515.

Kumosinski TF, Brown EM and Farrell Jr HM (1991a) Three Dimensional Modeling of Bovine Caseins:  $\kappa$ -Casein. *Journal of Dairy Science*, **74**, 2879-2887.

Kumosinski TF, Brown EM and Farrell Jr HM (1991b) Three Dimensional Modeling of Bovine Caseins:  $\alpha_{s1}$ -Casein. *Journal of Dairy Science*, **74**, 2889-2895.

Laue TM and Stafford III WF (1999) Modern Applications of Analytical Ultracentrifugation. *Annual Reviews in Biophysics and Biomolecular Structure*, **28**, 75-100.

Li P, Liu Z and Xu R (in press). Chemical Characterization of the Released Polysaccharide from the Cyanobacterium *Aphanothece halophytica* GR02. *Journal of Applied Phycology*.

Lin SHC, Dewan RK, Bloomfield VA and Morr CV (1971) Inelastic Light Scattering Study of the Size Distribution of Bovine Milk Casein Micelles. *Biochemistry*, **10**, 4788-4793.

Maroziene A and de Kruif CG (2000) Interaction of Pectin and Casein Micelles. *Food Hydrocolloids*, **14**, 391-394.

Parry Jr. RM and Carroll RJ (1969) Lactation of  $\kappa$ -Casein in Milk Micelles. *Biochimica et Biophysica Acta*, **194**, 138-150.

Payens TAJ (1979) Casein Micelles: The Colloid-Chemical Approach. *Journal of Dairy Research*, **46**, 291-306.

- Payens TAJ and van Markwijk BW (1963) Some Features of the Association of  $\beta$ -Casein. *Biochimica et Biophysica Acta*, **71**, 517-530.
- Pavlov GM, Rowe AJ and Harding SE (1997) Conformation Zoning of Large Molecules Using the Analytical Ultracentrifuge. *Trends in Analytical Chemistry*, **16**, 401-405.
- Pedersen KO (1936) CXXXVIII. Ultracentrifugal and Electrophoretic Studies on Milk Proteins. I. Introduction and Preliminary Results with Fractions from Skim Milk. *Biochemical Journal*, **30**, 948-960.
- Pepper L and Thompson MP (1963) Dephosphorylation of  $\alpha_s$ - and  $\kappa$ -Caseins and its Effect on Micelle Stability in the  $\kappa$ - $\alpha_s$ -Casein System. *Journal of Dairy Science*, **46**, 764-767.
- Ralston G (1993) *Introduction to Analytical Ultracentrifugation*. Beckman Instruments Inc., California.
- Robinson G, Ross-Murphy SB and Morris ER (1982) Viscosity-Molecular Weight Relationships, Intrinsic Chain Flexibility, and Dynamic Solution Properties of Guar Galactomannan. *Carbohydrate Research*, **107**, 17-32.
- Rowe AJ (1977) Concentration-Dependence of Transport Processes – General Description Applicable to Sedimentation, Translational Diffusion, and Viscosity Coefficients of Macromolecular Solutes. *Biopolymers*, **16**, 2595-2611.
- Saril PM (2000) Molecular Weight and Sedimentation Characteristics of Milk Proteins. University of Nottingham. BSc.
- Schachman HK (1959) *Ultracentrifugation in Biochemistry*. Academic Press, New York.

- Sharman WR, Richards EL, Malcolm GN (1978) Hydrodynamic Properties of Aqueous Solutions of Galactomannans. *Biopolymers*, **17**, 2817-2833.
- Stafford III WF (1992a) Boundary Analysis in Sedimentation Transport Experiments: A Procedure for Obtaining Sedimentation Coefficient Distributions Using the Time Derivative of the Concentration Profile. *Analytical Biochemistry*, **203**, 295-301.
- Stafford III WF (1992b) Methods for Obtaining Sedimentation Coefficient Distributions. In: Harding SE, Rowe AJ and Horton JC (Eds.) *Analytical Ultracentrifugation in Biochemistry and Polymer Science*, pp. 359-393. Royal Society of Chemistry, Cambridge.
- Swaigood HE and Brunner JR (1962) Characterisation of  $\kappa$ -casein Obtained by Fractionation with Trichloroacetic Acid in a Concentrated Urea Solution. *Journal of Dairy Science*, **45**, 1-11.
- Swaigood HE and Brunner JR (1963) Characterisation of Kappa-Casein in the Presence of Various Dissociating Agents. *Biochemical and Biophysical Research Communications*, **12**, 148-151.
- Swaigood HE, Brunner JR and Lillevik HA (1964) Physical Parameters of  $\kappa$ -Casein from Cow's Milk. *Biochemistry*, **3**, 1616-1623.
- Sullivan RA, Fitzpatrick MM, Stanton EK, Annino R, Kissel G and Palermi F (1955) The Influence of Temperature and Electrolytes upon Apparent Size and Shape of  $\alpha$ - and  $\beta$ -Casein. *Archives of Biochemistry and Biophysics*, **55**, 455-468.
- Tanford C (1961) *Physical Chemistry of Macromolecules*, Chapter 6. John Wiley and Sons, New York.

- Thompson MP (1971)  $\alpha_s$  and  $\beta$ -Caseins. In: MacKenzie HA (Ed.) *Milk Proteins: Chemistry and Molecular Biology Vol II*, pp. 117-174. Academic Press, New York
- Thompson MP and Pepper L (1962) Effect of Neuraminidase on  $\kappa$ -casein. *Journal of Dairy Science*, **45**, 794-796.
- Tombs MP and Harding SE (1998) *An Introduction to Polysaccharide Biotechnology*. Chapter 2. Taylor and Francis, London.
- Tongdang T, Bligh HFJ, Jumel, K. and Harding SE (1999) Combining Sedimentation Velocity With SEC-MALLS to Probe the Molecular Structure of Heterogeneous Macromolecule Systems that Cannot be Preparatively Separated: Application to Three Rice Starches. *Progress in Colloid and Polymer Science*, **113**, 185-191.
- von Hippel PH and Waugh DF (1955) Casein: Monomers and Polymers. *Journal of the American Chemical Society*, **77**, 4311-4319.
- Waugh DF, Creamer LK, Slattery CW and Dresdner GW (1970) Core Polymers of Casein Micelles. *Biochemistry*, **9**, 787-795.
- Waugh DF and von Hippel PH (1956)  $\kappa$ -Casein and the Stabilization of Casein Micelles. *Journal of the American Chemical Society*, **78**, 4576-4582.
- Zittle CA, Thompson MP, Custer JH and Cerbulis J (1962)  $\kappa$ -Casein -  $\beta$ -Lactoglobulin Interactions in Solution when Heated. *Journal of Dairy Science*, **45**, 807-810.

## A. APPENDIX A – TYPES OF AVERAGE MOLECULAR WEIGHTS

If a solution is polydisperse, then we can only calculate average molecular weights. In general there are three molecular weight averages, “number average”; “weight average” and “z-average” –  $M_n$ ,  $M_w$  and  $M_z$  which give increasing significance respectively, those components in a mixture with the highest molecular weight (McRorie and Voelker, 1993) (see equations A-1 to A-3). Therefore in a polydisperse system  $M_n < M_w < M_z$  and in a monodisperse system  $M_n = M_w = M_z$  and a comparison of molecular weight averages can therefore give a good indication of homogeneity.

$$M_n = \frac{\sum n_i M_i}{\sum n_i} \quad (\text{A-1})$$

$$M_w = \frac{\sum n_i M_i^2}{\sum n_i M_i} \quad (\text{A-2})$$

$$M_z = \frac{\sum n_i M_i^3}{\sum n_i M_i^2} \quad (\text{A-3})$$

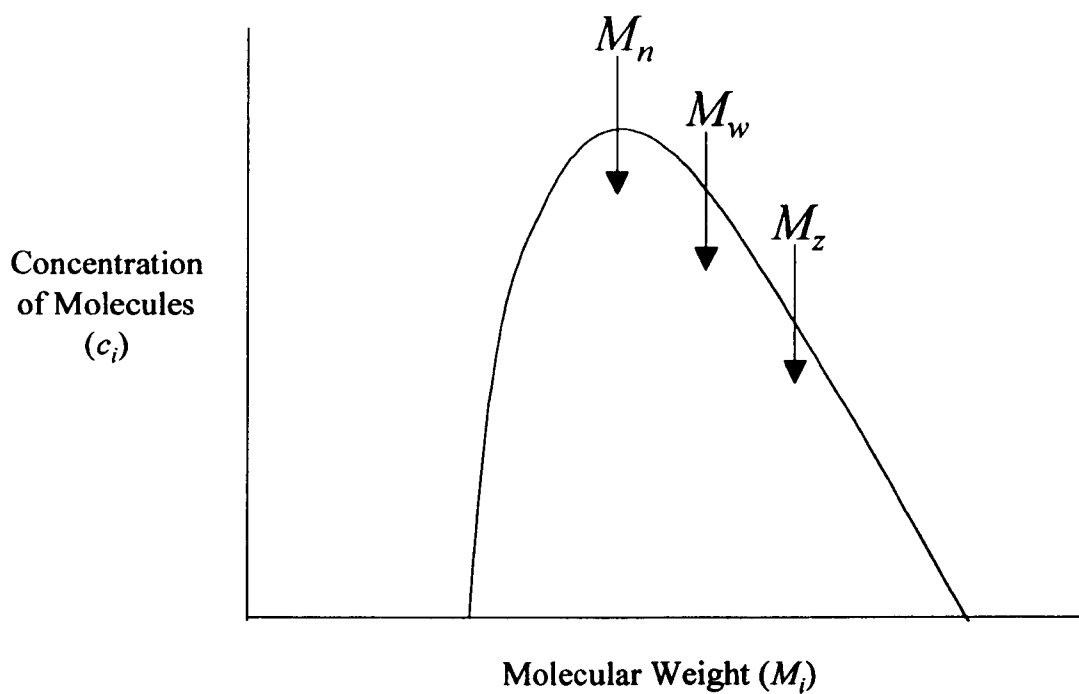


**Figure A-1** A graph showing the distribution of molecular weight “averages” in a polydisperse system (adapted from McRorie DK and Voelker PJ (1993) *Self-Associating Systems in the Analytical Ultracentrifuge*. Beckman Instruments Inc., California).

Appendix B not copied on instruction  
from the University.